

# **Optical Fibre Refractive Index, Voltage and Strain Sensors: Fabrication and Applications**

A thesis submitted

by

**Harpreet Kaur Bal**

MSc (App Phy), BSc, GCert (TE)

*for the degree of*

**DOCTOR OF PHILOSOPHY**

Centre for Telecommunication and Microelectronics

Faculty of Health, Engineering and Science

Victoria University

Australia

(2011)

To my family

## Abstract

The focus of this thesis is the study of intensity and wavelength-based optical fibre sensors (OFSs) for various applications in three major sensing areas: refractive index (RI), voltage and strain. The thesis aims to provide detailed information on the design and performance of particular intensity-based and wavelength-based (fibre Bragg gratings (FBGs)) OFSs in these three major areas. Furthermore, the thesis provides details of multiplexing strategies for some of these sensors.

Although various fibre optic sensors exist for RI, voltage and strain measurements, developing new sensing schemes aids understanding and provides improvements for these devices.

This thesis provides the relevant background of intensity-based sensors for RI measurements and introduces a simple optical principle that offers a multipoint sensing scheme for RI measurements for different applications. The etching of fibre as an evanescent field sensor for RI measurements is presented. RI sensing in terms of wavelength modulation is detailed, where a fibre Bragg grating was used for sensing. These sensors are compared for their performance based on factors including sensitivity, design complexity and cost.

The thesis gives detailed design and performance characteristics of a multipoint voltage sensor designed for high voltage power lines, which would allow direct measurement of up to 400 kV/m AC voltage at multiple points along power lines with high precision. A simple design of an electric field amplifying probe (EFAP) is also evaluated.

The complex structure of a FBG fabricated using the standard phase mask gives rise to an alternative type of pi-phase-shifted fibre Bragg grating (APPhSFBG). This thesis aims to investigate these APPhSFBGs to understand the complex structure inside the core of an optical fibre by their sensing behaviour, e.g. in transverse strain and bending. The effect of lateral pressure in pi-phase-shifted FBGs (APPhFBGs and standard) inscribed in various fibres is also evaluated.

The suitability of standard uniform FBGs for human skin pressure measurements is studied. Compression garments are used for patients' suffering from varicose veins, lymph-oedema, oedema or deep vein thrombosis. Evaluation of these garments is crucial in order to maintain recommended pressure levels. This study indicates that the standard FBGs have low sensitivity for such a low pressure measurements, and indicates that further investigation of suitability of FBGs in different types of fibres (in particular microstructured plastic optical fibre) is required.

## Declaration

"I, Harpreet K. Bal, declare that the PhD thesis entitled

**Optical fibre refractive index, voltage and strain sensors: fabrication and applications**

is no more than 100,000 words in length including quotes and exclusive of tables, figures, appendices, bibliography, references and footnotes. This thesis contains no material that has been submitted previously, in whole or in part, for the award of any other academic degree or diploma. Except where otherwise indicated, this thesis is my own work".

.....

Harpreet Kaur Bal

Dated the 3<sup>rd</sup> day of March, 2011

## Acknowledgements

I am indebted to many individuals who have provided assistance and support during the period of this research. First of all, I devote all my achievements to the Almighty God for instilling in me strength and spirit to accomplish this project.

I am extremely obliged to my supervisor Assoc. Prof. Stephen Collins, Director, Centre for Telecommunications and Microelectronics, Victoria University, Melbourne for inculcating research aptitude in me. His inspiration, encouragement, free and informal discussion, and valuable suggestions have gone a long way in the completion of my work. His reminders to stay determined helped me to focus on my work and completion in time. His comments on results and experiments have always provided a direction to this candidature. His tremendous attention to detail and endless efforts in reviewing this thesis and many manuscripts are highly appreciated. He has proved to be an invaluable mentor.

A special thanks to Dr. Zourab Brodzel, whose motivation and encouragement helped me through some difficult times during this journey. His continuous advice on effective writing skills facilitated to write journal papers and this thesis. I owe many thanks to him for discussing and helping in various laboratory experiments. I am grateful to him for the characterization of fibre sensor with liquid crystal at Hong Kong university of Science and Technology (HKUST). His readiness to help out in every aspect of life and direction during this candidature encouraged me to complete my journey from a graduate student to a scientist.

I would like to acknowledge Professor Gregory W. Baxter for his valuable suggestions in manuscripts and in this thesis. His friendly and welcoming nature always filled me with joy and eagerness to complete my task. I can never forget the time he stole from his busy schedule to attend my graduation ceremony of a graduation certificate.

I wish my gratitude to Dr. Fotios Sidroglou for his assistance in the laboratory and helpful comments. Special thanks to Dr. Nicoleta Dragomir for her help in imaging lab for FBG characterization. Her friendly nature and informal

discussions on the structure of this thesis were very helpful. Her personality and independent aptitude became a role model for me. Her constant motivation always encouraged me to do something special in research. I am highly thankful to her for her invaluable suggestions and assistance for this work.

I am grateful to Professor Akhtar Kalam for his unconditional support, helpful discussions and assistance in high power lab for characterization of an electric field amplifying probe (EFAP). I acknowledge Professor Valdimir Chigrinov from HKUST for his assistance with liquid crystals. I also extend my special thanks to all my friends and my research colleagues especially Zahir Pracha and Mohammad Reza Pourakbar for their co-operation throughout this work.

I also acknowledge the Victoria University Postgraduate Scholarship scheme for providing a scholarship for this research. I would like to thank technical and administrative staff of the School of Health Engineering and Science for their assistance. In particular, I am grateful to Donald Ermel for his time and effort for various job requests especially for characterization of EFAP.

The list of above acknowledgements would be incomplete had I not mentioned the encouragement, inspiration and advice from my family, especially my husband Navdeep Singh Bal. This big project could not be accomplished without his support and continuous encouragement during each day of my PhD. Special thanks to my father Harwinder Singh and my mother Sawraj Kaur, their love, support and encouragement during these many years. While my father never lived to see this achievement, during his life he and my mother were always there to be the best possible parents. I can never forget the love, support and inspiration from my uncle Balwinder Singh. I owe them my deepest gratitude. I owe a loving thanks to my father-in-law Gurninder Singh, mother-in-law Dyal Kaur and family for keeping my morale high throughout the period of this work and giving me time to study while not expecting anything from me. At last, my gratitude to my brother Amandeep Singh and my sister Sandeep Kaur for their love and support during these many years. Their wish to see their younger sister as a scientist helped me to complete my task with enthusiasm.

# Table of Contents

<b>ABSTRACT .....</b>	<b>II</b>
<b>DECLARATION .....</b>	<b>IV</b>
<b>ACKNOWLEDGEMENTS.....</b>	<b>V</b>
<b>TABLE OF CONTENTS .....</b>	<b>VII</b>
<b>LIST OF FIGURES .....</b>	<b>XIV</b>
<b>LIST OF TABLES.....</b>	<b>XXI</b>
<b>CHAPTER 1.....</b>	<b>1</b>
<b>INTRODUCTION.....</b>	<b>1</b>
1.1 OPTICAL FIBRE SENSORS BACKGROUND .....	1
1.2 SCOPE OF THE THESIS.....	5
1.3 CHAPTER SUMMARY.....	5
<b>CHAPTER 2.....</b>	<b>8</b>
<b>REVIEW OF OPTICAL FIBRE SENSORS .....</b>	<b>8</b>
2.1 THEORY OF OPTICAL FIBRE SENSORS.....	8
2.1.1 <i>Propagation of light in optical fibre .....</i>	<i>8</i>
2.2 TYPES OF OPTICAL FIBRE SENSORS .....	10
2.2.1 <i>Intensity-modulated OFSs.....</i>	<i>11</i>
2.2.1.1 Transmissive/ reflective OFSs.....	12
2.2.1.2 Micro-bend sensors .....	19
2.2.1.3 Fibre Bragg grating sensors .....	19
2.2.2 <i>Phase-modulated OFSs.....</i>	<i>20</i>
2.2.3 <i>Polarisation-modulated OFSs .....</i>	<i>21</i>

2.2.4 Wavelength-modulated OFSs.....	21
2.2.4.1 Fibre Bragg grating sensors .....	21
(a) Photosensitivity.....	22
(b) Hydrogenation for enhanced photosensitivity.....	23
(c) Fabrication of FBGs.....	25
(d) Apodisation of FBGs.....	28
2.2.4.2 Types of Fibre Bragg gratings.....	29
(a) Uniform FBGs .....	29
(b) Chirped gratings .....	30
(c) Long Period gratings (LPGs).....	30
(d) Blazed or Tilted gratings .....	30
(e) Pi-phase-shifted FBGs .....	30
2.2.4.3 Scope of fibre Bragg gratings in sensing.....	33
2.2.4.4 Properties of fibre Bragg gratings in sensing.....	34
(a) Tuning FBGs .....	34
(b) Varying the pitch of the FBG .....	34
(c) Varying the refractive index of the FBG .....	35
2.3 MULTIPLEXING OF OPTICAL FIBRE SENSORS BASED ON FIBRE BRAGG GRATINGS.....	37
2.4 APPLICATIONS OF OPTICAL FIBRE SENSORS.....	39
2.4.1 Applications of OFSs Studied in this thesis.....	39
2.5 CONCLUSIONS .....	40
<b>CHAPTER 3 .....</b>	<b>41</b>
<b>FABRICATION AND CHARACTERIZATION OF FIBRE BRAGG GRATINGS.....</b>	<b>41</b>
3.1 PHASE MASK METHOD (VU FBG INSCRIPTION METHOD) .....	41
3.1.1 Uniform FBG.....	43

3.1.2 Alternative type of pi-phase-shifted FBGs.....	43
3.2 CHARACTERIZATION OF FIBRE BRAGG GRATINGS.....	44
3.2.1 Spectral characterization of FBGs.....	44
(a) Characterization using OSA.....	44
(b) High resolution full spectrum characterization.....	46
3.2.2 Microscopic characterization of FBGs.....	47
(a) Set –up.....	47
(b) Sample preparation.....	50
(c) FBG images and analysis.....	50
3.3 CONCLUSIONS.....	55
<b>CHAPTER 4.....</b>	<b>56</b>
<b>REFRACTIVE INDEX SENSOR AND APPLICATIONS.....</b>	<b>56</b>
4.1 REFRACTIVE INDEX SENSOR.....	56
4.2. FIBRE OPTIC RI SENSOR BASED ON BROADBAND REFLECTOR.....	60
4.2.1 Introduction.....	60
4.2.2 Multipoint broadband reflector.....	62
(a) Theoretical analysis.....	64
(b) Experimental results.....	64
4.3. APPLICATION OF FIBRE OPTIC RI SENSOR BASED ON BROADBAND REFLECTOR-STATE OF CHARGE OF A BATTERY.....	69
(a) Introduction.....	69
(b) Principle of operation.....	71
(c) Experimental details and results.....	72
4.4. OPTICAL FIBRE RI SENSOR BASED ON ETCHED FIBRE BRAGG GRATINGS.....	76
4.4.1 Introduction: Communication with outside environment.....	76

4.4.1.1 D-shaped fibre .....	77
4.4.1.2 Etched, thinned or reduced cladding FBGs .....	78
(a) Theoretical analysis .....	78
(b) Experimental analysis .....	79
i. Special etching mount .....	80
ii. Fibre preparation for etching.....	81
iii. Spectral characterization of etched FBGs .....	83
iv. Microscopic characterization of etched FBGs .....	84
4.5 APPLICATIONS OF ETCHED FBGs.....	86
4.5.1 Etched fibre refractometer.....	86
4.5.2 Liquid RI sensor based on etched FBGs.....	87
4.5.3 Performance of etched FBGs for longitudinal strain .....	89
4.5.4 Pi-phase FBGs based on wet chemical etching .....	91
4.6 CONCLUSIONS .....	94
4.7 COMPARISON OF INTENSITY-MODULATED AND WAVELENGTH- MODULATED RI SENSOR STUDIED IN THE THESIS .....	96
4.7.1 Comparison of main parameters.....	97
<b>CHAPTER 5 .....</b>	<b>98</b>
<b>VOLTAGE SENSOR: INTERFACING FIBRE OPTIC AND LIQUID CRYSTAL TECHNOLOGY .....</b>	<b>98</b>
5.1 MOTIVATION.....	98
5.2 INTRODUCTION TO VOLTAGE SENSORS.....	99
5.2.1 Background.....	99
5.3 DEVICES BASED ON INTERFACING OF LIQUID CRYSTALS WITH OPTICAL FIBRE.....	100
5.3.1 Introduction to liquid crystals.....	103
5.3.1.1 Electro-optical properties of LCs.....	104

5.3.1.2 Alignment of LCs .....	106
5.4 MULTIPOINT OFLC VOLTAGE SENSOR .....	106
5.4.1 Principle of operation.....	107
5.4.2 Materials and methodologies.....	109
(a) Sensor head (SH).....	110
i. Fabrication of liquid crystal cell (LCC) .....	110
i.i Choice of LC .....	110
i.ii Initial alignment of LC .....	111
(b) Fibre optic circuit – multiplexer.....	111
i. Transmission characterization of LCC.....	111
(c) Electric field amplifying probe (EFAP).....	114
5.4.3 Characterization of EFAP.....	116
5.5 CONCLUSIONS .....	120
<b>CHAPTER 6 .....</b>	<b>122</b>
<b>OPTICAL FIBRE STRAIN SENSORS.....</b>	<b>122</b>
6.1 OPTICAL FIBRE STRAIN SENSOR .....	122
6.2 FIBRE BRAGG GRATING TRANSVERSE STRAIN SENSOR.....	123
6.2.1 Transverse strain measurements at twice the Bragg wavelength .....	126
(a) Experimental Analysis .....	126
(b) Theoretical Analysis.....	132
6.2.1.1 Applications of fibre Bragg grating transverse strain sensor .....	133
6.2.1.2 Low cost interrogation technique for simultaneous longitudinal and transverse strain sensor.....	134
6.2.3 Temperature independent bend measurements at twice the Bragg wavelength.....	135
6.3 FIBRE BRAGG GRATING PRESSURE SENSOR.....	139

6.3.1 Response of various pi-phase-shifted FBGs to elevated pressures .....	141
6.3.2 Fibre Bragg grating sensors for human skin pressure measurements .....	145
(a) Motivation.....	146
(b) Results and Discussion .....	148
6.4 CONCLUSIONS .....	151
<b>CHAPTER 7 .....</b>	<b>153</b>
<b>CONCLUSIONS AND FUTURE WORK .....</b>	<b>153</b>
7.1 SUMMARY OF THE KEY OUTCOMES .....	153
7.2 DIRECTIONS FOR FUTURE WORK .....	156
<i>Chapter 3 Fabrication and characterization of fibre Bragg gratings.....</i>	<i>156</i>
<i>Chapter 4 Refractive index sensor.....</i>	<i>156</i>
<i>Chapter 5 Hybrid voltage sensor .....</i>	<i>157</i>
(a) Fabry-Perot interferometer .....	157
(b) Corrugated Fibre Bragg gratings .....	157
(c) Fibre Taper .....	157
(d) Etched fibre Bragg gratings.....	158
(e) Long period gratings.....	158
<i>Chapter 6 Strain sensor .....</i>	<i>158</i>
Pi-phase-shifted FBGs .....	158
Transverse strain measurements.....	158
Bend measurements .....	159
Lateral Pressure measurements .....	159
<b>REFERENCES.....</b>	<b>161</b>
<b>APPENDIX A.....</b>	<b>183</b>
<b>LIST OF PUBLICATIONS .....</b>	<b>183</b>

JOURNAL PUBLICATIONS.....	183
INTERNATIONAL CONFERENCE PUBLICATIONS .....	183
NATIONAL CONFERENCE PUBLICATIONS.....	184
<b>APPENDIX B.....</b>	<b>186</b>
<b>PRECAUTIONS WHILE DEALING WITH HF ACID .....</b>	<b>186</b>

## List of Figures

Figure 2-1 Schematic of optical fibre, showing typical diameters.....	8
Figure 2-2 Refraction and reflection of light.....	8
Figure 2-3 Propagation of light inside the fibre based on total internal reflection ...	9
Figure 2-4 Transmissive concept .....	13
Figure 2-5 Schematic of a reflective type fibre optic displacement sensor.....	13
Figure 2-6 Schematic of an intensity-based fibre optic force sensor (Bakalidis <i>et al.</i> , 1996) .....	13
Figure 2-7 Reflection of light from angled end of fibre.....	15
Figure 2-8 Intrinsic FPI sensor configurations schematic: (a) cavity formed by an internal mirror and fibre end; (b) cavity formed by two internal mirrors; and (c) cavity formed by two fibre Bragg gratings (Taylor, 2002).....	18
Figure 2-9 Intrinsic sensor configurations: (a) reflective FPI sensor with internal cavity; (b) FPI sensor with hollow core (Taylor, 2002) and (c) miniature FPI using laser micromachining (*after (Wei <i>et al.</i> , 2008)). .....	19
Figure 2-10 After the patent entitled: "Accelerated method for increasing the photosensitivity of glassy material" by (Brennan <i>et al.</i> , 2001).....	25
Figure 2-11 Schematic representation of a fibre Bragg grating .....	25
Figure 2-12 Typical optical response/spectra of a FBG in reflection and transmission .....	26
Figure 2-13 Phase-mask writing method.....	27
Figure 2-14 Schematic of an apodised FBG .....	28
Figure 2-15 Spectrum of an unapodised and apodised FBG fabricated at VU .....	29
Figure 2-16 Schematic of a chirped FBG.....	30
Figure 2-17 DIC images of the core region of a fibre Bragg grating (a) image is taken from a direction orthogonal to that of the writing beam. (b) The same fibre Bragg grating, after the fibre has been rotated about its axis by $\pm 90^\circ$ (after (Dragomir <i>et al.</i> , 2003)).....	32

Figure 3-1 Schematic of the optical arrangement of the scanning FBG fabrication facility at VU .....	42
Figure 3-2 Schematic showing the fibre clamps, strain sensors and alignment facility for FBG fabrication located at VU .....	42
Figure 3-3 Hydrogenation chamber located at VU .....	43
Figure 3-4 Schematic of set-up used to measure (a) transmission and (b) reflection spectrum of FBGs .....	45
Figure 3-5 Transmission and reflection spectra of a uniform FBG written at VU ....	45
Figure 3-6 Reflection spectrum of an alternative type of pi-phase-shifted FBG at twice the Bragg wavelength fabricated using phase-mask writing method at VU...	46
Figure 3-7 Schematic of high resolution FBG characterization set-up .....	46
Figure 3-8 Spectrum showing reflection and group delay for a chirped FBG fabricated at VU .....	47
Figure 3-9 Schematic of DIC microscope .....	48
Figure 3-10 Schematic representation of the acquisition system used to acquire DIC images. The imaging platform can be interactively controlled through the Windows NT workstation via the Fluoview™: with a stepper motor that translates the objective in 0.1 μm increments along the optical axis (Kouskousis, 2009).....	49
Figure 3-11 Schematic representation of prepared sample on a cover slip .....	50
Figure 3-12 DIC image of an (a) FBG inside the core of an optical fibre (b) FBG with etched cladding where a small portion of cladding is present.....	51
Figure 3-13 DIC image of a fully etched FBG.....	51
Figure 3-14 Pixel intensity plots for a (a) line and (b) 3D surface plot of a region across the fibre core for the FBG in GF1 fibre shown in Figure 3-12 (a) .....	52
Figure 3-15 Pixel intensity plots for a (a) line and (b) 3D surface plot of a region across the fibre core for the partially etched FBG in GF1 fibre shown in Figure 3-12 (b).....	53
Figure 3-16 Pixel intensity plots for a (a) line and (b) 3D surface plot of a region across the fibre core for the fully etched FBG in GF1 fibre shown in Figure 3-13 ...	54
Figure 4-1 Basic principle of operation of fibre optic RI sensor based on broadband reflector .....	61

Figure 4-2 Response of fibre optic broadband reflector when sensor head was in air and in isopropyl alcohol .....	62
Figure 4-3 Relationship between RI of liquid and reflected signal .....	62
Figure 4-4 Schematic of module 1 (M1).....	63
Figure 4-5 Multiplexing of fibre optic reflective sensors consisting of n modules, each of which has a sensor head and a unique wavelength (Bal <i>et al.</i> , 2010d).....	64
Figure 4-6 Example of the spectrum of two FBGs when both sensor heads M1 (operating at 1559.5 nm) and M2 (operating at 1543.5 nm) were in air .....	65
Figure 4-7 Examples of spectra when sensor head M2 (1543.5 nm) (a) was in air and (b) was in isopropyl alcohol.....	66
Figure 4-8 Performance of M1 when an isolator was used in between M1 & M2....	67
Figure 4-9 (a) Variation of the reflected power for measurement over a range of refractive indices using sensor heads M1 & M2 with (b) showing the same data over a smaller range (Bal <i>et al.</i> , 2010d).....	68
Figure 4-10 Set-up used to measure state of charge (SOC) of battery .....	73
Figure 4-11 Set-up used to calibrate sensor and to measure state of charge of battery.....	73
Figure 4-12 Output of the sensor vs. temperature .....	74
Figure 4-13 Output of the sensor vs. voltage measured between the load applied to the battery and battery itself.....	75
Figure 4-14 The theoretical representation of shift in Bragg wavelength with outer RI for a standard SMF 28 fibre core (Brodzeli <i>et al.</i> , 2009b) .....	79
Figure 4-15 Spectrum of unevenly etched FBG.....	80
Figure 4-16 HF acid etching mount .....	80
Figure 4-17 A prepared FBG with Teflon tubing for etching .....	81
Figure 4-18 Set-up used for etching of FBG.....	82
Figure 4-19 Shift of Bragg wavelength ( $\lambda_B$ ) while etching .....	82
Figure 4-20 Representation of etched FBG.....	83
Figure 4-21 Spectrum of etched FBG, when fixed at the ends on Teflon holder using a sticky tape.....	83

Figure 4-22 Spectrum of a uniformly etched FBG before and after etching using special etching mount .....	84
Figure 4-23 Spectrum of a chirped FBG before and after etching using special etching mount .....	84
Figure 4-24 DIC images of (a) un-etched FBG (b) etched fibre without FBG and (c) etched FBG.....	85
Figure 4-25 Reflected power intensity of an etched fibre with different surrounding RI.....	86
Figure 4-26 Reflected power of a partially etched FBG with the surrounding RI greater than the core RI.....	87
Figure 4-27 Spectrum of a uniform FBG before and after etching .....	88
Figure 4-28 Bragg wavelength shift with respect to RI (Bal <i>et al.</i> , 2010e).....	88
Figure 4-29 Set-up for longitudinal strain measurement (Trpkovski <i>et al.</i> , 2005) .	90
Figure 4-30 FBGs wavelength shift with applied longitudinal strain.....	90
Figure 4-31 Schematic of FBG (a) with Teflon drop in the middle, (b) Teflon tape knot and (c) an etched phase-shifted FBG .....	92
Figure 4-32 Reflection spectrum of the FBG before (dotted) and after (solid) etching (with Teflon drop).....	92
Figure 4-33 Reflection spectrum of the FBG before (dotted) and after (solid) etching (with Teflon tape knot) .....	93
Figure 4-34 (a) DIC image of un-evenly etched FBG and (b) microscopic image of un-etched fibre region .....	93
Figure 4-35 Reflection spectrum of the FBG before (dotted) and after (solid) etching.....	94
Figure 5-1 Schematic of a hybrid device based on OFLC.....	102
Figure 5-2 LC arrangements (a) solid (b) liquid and (c) liquid.....	103
Figure 5-3 Example of orientation of (a) Nematic, (b) Smectic A and (c) Smectic C .....	104
Figure 5-4 Schematic representing of liquid crystal molecule (a) depicting ordinary and extra-ordinary refractive indices (b) alignment of molecules when an electric field is applied along direction of propagation of light and (c) alignment of	

LC molecules when external electric field is applied perpendicular to the direction of propagation of light.....	105
Figure 5-5 The propagation of light through two transparent materials with different refractive indices when angle of incidence = 0.....	107
Figure 5-6 Basic idea of the multipoint sensor .....	107
Figure 5-7 Interaction of light with fibre end and LC (a) no external electric field, (b) with external electric field .....	109
Figure 5-8 Refractive index vs. angle between the director of the molecule of LC and polarisation of transmitting through LC light (using equation 5-2) .....	109
Figure 5-9 Reflectivity of the cleaved end of fibre emerged into LC vs. angle between the director of the molecule of LC and polarisation of transmitting through optical fibre light.....	109
Figure 5-10 (a) Sensor head inside a LCC and (b) Cleaved fibre submerged in LCC .....	110
Figure 5-11 Set-up for characterization of transmittance of LCC.....	111
Figure 5-12 Retardation of 180 $\mu\text{m}$ thick LCC vs. applied voltage (TVC curve).....	111
Figure 5-13 Signal power reflected off FBG vs. external voltage applied to LCC...	112
Figure 5-14 Schematic representation of alignment of LC molecules inside SH around cleaved fibre end; (a) no field, (b) with electric field.....	113
Figure 5-15 LCC placed inside an electric field .....	114
Figure 5-16 Schematic representation of EFAP connected to LCC (SH).....	114
Figure 5-17 Transmittance of light through the 10 $\mu\text{m}$ gap LCC vs. external voltage .....	115
Figure 5-18 Set-up for demonstrating ability of EFAP to provide enhanced field and switching LCC.....	116
Figure 5-19 Switching of 10 $\mu\text{m}$ LCC by EFAP placed in an external electric field	116
Figure 5-20 Set-up used to test geometrical properties of EFAP.....	117
Figure 5-21 Output voltage vs. distance between the probes of EFAP .....	117
Figure 5-22 Parallel conducting probes inside uniform electric field (a) inferred field lines (b) electric potential profile along path a→b.....	118

Figure 5-23 Coefficient B vs area of probe of and EFAP .....	119
Figure 5-24 Calculated output voltage placed inside uniform electric field of 2.5 kV/m when changing distance between the probes .....	119
Figure 6-1 Schematic showing direction of force applied .....	127
Figure 6-2 Set-up used for transverse strain measurements .....	127
Figure 6-3 FBG spectra at various applied loads (a) 3D representation and (b), (c), (d) FBG spectra at various applied loads.....	129
Figure 6-4 Splitting of the lower wavelength peak vs. applied weight.....	129
Figure 6-5 Uniform splitting of two peaks under transverse load .....	130
Figure 6-6 Separation between two peaks with applied load.....	130
Figure 6-7 Variation in the dip wavelength against transverse strain at $\lambda_{2/3B}$ (Yam <i>et al.</i> , 2006).....	131
Figure 6-8 Transverse strain response (Figure 6-4) with respect to actual load on the FBG calculated using equation 6-2 .....	132
Figure 6-9 Experimental results of low cost FBG strain interrogation system showing overall wavelength shift on application of longitudinal strain.....	135
Figure 6-10 Schematic diagrams, showing (a) bending directions of an embedded FBG, and (b) set-up used for measuring the spectral response of the pi-phase-shifted FBG, when bending in one direction .....	136
Figure 6-11 Spectrum of FBG at double the Bragg wavelength without (solid line) and with bending (dotted line).....	137
Figure 6-12 Behaviour of the double peaks (L and R) when subject to bending in two directions (+ and - ), with (a) showing the normalized peak area intensity ratios of two peaks and (b) illustrates the peak separation of wavelength with bending, while (c) depicts the peak separation of wavelength with respect to temperature .....	138
Figure 6-13 Set-up used for FBG pressure sensor calibration, where BBS - broadband light source, OSA - optical spectrum analyser .....	141
Figure 6-14 Examples of reflection spectra for 3 different pressures, for the 3 fibre and FBG combinations, where (a) & (b) APPhSFBG and (c) standard pi-phase-shifted FBG .....	143
Figure 6-15 Wavelength shift (first peak) against applied pressure for pi-phase-shifted gratings in the three fibre types.....	144

Figure 6-16 Linear wavelength shift (first peak) against applied pressure (for a range 0-20 kPa) for pi-phase-shifted gratings in the three fibre types ..... 145

Figure 6-17 Leg layout showing different positions of measurements, HT- hard tissue & ST-soft tissue ..... 147

Figure 6-18 Spectral response of FBG1 sensor for two different loads..... 149

Figure 6-19 Pressure calibration for different lengths of FBGs..... 149

Figure 6-20 Pressure response demonstrating the effect of changing position and posture ..... 150

Figure 7-1 DIC images with highpass filter in Y direction (For display purposes) of the core region of a fibre Bragg grating in small core Hi 1060 FLEX fibre (a) image was taken from a direction orthogonal to that of the writing beam (b) The same fibre Bragg grating, after the fibre has been rotated about its axis by  $\pm 90^{\circ}$ ..... 155

## List of Tables

Table 2-1 OFSs for different applications (Krohn, 2000).....	39
Table 2-2 Applications of OFSs based on different sensing techniques (Krohn, 2000) .....	39
Table 2-3 Applications of OFSs studied in this thesis.....	39
Table 4-1 Details of equipment used to measure SOC of a battery .....	72
Table 4-2 Details of FBGs used for longitudinal strain sensing .....	89
Table 4-3 Summary of the performance of the various RI sensing techniques.....	97
Table 4-4 Summary of the performance of the various RI sensing technique.....	97
Table 5-1 Compatibility of optical fibre and liquid crystal technology for OFLC device.....	100
Table 5-2.....	119
Table 5-3 Calculated output voltage of EFAP for various probe sizes .....	120
Table 6-1 Response of various types of FBGs to transverse load .....	124
Table 6-2 Transverse load response for various fibre types (after (Chehura <i>et al.</i> , 2004)).....	125
Table 6-3 Transverse response for various core diameters and dopant concentration .....	125
Table 6-4 (after (Wang <i>et al.</i> , 2009) .....	126
Table 6-5 Transverse strain response at different harmonics of FBG .....	131
Table 6-6 Properties of optical fibre used for theoretical analysis (Wagreich <i>et al.</i> , 1996) .....	133
Table 6-7 (after (Brodzeli <i>et al.</i> , 2008a)).....	135
Table 6-8 (Sharifian, 2003).....	139
Table 6-9 Fibre and FBG types used to measure pressure response .....	142

# Chapter 1

## Introduction

One of the most promising areas of measurement technology that continue to develop rapidly, particularly over the past two decades, is that of optical fibre sensors (OFSs). This chapter highlights the scope of the thesis, where the telecommunications background to OFSs is detailed and a chapter summary is provided.

### 1.1 Optical Fibre Sensors Background

The history of OFS technology is allied to an optical revolution started in 1790 when French engineer Claude Chappe reported an 'optical telegraph'. After that it evolved from the invention of an optical photophone by Alexander Graham Bell in 1880 to the understanding of a light guiding medium by Swiss physicist Daniel Collodon and French physicist Jacques Babinet in the 1840s. About a decade after, in 1854, British physicist John Tyndall popularized light guiding properties and demonstrated that light could be guided in a jet of water flowing from a tank. Later, in the 1920s, the use of arrays of hollow pipes or transparent rods to transmit images for television or facsimile systems were demonstrated by John Logie Baird in England and Clarence W. Hansell in the United States. Initially the use of optical fibres was limited to medical technology. In 1951, Holger Møller announced its scope in imaging. In the earlier version of fibres no cladding was present and light was guided from the glass-air interface.

The era of today's fibres with waveguiding properties using cladding began with an invention of Van Heel, who used a transparent cladding of lower refractive index (RI) to cover a bare fibre and reduced the crosstalk between fibres. Later, in 1966, Charles K. Kao revolutionized the industry by demonstrating that loss could be reduced to less than 20 dB/km (Kao & Hockham, 1966). He did his pioneering work in anticipation of glass fibre optics as a telecommunications medium and is known as the "Father of Fibre Optics" (Shampo *et al.*, 2011). These novel discoveries are the basis of today's optical fibre communications and optical

sensing networks. Recently, in 2009, he was awarded half of the Nobel Prize in Physics for “groundbreaking achievements concerning the transmission of light in fibres for optical communication”. Finally, in September 1970, at the Corning Glass Works (now Corning Inc.), Robert Maurer, Donald Keck and Peter Schultz announced the production of the first single-mode fibres (SMF). The modern photonic industry began in earnest with the development of the first semiconductor laser by Bell Labs (Schawlow, 1960) and a team at the Ioffe Physical Institute in Leningrad, in the same year (Hecht, 2004).

The properties of optical fibre like large bandwidth, low transmission loss, high optical damage threshold and low optical nonlinearity made possible the use of optical fibre in telecommunications (Sandbank, 1977). Telecommunication applications are widespread involving global and local networking of a vast number of devices including desktop computers. These involve the transmission of voice, data, or video over distances of less than a metre to thousands of kilometres, using one of a few standard fibre designs in one of several cable designs.

As fibre-optic communications networks matured and became a promising transporting medium for high speed communication, the need for improved photonics products continued. This demand resulted in an exponential growth of the industry and as a result other potential applications of photonics technology emerged.

Optical fibre sensor technology is an offshoot of fibre optic communication technology, and a low loss optical fibre was used for the first time for sensing purposes in the early 1970s. In 1967, the first “Fotonic” sensor was suggested (Menadier *et al.*, 1967) to measure position and spacing in the machine tool industry. For the last two decades, an increasing amount of resources has been expended on research and development worldwide on the application of novel fibre-optic sensor systems. Fibre-optic sensors offer the possibility of measurement in harsh environments where conventional electrical and electronic sensors have difficulties. Their demand from industry is increasing because of the advantages of small size, high multiplexing capability, immunity to EMI, high

temperature operation, improved measurement accuracy and reliability. Their applications are emerging in industrial automation, health care, aerospace and aviation. Compared to conventional sensor technology, OFSs offer numerous other advantages such as high sensitivity, all-solid-state construction, no moving parts and a sufficiently long lifetime (Krohn, 2000). It is now feasible to process an optical signal all-optically with optical fibre components such as filters, dispersion compensators (Ibsen *et al.*, 1999), amplifiers (Mears *et al.*, 1987), lasers (Zyskind *et al.*, 1991), phase modulators (Jarzynski, 1984), directional couplers (Masuda & Iwama, 1982) and polarisers (Stewart *et al.*, 1989).

The main limitations of OFSs are the high cost and unfamiliarity to the end user. Although familiarity with fibre sensor technology has increased and sensor prices have decreased, fibre sensors still find most applications in areas where electronic sensors cannot compete with the advantages offered by optical technologies such as the promise of faster speeds or an ability to operate under harsh conditions (Weisenbach, 2008). Other main challenges in OFSs market are sensor reliability and durability as compared to electronic sensors, requirement of the packaging and connectorisation issues.

Considering OFSs are still an emerging technology, a report from BCC Research (Wellesley, MA, USA) indicated the U.S. markets and opportunities for OFSs in telecommunications, oil and gas exploration, drilling, medical, and industrial markets (Weisenbach, 2008), as follows:

- “• The U.S. fibre optic sensor market was valued at \$235.0 million in 2007. This is expected to reach \$430.0 million in 2009 and \$1.6 billion in 2014, for a compound annual growth rate (CAGR) of 30.1%.
- Intrinsic sensors, in which the fibre itself acts as the sensor, have the larger market share, worth \$170.0 million in 2007 and an estimated \$306.0 million in 2009. This segment should reach \$1.4 billion in 2014, a CAGR of 35.2%.
- Extrinsic sensors, in which the fibre is simply the means of signal transmission, generated \$65.0 million in 2007 and an estimated \$124.0 million in 2009. This segment is expected to reach \$219.0 million in 2014 for a CAGR of 12.1%”.

From this report it is clear that market for OFSs will grow rapidly in the coming years.

OFS and large-scale fibre sensor systems are also attractive components for sensing in materials and structures. The monitoring of these structures usually requires the sensors and measurement devices to have features such as large area coverage, non-attendance with minimum maintenance, low cost per measurement point, capability of operation in harsh environments, explosion proof operation, low intrusion of the optical fibres in the host structure, high accuracy and secure data transmission. Another example where optical fibre sensing has a unique property is in the field of distributed sensing, where the location of a measured event can be obtained continuously along the length of the sensing fibre. OFSs have successfully been used in mechanical, electrical, biomedical, and chemical technologies also.

The market revenue of fibre optic chemical sensors was predicted to be over ~ \$300 million, for power lines it was ~\$50 million and for smart structures is approximately over \$600 million in 2010 (Ignacio *et al.*, 2007). This market share will increase continuously as predicted by Weisenbach in a report in 2008. As the market for fibre optic voltage sensors is low continuing efforts will be necessary to demonstrate the long-term reliability and further improve the acceptance and confidence in the new technology. So these three sensing areas were chosen in this work. Of particular interest for this thesis, RI sensors, voltage sensors and strain sensors are in demand for a wide range of applications, which include real-time monitoring of industrial processes, health monitoring of power lines and industrial and civil infrastructures, etc. Such applications range from RI measurements for chemical, biological, food, oil and gas, pharmaceutical, medical and biotechnology etc., voltage sensing is important to detect faults in the power supply in high power transmission lines. Strain sensing is valuable for large bridges and dams to even commercial and residential buildings. Although a significant body of research has been undertaken in extensive applications of fibre Bragg grating (FBG) based sensors in the civil engineering and aerospace industry, limited work has been done in the field of healthcare towards synergizing photonic sensing with biomechanics, orthopaedics or rehabilitation applications. The potential

applications of FBGs pressure sensors may provide important advances for the health sector.

Many different types of OFSs have been developed that operate principally by modulating the intensity, phase, wavelength or polarisation of light passing through these sensors. These sensors have been developed to measure strain, temperature, pressure, proximity, current, voltage and chemical composition.

## **1.2 Scope of the Thesis**

Although various fibre optic sensors exist for RI, voltage and strain measurements, developing new sensing schemes aids understanding and provides improvements for these devices. Refractive index sensors, a voltage sensor and strain sensors were studied and new sensors are proposed for these measurements. The performance of these sensors was evaluated by comparing the experimental outcomes with theoretical results. For each application area different sensors were developed and characterized for their optimal performance. The prospect of FBGs in low pressure (1.9 to 3.0 kPa) sensing in compression stockings was also studied. Accordingly this project was divided into three major sections where sensors for each of the above application areas were investigated.

This thesis is divided into 7 chapters. The next section provides the chapter summary of the thesis.

## **1.3 Chapter summary**

A literature review is presented in Chapter 2, which provides a review of OFSs, FBGs and the main applications of FBGs in general. In addition, fabrication and operation of a FBG sensor and the concept of tuning of Bragg wavelength is presented. Finally the main applications of FBGs are outlined.

The fabrication method and characterization of FBGs used in this project is outlined in Chapter 3. Spectral and microscopic characterization methods are discussed in detail in this chapter.

Chapter 4 presents an introduction to RI sensors and an insight into the different RI sensors present in the literature. This chapter summarises the details of two types of RI sensors, i.e. intensity-based (broadband reflector) and wavelength-modulated (reduced cladding FBGs) sensors. Among the two main sections of the chapter, the first part provides information about different broadband reflector applications such as multipoint RI sensor for liquids and state of charge of battery indicator. In the second part of the chapter the scope of etched fibre for RI measurements and etched FBGs as a highly sensitive glycerine concentration sensor is highlighted. In particular, the basic principle of operation of the sensor, materials and methodologies, experimental details and finally results and discussions of each RI sensor application is explored. This chapter concludes by providing an analysis of these sensors and a comparison is provided in terms of reliability, repeatability, lifetime and cost.

The outline of the hybrid high-voltage sensor for high-voltage transmission lines, its background, principle of operation and working is presented in Chapter 5. This voltage sensor is based on the combination of two independently well established technologies, i.e. optical fibre and liquid crystals (OFLC). The details of existing methods of voltage sensing are presented. In addition, the fundamentals of liquid crystals are discussed. The use of a broadband reflector for this specific application and the performance of this sensor are emphasized in this chapter. The proposed sensor monitors the optical properties of an OFLC hybrid device that is placed within an electric field. A low cost electric field amplifying probe (EFAP) is developed to obtain sufficient electric energy to operate this sensor.

Chapter 6 summarizes strain sensors based on fibre Bragg gratings. In particular, it details the effect of transverse strain in an alternative type of pi-phase-shifted FBG (APPhSFBG). The complex RI structure of a FBG fabricated using the phase mask technique produced an APPhSFBG at twice the Bragg wavelength. To study the sensing behaviour of these FBGs bend experiments were performed. Finally, this chapter provides an outline on the possibilities of the use of optical fibre Bragg gratings as a low pressure sensor for biomedical applications. It also provides an overview on the use of other types of fibres to enhance the sensitivity of the pressure sensor.

The detailed conclusions of this work on RI sensor, voltage sensor and strain sensor are provided in Chapter 7. In addition, the discussion of main advantages, limitations along with future work proposals are presented.

# Chapter 2

## Review of Optical Fibre Sensors

This chapter presents a literature review on different OFSs. Information was collected to provide a background to OFSs, fibre FBGs and main applications of FBGs in general. The basics of propagation of light in optical fibre and types of OFSs are presented. In addition, fabrication and operation of a FBG sensor, the concept of tuning of the Bragg wavelength, and the main applications of FBGs are outlined.

### 2.1 Theory of Optical Fibre Sensors

#### 2.1.1 Propagation of light in optical fibre

An optical fibre consists of a wave-guiding core, surrounded by a cladding, as shown in Figure 2-1. A proper description of the characteristics of an optical fibre is derived by solving Maxwell's equations. However, in order to get an overview of the function of an optical fibre, it is sufficient to consider the approximations of geometrical optics.

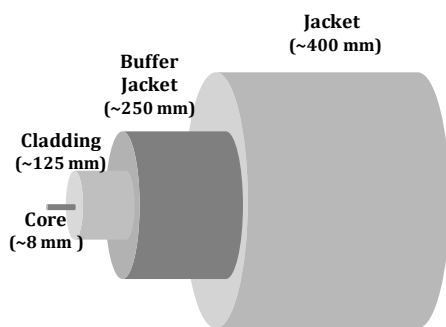


Figure 2-1 Schematic of optical fibre, showing typical diameters

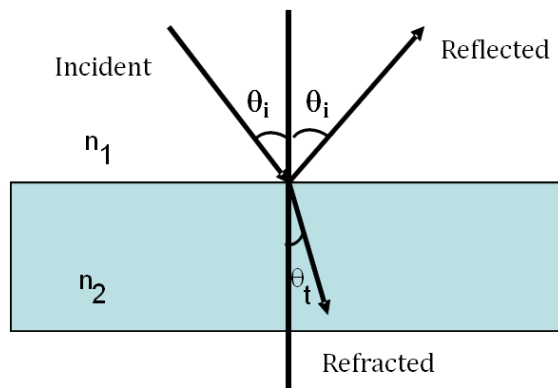


Figure 2-2 Refraction and reflection of light

According to geometrical optics, when a plane wave impinges at an angle  $\theta_i$  (incident angle) upon a boundary between two media with different refractive indices ( $n_1$  and  $n_2$ , respectively) (Figure 2-2), the light is partially reflected and partially transmitted into the second medium, according to Snell's law

$$n_1 \sin \theta_i = n_2 \sin \theta_t, \quad 2-1$$

where  $\theta_t$  is the transmission angle.

Light propagates inside an optical fibre of core and cladding refractive indices,  $n_{co}$  and  $n_{cl}$  respectively (Figure 2-3) according to the phenomenon of total internal reflection that occurs when a ray of light strikes boundary at an angle larger than a particular critical angle ( $\sin^{-1}(n_{cl}/n_{co})$ ) with respect to the normal to the surface and only when light is travelling within the medium of higher RI, i.e ( $n_{co} > n_{cl}$ ) (Buck, 2004).

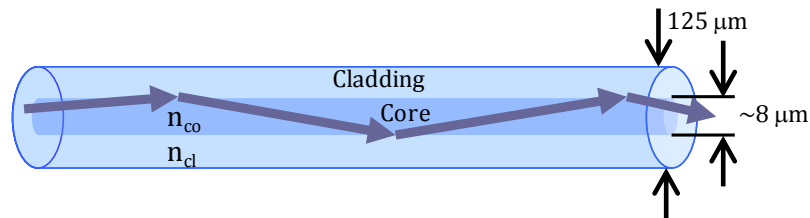


**Figure 2-3** Propagation of light inside the fibre based on total internal reflection

Thus, the light is confined to the core through total internal reflection, and as long as the fibre is not bent too much, light of the appropriate frequency will propagate a very long distance with very low loss, in the order of 0.2-1 dB/km.

That criterion of total internal reflection limits the required angle of incidence of a light beam which hits the fibre core from outside, as guidance is obtained only if the angle between the beam and the fibre axis is below a certain maximum which is defined as the numerical aperture (NA) of the fibre.

$$NA = \sqrt{n_1^2 - n_2^2} \quad 2-2$$

Any beam with an incidence angle larger than arcsine NA is not guided by the core and it thus experiences high losses at the outer interface of the cladding.

The waveguide modes are electromagnetic field configurations (tangential between electrical (E) and magnetic (H) field, denoted  $LP_{lm}$ ) which maintain their intensity profile during propagation in the fibre core (Snyder & Love, 1983).

The normalized frequency ( $V$ ) determines the fraction of the optical power in a certain mode which is confined to the fibre core and is defined as (Keck, 1981):

$$V = \frac{2\pi a}{\lambda} NA \quad 2-3$$

where  $\lambda$  is the vacuum wavelength,  $a$  is the radius of the fibre core, and  $NA$  is the numerical aperture. A fibre with a large value of  $V$  supports many modes, but for  $V < 2.4$  all modes except the HE<sub>11</sub> mode reach cut-off, as shown in Figure 1.1.3. Such fibres support a single mode and are called single mode fibre, supporting only the HE<sub>11</sub> mode, known as the fundamental mode of the fibre. The lowest order mode HE<sub>11</sub> is denoted LP<sub>01</sub>. The single-mode condition is determined by the value of  $V$  at which the TE<sub>01</sub> and TM<sub>01</sub> reach cut-off and hence the  $V$  value is less than 2.405.

Optical fibres have been used in sensing due to many advantages offered by them as outlined in Chapter 1.

## 2.2 Types of Optical Fibre Sensors

Many different types of OFSs have been developed that operate principally by varying the intensity, phase, or polarisation of the light passing through these sensors. In general, fibre optic sensors are classified as “intrinsic” or “extrinsic”. In extrinsic sensors the optical fibre is only used as a means of light transport to an external sensing system, i.e. the fibre structure is not modified in any way for the sensing function. Examples of extrinsic fibre optic sensors include fibres terminated in active layers, e.g. optode, Doppler anemometers and non-contact vibration measurements systems (Jackson & Jones, 1986), fibres having end face mirrors or fibres confronting other transducer elements or fibres such as Fabry-Perot interferometers (FPI) (Ribeiro & Jackson, 1993). Their major advantage is that the flexible and dielectric link provided by the fibre allows the instruments to be used where access is difficult or prohibitive by means of electrical signals.

Intrinsic OFSs differ from extrinsic sensors, where light does not have to leave the optical fibre to perform the sensing function. In intrinsic OFSs, the optical fibre structure is modified and the fibre itself plays an active role in the sensing function,

i.e. modulation of light takes place inside the fibre to measure a particular parameter. Examples of intrinsic fibre sensors include fibres with Bragg gratings, modified claddings and micro or macro bends. Intrinsic sensors can be divided into various categories depending upon the electric field of the light from an intrinsic sensor, which can be expressed as

$$\vec{E} = -\vec{e}A\exp(j\omega t + \phi) \quad 2-4$$

where  $A$  is the amplitude,  $\omega$  is the angular frequency,  $\phi$  is the phase, and  $-\vec{e}$  is a unit vector that represents the state of polarisation. The intensity of the light is proportional to  $|A|^2$ . The wavelength of the light is  $\lambda = 2\pi c/\omega$  where  $c$  is the speed of light in vacuum. Intensity, phase, state of polarisation and wavelength are the four fundamental elements of the light field. A perturbation of the measurand will change either one or multiple fundamental elements. Correspondingly, OFSs can be further grouped into four broad categories i.e.,

1. Intensity-modulated OFSs
2. Phase-modulated OFSs
3. Polarisation-modulated OFSs
4. Wavelength-modulated OFSs

In this work intensity (Fresnel-reflection based) and wavelength-modulated (FBG-based) OFSs are investigated. As a consequence the following review will focus on these two categories.

### **2.2.1 Intensity-modulated OFSs**

In an intensity-modulated OFS the measured parameter causes a change in the intensity of the received light at the detector. Measurements of optical power are easier than measurements of complicated optical properties like phase interference, wavelength shift or polarisation state. Several mechanisms such as transmission, reflection, micro-bending, or other phenomenon such as scattering, absorption, or fluorescence can be associated with light loss. Depending upon which mechanism changes the intensity of a signal, a wide variety of architectures is possible for these sensors. Optical fibre intensity-based reflective sensors represent some of the initial, straightforward and, maybe, the most widely used

sensors. The popularity of these sensors is related to their robustness, simple configuration, low fabrication cost and flexibility because no speciality components or fibres are required except a stable optical source, a reasonable photo-detector and signal processing unit. However, by adding suitable components to the architecture of these sensors performance can be enhanced and sensing at multiple points becomes possible. The main limitation of intensity based sensors is intensity fluctuations which can be caused by the power source, deterioration of optical fibre, fluorophore, micro or macrobending in the fibre path. The deleterious effect of possible fluctuations in source optical power on the sensor output in these devices may be addressed through the use of a reference sensor (Kim & Su, 2004) and other effects can be minimised by the use of a suitable coating and packaging materials.

Although the sensitivity and accuracy reported in most intensity-based sensor schemes is limited due to possible fluctuations in source power and stability, but it is still sufficient for many applications. Intensity-modulated OFSs can be found in a variety of extrinsic and intrinsic configurations, and examples are given in the following subsections. The intensity-based sensors in this work are mainly based on a reflective configuration. So the main emphasise of the following review is on these sensors.

#### *2.2.1.1 Transmissive/ reflective OFSs*

These types of sensors involve coupling-based OFSs. Coupling based intensity-modulated OFS can be configured in basically two ways: either in a transmissive arrangement, using straightforward transmission from one fibre to the other, as shown in Figure 2-4, or in a reflective arrangement where light is reflected from the end face of the fibre and received by the receiving fibre, as shown in Figure 2-5.

The reflective configuration may involve a single fibre acting as an emitter and receiver, multiple receivers or fibre bundles (Krohn, 2000).

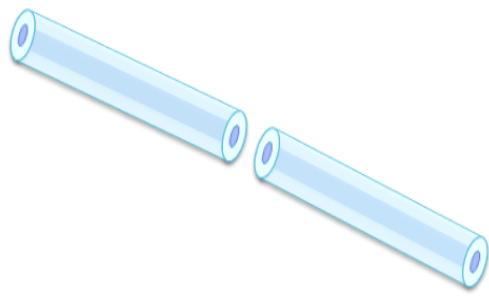


**Figure 2-4** Transmissive concept

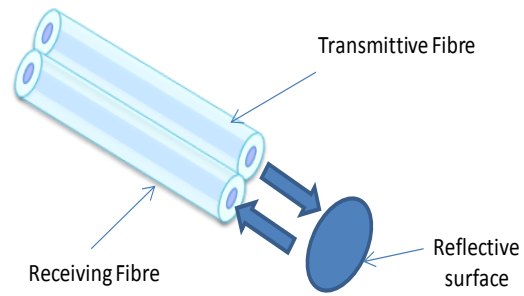


**Figure 2-5** Schematic of a reflective type fibre optic displacement sensor

A low cost reflective fibre optic force sensor was proposed by Bakalidis *et al.*, in 1996, utilising multimode fibre loops as a sensing probe. This arrangement was tested for different loop diameters and number of loops. This method relies on the additional optical power loss induced by the compression of a fibre optic loop as shown in Figure 2-6. The sensor exhibited long-term stability and repeatability of the order of 0.5% was achieved. The sensor provided a means of acquiring force values with accuracy sufficient for most robotics grippers (Bakalidis *et al.*, 1996).

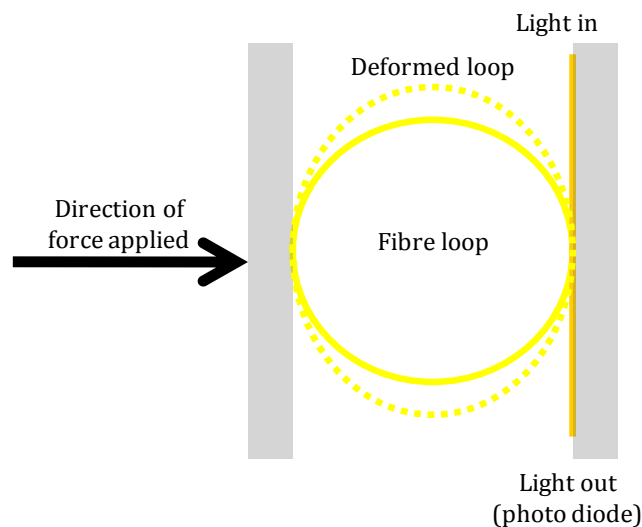


**Figure 2-6** Schematic of an intensity-based fibre optic force sensor (Bakalidis *et al.*, 1996)

There are several other architectures used for reflective type intensity-based sensors. A sensor can be made by coupling a reflective sensor to an elastic membrane to measure pressure. The light intensity transmitted to the second fibre is changed directly by deflection of a diaphragm. Single mode or multimode fibres can be used as the wave guide (Krohn, 2000).

Arregui *et al.* presented an intensity based sensor for simultaneous measurement of humidity and temperature. This combined humidity and temperature OFS described was based on a fibre Bragg grating (FBG) cascaded with a low finesse Fabry–Perot humidity sensor element. The sensing mechanism of this humidity sensor approach relies on the change in reflected optical power that the humidity creates in specific materials that may be used to form interferometric cavities. That is, some molecules of water may be trapped at the surface of the sensing coating, changing the optical reflectivity; therefore, the sensor works as an optical intensity sensor (Arregui *et al.*, 2002).

More recently a reflective type device for measuring thickness of transparent plates (1 to 2.5 mm) has been reported by Sastikumar *et al.* It was a displacement sensor, where two fibres were placed side by side. The concept of this sensor is given in Figure 2-5, where one fibre acts as an emitting fibre and other acts as a receiving fibre. The peak position in the output of the receiving fibre, which varies linearly, is related to the thickness of the transparent plate. The authors proposed a theoretical model and compared it with the experimental results, where parameters such as numerical aperture and diameter were taken into account to investigate output characteristics of the sensor (Sastikumar *et al.*, 2008).

Various other intensity-based sensors have been reported where the design of the sensors is based on a cladding modification approach. El-Sherif *et al.* developed a fibre optic chemical sensor for detection of toxic and biological materials. They removed the original passive cladding of the fibre in a small section and the fibre core was coated with a chemically sensitive material. Any change in the optical properties of the modified cladding material, due to the presence of a specific chemical vapour, changes the transmission properties of the fibre and results in modal power redistribution in multimode fibres. Both total intensity and modal power distribution (MPD) measurements were used to detect the output power change through the sensing fibres (El-Sherif *et al.*, 2007).

Dutta *et al.* reported an intensity-based optical pH sensor based on evanescent wave absorption, in which they removed the cladding of optical fibre and then coated it with a prepared solution of PVA, methyl red and de-ionized water (kept at

100 °C). Light from a He-Ne laser (632.8 nm) was launched into the coated fibre whose modified region was kept in the pH solution. Transmitted light intensity was measured by an optical power meter attached at the other end. It was noted that the absorption was lowest for pH 4.2 and highest for pH 6.0 where the modified region was red and yellow, respectively. This was due to the fact that at a lower pH value, the incident light and the modified region were both red, so absorption was least in the modified region resulting in the highest transmitted power, whereas at some higher pH value the modified region slowly turns yellow and at pH 6.0 the modified region was completely yellow and the transmitted power was least (Dutta *et al.*, 2010).

A low-weight, small-size, low-cost, repeatable and wide dynamic range temperature sensor was reported by Barbu *et al.* In this work a fibre taper was used as a temperature sensor, where temperature measurements were taken in terms of loss in the intensity of light carried by the fibre. It was assumed that a fibre taper has a constant ratio of core and cladding diameter. So the V value was not affected and it behaves single modedly. This tapered fibre was mounted in grooves in a polymer rod and temperature bending was introduced with expansion or contraction of a polymer rod, and the corresponding loss in optical power was recorded (Barbu *et al.*, 2002).

Another class of intensity-based fibre optic sensors is based on total internal reflection and Fresnel-reflection. In the sensor illustrated in Figure 2-7, light in the fibre core reaches the angled end of the fibre.

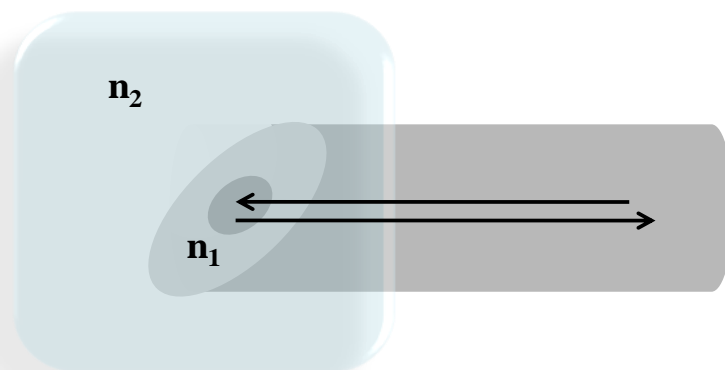


**Figure 2-7** Reflection of light from angled end of fibre

The total light reflected from the boundary between two media, as described by equation 2-1 also relies on the polarisation state of the incident light. Therefore, the reflection coefficients, which determine the intensity of the reflected light, are computed as (Buck, 2004)

$$\Gamma_{\perp}^b \Big|_{\mu_1=\mu_2} = \frac{\cos \theta_i - \sqrt{\frac{\varepsilon_2}{\varepsilon_1}} \sqrt{1 - \left(\frac{\varepsilon_1}{\varepsilon_2}\right) \sin^2 \theta_i}}{\cos \theta_i + \sqrt{\frac{\varepsilon_2}{\varepsilon_1}} \sqrt{1 - \left(\frac{\varepsilon_1}{\varepsilon_2}\right) \sin^2 \theta_i}} \quad 2-5$$

$$\Gamma_{\parallel}^b \Big|_{\mu_1=\mu_2} = \frac{-\cos \theta_i + \sqrt{\frac{\varepsilon_2}{\varepsilon_1}} \sqrt{1 - \left(\frac{\varepsilon_1}{\varepsilon_2}\right) \sin^2 \theta_i}}{\cos \theta_i + \sqrt{\frac{\varepsilon_2}{\varepsilon_1}} \sqrt{1 - \left(\frac{\varepsilon_1}{\varepsilon_2}\right) \sin^2 \theta_i}} \quad 2-6$$

where  $\varepsilon_1$ ,  $\varepsilon_2$  are the permittivity of medium 1 and medium 2, respectively.  $\Gamma_{\perp}^b$  and  $\Gamma_{\parallel}^b$  are known as the plane wave Fresnel reflection coefficients for perpendicular and parallel polarisation, respectively. For most dielectric media (excluding ferromagnetic materials) the permeability of the medium is given by  $\mu_1 \approx \mu_2 \approx \mu_0$ .

When the incident light is travelling close to the interface surface normal ( $\sin\theta \approx 0$  and  $\cos\theta \approx 1$ ) and using the RI of the core, both Fresnel reflection coefficients reduce to  $\frac{n_1 - n_2}{n_1 + n_2}$ . For ( $n_1 > n_2$ ) the reflection coefficient is negative. If the incident

light intensity is  $I_i$ , the reflected light intensity is  $I$ , then the reflectance  $R$  becomes

$$R = \frac{I}{I_i} = \left( \frac{n_1 - n_2}{n_1 + n_2} \right)^2 \quad 2-7$$

If the medium into which the cleaved end of the fibre is placed has a low enough index of refraction then approximately 3.5% (in air) of the light is reflected and returns via the fibre (Dakin & Brown, 2006). If, however, the index of refraction of the medium starts to approach that of the glass some of the light propagates out of the optical fibre and is lost, resulting in an intensity modulation.

A large number of optical fibre reflective sensors based on the Fresnel-reflection principle have been reported over the years, and new schemes continue to be reported, some of which are briefly discussed here (the detailed review for these techniques will be presented in Chapter 4, where a Fresnel reflection based broadband reflector is presented for RI measurements).

Su *et al.* reported a two channel RI sensor, which was used to measure solute concentrations in a solution, where a protected fibre end act as a sensing head. Three optical couplers, a diode laser and photo-detectors were used for RI measurements (Su & Huang, 2007).

An optical fibre coupler was used to measure RI of liquids at 1300 nm and 1500 nm with a double pulse measurement technique giving high resolution. Reflection signals from the liquid–fibre interface were compared with reflection signals from the air–fibre interface to obtain the RI (Kim & Su, 2004).

Another Fresnel-reflection-based fibre sensor that can measure liquid concentration and temperature simultaneously was reported recently. In this configuration wavelength division multiplexing was achieved by using thin film filters and an array of waveguide gratings (Zhao *et al.*, 2009).

In a recent report, an intensity-based RI sensor was used to measure the state of charge (SOC) of a battery, by determining the RI of the electrolyte. Chemical reaction inside the electrolyte during the operation of the battery changes the chemical compound within, which leads to a change of the RI of the electrolyte, which was monitored using a fibre optic sensor based on a broadband reflector (Paz & Acevedo, 2006).

The transmission-type sensor can also be used in several different structural designs. Transmissive sensors can be divided into two basic categories. In the first category, intensity variation is provided by the relative movement of two fibres whereas, in the second category, the relative movement of a shutter provides the modulation (Krohn, 2000). In the first category, the relative movement can include relative displacement of two fibres (transverse or longitudinal), or a change of angles between two fibres.

Two fibres may be coupled via free space coupling, where two cleaved ends of the fibre act as two mirrors and the sensor becomes a Fabry-Perot interferometer (FPI) (Figure 2-8 (a) & (b)). The gaps can be filled with different materials and this type of sensor can be used for chemical, biological, pH or humidity sensors.

One significant advantageous feature of a FPI sensor is that it can be configured as an in-line sensor (Fang *et al.*, 1998) and can be multiplexed along a single fibre for quasi-distributed sensing. The other possible design for intrinsic intensity-modulated FPI is by using two closely spaced FBGs (Kaddu *et al.*, 1997) (Figure 2-8(c)).

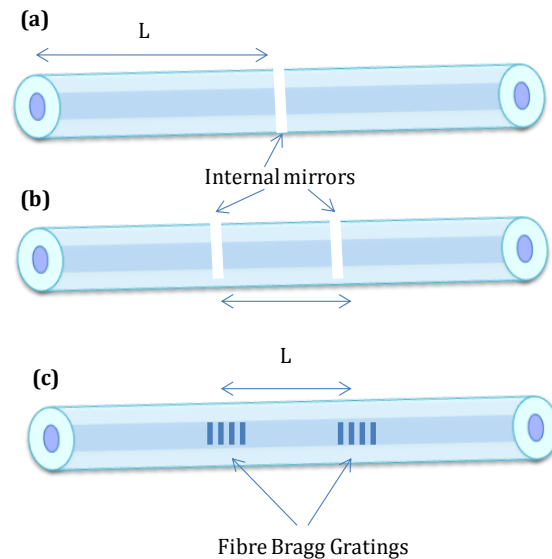


**Figure 2-8** Intrinsic FPI sensor configurations schematic: **(a)** cavity formed by an internal mirror and fibre end; **(b)** cavity formed by two internal mirrors; and **(c)** cavity formed by two fibre Bragg gratings (Taylor, 2002).

However, in an extrinsic FPI (EFPI), light is not totally confined. It exits and then re-enters the fibre, which causes optical loss. They can also be realised based on a hollow core fibre (Sirkis *et al.*, 1995, Rao *et al.*, 2009), combination of single mode and multimode fibres (Taylor, 2002) and miniature versions fabricated using laser micromachining (Wei *et al.*, 2008) (Figure 2-9).

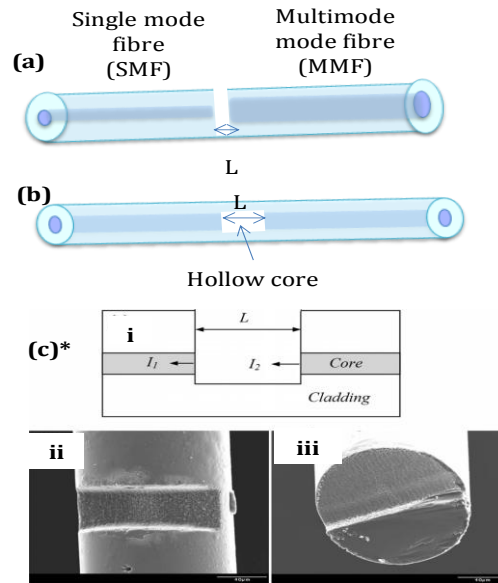


**Figure 2-9** Intrinsic sensor configurations: **(a)** reflective FPI sensor with internal cavity; **(b)** FPI sensor with hollow core (Taylor, 2002) and **(c)** miniature FPI using laser micromachining (\*after (Wei *et al.*, 2008)).

### 2.2.1.2 Micro-bend sensors

The micro-bend sensor is one of the earliest intrinsic OFSs. When an optical fibre is bent, small amounts of light will be lost as the angle of incidence between the transmitted light and the fibre walls change due to loss of total internal reflection conditions. This is called micro-bending and is a way to detect a displacement in a closed optical path. As the path is closed, the micro-bending optical sensor can be used in all environments.

The mechanical perturbation of a multimode fibre waveguide causes a redistribution of light power among the many modes in the fibre. The more severe the mechanical perturbation or bending, the more light is coupled to radiation modes and is lost. Thus, the important characteristics of a micro-bend sensor are that it uses a multimode optical fibre, it is a light intensity sensor and the light intensity decreases with increase in mechanical bending (Krohn, 2000).

### 2.2.1.3 Fibre Bragg grating sensors

The transition from electrical to optical communication networks requires components that are compatible with optical fibres. Recently there has been much

effort directed towards the development of various guided-wave optical solutions for use in integrated optics. Creation of technologically simple optical components became a reality after the demonstration of photosensitivity of optical fibre. It was shown that the RI of the fibre core was permanently changed when it was exposed to light at appropriate wavelengths. The most basic optical component, an optical bandpass filter, was created on the basis of this discovery. An optical bandpass filter is commonly called a fibre Bragg grating (FBG), which reflects a narrow wavelength band out of a broad input spectrum, with the rest of the spectrum being transmitted (Hill & Meltz, 1997), as discussed in section 2.2.4.1.

It is a building block in optical wavelength division-multiplexed (WDM) networks and is widely used as a sensor with numerous applications. A FBG may be regarded as an optical fibre with a periodic change of the RI (density of the light guiding media in regards to travelling/transmitting light) of the core with a period of the order of half of the wavelength of light of transmitting through the fibre (in case of telecommunications it is around 1  $\mu\text{m}$ ) (Kashyap, 1999, Othonos & Kalli, 1999).

Although FBGs are widely used as a wavelength-modulated sensors, there are some reports, where FBG based intensity-modulated sensors have been reported (Krohn, 2000). A report includes a reflectivity-tunable FBG reflector involving acoustic vibrations where the reflectivity of the FBG changes with respect to applied transverse vibrations through an acoustic wave (Huang *et al.*, 2000).

In this work the multiplexing capabilities of FBGs are explored and FBGs are used mainly as wavelength-modulated sensors. The detailed description and applications of FBGs will be discussed in section 2.2.4.1. As explained earlier, this work highlights the intensity-based and wavelength-based sensors so only a brief description is provided for phase and polarisation-modulated OFSs in the following sections.

### **2.2.2 Phase-modulated OFSs**

Phase-modulated sensors usually use an interferometer and sense the output signal by comparing the phase of the received signal with a reference fibre. These

are used to measure pressure, rotation and magnetic field, etc. The most commonly used phase-modulated sensor is the Mach-Zehnder interferometer. These sensors give a change in phase depending upon the change in length of an arm of interferometer or change in RI, or both. These sensors usually give accurate results, but are expensive to manufacture, and are mainly used in military applications (Krohn, 2000).

### **2.2.3 Polarisation-modulated OFSs**

Polarisation-modulated OFSs are sensors in which the polarisation state of light is changed due to an external perturbation such as electric field, magnetic field, etc. One example of polarisation-modulated sensor is an optical current sensor based on the magneto-optic (Faraday) effect, which will rotate the polarisation plane. Liquid crystals (LCs) have polarisation effects, so sensors based on LCs also exhibit polarisation effects (Krohn, 2000).

### **2.2.4 Wavelength-modulated OFSs**

Wavelength-modulated OFS change the spectrum of the light being transmitted, reflected or emitted. Such sensors include blackbody radiation, fluorescence, phosphorescence and FBG sensors. Wavelength-modulated sensors experience a shift in wavelength depending upon displacement, temperature or the presence of chemical species, which causes fluorescence. Fibre optic wavelength-modulated sensors are based mainly on FBGs.

FBGs have revolutionized modern telecommunications and subsequently that of optical fibre based sensor technology. In the latter case, FBGs are an excellent sensing element due to their high sensitivity, multiplexing ability and reasonable fabrication cost. In addition, several distinct types of FBGs have been developed in order to meet certain scientific needs. The following sections give details of FBGs.

#### *2.2.4.1 Fibre Bragg grating sensors*

The basic principle of FBGs, fabrication methods, types of FBGs and properties of FBGs are detailed in the next sections.

### (a) Photosensitivity

Photosensitivity is the ability of an optical fibre to incur change in its RI when exposed to an optical irradiation. This RI change can be erased by heat treatment at elevated temperatures or be made permanent via annealing at a suitable temperature. This was first observed by Hill *et al.* in 1978, when they were trying to test a stimulated Raman oscillator (Hill *et al.*, 1978) (Hill, 2000). The term “photosensitivity” encompasses a large number of effects caused by the sensitivity of a material to optical radiation, among which are photorefractivity, photoconductivity, photovoltaic effect, photochromic effect, etc. Several models have been proposed to date to understand this phenomenon.

According to the colour centre model, photosensitivity is related to defects present in glass. These defects have strong optical absorption known as colour centres. In particular, these result from Ge-Si ‘wrong’ bonds which are referred as germanium-oxygen deficiency centres (GODC). Absorption of ultraviolet (UV) light breaks a Ge-Si ‘wrong’ bond and creates a trapped hole with an oxygen vacancy (GeE’) (Hill & Meltz, 1997). Thus free electrons move randomly in the glass matrix and try to find an atom to which it can bond i.e. when a silicon fibre is doped with germanium, it becomes photosensitive. This will cause changes in UV absorption spectra which lead to changes in the RI through the Kramers-Kronig relation given by

$$\Delta n_{eff}(\lambda) = \frac{1}{2\pi^2} P \int_0^{\infty} \frac{\Delta \alpha_{eff}(\lambda')}{1 - (\lambda/\lambda')^2} d\lambda', \quad 2-8$$

where  $\lambda$  is the wavelength,  $\Delta \alpha_{eff}(\lambda)$  is the effective change in the absorption coefficient and  $\Delta n_{eff}(\lambda)$  is the effective RI change (Othonos & Kalli, 1999).

Another model known as the stress relief model is based on relaxation of thermoelastically-induced stress in the core of the fibre during UV irradiation (Wong *et al.*, 1992). The difference in thermal expansion coefficients of the core and cladding means that the core of a germanosilicate fibre is under tension. The compaction or densification model suggests that UV irradiation causes structural

changes in the glass matrix followed by an increase in glass density (Bernardin & Lawandy, 1990). It is evident that, along with colour centres, other effects are also present. The RI change remains unchanged even after 40% erasure of colour centres, and it gives evidence for two separate effects: first as E' centres' absorber and a second as structural changes that change the coordination number leading to a densification effect.

There are various other models like the electron charge migration model, permanent electric dipole model, ionic migration model and Soret effect, etc. which were used to explain photosensitivity in optical fibres (Othonos & Kalli, 1999). Later, it was observed by Brodzeli *et al.* that the spectrum of the FPI has been observed to shift to longer wavelengths due to UV irradiation of the selected region of the fibre, indicating that the UV-induced densification of glass is taking place and this is stretching the grating. The observed dynamics of the fibre FPI response to the UV treatment indicates that both elastic and non-elastic components contribute to the induced deformation, with the internal friction in the glass matrix defining the response time (Brodzeli & Stepanov, 1999).

The processes for writing in non-germanosilicate based fibres have also continued to develop and include multi-photon excitation directly into the band edge of the glass. It is now possible to customise a grating's property based on the application and the nature of production as well as customise the grating writing process to suit the type of fibre and application (Canning, 2008).

*(b) Hydrogenation for enhanced photosensitivity*

FBGs with sufficiently high reflection (large change in RI) are very important for OFSSs, where it is easy to detect the signal accurately. In addition, complex grating structures such as chirped fibre Bragg gratings, multi-channel fibre filters or multi-wavelength lasers require large magnitudes of RI change. For this reason, there is great interest in optical fibres with improved photosensitive properties. The most popular method to greatly enhance the UV photosensitivity of optical fibres is "loading" the fibres with molecular H<sub>2</sub> or D<sub>2</sub> at high pressure.

The mechanisms of enhancing RI both involve photolytically as well as thermally enhanced reactions between Ge and H<sub>2</sub> (Atkins *et al.*, 1993). The diffusion rate and concentration of hydrogen molecules depend upon the pressure and temperature of hydrogen gas. When the temperature is high, the hydrogen concentration reaches saturation very fast compared with room temperature (21 °C). High photosensitivity can be achieved in less time at high temperature (less than 100 °C) but at the expense of hydrogen concentration. Low temperature decreases the diffusion rate of H<sub>2</sub> into the core of the optical fibre. Shorter exposure times are possible at high temperatures but a temperature greater than 100 °C can cause overall fibre loss due to hydrogen reactions.

Lemaire *et al.* reported high pressure hydrogenation at low temperature (less than 100 °C). This hydrogen loading was carried out by diffusing H<sub>2</sub> molecules into fibres at low temperatures and high pressures. Subsequent exposure to UV or intense heat (e.g. a flame or a CO<sub>2</sub> laser) causes the dissolved H<sub>2</sub> to react in the glass, typically at Ge sites, resulting in large permanent index changes in the fibre core. Any germanosilicate fibre or even phosphosilicate fibre can be made photosensitive by this method (Lemaire *et al.*, 1993).

It was believed that high temperature hydrogen treatment involved a different physical mechanism than low temperatures, but in 2001 Brennan *et al.* proposed a new approach to hydrogenate fibres, in which, high temperature (more than 250 °C) was used to hydrogenate fibre in a time less than one hour (Figure 2-10). The change in normalised RI was reported to be at least 10<sup>-5</sup> (Brennan *et al.*, 2001).

For a 12 day exposure at 21 °C temperature, H<sub>2</sub> solubility is ~116 ppm/atm (Othonos & Kalli, 1999).

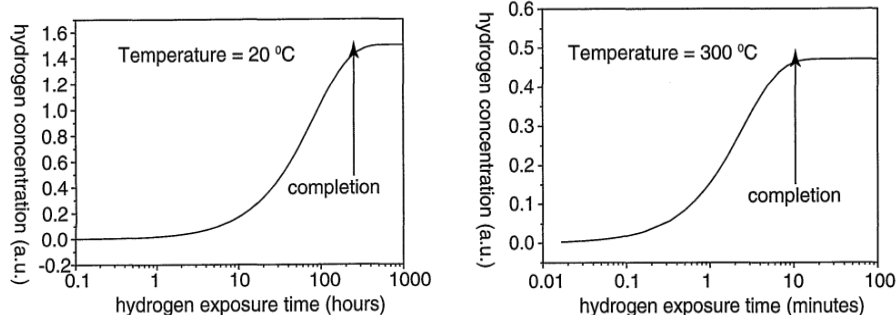


**Figure 2-10** After the patent entitled: "Accelerated method for increasing the photosensitivity of glassy material" by (Brennan *et al.*, 2001)

(c) Fabrication of FBGs

As discussed earlier in section 2.2.1.3, a FBG is defined as an optical fibre with a periodic change of the RI (density of the light guiding media in regards to travelling/ transmitting light) of the core with a period of the order of half of the wavelength of light of transmitting through the fibre (in case of telecommunications it is approximately 1  $\mu\text{m}$ ) (Figure 2-11).



**Figure 2-11** Schematic representation of a fibre Bragg grating

When broadband light transverses along the fibre core, a narrow band, centred on the Bragg wavelength ( $\lambda_B$ ) of the incident optical field, is reflected by successive, coherent scattering from the periodical index variations. When the reflection from a crest in the index modulation is in phase with the next one, a maximum mode coupling or reflection is achieved. The Bragg condition for back reflection of transmitting light from the periodic structure is

$$\lambda_B = 2n_{eff} \Lambda, \quad 2-9$$

where  $\lambda_B$  is the wavelength of the Bragg reflection,  $\Lambda$  is the period of the grating and  $n_{eff}$  is the effective RI of the fibre core. Figure 2-12 shows the reflection and transmission spectra of a uniform FBG in a 1060 nm fibre written with a phase

mask of pitch 1070.3 nm. The grating length was 5 mm and FBG was written with a scanning phase mask method (as described below) with a scanning speed of 1.5 mm/min.

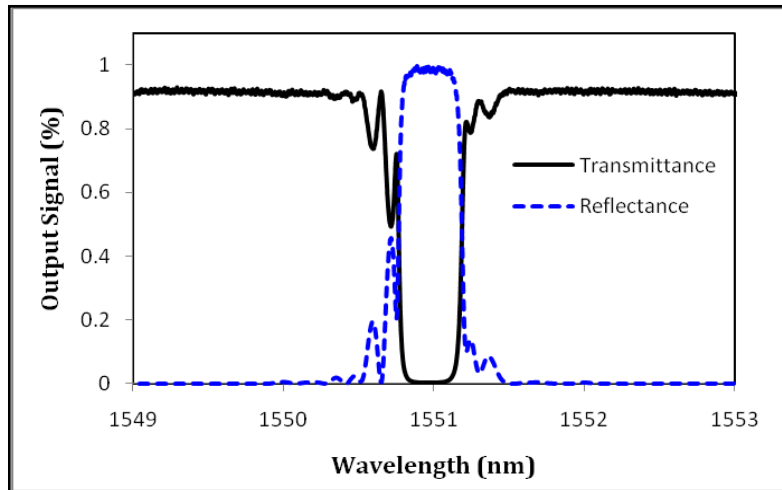


**Figure 2-12** Typical optical response/spectra of a FBG in reflection and transmission

The periodic change in the index of refraction is created typically by exposing the fibre core to an intense interference pattern of UV energy. The formation of permanent grating structures in optical fibre was first demonstrated by Hill and Meltz in 1978 (Kashyap, 1999). The first FBGs were fabricated with a visible laser beam propagating along the fibre core, but in 1989 a more versatile technique was demonstrated by Meltz *et al.* using the interferometric superposition of a pair of ultraviolet beams directed onto the fibre (Meltz *et al.*, 1989). The angle between the ultraviolet beams determines the period of the light pattern in the fibre core and thus the Bragg wavelength. There are various different techniques for fabricating standard and complex Bragg grating structures in optical fibres. Among these techniques include point-by-point fabrication, internal writing method often referred to as Hill gratings, and the transverse holographic method (Meltz *et al.*, 1989, Kashyap, 1999). The two ultraviolet beams are often generated as two first-order diffracted beams from a periodic phase mask exposed to a single UV beam (phase mask technique).

The phase mask method is the most widely used and effective method for inscription of FBGs in photosensitive fibres (Figure 2-13). Using holography or

electron-beam lithography, the phase mask is produced as a one-dimensional periodic surface-relief pattern, with period  $\Lambda_{pm}$  etched into fused silica.

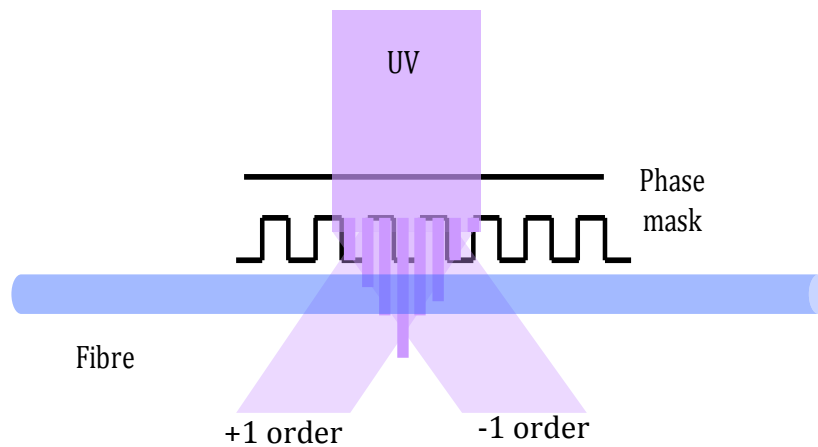


**Figure 2-13** Phase-mask writing method

Ultraviolet light is directed normally onto the phase mask and is diffracted by the periodic corrugations of the phase mask which generates an interference pattern of the 0,  $\pm 1$ ,  $\pm 2$ ,  $\pm 3$ , etc diffraction orders. Typically, they are designed so that zero and higher diffraction orders (e.g.  $\pm 2$ ,  $\pm 3$ , etc) are suppressed to less than 5% with approximately 80% of the total light intensity divided equally in the  $\pm 1$  diffraction orders as shown in Figure 2-13. When the phase mask is placed in close proximity to the fibre, the inscribed period is equal to half of the period of the phase mask. The use of the phase mask allows highly reproducible fabrication of FBGs with fixed characteristics determined by the phase mask properties.

The popularity of the phase mask fabrication method is for many reasons as outlined below:

- Simple fabrication process.
- Stable method for producing FBG.
- Minimum sensitivity to mechanical vibrations.
- Possibility of manufacturing several gratings in a single exposure.
- Lower coherence requirement on UV laser beam.
- Easier alignment of fibre.

A disadvantage of the phase mask method stems from the need to have a separate phase mask for each Bragg wavelength. To produce quality gratings, the separation between phase mask and fibre is an important factor.

However, advances in grating fabrication methods and fibre photosensitivity enhancement techniques have made it possible to fabricate a variety of index-modulated structures within the core of an optical fibre including Bragg grating, long period gratings, pi-phase-shifted grating, blazed or tilted gratings, and various types of chirped gratings (Othonos & Kalli, 1999).

*(d) Apodisation of FBGs*

Apodisation corresponds to the modulation of the index of refraction of the fibre grating with a much larger period than the period of the grating. The Fourier transform of a finite periodically varying rectangular structure (uniform Bragg grating) leads to the spectrum of its optical response which is a sinc function with multiple side lobes. It is well known that the Fourier transform of a Gaussian function is a Gaussian function. It was proposed and shown by Matsuhara and Hill that as a result of a slowly varying coupling coefficient along the length of the coupling region, it is possible to design band-rejection filters with very low side lobes (Matsuhara & Hill, 1974). The method of suppression of side lobes of fibre Bragg gratings by varying RI change is referred to as apodisation (Figure 2-14).



**Figure 2-14** Schematic of an apodised FBG

Apodised gratings are used to define channels through which the information is transmitted in communication networks. The side lobes may cause crosstalk between the channels in dense WDM systems, where bandpass filters are used to define the channels, and hence there is a requirement in suppression of side lobes for dense packing of the channels. Side lobes of fibre Bragg gratings can be suppressed by varying the RI change along the grating. In Figure 2-15, the dotted

line spectrum is for an unapodised FBG, whereas the solid line is the spectrum of an apodised FBG.

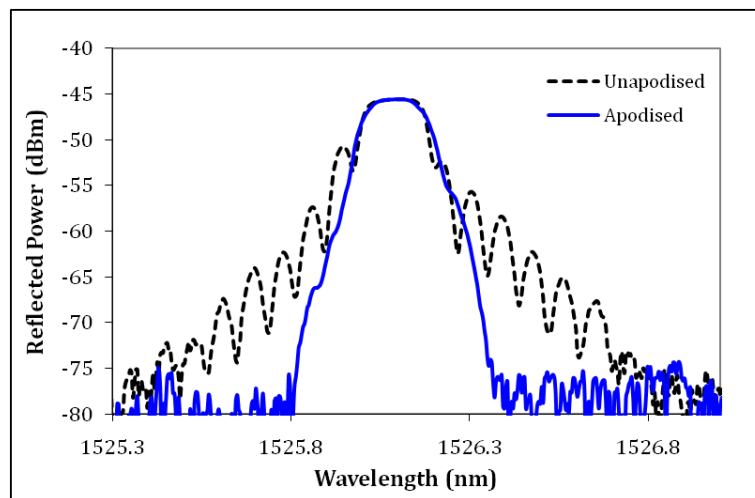


**Figure 2-15** Spectrum of an unapodised and apodised FBG fabricated at VU

There are several different methods of fibre Bragg grating apodisation described in the literature including variable diffraction efficiency phase mask technique (Albert *et al.*, 1995), the amplitude mask technique (Albert *et al.*, 1996), multiple printing of in-fibre gratings (Storoy *et al.*, 1997), intrinsic apodisation using UV-pulse interferometry (Cortes *et al.*, 1998), and the moving fibre/phase mask – scanning beam technique (Cole *et al.*, 1995). Apodisation of gratings was achieved by applying dither to the fibre (Cole *et al.*, 1995), and in a more steady approach based on dithering of the phase mask, instead of the fibre results in increased mechanical stability of the grating writing set-up (Stephens *et al.*, 1996). The method also enables a phase shift to be added to the fibre grating.

#### 2.2.4.2 Types of Fibre Bragg gratings

##### (a) Uniform FBGs

A uniform or standard Bragg grating has a sinusoidal modulation in the RI of the optical fibre core, with a period of the order of 1  $\mu\text{m}$ . Depending on parameters such as grating length and magnitude of induced index change, the Bragg reflector can function as narrowband transmission or reflection filter.

### *(b) Chirped gratings*

Chirped gratings have a non-uniform period along their length and exhibit a broadened spectral response reflecting a band of wavelengths related to the range of grating periods along the grating length.



**Figure 2-16** Schematic of a chirped FBG

They are used as dispersion compensators to compensate for dispersion in communication networks and for intra-grating sensing (Nand, 2007).

### *(c) Long Period gratings (LPGs)*

A long-period grating has a period of the order of 100  $\mu\text{m}$ . These were first demonstrated by Vengsarkar *et al.*. An amplitude phase mask is used to fabricate LPGs (Vengsarkar *et al.*, 1996). In LPGs, light couples from the fundamental core mode into the forward propagating cladding modes, where it is lost due to absorption and scattering. These have been used for various sensing applications because they can interact with the fibre jacket or any other material surrounding the cladding (Smietana *et al.*, 2008).

### *(d) Blazed or Tilted gratings*

In standard FBGs, the variation of the RI is typically uniform across the width of the fibre whereas it is at an angle to the optical axis in a tilted FBG (TFBG). The RI modulation is purposely tilted in order to enhance coupling between the forward propagating core mode and the contra propagating cladding modes. The angle of tilt in a TFBG has an effect on the reflected wavelength, and bandwidth (Kashyap, 1999). It has been used for RI measurements (Caucheteur *et al.*, 2009).

### *(e) Pi-phase-shifted FBGs*

Pi-phase-shifted FBGs constitute an important family of gratings that have found applications in optical communications and especially in the production of

distributed feedback fibre lasers. To date, many different methods have been reported for fabrication of phase-shifted FBGs including UV post processing (Canning & Sceats, 1994), etching of the middle of pre-fabricated FBGs (Iadicicco *et al.*, 2007), non-uniform etching of a FBG containing an optical waveguide (Brodzeli *et al.*, 2009b), shifting of the phase mask at half of its period during the FBG manufacturing process (Stepanov *et al.*, 1998) or simply using a phase-shifted phase mask (Kashyap *et al.*, 1994).

Recently, an alternative type of pi-phase-shifted FBG (APPhSFBGs) was observed near 1550 nm, in 1060 nm fibre, which was at twice the Bragg wavelength (Yam *et al.*, 2009a). An example of a reflection spectrum for these APPhSFBGs is given in Figure 3-6. APPhSFBGs result due to the formation of a complex RI structure inside the core of an optical fibre while writing with the standard phase mask technique. Although phase masks are manufactured to suppress the zeroth order while maximizing the  $\pm 1$  orders, generally the zero-order diffraction beam is suppressed to less than a few percent (typically less than 3% ) of the total transmitted power, while each of the  $\pm 1$  diffracted orders typically contain more than 35% of the total transmitted power. Investigations determining the effects of the zeroth and higher diffraction orders of a phase mask for fibre Bragg grating fabrication have been performed previously (Dyer *et al.*, 1995). The complex RI structure inside the core has observed by Dragomir *et al.* and reproduced in Figure 2-17 (a) & (b). These two images correspond to the views transverse and parallel to the direction of the writing beam, respectively. Figure 2-17 (a) shows how the two interleaved gratings have a pi-phase shift with respect to each other in the effective index profile. Analysis of this image showed that there are co-existing FBG periodicities ( $\Lambda_{pm}/2$  and  $\Lambda_{pm}$ ) in a phase-mask-written FBG (Dragomir *et al.*, 2003).

These results have been further verified by modelling the phase mask and it was demonstrated that the second periodicity is due to zeroth or higher phase mask diffraction orders (Kouskousis *et al.*, 2006). Later the spectral consequences of the complex structure of fibre Bragg gratings were investigated by Rollinson *et al.* including the reflection at 2/3 of the Bragg wavelength (Rollinson *et al.*, 2005b).

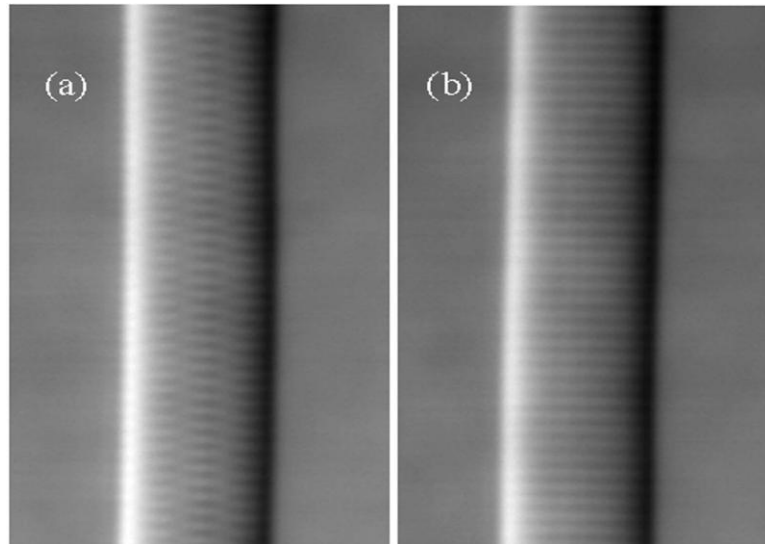


**Figure 2-17** DIC images of the core region of a fibre Bragg grating (a) image is taken from a direction orthogonal to that of the writing beam. (b) The same fibre Bragg grating, after the fibre has been rotated about its axis by  $\pm 90^\circ$  (after (Dragomir *et al.*, 2003))

It was further demonstrated by Yam *et al.* that the variation of the wavelength of both transmission dips was proportional to the increase in periodicity of the phase mask. The ratios of these wavelengths, for the irradiation of each phase mask section, were well matched with the theoretical value, in agreement with the proposition that features at  $\sim 1030$  nm are the 3<sup>rd</sup> harmonic of a grating having the phase mask periodicity, rather than an artefact of the fabrication process (Yam *et al.*, 2007). Furthermore, it was demonstrated that by introducing a Talbot interferometric set-up, when phase mask orders other than  $\pm 1$  were absent during fabrication, the features at 1552 nm were not evident, which verifies that the formation of this diffraction wavelength is due to the presence of higher diffraction orders of a phase mask during the fabrication process (Yam *et al.*, 2009a).

The response of the double peak structure of these gratings at twice the Bragg wavelength to temperature, longitudinal strain and transverse strain, has been investigated (Bal *et al.*, 2010b, Rollinson *et al.*, 2005a, Yam *et al.*, 2009b, Yam *et al.*, 2006), with the results being similar to those for standard FBGs. Recently the use of these gratings for multi-parameter sensing was investigated (Collins *et al.*, 2010).

In this thesis alternative type of pi-phase-shifted FBGs (APPhSFBGs) at the twice the Bragg wavelength are used specifically for transverse strain sensing (Bal *et al.*, 2010b) and bending (Bal *et al.*, 2010c). Pressure measurements were carried out in a uniform pressure chamber for further study of these pi-phase-shifted FBGs. The detailed fabrication technique for these FBGs is described in Chapter 3.

A new method of fabrication of pi-phase-shifted FBG is proposed based on un-even etching of a FBG. The fabrication of these pi-phase-shifted FBGs is discussed in section 4.5.4. FBGs in fibres of reduced cladding constitute a unique family of post-processed optical media that have found numerous applications in tunable devices and chemical sensing (Brodzeli *et al.*, 2009b).

Other types of FBGs constitute sampled FBGs (Ibsen *et al.*, 1995) and micro-structured FBGs (Iadicicco *et al.*, 2007).

#### *2.2.4.3 Scope of fibre Bragg gratings in sensing*

FBGs are an excellent sensing element due to their high sensitivity, multiplexing ability and low fabrication cost. Depending upon applied strain or temperature, a corresponding shift in reflected light is observed in FBGs. These have been successfully used for longitudinal strain, transverse strain, temperature, pressure, bend, simultaneous strain and temperature measurements and smart structures, etc. (Kersey *et al.*, 1997). Recently a wavelength-modulated fibre optic sensor has been used for RI measurements (Iadicicco *et al.*, 2003). In addition, several distinct types of FBGs have been developed in order to meet certain scientific needs. FBGs have become key passive devices for application in optical fibre telecommunications and in the rapidly developing field of OFSs due to a number of advantages over other OFSs (Rao, 1997 and 1999). These include:

- when interrogated are insensitive to fluctuations in the irradiance of the illuminating source,
- can be fabricated without changing the fibre diameter,
- have the potential to be mass-produced at low cost,
- have unique wavelength-division (WDM) and time-division multiplexing (TDM) capabilities,

- have great potential in sensing applications for simultaneous measurements of important physical parameters and in quasi-distributed sensor networks,
- can be used in fibre-optic smart structures where they can be attached or embedded into structures for the provision of real-time sensing information,
- a number of companies sell FBG sensing solutions.

#### 2.2.4.4 Properties of fibre Bragg gratings in sensing

##### (a) Tuning FBGs

The central wavelength of a FBG is determined by the Bragg condition, in equation 2-9 (Othonos & Kalli, 1999). Differentiating equation 2-9 gives

$$\Delta\lambda_B = 2(n_{eff}\Delta\Lambda + \Lambda\Delta n_{eff}), \quad 2-10$$

which gives

$$\frac{\Delta\lambda_B}{\Delta\lambda} = \frac{\Delta n_{eff}}{n_{eff}} + \frac{\Delta\Lambda}{\Lambda} \quad 2-11$$

From equation 2-11 it is clear that either varying the pitch,  $\Delta\Lambda$ , or the RI,  $\Delta n_{eff}$ , the central wavelength can be shifted, via one or more of the following effects.

##### (b) Varying the pitch of the FBG

The periodicity, or pitch, of the grating is simply the distance between the fringes. If the grating has length L with N number of fringes, the pitch will be:

$$\Lambda = \frac{L}{N}, \quad 2-12$$

Which, when differentiated gives

$$\Delta\Lambda = \frac{\Delta L}{N}. \quad 2-13$$

Dividing equation 2-13 by equation 2-12 gives

$$\frac{\Delta\Lambda}{\Lambda} = \frac{\Delta L}{L} . \quad 2-14$$

Thus, the relative change of the pitch is identical to the relative change of the grating length.

This change in grating pitch can either be achieved through tensile stress, by simply stretching the fibre or through thermal expansion. The thermal expansion can be determined by the following relation

$$\frac{\Delta L}{L} = \alpha \Delta T , \quad 2-15$$

where  $\alpha$  is the thermal expansion coefficient and can be determined by

$$\alpha = \frac{1}{L} \frac{\partial L}{\partial T} . \quad 2-16$$

However, the thermal expansion coefficient for silica is only  $\alpha = 5 \times 10^{-7} \text{ K}^{-1}$ , which only gives a negligible contribution to the shift in wavelength compared to temperature and tensile stress (Othonos & Kalli, 1999).

*(c) Varying the refractive index of the FBG*

The RI of the fibre can be either through the photo-elastic effect or the thermo-optic effect. The relative change in RI, due to the thermo-optic effect is given by

$$\frac{\Delta n_{eff}}{n_{eff}} = \xi \Delta T , \quad 2-17$$

where  $\xi$  is the thermo-optic coefficient given by

$$\xi = \frac{1}{n} \frac{dn}{dT} . \quad 2-18$$

The thermo-optic coefficient ( $\xi$ ) for silica is  $\sim 6.5 \times 10^{-6}$  which is an order of magnitude larger than the thermal expansion coefficient in equation 2-17.

The photo-elastic effect is a response of the RI to the tensile stress along the direction perpendicular to the direction of the propagation of light. If the light propagates along the  $z$ -axis, the response of the polarisation component aligned with the  $x$ - and  $y$ - eigenaxes to strain or a temperature,  $T^f$ , relative to a reference temperature,  $T^0$ , has been described by Sirkis (Sirkis, 1993):

$$\begin{aligned}\lambda_{Bx} &= \lambda_{Bx}^0 \left\{ 1 + S_z^f - \frac{1}{2} n_0^2 [p_{11} S_x^f + p_{12} (S_z^f + S_y^f)] + \xi T^f \right\}, \\ \lambda_{By} &= \lambda_{By}^0 \left\{ 1 + S_z^f - \frac{1}{2} n_0^2 [p_{11} S_y^f + p_{12} (S_z^f + S_x^f)] + \xi T^f \right\}.\end{aligned}\quad 2-19$$

where  $p_{11}$  is the strain-optic coefficient for parallel stress and  $p_{12}$  is the strain-optic coefficient for perpendicular stress. The Bragg wavelengths for zero applied strain and operation at the reference temperature,  $T_0^f$ , are given by  $\lambda_{Bx}^0$  and  $\lambda_{By}^0$  for the  $x$ - and  $y$ -directions, respectively. The superscript,  $f$ , indicates that the temperature and strain refer to the optical fibre. From equation 2-19 it is clear that application of transverse strain, i.e., in either the  $x$ - or  $y$ - directions (or in both), will result in a change in the Bragg wavelength that is dependent upon the orientation of the light with respect to the eigenaxes.

When stress is applied to a material, indices of refraction in the plane of polarisation will change with respect to each other causing the material to become anisotropic. When a light beam is incident on an anisotropic material, retardation between orthogonal polarisation states occurs because of the change in speed due to the index of refraction variation. Similarly the transverse loading of fibre results in a change in the relative index of refraction of the polarisation axes of the fibre and the net result is that the difference in wavelength between the spectral peaks changes as well.

Changes in RI in response to the applied load are derived from photoelastic theory described by Equation 2-19.

$$(\Delta n_{eff})_x = -\frac{n_0^3}{2E} \{ (p_{11} - 2\nu p_{12}) \sigma_x + [(1 - \nu) p_{12} - \nu p_{11}] (\sigma_y + \sigma_z) \} \quad 2-20$$

$$(\Delta n_{eff})_y = -\frac{n_0^3}{2E} \{ (p_{11} - 2\nu p_{12})\sigma_y + [(1-\nu)p_{12} - \nu p_{11}](\sigma_x + \sigma_z) \}, \quad 2-21$$

where  $E$  is the Young's modulus,  $\nu$  the Poisson's coefficient of the fibre,  $p_{11}$  and  $p_{12}$  the photo-elastic constants (Gafsi & El-Sherif, 2000), and  $\sigma_x$  and  $\sigma_y$  are the stress components in the  $x$  and  $y$  direction, respectively and given by

$$\sigma_x = \frac{2F}{\pi h D} \quad 2-22$$

$$\sigma_y = -\frac{6F}{\pi h D} . \quad 2-23$$

Transverse strain sensitivity can be calculated by using following equations

$$\frac{\Delta \lambda_{Bx}}{\lambda_{Bx}} = \frac{1}{2} n_o^2 (p_{11} \varepsilon_{xx} + p_{12} \varepsilon_{yy}) \quad 2-24$$

$$\frac{\Delta \lambda_{By}}{\lambda_{By}} = \frac{1}{2} n_o^2 (p_{11} \varepsilon_{yy} + p_{12} \varepsilon_{xx}), \quad 2-25$$

where,  $\varepsilon_{xx}$  &  $\varepsilon_{yy}$  are calculated using Hooke's law for plane strain.

$$\varepsilon_{xx} = \frac{1+\nu}{E} (\sigma_{xx}(1-\nu) - \nu \sigma_{yy}) \quad 2-26$$

$$\varepsilon_{yy} = \frac{1+\nu}{E} (\sigma_{yy}(1-\nu) - \nu \sigma_{xx}) \quad 2-27$$

If two transverse components are not equal then the two Bragg wavelengths will differ as given by equations 2-24 & 2-25 (Wagreich *et al.*, 1996). Similarly equations 2-19 can be solved in terms of pressure to find pressure sensitivity.

## 2.3 Multiplexing of Optical Fibre Sensors based on Fibre Bragg Gratings

For many sensing strategies, it is of great advantage to incorporate many sensors into a single system. This may be done to reduce overall system cost by reducing

the number of components required per sensor. Multiplexing can also make installation and monitoring of sensor systems substantially easier. When the primary choice of sensor technology has been made, the next step is to choose a suitable network topology and multiplexing technique. The ability to multiplex many, possibly hundreds, OFSs so that they can be monitored through a single instrumentation unit is an added attraction of OFSs. Several different multiplexing topologies can be used for reflective and transmissive types of sensor. For example, linear, star and tree are common configurations used in reflective type sensors whereas ring, star and ladder are commonly used in transmissive type sensors. There are a variety of different multiplexing techniques such as time, frequency, wavelength, coherence, polarisation, and spatial-division multiplexing schemes, used to sense at multiple points.

Wavelength division multiplexing has been proven to be a powerful technique to increase the capacity of optical communication systems and has been widely deployed in long-haul optical communication links and local optical networks. FBGs are a versatile tool for wavelength division multiplexing techniques, in which many gratings can be combined on a single fibre and addressed simultaneously provided each has a different Bragg wavelength. This is achieved in practice either by using a broadband light source and a spectrometer for detection or a tunable, swept-wavelength light source and simple photodiode detectors (Kersey *et al.*, 1997, Rao *et al.*, 1996).

Time-division multiplexing (TDM) systems employ a pulsed broadband light source and identify different gratings by the time taken for their return signals to reach a detector. The pulses from closer gratings are received before those from more distant FBG (Kersey *et al.*, 1997).

In this thesis the multiplexing capabilities of uniform FBG are explored and multipoint RI sensor (Bal *et al.*, 2010d) and a multipoint voltage sensor (Brodzeli *et al.*, 2010) are demonstrated. FBGs were written at different wavelengths to extract signals from a reflective type of sensor at various points.

## 2.4 Applications of Optical Fibre Sensors

OFSs offer numerous advantages that are significant in a wide variety of industrial, military and medical applications. In this thesis a few applications are highlighted and experimentally demonstrated.

Applications	Sensor
<b>Military</b>	Sound, rotation, vibration, position, liquid level, temperature, pressure, position
<b>Medical</b>	Temperature, refractive index (RI), pressure
<b>Industrial</b>	Temperature, refractive index (RI), pressure, position, thickness, flow, velocity, displacement, rotation, strain, leak, liquid level, etc.

**Table 2-1** OFSs for different applications (Krohn, 2000)

Sensing Technique	Parameter
<b>Intensity-modulated sensor</b>	Vibration, pressure, displacement, rotary position, liquid RI, liquid level, bend, temperature, strain, etc.
<b>Wavelength-modulated sensor</b>	Strain, transverse strain, position, bend, pressure, voltage, RI, liquid level, etc.

**Table 2-2** Applications of OFSs based on different sensing techniques (Krohn, 2000)

### 2.4.1 Applications of OFSs Studied in this thesis

Parameter	Sensing Technique	Applications	References
<b>Refractive-index (RI) sensors</b>	Intensity-modulated sensor	<ul style="list-style-type: none"> <li>• Multipoint liquid refractometer</li> <li>• State of charge (SOC) of battery indicator</li> </ul>	(Bal <i>et al.</i> , 2009a, Bal <i>et al.</i> , 2010d), (Bal & Brodzeli, 2010a)
	Wavelength-modulated sensor	<ul style="list-style-type: none"> <li>• Etched fibre based RI sensor</li> <li>• Etched FBG based liquid refractometer</li> </ul>	(Bal <i>et al.</i> , 2010e)
<b>Hybrid Voltage sensor</b>	Intensity-modulated sensor	<ul style="list-style-type: none"> <li>• High-voltage sensing for power transmission lines</li> </ul>	(Brodzeli <i>et al.</i> , 2009a, Brodzeli <i>et al.</i> , 2010)
<b>Strain sensor</b>	Wavelength-modulated sensor	<ul style="list-style-type: none"> <li>• Transverse strain sensor based on alternative type of pi-phase-shifted FBGs</li> <li>• Pressure sensor for compression garments based on uniform FBGs</li> </ul>	(Bal <i>et al.</i> , 2010b)(Bal <i>et al.</i> , 2009b) (Bal <i>et al.</i> , 2009c)(Bal <i>et al.</i> , 2010f)

**Table 2-3** Applications of OFSs studied in this thesis

## 2.5 Conclusions

This chapter summarises the background of optical fibre and optical fibre sensor technology. Different types of optical sensors are highlighted. The fabrication, types and properties of fibre Bragg gratings based sensors are explored. The scope of FBGs in different applications was detailed in this chapter, which also overviewed details of the applications of different fibre optic sensors and highlights the applications investigated in this thesis. The fabrication method and characterization of FBGs used in this project will be discussed in the next chapter.

## Chapter 3

### Fabrication and Characterization of Fibre Bragg Gratings

This chapter summarizes the fabrication method of fibre Bragg gratings used in this thesis which consists of fabrication of uniform FBGs and an alternative type of pi-phase-shifted FBGs (APPhSFBGs) with Victoria University (VU) phase-mask writing method. In addition, the characterization techniques are presented where spectral and microscopic characterization is outlined.

#### 3.1 Phase Mask Method (VU FBG Inscription Method)

This system is based on the phase-mask writing approach, where the optical fibre is exposed to UV light through a phase mask and used for all of the FBGs used for this project with a number of standard, commercially produced phase masks at different wavelengths. The FBG writing system shown in Figure 3-1 is a fully automated computer-controlled system which is optimized to produce repeatable fabrication conditions.

The system consists of a Coherent frequency doubled (FreD) (CW) argon-ion laser operating at 244 mW mounted on a table. Beam location and stability were monitored by computer controlled beam steering mirrors and a beam height adjusting telescope. A computer controlled (Aerotech) high precision translation stage was used to redirect and focus the laser beam onto a small section of the optical fibre as shown in Figure 3-1. It was mounted on a granite block to reduce mechanical vibrations during grating fabrication. The tight focussing was achieved by a steering mirror and a cylindrical lens was mounted on the translation stage. The optical fibre was placed almost in contact with and at right angles to the corrugations of the phase mask. The precise position of the fibre in the interference field pattern behind the uniform phase mask was monitored through a computer controlled camera located at the top of the stage. The fibre was mounted on the stage behind the phase mask and a uniform strain was applied to

the fibre. The same amount of tension is applied for each grating which was controlled precisely through a strain sensor connected to the fibre mount.

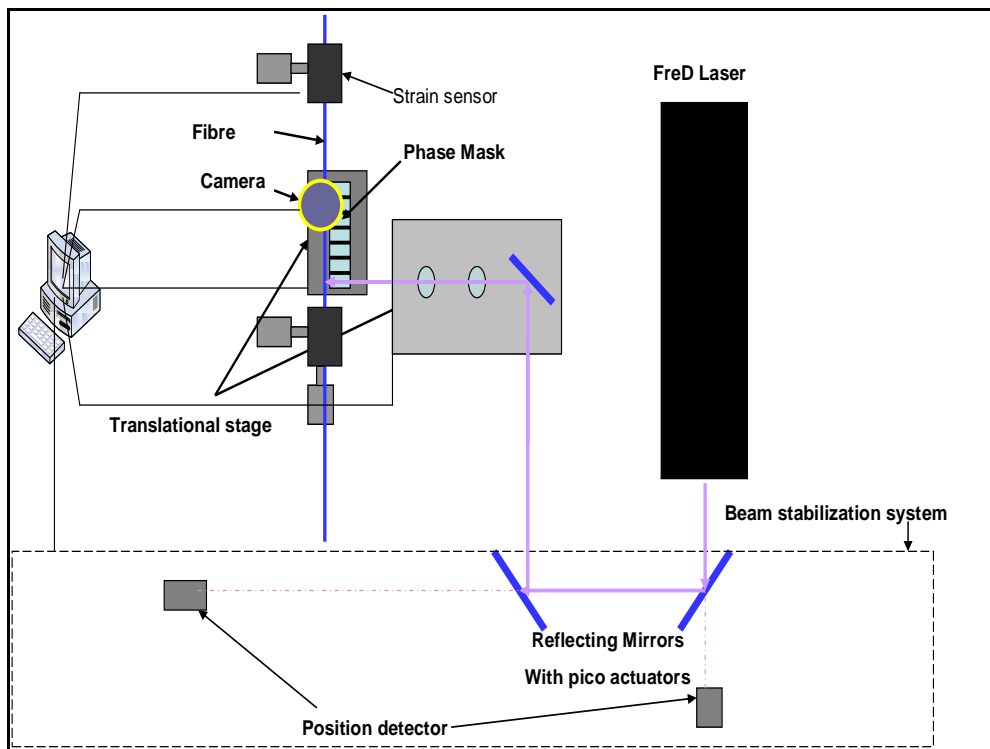


**Figure 3-1** Schematic of the optical arrangement of the scanning FBG fabrication facility at VU

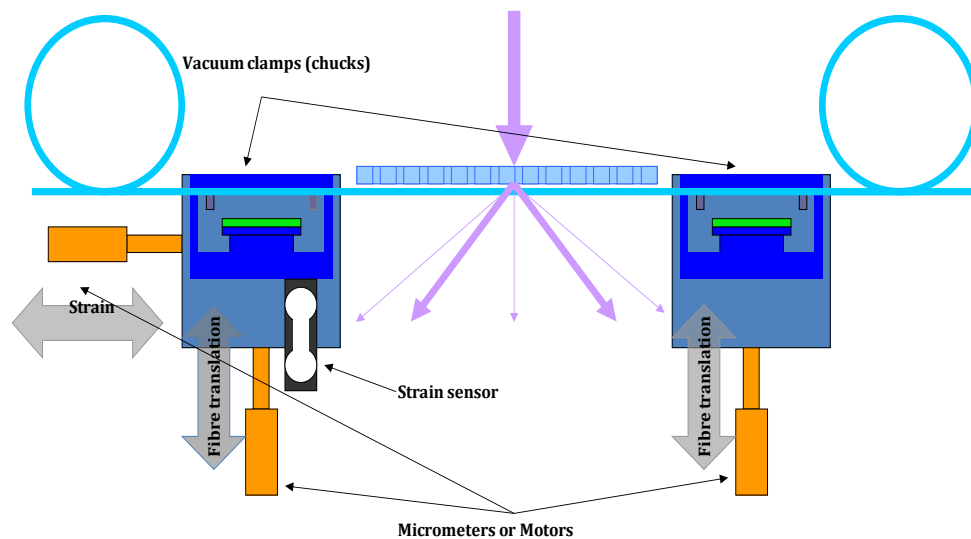


**Figure 3-2** Schematic showing the fibre clamps, strain sensors and alignment facility for FBG fabrication located at VU

This system allows the grating parameters such as apodisation profile, length, bandwidth and reflectance to be user defined and controlled. The grating

reflectance (exposure) was controlled by varying the scan rate of the laser beam along the phase mask using the high performance linear translation stage. Fibre gratings are written by scanning the laser beam across the phase mask at a rate determined by the user – a slower scan rate will give a longer exposure time and relatively stronger grating reflectance. A piezo phase mask shaker (dither) was used to reduce the index contrast, and apply controlled apodisation by gradually increasing the dither towards the grating ends. This suppresses the side lobes at the ends of the grating spectrum.

This system also allows grating production of almost any arbitrary design.

### 3.1.1 Uniform FBG

The fabrication technique described in section 3.1 was used to inscribe a uniform FBG in an optical fibre. Prior to fabrication, fibre was hydrogenated to increase photosensitivity. Figure 3-3 shows the hydrogen loading vessel.



**Figure 3-3** Hydrogenation chamber located at VU

A uniform pitch phase mask (Product: LASIRIS, model: PM-244-1054.7-50.8) was used to write uniform FBGs at wavelengths around 1550 nm. A constant strain ( $\sim 394 \mu\epsilon$ ) was applied to all fibres when mounted on the stage behind the phase mask.

### 3.1.2 Alternative type of pi-phase-shifted FBGs

Several distinct types of FBGs have been developed in order to meet certain scientific needs. Pi-phase-shifted FBGs constitute an important family of gratings that have found applications in optical communications and especially in the production of distributed feedback fibre lasers (Section 2.2.4.2 (e)).

As wavelengths near  $3\ \mu\text{m}$  are inaccessible with conventional optical fibre technology; observation of features at twice the Bragg wavelength requires a phase mask of much smaller pitch. Thus, a standard phase mask with a design wavelength of  $\lambda_B = 785\ \text{nm}$  (i.e. a phase mask with  $536\ \text{nm}$  uniform pitch) was used to investigate the sensor properties of spectral features at twice the Bragg wavelength (i.e. near  $1.55\ \mu\text{m}$ ), which behaves as an APPhSFBG (Yam *et al.*, 2009a). The complex structure was credited to multiple-beam interference produced by the phase mask technique (Yam *et al.*, 2009a).

## 3.2 Characterization of Fibre Bragg Gratings

The success of fabrication technique involves measuring reflection and transmission spectra. Complete characterization of FBGs is achieved by determining the reflection, transmission and phase spectrum. Absolute characterization of fibre Bragg gratings requires knowledge of the complex coupling coefficient or the complex reflection spectrum. Characterization of fibre gratings is not a trivial problem; an optical phase is usually difficult to measure. The following two techniques, which are the most commonly used, were used to characterize FBGs.

### 3.2.1 Spectral characterization of FBGs

The most commonly used technique consists of an optical spectrum analyser (OSA) and a broadband source but due to limited resolution of OSA this technique has limited scope.

#### *(a) Characterization using OSA*

Measurement of a transmission spectrum requires a broadband source and an Optical Spectrum Analyser (OSA). An erbium broadband light source ( $\text{Er}^{3+}$  EBS-

7210) and an optical spectrum analyser (ANDO, AQ 6317B, resolution 10 pm) was used. The reflection spectrum was retrieved by using a 50:50, optical coupler (1550 nm, Thorlabs Ltd.). Figure 3-4 (a) & (b) shows the set-up used to monitor transmission and reflection spectrum, respectively.

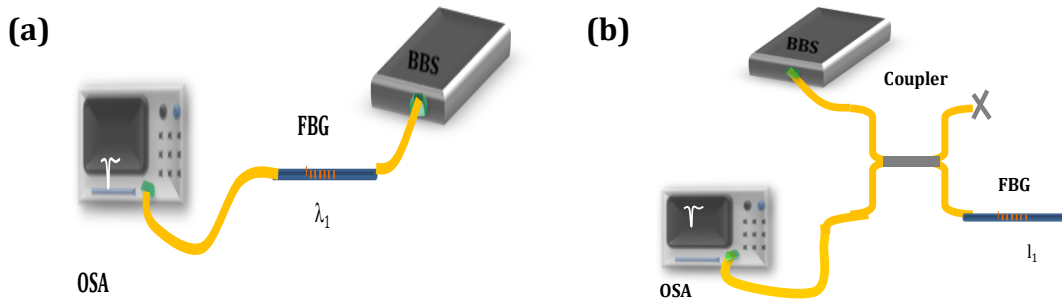


**Figure 3-4** Schematic of set-up used to measure **(a)** transmission and **(b)** reflection spectrum of FBGs

The transmission and reflection spectrum of a uniform FBG is depicted in Figure 3-5. The set-up described in section 3.1 was used to produce apodised FBGs. The detailed description and spectrum of apodised FBG is given in section 2.2.4.1 (c) (Figure 2-15).

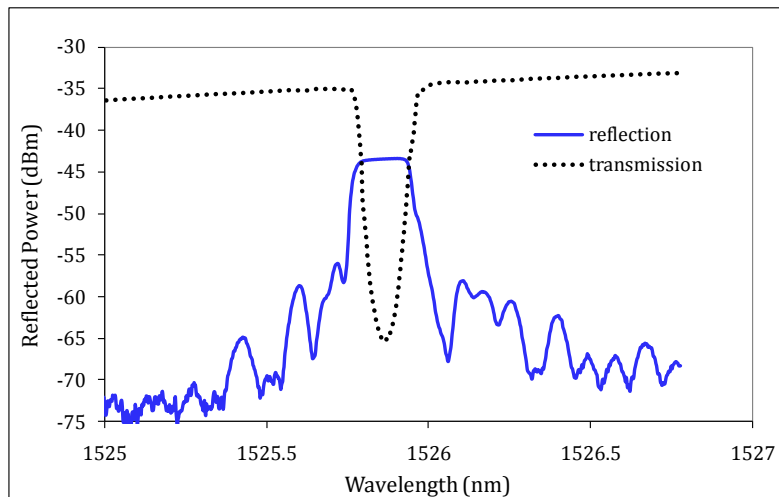


**Figure 3-5** Transmission and reflection spectra of a uniform FBG written at VU

An APPhSFBG was observed near 1550 nm (twice the Bragg wavelength), in 1060 nm fibre, while Bragg wavelength was near to 780 nm (Section 3.1.2). A typical spectrum of an APPhSFBG at twice the Bragg wavelength is shown in Figure 3-6.

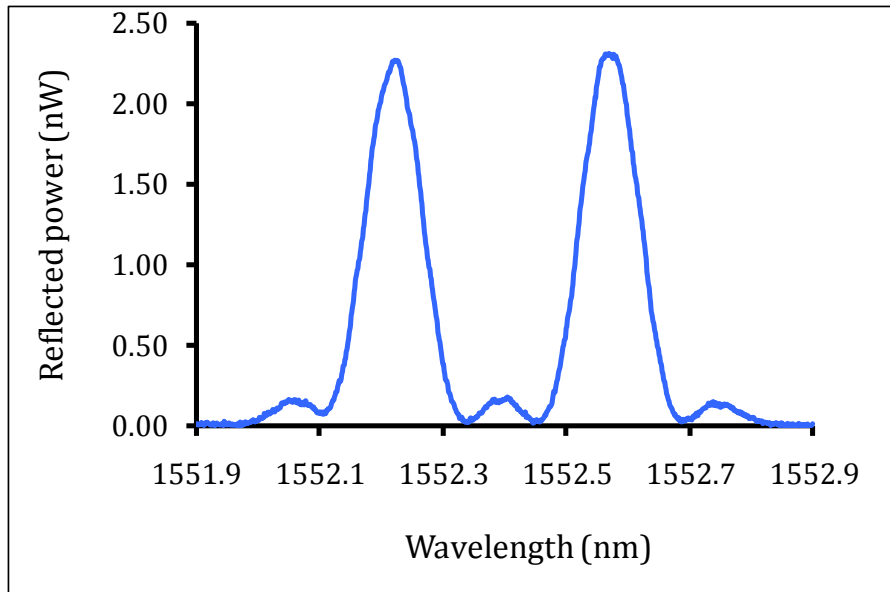


**Figure 3-6** Reflection spectrum of an alternative type of pi-phase-shifted FBG at twice the Bragg wavelength fabricated using phase-mask writing method at VU

*(b) High resolution full spectrum characterization*

The previous described characterization technique has wavelength resolution limited by the OSA. So another characterization method was used, involving a network analyser and photo receivers along with a tuneable laser source. This method has very high resolution (1 pm) and it can detect changes in reflection, transmission as well as in phase and is illustrated in Figure 3-7.

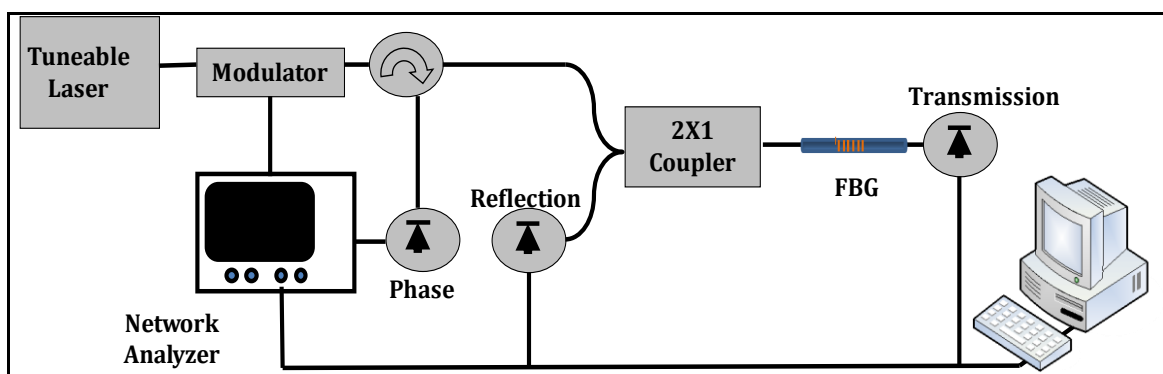


**Figure 3-7** Schematic of high resolution FBG characterization set-up

The reflection and group delay (phase) spectrum for a chirped grating fabricated at VU, which was monitored using high resolution set-up is depicted in Figure 3-8.

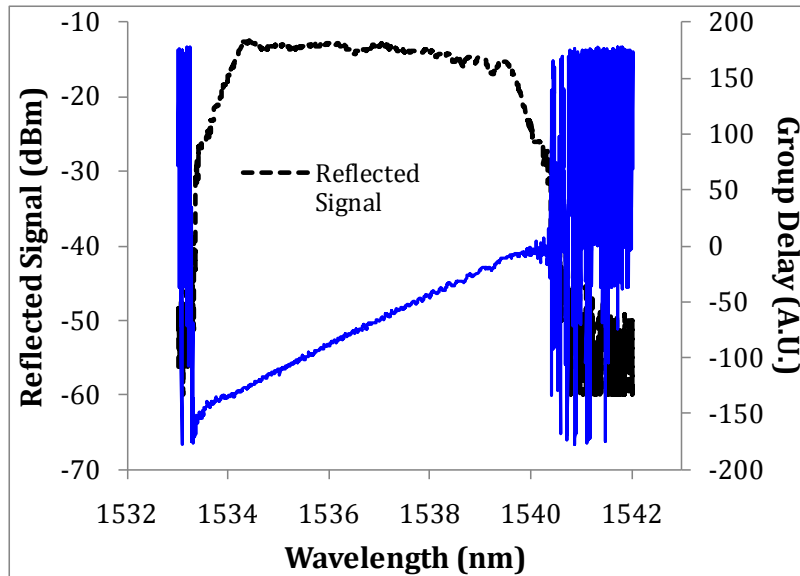


**Figure 3-8** Spectrum showing reflection and group delay for a chirped FBG fabricated at VU

### 3.2.2 Microscopic characterization of FBGs

Although various methods exist for characterizing phase and RI information of optical fibres, refinement and development of optical fibres and optical devices such as fibre Bragg gratings require new methods to aid understanding and provide further improvement of these devices. Current characterization techniques are limited in obtaining structural information of fibre Bragg gratings, where gratings are generally characterized using their reflection or transmission spectra in conjunction with coupled-mode theory. Thus, imaging techniques, such as those used to study the complex RI interference pattern within FBGs inscribed using the standard phase mask technique, can be used to confirm the etching of fibres. An inverted Olympus IX FL microscope at VU was used for the differential interference contrast (DIC) microscopy images presented in this thesis following methodology used previously for the imaging of FBGs (Dragomir *et al.*, 2003, Kouskousis, 2009). This microscope is infinity corrected, equipped with high resolution Nomarski optics and uses an argon ion laser, operating at 488 nm as the light source.

(a) Set-up

Microscopes with differential interference contrast capabilities are suitable for high modulation imaging of phase shifting objects such as biological objects (in transmission) and glass or metal surfaces (in reflection). DIC microscopy is one of the most popular microscopic techniques for high contrast depiction of phase objects. DIC theory was introduced by G. Nomarski (Pluta, 1994) and is based on interferometry to gain information about the optical density of the sample, to see otherwise invisible features. The light path through an inverted DIC microscope is represented schematically in Figure 3-9.

Advantages also include high sensitivity and high resolution, revealing detailed structures in the specimen under investigation. DIC works by separating a polarised light source into two beams which take slightly different paths through the sample. When the optical length of each path differs, the beams interfere when they are recombined. A DIC image is formed from the interference of two mutually coherent waves that have a lateral displacement, (called the lateral shear), of a few tenths of a micrometre, that are phase-shifted relative to each other.

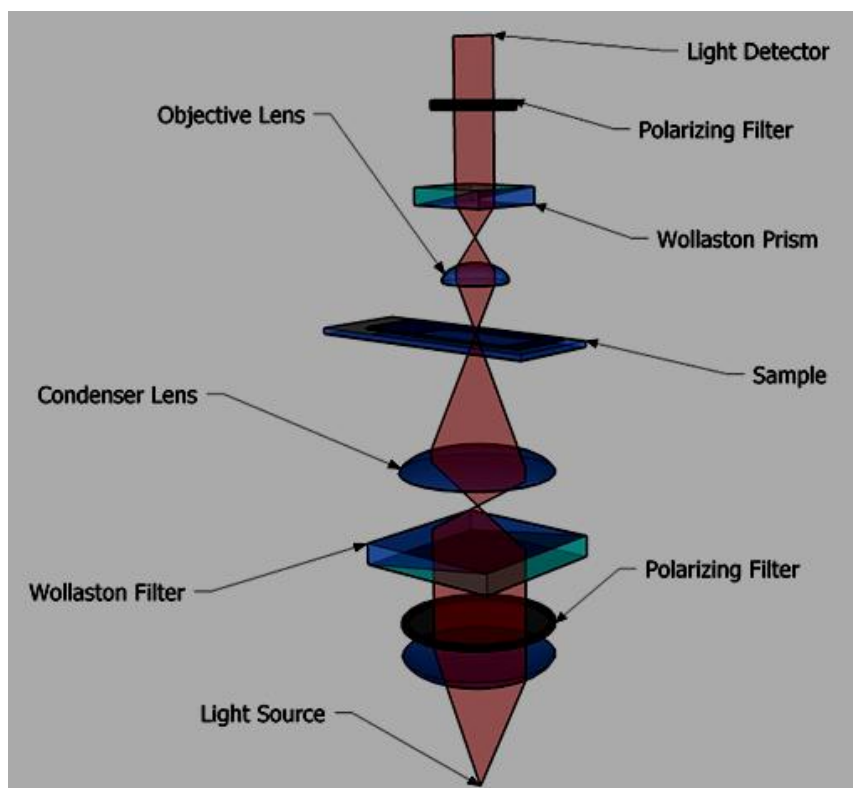


**Figure 3-9** Schematic of DIC microscope

DIC images were acquired using an Olympus Fluoview laser scanning microscope in conjunction with a Melles Griot argon ion air-cooled laser, wavelength selectable operating at 488 nm (model 35-Lap-321-240), with an Olympus IX-70 inverted microscope equipped with DIC optics attached to a laser scanning device using Fluoview software.

The system computer with software enabled easy user interface with the instrument. The specifications for the argon ion laser include a maximum output power of 40 mW, with a beam diameter ( $1/e^2$ ) of  $0.66 \pm 5\%$  mm and a beam divergence ( $1/e^2$ ) of 1.1 mrad. All images were acquired using an Olympus Uplan Apo  $40 \times /0.85$  NA objective, which is flat field, chromatic, spherical aberrations and infinity corrected. Figure 3-10 represents schematically the acquisition system.

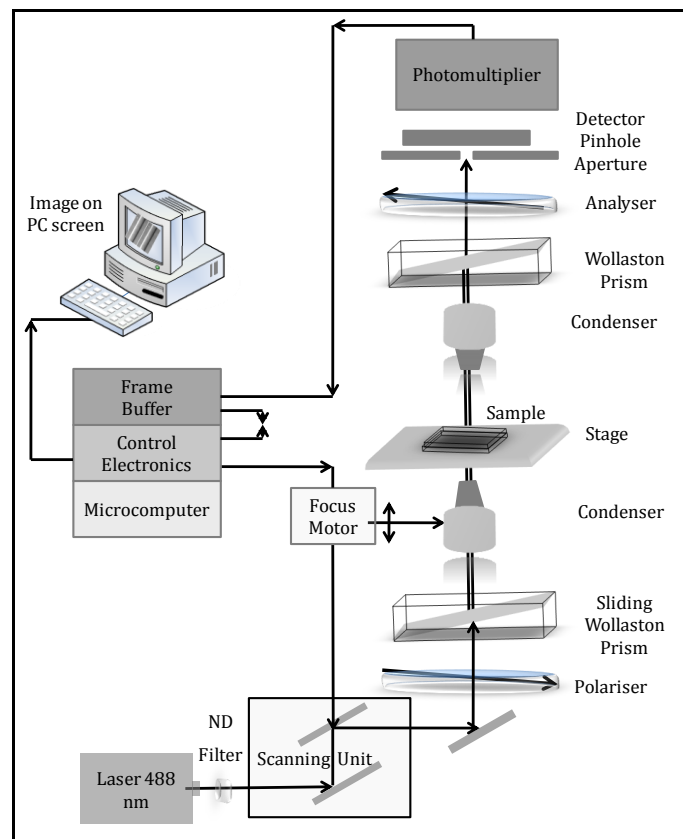


**Figure 3-10** Schematic representation of the acquisition system used to acquire DIC images. The imaging platform can be interactively controlled through the Windows NT workstation via the Fluoview™; with a stepper motor that translates the objective in 0.1  $\mu\text{m}$  increments along the optical axis (Kouskousis, 2009).

*(b) Sample preparation*

In order to achieve the optimum contrast in DIC images of the fibre core region, a high level of index matching is required between the immersion oil and the cladding of the fibre sample. An oil (Cargille Series AA) was used in this work which was specified as having a RI of  $1.458 \pm 0.0002$  at 25 °C. The temperature dependent RI of the oil was specified to change at a rate of  $-3.73 \times 10^{-4}/^{\circ}\text{C}$ .

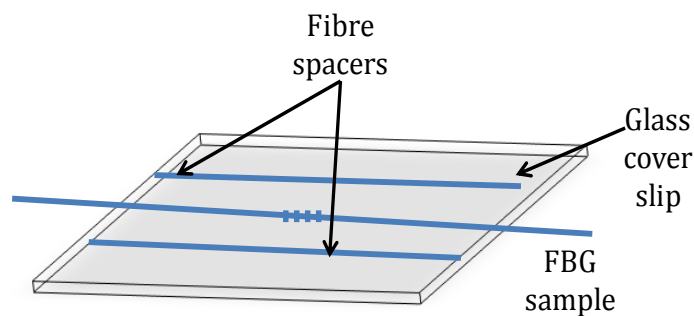


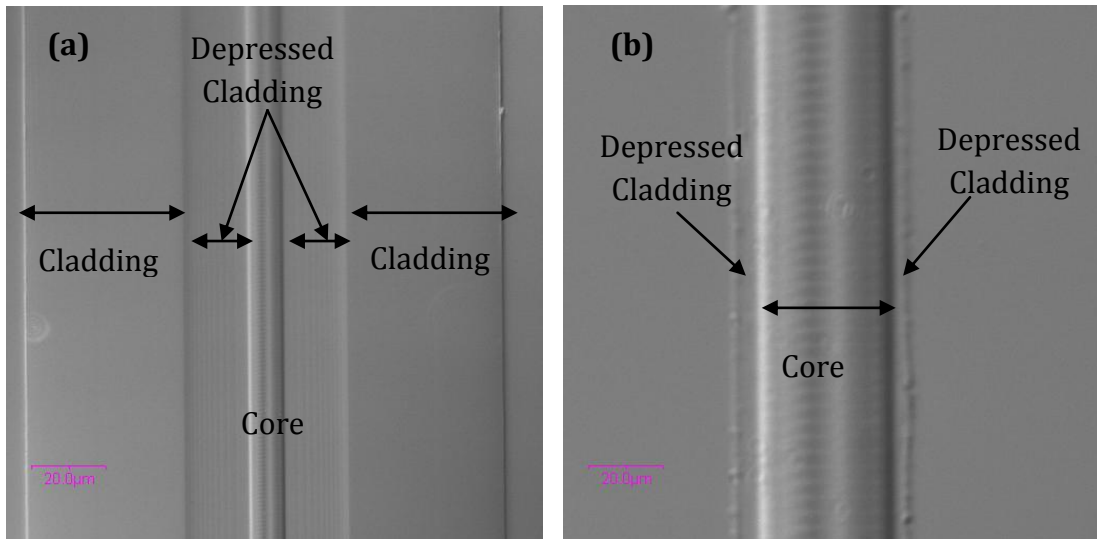
**Figure 3-11** Schematic representation of prepared sample on a cover slip

The sample was placed on a cover slip. Small length fibres (called spacers) were placed on both sides of the test sample in order to form a 'well' with the index matching oil and also to prevent tilting in the microscope slide that is then placed on top of the sample (Kouskousis, 2009). The cover slip was then covered with another cover slip and immersion oil was dripped in between the glass slides. Care was taken in order to avoid any occurrence of bubbles. Small tapping using tweezers was helpful in this case. Immersed samples were mounted on a stage on the microscope.

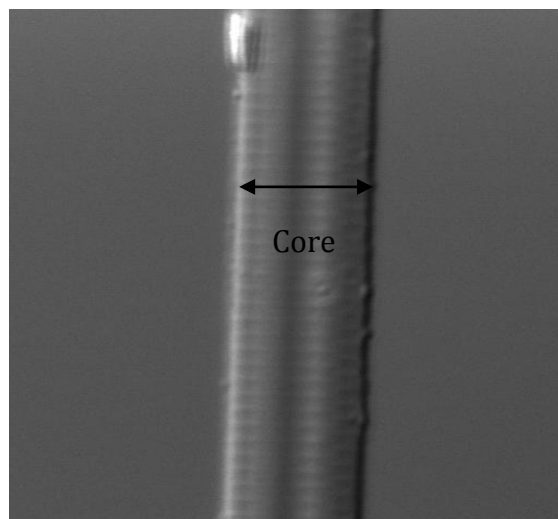
*(c) FBG images and analysis*

Figure 3-12 (a) is a DIC image of a FBG in the core of an optical fibre. The depressed cladding region of the fibre and full cladding is present, where the intensity variation within the cladding region produced by the deposition of dopants during the preform fabrication process is also visible. However, it should be noted that the GF1 fibre has a core doped with germanium and boron with a fluorine doped inner cladding. The inclusion of fluorine in the cladding will result in a smaller RI difference between the core-cladding interface. DIC imaging of

etched cladding FBGs presents a clear picture of the FBG structure inside the fibre core and illustrates the remaining diameter of the cladding on the fibre (Figure 3-12 (b)). A fully etched FBG where no cladding is left is depicted in Figure 3-13, where a clear dip and grating planes across the core are more evident.



**Figure 3-12** DIC image of an (a) FBG inside the core of an optical fibre (b) FBG with etched cladding where a small portion of cladding is present



**Figure 3-13** DIC image of a fully etched FBG

The line and 3 dimensional plot of DIC image of the FBG of Figure 3-12 (a) is illustrated in Figure 3-14 (a) & (b). As this is un-etched FBG so line plot and 3 D plot with the cladding, inner cladding and core regions are clearly visible.

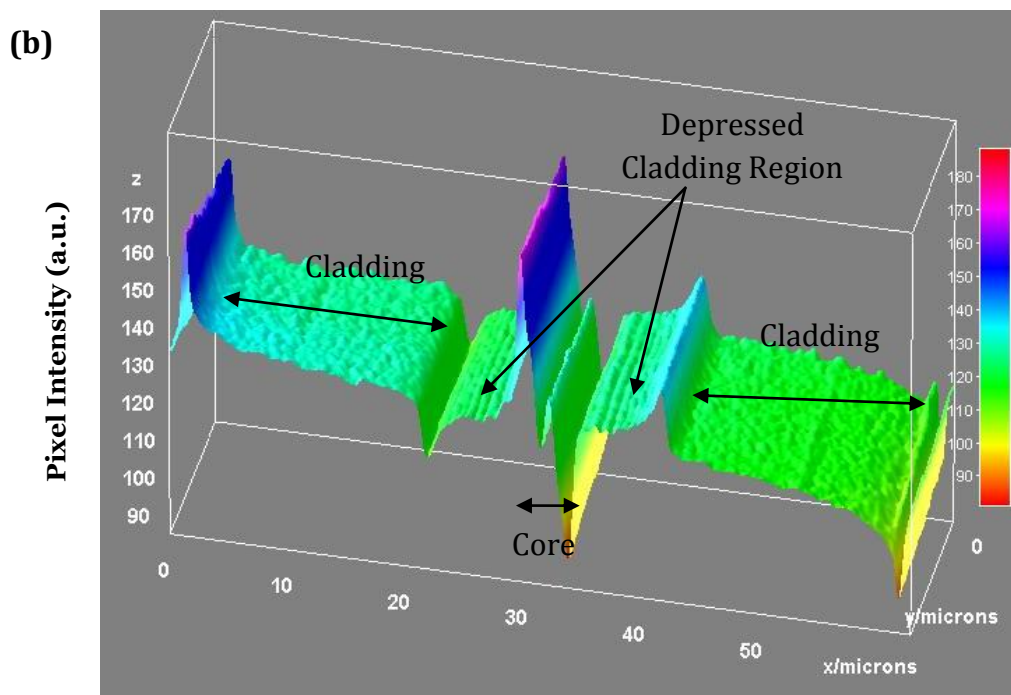
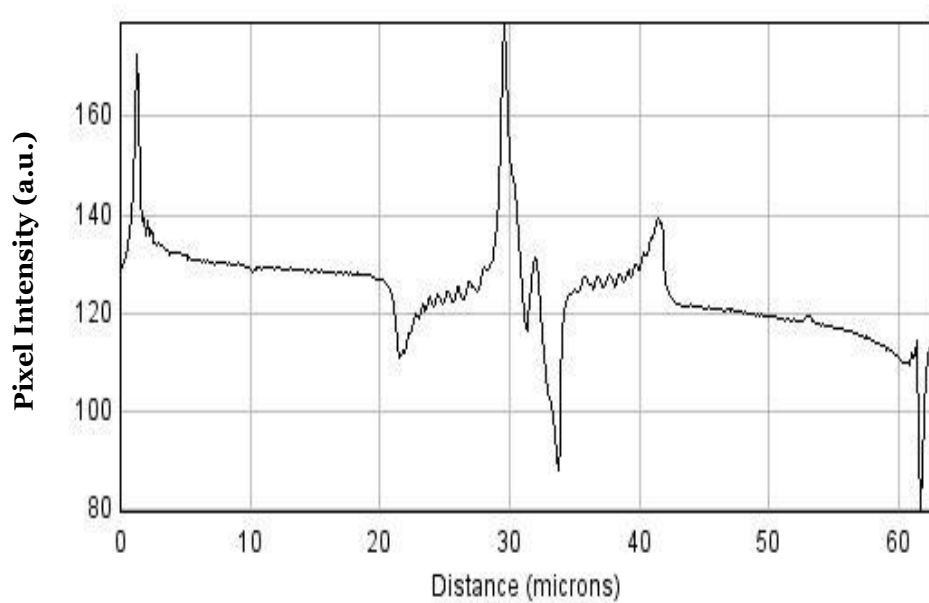


**Figure 3-14** Pixel intensity plots for a (a) line and (b) 3D surface plot of a region across the fibre core for the FBG in GF1 fibre shown in Figure 3-12 (a)

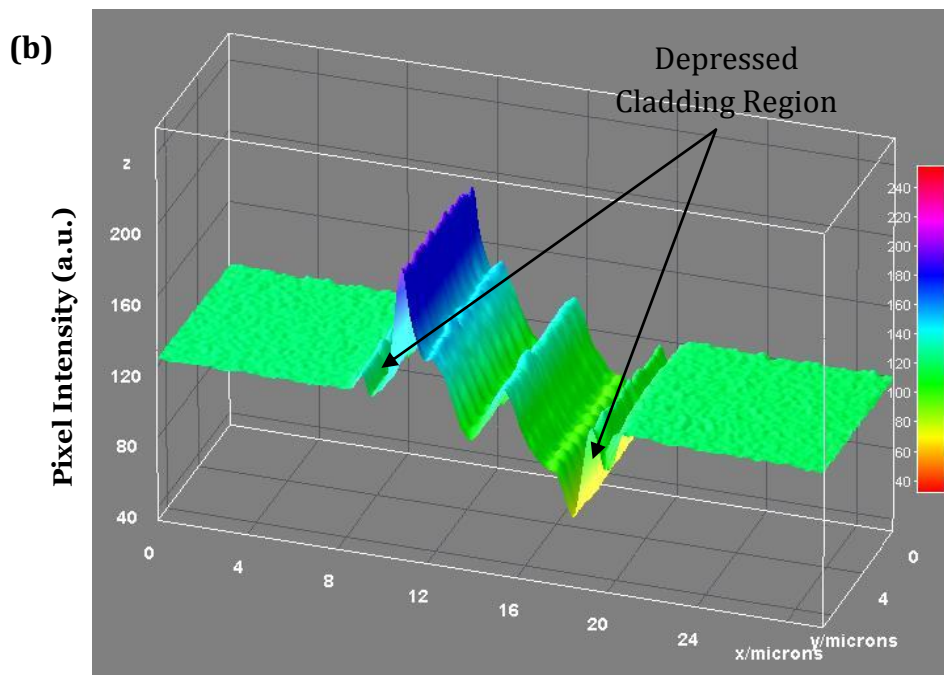
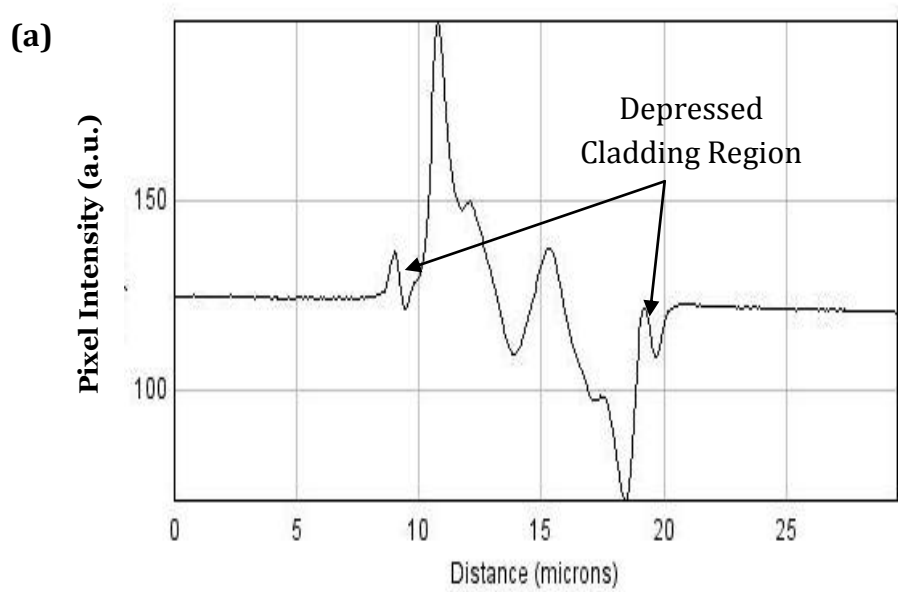


**Figure 3-15** Pixel intensity plots for a (a) line and (b) 3D surface plot of a region across the fibre core for the partially etched FBG in GF1 fibre shown in Figure 3-12 (b)

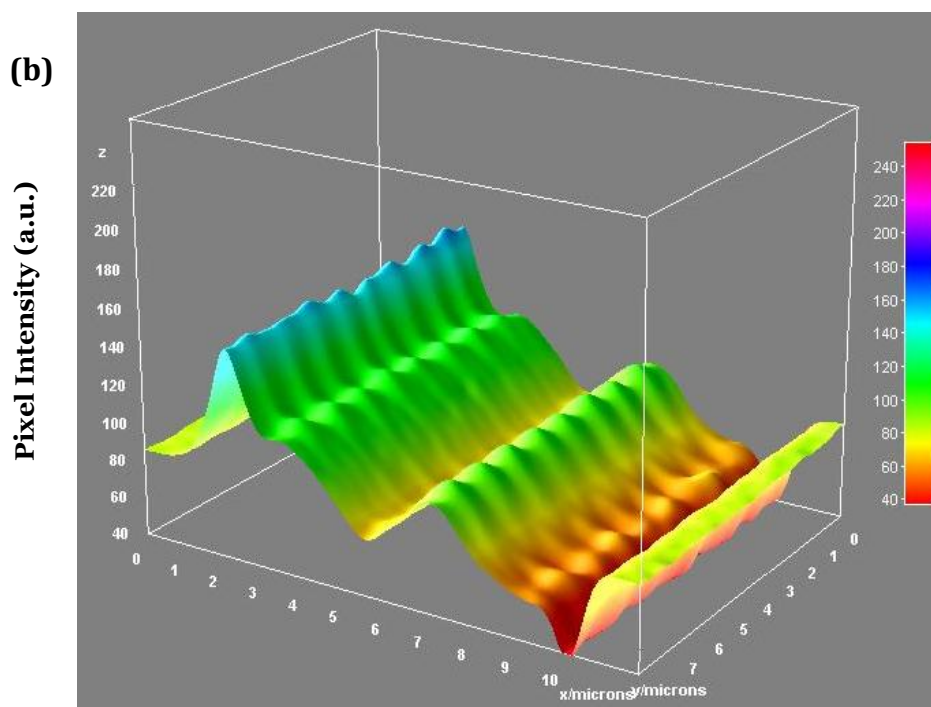
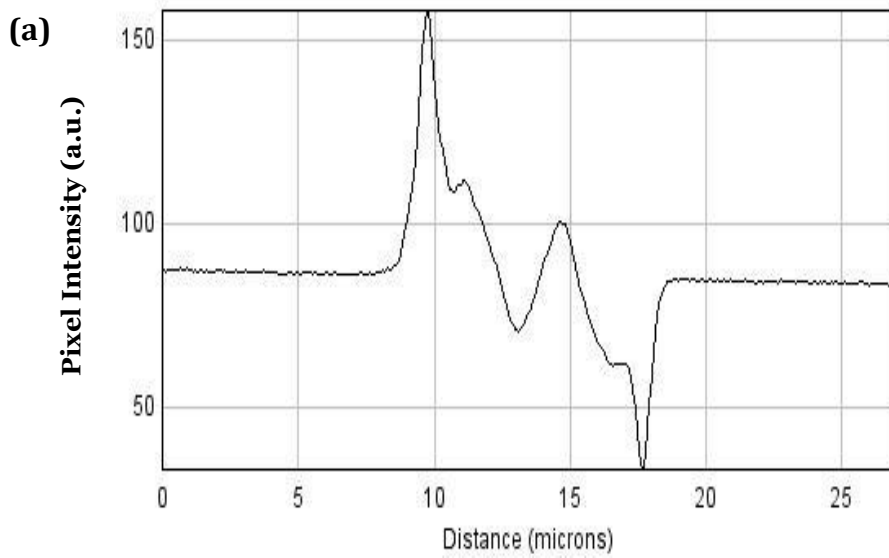


**Figure 3-16** Pixel intensity plots for a **(a)** line and **(b)** 3D surface plot of a region across the fibre core for the fully etched FBG in GF1 fibre shown in Figure 3-13

Figure 3-15 (a) shows the RI profile of the etched FBG which has some cladding left on it. Figure 3-15 (b) depicts the surface plot of this etched FBG, where a small portion of the cladding is visible and the gratings planes are also visible.

The RI profile and 3D view (Figure 3-16 (a) & (b)) of the fully etched FBG shown in Figure 3-13, gives clearer picture of the core of the GF1 fibre with FBG inscribed in it. It illustrates the gratings planes very clearly. And also it can be noted that RI variation on one side of the fibre facing the UV are more than other side, which is in good agreement with (Kouskousis, 2009).

### **3.3 Conclusions**

This chapter presents the fabrication technique of standard uniform FBGs and pi-phase-shifted FBGs and APPhSFBGs (at twice the Bragg wavelength) used in this thesis utilising the phase-mask writing approach. The spectral characterizations and microscopic characterization of these FBGs was discussed. A high resolution spectral characterization technique was used to get full spectral information regarding transmission, reflection as well as phase.

In the microscopic characterization using DIC images 3D surface plots of etched FBGs were revealed. This was first time that etched FBG were studied using the DIC microscope. These illustrate a clear dip in the RI in the core region and FBG grating planes are clearly visible.

## Chapter 4

### Refractive Index Sensor and Applications

**R**efractive index (RI) is a basic optical property of materials and its accurate measurement is of great importance. This chapter summarises the details of two types of RI sensors, i.e. intensity-based (broadband reflector) and wavelength based (reduced cladding FBGs) sensors. Among the two main sections of the chapter, the first part explores the multiplexing capabilities of a broadband reflector and provides the information of its different applications such as multipoint RI sensor for liquids and state of charge of battery indicator. In the second part of the chapter the scope of etched fibre and etched FBGs as highly sensitive liquid RI sensors is highlighted. In particular, the basic principle of operation of the sensor, materials and methodologies, experimental details and finally results and discussions of each RI sensor application is explored. A reliable and stable method of etching FBGs using a special mount is discussed. The prospects of etched FBGs in other applications such as strain sensor are also discussed. A new pi-phase-shifted FBG fabrication method based on wet chemical etching technique is demonstrated. This chapter concludes by providing analysis of these sensors and a comparison in terms of reliability, repeatability, life time and cost.

#### 4.1 Refractive Index Sensor

The measurement of the RI of liquids is important in engineering and science. The RI has various potential applications in chemical, biological, food, oil and gas, pharmaceutical, medical, biotechnology and many more. Apart from being a fundamental property of a material it also offers indication of several physical and chemical parameters. The determination of RI finds prospects in industries for finding the physical parameters such as concentration, temperature, pressure and in a variety of chemical and biological applications (Li & Xie, 1996, Liang *et al.*, 2007). Most notably, an estimate of RI must be given to calculate the particle size from the scattering data for inorganic and organic particle size determinations using light scattering, and in the biological realm, it is important in terms of phase

contrast microscopy, flow cytometry, and light scatter based detection methods. So RI determination is very important to enhance existing and emerging optical detection technologies. RI measurements for biological particles have been reported where the microscope image has been replaced by optical density measurements (Sean & Tomasz, 2006).

The RI determination of liquids in the chemical industry is well established. It is commonly used to help identify or confirm the identity of a sample by comparing its RI to known values (Shugar *et al.*, 1996), assess the purity of a sample by comparing its RI to the value for the pure substance (Shugar *et al.*, 1996) and determine the concentration of a solute in a solution by comparing the solution's RI to a standard curve (Suhadolnik, 2007). The classical methods involve bulk optics and incorporate measurements from critical angle and Brewster angle (Bali *et al.*, 2005, Castrejon-Pita *et al.*, 2006, Kejalakshmy & Srinivasan, 2001). Typically, in these types of instruments, light passing through (or reflecting from) an optical interface with the liquid in question is analysed for angular displacement. The extent of displacement is related to the RI of the liquid. As light refraction occurs at the exact boundary between the two chemically different regions, it is a bulk sample measurement technique. These RI measurements can be performed using an Abbe or reflection type refractometer. Singh S. reviewed techniques for measurements of RI of solid, liquid and gas and for polymers and crystals. These includes various prism methods where measurements were based on the deflection angle or on the Brewster angle, Pulfrich refractometer, thin film based measurements, transmittance envelopes method and different interferometric techniques (Singh, 2002).

However, the most of the traditional methods and devices are not suitable for some applications due to size and weight. In that case optical fibre based RI sensors can be a substitute in various applications as they offer many advantages (Krohn, 2000), as listed in Chapter 2. To date various methods of fibre optic RI measurement has been reported. Transmission or reflection detections near critical angles related to total internal reflections are the earliest and most common methods in RI measurements. Govindan *et al.* reported reflective type fibre optic displacement sensor to determine the RI of liquids. This sensor consists

of two multimode step index fibres and a mirror. The output light intensity from the receiving fibre was measured as a function of displacement of the fibre with respect to a mirror. Different liquids were used as a medium and it was reported that the light peak intensity position depends upon the RI of the medium. However, these types of sensors are prone to coupling losses. It is further demonstrated that the light intensity peak in a given medium is independent of the change in the light power or any light absorption by the medium (Govindan *et al.*, 2009).

More recently, a refractometer has been demonstrated by Liao, where a Mach-Zehnder interferometer (MZI) was integrated in fibre Bragg grating (FBG) for temperature independent RI measurements. By using the Bragg wavelength and the interference dip of MZI, RI and temperature can be distinguished (Liao *et al.*, 2010).

In another report, a U-shape optrodes were used to measure RI, where fibre was bent in U-shape and RI was measured in terms of light transmission (Kalvoda *et al.*, 2010).

A RI sensor based on Fresnel reflection has been demonstrated (Kim & Su, 2004) with an optical coupler and ratio of signals between air and liquid used to estimate the RI of liquids. A pulse generator was used along with laser diode to send pulses to the optical coupler at port 1 of the coupler whereas port 3 act as a sensor head, port 4 of optical coupler was used for the reference and reflected signal was detected using a detector at port 2. The authors proposed a double pulse measurement technique to avoid undesirable effects due to possible source power drifts and detector response changes. The resolution of the sensor was greatly increased using a double pulse technique and was reported to be  $2.5 \times 10^{-5}$ . Recently Su *et al.* reported a similar approach where a Fresnel-reflection-based two-channel RI sensor has been used to measure solute concentrations in the solutions, where protective fibre ends act as the sensor. One of the two sensing heads were left in air and used as a reference and the other was submerged into the solution under test. The ratio between the two intensities provided information on the RI value of the liquid. Three optical couplers, a diode laser and a photo-detector were used for RI measurements (Su & Huang, 2007). Modelling can

provide expected outcomes of a particular sensor and Zhang Zhi-Wei *et al.* demonstrated a new method of mathematical modelling for measuring RI of a liquid based upon the Fresnel formula and a prism internal reflection at an incident angle less than the critical angle (Zhang *et al.*, 2007). Turan *et al.* proposed a refractometer based on Fresnel reflection principle where they analysed various microprocessor-controlled operation architectures (Turan *et al.*, 2001). Another report included a Fresnel-reflection-based fibre sensor that can measure liquid concentration and temperature simultaneously where wavelength division multiplexing was achieved by using thin film filters and an array of waveguide gratings. By measuring the Fresnel-reflection signals from the sensing heads, each of which consists of two fibre sensing tips, simultaneous measurement of liquid concentration and temperature was obtained (Zhao *et al.*, 2009).

Other reports include optical fibres in conjunction with thin films deposited on them and metal coated fibres with surface plasma resonance have been used as RI sensors (Jorgenson & Yee, 1993, Le Goullon & Goswami, 1990, Smietana *et al.*, 2008). Other method involves the side polishing of D-shape optical fibre to get access to evanescent fields from FBGs (Chen *et al.*, 2007). In another approach D-shape fibre was used, in which the phase difference between internal reflection from S and P polarisations was measured using a heterodyne interferometer, and results were compared with a prism RI measurement method (Chiu & Wang, 2004). More recently, an intensity-based RI sensor was reported by Chen *et al.*, where D-shaped grooves were fabricated in optical fibre using femtosecond laser. The sensitivity of the sensor was  $\sim 1.13 \times 10^{-4}$  RIU for RI of 1.403 (Chen *et al.*, 2010). Banerjee *et al.* demonstrated a refractometer based on an evanescent field sensor using hydrofluoric (HF) acid etching of a fibre (Banerjee *et al.*, 2007). Long period gratings and tilted FBGs as RI sensor have also been reported (Bhatia & Vengsarkar, 1996, Chiang & Liu, 2006, Rui *et al.*, 2008). FBGs inscribed in some specialized fibre such as photonic crystal fibre and microstructure fibre also acts as highly sensitive RI sensors (Martelli *et al.*, 2007, Phan *et al.*, 2007).

Evanescent field coupling to the surrounding environment was also used, which involves RI sensor based on thinned gratings or etch-eroded gratings, where a portion of cladding above the core is removed using HF acid and when this etched

portion is immersed in different liquids, giving a shift in the Bragg wavelength. These etched FBGs have been used for various applications. Recently, very high sensitivity (resolution  $\sim 10^{-4}$  RIU) RI sensors have been reported based on etched fibre Bragg gratings (Huang *et al.*, 2008, Iadicicco *et al.*, 2005b, Iadicicco *et al.*, 2004, Iadicicco *et al.*, 2003, Liang *et al.*, 2005). Other reports include the use of etched FBG (and twin FBG) as temperature independent chemical sensors (Iadicicco *et al.*, 2005a, Sang *et al.*, 2007, Sang *et al.*, 2006), where half of the FBG remain un-etched in order to reduce temperature sensitivity. Then the peak wavelength difference between etched and un-etched FBG was calculated for temperature-independent RI measurements of various propylene glycol solution concentrations and sugar solution concentrations.

Another type of evanescent field RI sensor is based on an optical coupler where an optical coupler has been tapered and used for solution concentrations sensors. This type of sensor is demonstrated by Shi *et al.*, where a  $2 \times 2$  fused tapering single-mode optical fibre coupler when immersed in the solution, the light propagating through the fused tapered coupler and makes the coupling ratio sensitive to the variation of the liquid's concentration surrounding the fused tapering zone of the coupler (Shi *et al.*, 2007). Baptista *et al.* proposed a self-referenced intensity-based sensor for the measurement of RI of oils, where the sensing head consists of a short length of un-cladded multimode fibre (etched using 40% hydrofluoric acid (HF) solution). The sensing head relies on the change of the RI of the medium that surrounds the unclad portion of multimode fibre, which results in different attenuation of the guided modes that propagate in the fibre (Baptista *et al.*, 2001). More recently, Fang *et al.* demonstrated a RI sensor in microfibre, where microfibre has only core ( $\sim 10 \mu\text{m}$ ) surrounded by air and FBG was written using femtosecond laser (Fang *et al.*, 2010).

## **4.2. Fibre Optic RI Sensor based on Broadband Reflector**

### **4.2.1 Introduction**

The broadband reflector comes in the family of intensity-based sensor and these are one of the earliest sensing methods and are popular due to their straightforward, economic and simple operation. The following section emphasizes

the operation of a broadband reflector, their multiplexing topology and the main applications which were experimentally demonstrated.

A broadband reflector consists of a cleaved fibre end of an optical coupler which acts as a sensor head and used to measure the RI of medium under test. Light launched into port 1 of the  $50 \times 50$  4 port optical coupler is directed via port 3 towards the cleaved end of the fibre, which serves as a sensor head (Figure 4-1).

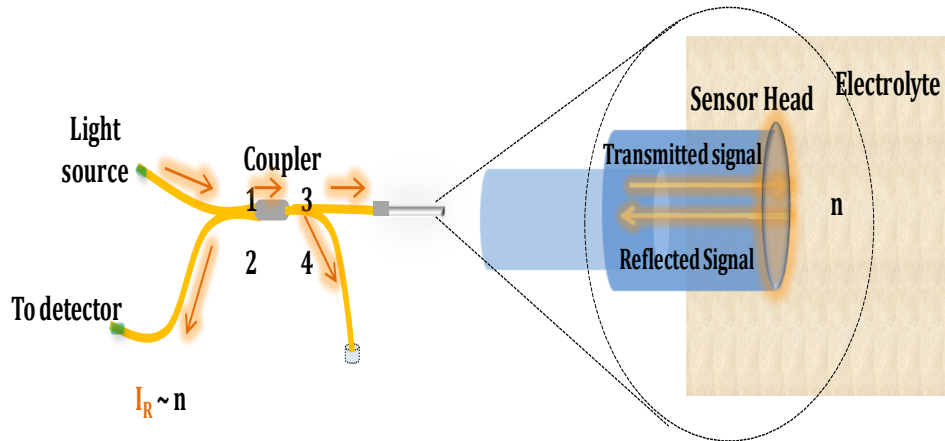


**Figure 4-1** Basic principle of operation of fibre optic RI sensor based on broadband reflector

Light reflected off the optical fibre end submerged into the medium under test into ports 1 and 2 and is detected at port 2. Submerging of port 3 (sensor head) into different media results in change of reflectance at the sensing end which results in a variation of the signal intensity reflected back to port 2. Information about the RI of the medium under investigation can be retrieved by monitoring the relative intensity of the signal reflected back from the sensor head to the detector (equation 2-7). Intensity of the reflected light depends upon the reflectivity of the surface between the optical fibre and the medium under test.

In equation 2-7, if  $n_2$  is the RI of the substance surrounding the sensor head then  $n_1$  is the effective group RI for the fibre, which is best determined by the use of standard RI oils (i.e. for  $n_2$ ) in the region of the nominal value of 1.47 and locating the RI where there is zero reflection. Subsequently, an unknown RI,  $n_2$ , can be determined from a measurement of R.

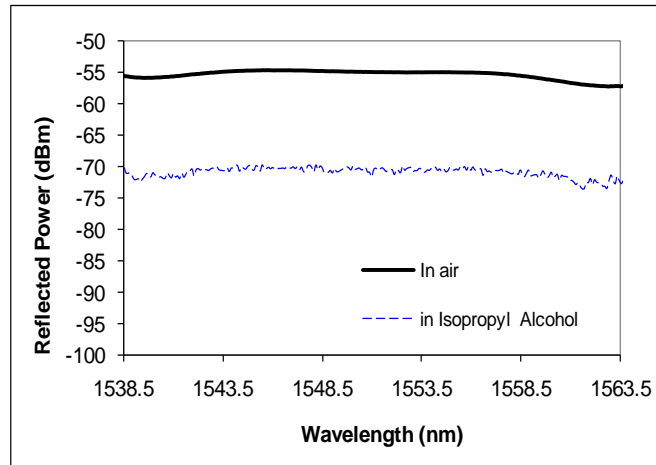


**Figure 4-2** Response of fibre optic broadband reflector when sensor head was in air and in isopropyl alcohol

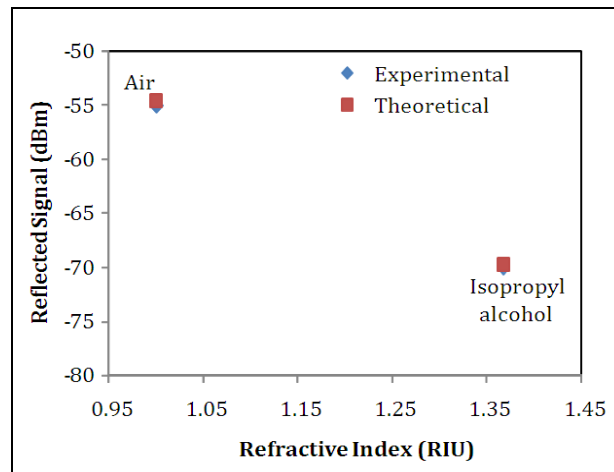


**Figure 4-3** Relationship between RI of liquid and reflected signal

Figure 4-2 depicts the response of the broadband reflector for two different media. A clear change in intensity of reflected signal is observed when the medium under test was changed from air to isopropyl alcohol, whereas Figure 4-3 shows the relationship between RI and output signal. The reflected signal from the fibre was compared for the known value of RI of isopropyl alcohol (i.e. 1.3677 RIU) and air (1.003 RIU) using equation 2-7.

#### 4.2.2 Multipoint broadband reflector

Multipoint measurements are often required for several applications where different information at various points is required at one time. The multiplexing

technique can easily be achieved by using fibre Bragg gratings (FBGs). There are several different multiplexing topologies which can be used to multiplex FBG based sensor arrays (Section 2.3). In (Caucheteur *et al.*, 2009) authors incorporated tilted FBGs for multipoint RI measurements. Baptista *et al.* have also explored a self referenced intensity-based sensor for multiplexing capabilities based on Michelson topology using optical couplers and pair of FBGs (Baptista *et al.*, 2002).

The broadband reflector discussed above in section 4.1.1 can easily be multiplexed using FBGs. FBGs can reflect a particular wavelength, so by using FBGs at different unique wavelengths and optical couplers, the broadband reflector can serve as a multipoint sensor. Figure 4-4 illustrates the schematic of module 1 (M1) using one FBG at a specific wavelength. This module consists of two 3-dB  $2 \times 2$  bi-directional couplers and incorporates a FBG. Port 4 of coupler 1 is used as the sensor head (SH). The fibre end at this port is cleaved before being submerged into the liquid under test. Light from a broadband source (BBS) is introduced into coupler 1 through port 1, while any change of reflectance at the sensing end results in a variation of the signal intensity reflected back to port 2. Connecting port 2 of coupler 1 with port 3 of coupler 2 through an isolator enables the reflected sensing signal to reach the FBG connected to port 2 of coupler 2. As discussed earlier the FBG was used to selectively reflect back to port 4 of coupler 2 (signal detection end) only the part of the reflected sensing signal that matches the narrow spectral band of the FBG. As a result, information about the RI of the liquid under investigation can be retrieved by monitoring the relative intensity of the signal reflected back from the sensor head to the detector via the FBG reflection.

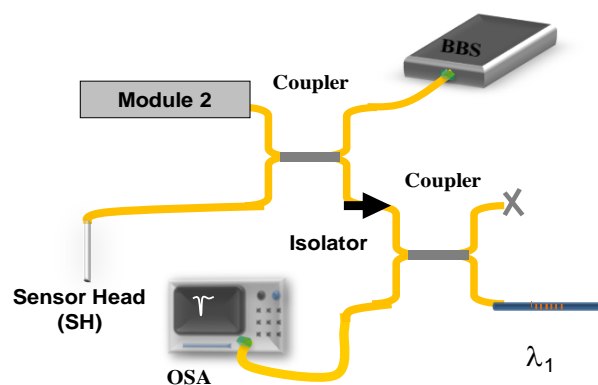


**Figure 4-4** Schematic of module 1 (M1)

Importantly, this sensing module allows multiplexing capability by directly connecting a similar module, involving a FBG that has a different Bragg wavelength, with port 3 of coupler 1, as depicted in Figure 4-5. Each FBG reflects a different wavelength, so depending upon wavelength, different sensor heads can be distinguished and the corresponding intensity of reflected signal yields the specific RI.

The capability of this multipoint sensor was evaluated for two sensor modules, theoretically and experimentally.

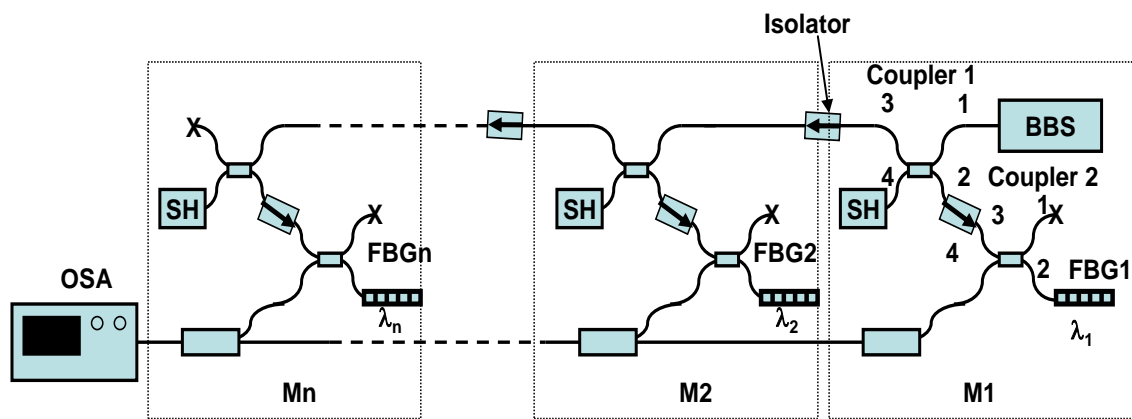


**Figure 4-5** Multiplexing of fibre optic reflective sensors consisting of n modules, each of which has a sensor head and a unique wavelength (Bal *et al.*, 2010d).

*(a) Theoretical analysis*

Theoretical analysis of this multipoint sensor was achieved by using Fresnel equation 2-7.

The RI of 1.46 RIU for the core of the optical fibre was used and the relative intensity for different RI values was calculated for various oils.

*(b) Experimental results*

In two sensor modules, each sensor consists of two  $2 \times 2$  fibre couplers and a FBG (Figure 4-4). Modules 1 and 2 (denoted M1 and M2, respectively), as depicted in Figure 4-5, were constructed using four fibre optic couplers that were single mode in the C band with 50:50 splitting ratios and apodised FBGs centred on

wavelengths of 1559.43 nm and 1543.5 nm, respectively. The detailed fabrication technique of these uniform FBGs is explained in section 3.1. Sidelobe suppression (apodisation) was employed in FBGs, and SMF-28 telecommunications fibre was used for each sensor head. An optical isolator was used to avoid crosstalk between the modules and an isolator within the modules can be used to improve the output signal. Light from a broadband erbium-doped fibre source (MPB model 7210) was launched into the sensor network. An OSA (ANDO, model AQ6317B, resolution of 0.1 nm), was used to monitor the sensor outputs. The spectrum of the output signal from these two sensors, M1 and M2, when both sensor heads were in air, is presented in Figure 4-6.

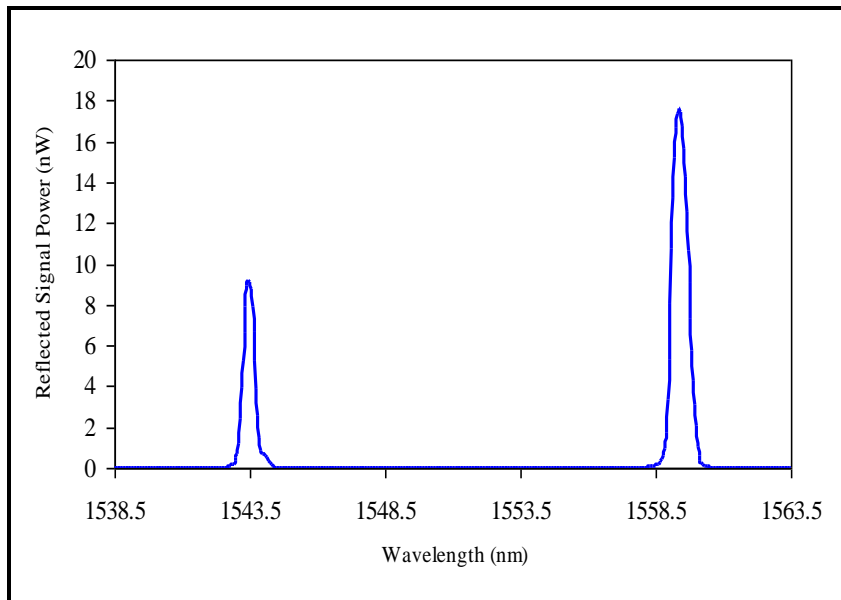


**Figure 4-6** Example of the spectrum of two FBGs when both sensor heads M1 (operating at 1559.5 nm) and M2 (operating at 1543.5 nm) were in air

The two reflection bands in the spectrum correspond to FBG1 at 1559.5 nm (M1) and FBG2 at 1543.5 nm (M2), and provide a reference to convert power levels to reflectance based on the RI of air. The optical power reflected from FBG1 in M1 is almost twice as large as the power reflected from FBG2 in M2. This difference in reflected power is due to the design of the system (Figure 4-5), which is necessary as reflective sensors necessarily have to be multiplexed in parallel.

Subsequent monitoring of the intensity of the reflected signal from each grating enabled the value of an unknown reflectance, and hence the RI, at each sensor (i.e.

M1 and M2), when the sensor head was immersed into solutions, to be determined. The sensor head was cleaned with ethanol solution between each measurement and the intensity of light reflected off the surface of the fibre surrounded with air was compared to the control measurement taken in the beginning of the experiment. This procedure ensures that there is no influence of any residual liquid contamination left on the surface of the sensor head after each measurement. In addition, the device was tested for stability by performing repeatable and cyclic (reverse order) measurements.

An example of a spectrum of module 2 (M2), when the sensor was in air and in isopropyl alcohol is shown in Figure 4-7 (a) and (b), respectively. The use of a set of index matching oils enabled detailed measurements at many RI values.

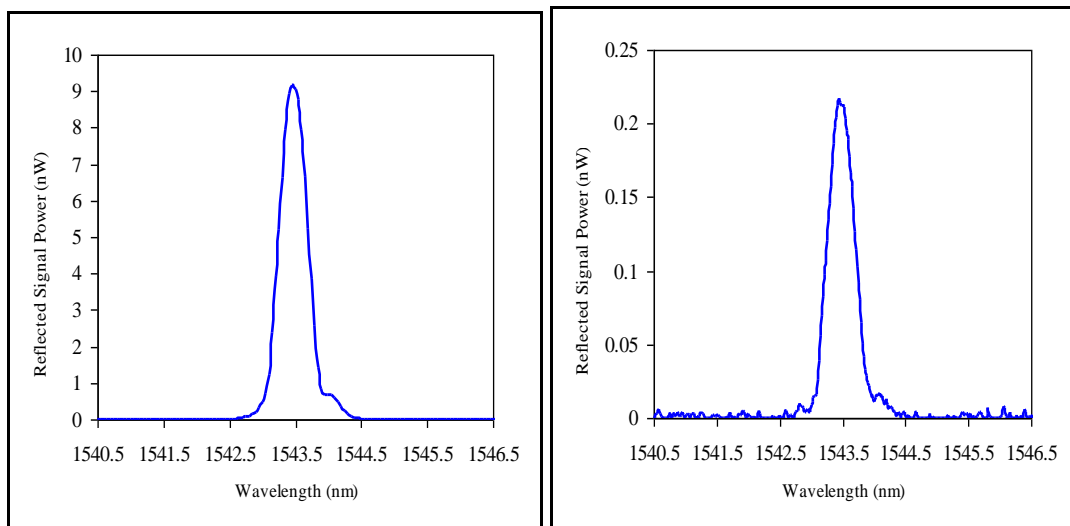


**Figure 4-7** Examples of spectra when sensor head M2 (1543.5 nm) **(a)** was in air and **(b)** was in isopropyl alcohol

As mentioned earlier an optical isolator was used in between M1 & M2 and both modules were tested for their performance. Figure 4-8 illustrates the performance of the sensor with an optical isolator. It is clear that the performance of M1 is not affected by the other module. A set of liquids, having refractive indices lying in the range 1.400 – 1.640 ( $\pm 0.0002$ ) RIU, were chosen for testing the performance of the final sensor.

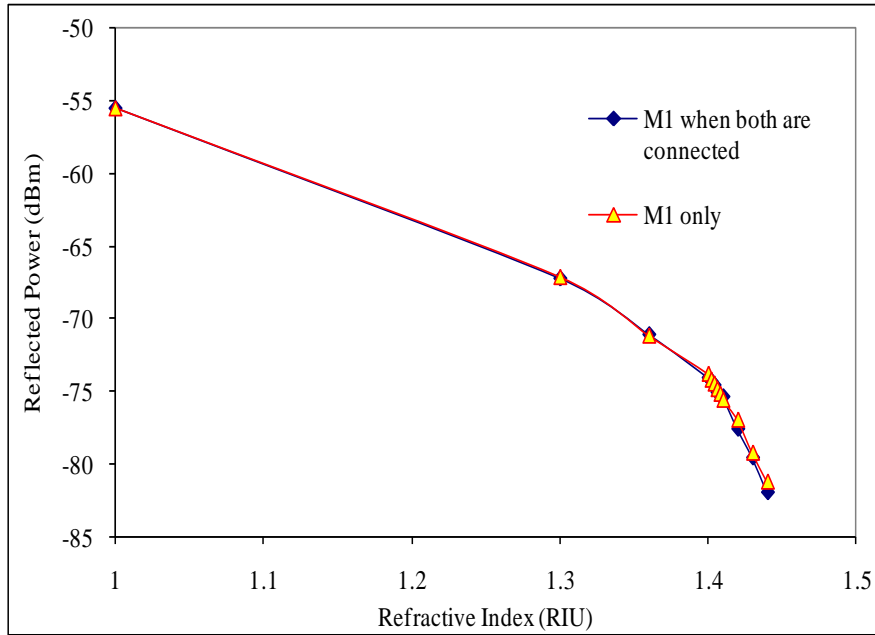


**Figure 4-8** Performance of M1 when an isolator was used in between M1 & M2

The measured reflected power as a function of RI is shown in Figure 4-9 (a), while Figure 4-9 (b) shows the same data over a more limited range. A decrease in the intensity of the signal reflected off FBGs in both modules was observed up to  $n_2 = 1.460 \pm 0.002$  RIU (which was taken to be the value for  $n_1$ ). Any further increase in the RI of oils surrounding the sensor head resulted in the intensity of the signal increasing, as expected. This behaviour is in excellent agreement with the theory, based on equation 2-7 using  $n_1 = 1.460$  RIU, as depicted by the two curves. The theoretical curves in Figure 4-9 (a) include the situation when the sensor heads were surrounded by air.

As discussed in section 2.2.1.1, when the value of  $n_2$  becomes equal to  $n_1$ , there is no reflection and intensity of signal becomes zero. This RI (i.e. the “index matching” condition) adds uncertainty in the situation when two different refractive indices correspond to one value of intensity of reflected light. This adds possible complexity to the interrogation system if the range of refractive indices of interest crosses through this point. A better alternative, in this situation, would be to cause a shift in the bifurcation point by a change in the RI of the optical fibre used at the tip of the sensor head.

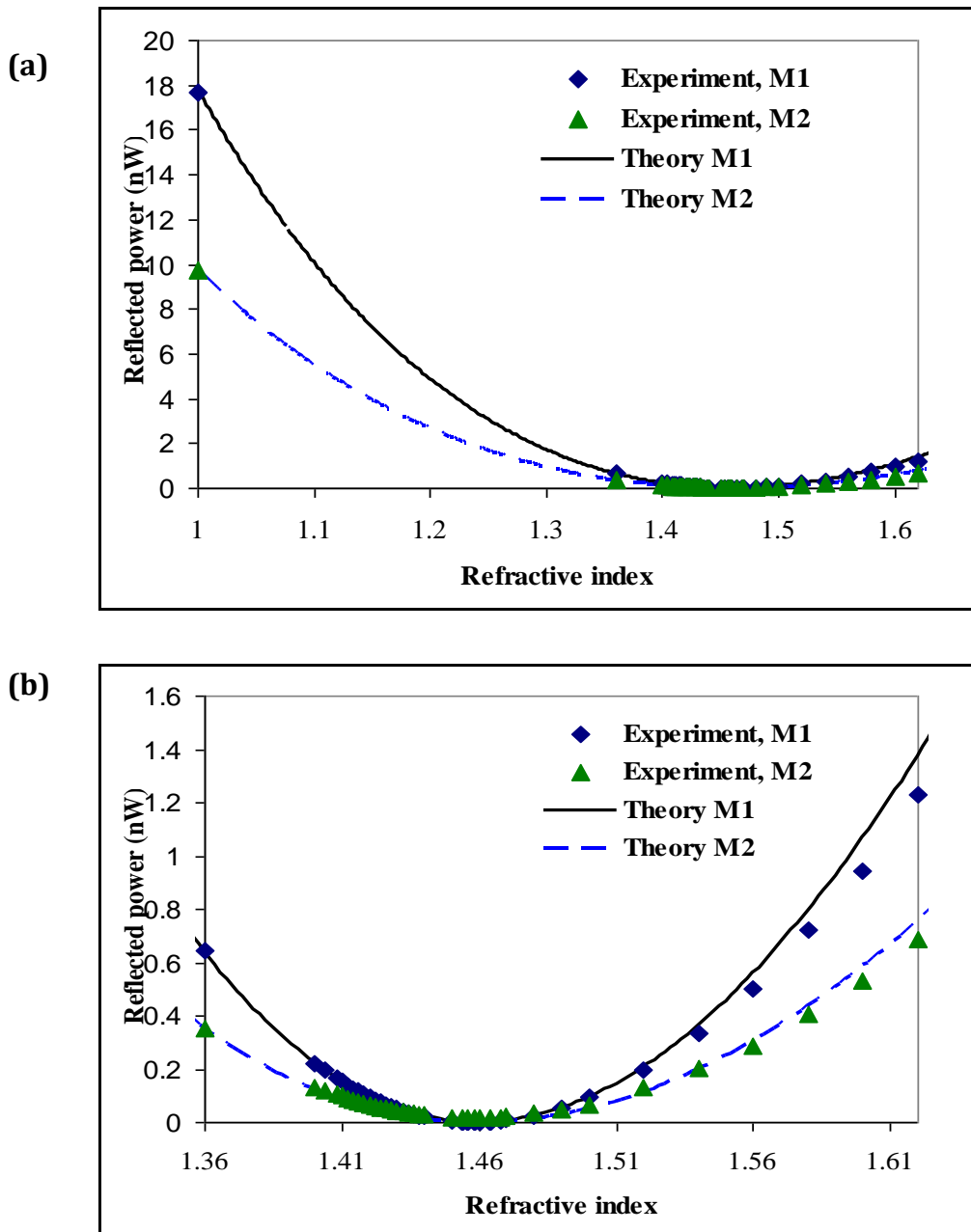


**Figure 4-9 (a)** Variation of the reflected power for measurement over a range of refractive indices using sensor heads M1 & M2 with **(b)** showing the same data over a smaller range (Bal *et al.*, 2010d).

An optical coupler induces a 3 dB loss. So half of the light launched into M1 from the broadband source is directed into the sensor head while another half is launched into M2. Thus the number of channels will be limited by the power of the optical source since there is at least 3 dB less power delivered to each successive module, and by the dynamic range of the OSA for a larger number of channels. Nevertheless, the sensor can easily be made to measure the reflectance of multiple

sensors (10 or less) through use of high power super-luminescent diodes, replacing some couplers with circulators or by amplifying the power using an amplifier. When a larger number of sensors are in use, a calibration procedure, similar to that outlined above, will need to be followed for each sensor head to ensure that variations in source power and grating properties across the spectral range of the sensor heads is taken into account. For the gratings used here the minimum wavelength separation between modules will be about 2 nm, and the limit of the number of channels will depend on the power and spectral width of the light source. It is also noted that through the use of circulators, instead of couplers, that some of the losses mentioned above could be reduced significantly.

Although this device was tested at telecommunication wavelengths, the multipoint sensor can be used at visible wavelengths, provided that components (i.e. light source, FBGs, fibres and couplers) at the appropriate wavelength band are employed. This will enable the use of this reflective sensor in biomedical and chemical applications where RI measurement of liquids at specific visible wavelengths is required.

This technique allowed detection of RI changes as small as  $10^{-3}$  RIU, and the estimated precision is 0.002 RIU. This performance could be enhanced by using a high-power source at the input of the interrogation system.

### **4.3. Application of Fibre Optic RI Sensor based on Broadband Reflector-State of Charge of a Battery**

The RI measurement based on broadband reflector as discussed in section 4.2 can be used for various different applications. As discussed in section 4.2.2 multipoint RI measurements of various liquids can be realised using this sensor. In this section another application area will be explored.

#### *(a) Introduction*

Batteries have revolutionised the way electricity can be stored and paved the way for greater mobility in our day-to-day lives. These have been used from portable cell phones to high-tech space equipments. Lead-acid batteries have been widely

used as automotive and submarine batteries, etc. It is very important to measure capacity of the batteries. Knowing the amount of energy left in a battery compared with the energy it had when it was full gives the user an indication of how long a battery will continue to perform before it needs recharging. Using the analogy of a fuel tank in a car, state of charge (SOC) estimation is often called the "Gas Gauge" or "Fuel Gauge" function. The SOC is defined as the available capacity expressed as a percentage of some reference, sometimes its rated capacity but more likely its current (i.e. at the latest charge-discharge cycle) capacity but this ambiguity can lead to confusion and errors. It is not usually an absolute measure in coulombs, kWh or Ah of the energy left in the battery, which would be less confusing. The preferred SOC reference should be the rated capacity of a new cell.

Electric batteries, which comprise the bulk of the storage batteries currently in use worldwide, require the plates of the battery to be immersed in an electrolyte, which could be a sulphuric acid solution or gel. Batteries are made up of several interconnecting cells and the number of connected cells determines the battery's operating voltage. In the charged state, each cell contains electrodes of elemental lead (Pb) and lead (IV) dioxide (PbO<sub>2</sub>) in an electrolyte of approximately 33.5% v/v (6 molar) sulphuric acid (H<sub>2</sub>SO<sub>4</sub>). Chemical reaction inside the electrolyte during operation of the battery changes concentration of chemical compound of it, which leads to the change of the RI of the electrolyte.

There are various methods to determine state of charge of a battery; some methods are based on the electrical characteristics of the batteries which include battery voltage, charge integration, or cell impedance with various degrees of accuracy, price and ease of use (Aglzim *et al.*, 2007, Basell & Hawkins, 1998, Blanke *et al.*, 2005, Dowgiallo, 1976, Ohsawa, 2001, Ullrich *et al.*, 2004). Other methods embrace various techniques to determine the concentration of the sulphuric acid in the electrolyte (Hancke, 1990, Matsui, 1987, Nagai *et al.*, 1987, Tsubota, 1985). However, it evident that voltage-based methods of fuel gauging cannot achieve today's required accuracy of SOC estimation. Further, correction for internal impedance of the battery suffers from transient effects and variability of impedance with aging and from cell to cell. Radical new solutions to this problem use voltage-based methods where no correction is needed. Current integration

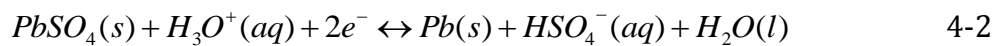
during periods of activity allows precise estimation of the change in SOC from the last voltage-based estimation. Impedance information is still needed for calculating the usable capacity under a particular load and can be acquired by real-time measurement. Sensors based on use of optical fibre stand out of other sensing methods due to their numerous advantages such as ease of use and integration, multiplexing capabilities, comparatively low cost, etc. (Grattan & Meggitt, 1994). Due to these advantages there are few methods of monitoring SOC based on optical approaches.

A fibre-optic technique for measuring specific gravity based on the principle of variation of the critical angle of reflection due to a change in the density of the surrounding medium is demonstrated, caused an equivalent change in the leakage of light through the walls of the fibre in contact with the fluid. This change can be measured and converted to a related specific gravity value (Hancke, 1990). Another method involves the measurement based on light ray trajectory variations produced by the electrolyte media when its density changes. The changes in the electrolyte RI are produced due to changes in density, and the system measures such changes by means of an optical sensor coupled with a fibre optic bundle. SOC is indirectly measured via an optical specific gravity measurement. A set of equations based on a paraxial ray model perform the optical sensor design, describing its behaviour for different design parameters, thereby allowing for the optimization of signal response (Cortazar & Feliu, 2006). In a lead-acid battery the sensor comprises a fibre optic system with an absorption cell or, an optical fibre woven into an absorbed-glass-mat battery (Weiss, 2002). A sensor for measuring the change in RI of a liquid uses the lowest critical angle of a normal to achieve sensitivity when the index of the liquid is significantly less than the index of the fibre core. Another embodiment uses a liquid filled core to ensure that its index is approximately the same as the liquid being measured (Accetta, 2008). A fibre optic sensor was reported recently, where etched portion of the fibre was used to determine the SOC of the battery (Paz *et al.*, 2010).

*(b) Principle of operation*

In a lead acid battery, the SOC or energy content is linearly related to the concentration of the electrolyte, which is a sulphuric acid solution (or gel) in conventional wet batteries. As the battery is charged or discharged, the concentration of acid increases or decreases ranging from 40% to 10% by weight, depending on the type of battery. In most solutions, the index of refraction of the sulphuric acid solution is very nearly linear with respect to concentration.

Measurement of state of the charge of battery was utilised by determining its chemical state via the change of the RI of the electrolyte, which turned both electrodes turn into lead (II) sulphate ( $PbSO_4$ ) and the electrolyte primarily water as given by following equations.



RI of the electrolyte was measured using Fresnel-reflection as given in section 4.2.

*(c) Experimental details and results*

An optical coupler was used to determine the RI of electrolyte of the battery (similar to section 4.2.1). Table 4-1 shows the details of the equipment used for this experiment.

Equipment	Manufacturer	Details
Optical coupler	Thorlabs Ltd.	2 × 2, 10202A-50 - 1550nm, 50/50 split ratio coupler
Light Source	MPB	Erbium dual band light source, MPB model 7210
Battery	G/N/B Technologies Australia Ltd.	Part No. 92093604
Detector	Optiphase Ltd.	V - 600 FC tunable optical converters
Load	MaxLite	130 watt halogen car bulbs (H3U12V 130W)

**Table 4-1** Details of equipment used to measure SOC of a battery

The cleaved end of the fibre at port 3 of coupler serves as a sensor head. Sensor head was submerged into the electrolyte (33.5% mixture of sulphuric acid in  $H_2O$ ) of the battery. A load of two halogen bulbs were connected to the battery to discharge it, and the reflected signal was monitored.

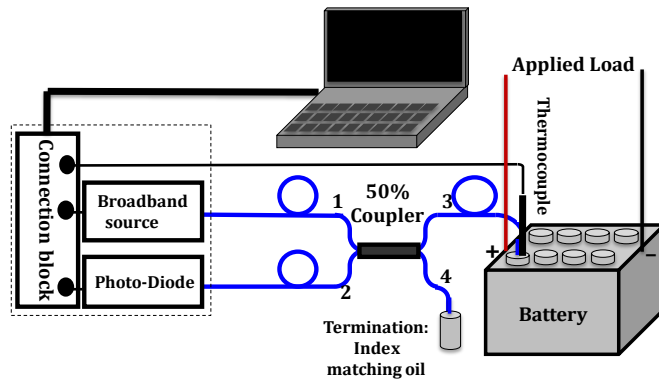


**Figure 4-10** Set-up used to measure state of charge (SOC) of battery

A thermocouple was submerged into the battery electrolyte to measure temperature and all information was sent to computer through a LabView and GPIB interface as shown in Figure 4-10.

To avoid any fluctuations due to unexpected change of intensity of the light source the set-up in Figure 4-10 was modified using another 2 x 2 coupler as shown in Figure 4-11. Port 3 of (Coupler 1) was used to calibrate the sensor to any unexpected change of intensity of the light source. Isolator (4015SA - Single Stage Fibre Optic Isolator, 1550nm, Thorlabs Ltd.) between coupler 1 and 2 is used to prevent cross-talk from the measurement signal from reaching detector 1 and to calibration signal.

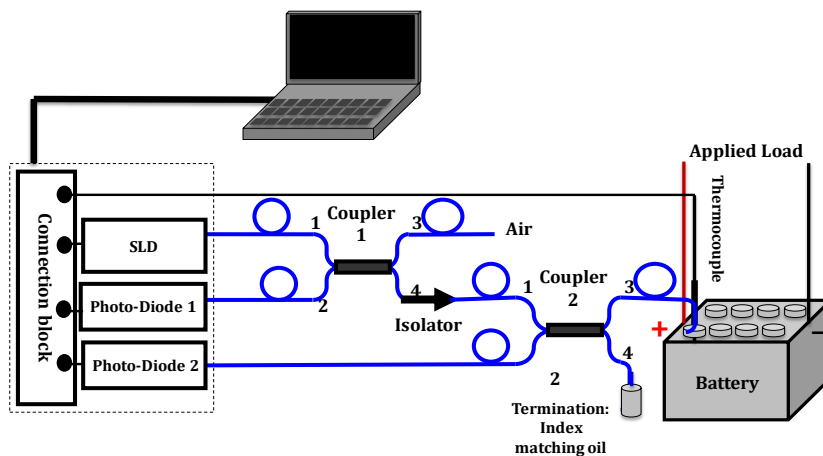


**Figure 4-11** Set-up used to calibrate sensor and to measure state of charge of battery

The intensity of light at detector 2 was compared to the intensity of light launched into the sensor at detector 1 and the ratios of these intensities was analysed as an

indication of the concentration of sulphuric acid in water. As the RI of an electrolyte changes with temperature, a thermocouple was used to measure the temperature of the electrolyte and to calibrate any temperature fluctuations (to discriminate between RI change due to decomposition of sulphuric acid or due to increase of temperature).

The output of the sensor was measured while changing the temperature of the 40% concentration of sulphuric acid in H<sub>2</sub>O (Figure 4-12). The acid was heated on a hot plate and a thermocouple was used to record the temperature variations. The data were fitted using linear regression as shown in Figure 4-12.

$$V = 0.0057T + 15.539, \quad 4-3$$

where  $V$  is the sensor output (pW) and  $T$  is temperature of the solution. Figure 4-13 shows the sensor output vs. voltage, corrected for temperature changes, measured between the load applied to the battery and the battery itself.

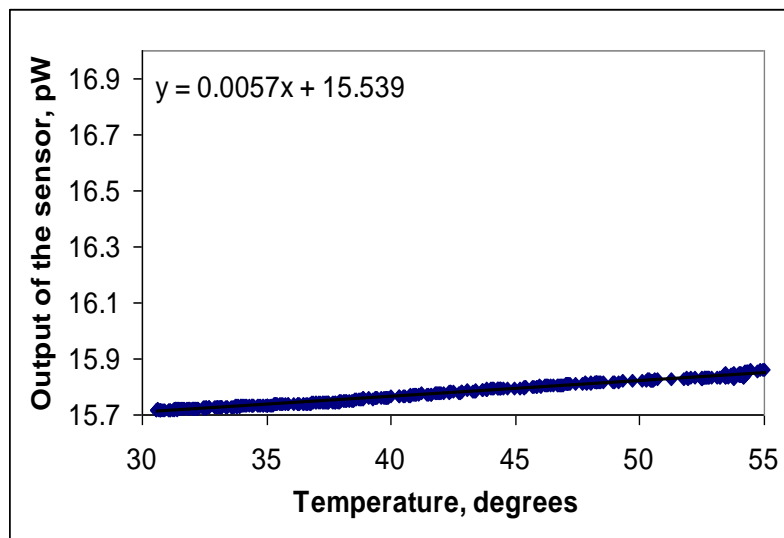


**Figure 4-12** Output of the sensor vs. temperature

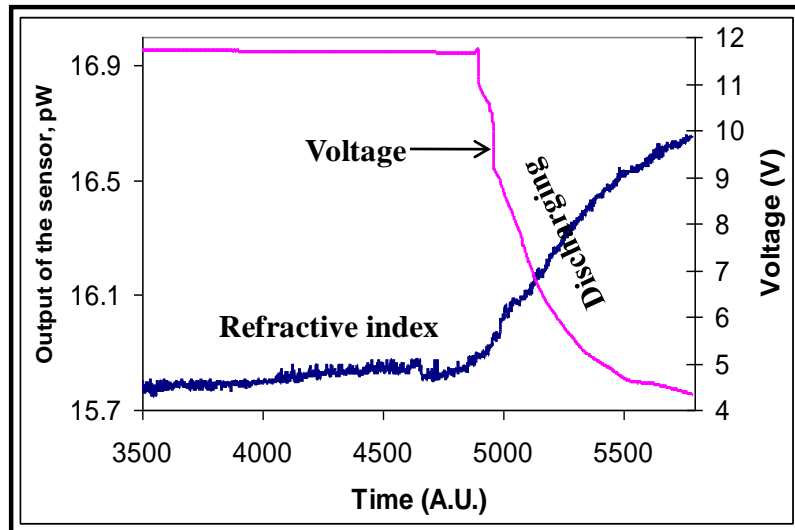


**Figure 4-13** Output of the sensor vs. voltage measured between the load applied to the battery and battery itself

This fibre optic probe can be extended to serve as a multipoint sensor for real time monitoring of state of charge of several stock batteries at one time. It is quite important to monitor state of charge of several batteries in stock in real time. As batteries consist of electrolyte or gel, while in stock for several months, batteries deplete in charge. So to monitor health of these batteries multipoint sensor is required, which can determine charge state of batteries continuously. By using FBGs a multipoint sensor similar to that described in section 4.2.2, can be realised which would be used to estimate SOC of stock batteries. The environmental long term accuracy of this sensor was not investigated experimentally in our case. However, recently it has been observed that polymer optical fibres (POF) in battery electrolyte for 9,552 hrs showed no acidic degradation. Photographs of the fibre before and after the experiment revealed minimum change. It has been verified through a theoretical model that due to the high activation energy and low operating temperature (below 50 °C) the mean life expectancy of the fibres will be larger than the battery life (Acevedo *et al.*, 2008). It should be noted that the attenuation of the cleaved tip of the fibre is possible in long term use, which needs to be cleaved again occasionally.

## 4.4. Optical Fibre RI Sensor based on Etched Fibre Bragg Gratings

The sensitivity and accuracy of intensity-based sensors is suitable for many applications but still some applications require enhanced sensitivity. In this section another type of RI sensor is highlighted, where the signal can be detected as a wavelength change using FBGs. Thus problems associated with source power fluctuations, bending losses, backscattering/reflection losses are eliminated. The sensitivity of these sensors is very high, but their manufacture is more expensive. In the following section a RI sensor based on etched FBGs is presented.

### 4.4.1 Introduction: Communication with outside environment

As discussed in section 2.2.4.3, standard FBGs have been have been successfully used for various applications (Rao, 1999). The FBG sensing operation relies on the dependence of its Bragg wavelength on the grating period and modal effective index, which in turn, depends upon the refractive indices of both cladding and core as well as upon the overlap of guided mode with the grating structure. Typically, FBGs are insensitive to the RI of their surroundings since light coupling occurs predominantly in the core. Recent developments in guided optics involve squeezing light out of the bulk and having a large fraction of the optical field outside of the waveguide with low transmission losses. Etched FBGs, corrugated gratings or a Fabry-Perot interferometer can be used for this purpose. A corrugated grating is a one-dimensional periodic surface relief structure etched into the waveguide, e.g. optical fibre or planar structure. In etched/thinned FBGs, removal of the fibre cladding enables light propagating into the evanescent field to interact with the surrounding environment.

When the cladding is removed, or sufficiently reduced, the effective RI of the fundamental mode is strongly affected by the surrounding RI and a change in the RI also causes a wavelength shift given by:

$$\Delta\lambda_B = 2\Delta n\Lambda\Delta\eta_P, \quad 4-4$$

where  $\Delta\lambda_B$  is the change in wavelength of the Bragg reflection,  $\Lambda$  is the period of the grating,  $\Delta n$  is the difference between the cladding RI and the surrounding RI and  $\Delta\eta_p$  is the variation of the fraction of the total power of the unperturbed mode that exists in the etched region.

Several methods have been used to reduce the cladding diameter of the fibre to enable access to the evanescent field:

- polishing or D-shaped method;
- chemical etching.

The material of the cladding determines the best process to be used to remove it and, as optical fibres used in telecommunication has a cladding of silica; chemical attack is the preferred solution to remove the cladding.

#### 4.4.1.1 D-shaped fibre

D-shaped optical fibre provides an alternative to circular fibre for creating in fibre optical devices because of the proximity of the core to the flat side of the fibre. It can have an elliptical core. The elliptical core supports two fundamental modes, one polarized along each of the axes of the core. The mode polarized along the vertical (short) axis of the core has a lower effective index of refraction than the mode polarized along the horizontal (long) axis of the core. Thus, the vertical mode has a lower mode confinement, meaning that a larger portion of the modal energy resides in the cladding. The geometry of the single mode D-fibre offers increased evanescent field strengths for interaction with surrounding material. This geometry also provides access to the evanescent field of the propagating light without significantly weakening structural integrity (Gordon, 2007).

D-shaped fibre can be manufactured by polishing the side of the fibre, mechanical lapping by making a groove through the fibre by using a large diameter cylinder (Cordaro *et al.*, 1994), by drawing D-shaped fibre during fibre manufacturing process using a D-shape preform (Renner *et al.*, 2003) or using wet chemical etching (Zaatar *et al.*, 2000). As the fibre cladding is reduced to expose the core to air, the effective index of the fibre can be changed, resulting in a shift of the Bragg

wavelength and bandwidth broadening. The use of mechanical polishing for the production of the D-section may put at risk the strength and durability of the sensor. In some cases special fibres are also needed, which would raise the costs and limit the possible applications.

#### *4.4.1.2 Etched, thinned or reduced cladding FBGs*

If the fibre cladding diameter is reduced symmetrically along the grating region, the effective RI is significantly affected by the external RI. The resultant FBG is often termed as an etched, thinned or reduced cladding FBG. A shift in the Bragg wavelength combined with a modulation of the reflected amplitude is expected as explained in section 4.4.1. It should be noted that in both D-shaped fibre and etched gratings, the strength of each sensor was greatly reduced as compared to un-etched fibre.

##### *(a) Theoretical analysis*

A theoretical analysis provided the relationship between outer cladding diameter and the shift in the Bragg wavelength. FIMMWAVE from Photon Design was used for this analysis. FIMMWAVE is a generic, fully vectorial mode finder for 2D+z waveguide structures, which may be of almost any geometry, including SOI, polymer and etched GaAs/AlGaAs waveguides, as well as single and multicore fibres (Photon Design).

Figure 4-14 depicts the resultant dependence of the wavelength shift on the surrounding RI, where it is evident that a shift of  $\sim 2$  nm (difference between fibre core i.e.  $\sim 1.45$  RIU-air RI i.e.  $\sim 1.3$  RIU) indicates complete removal of cladding.

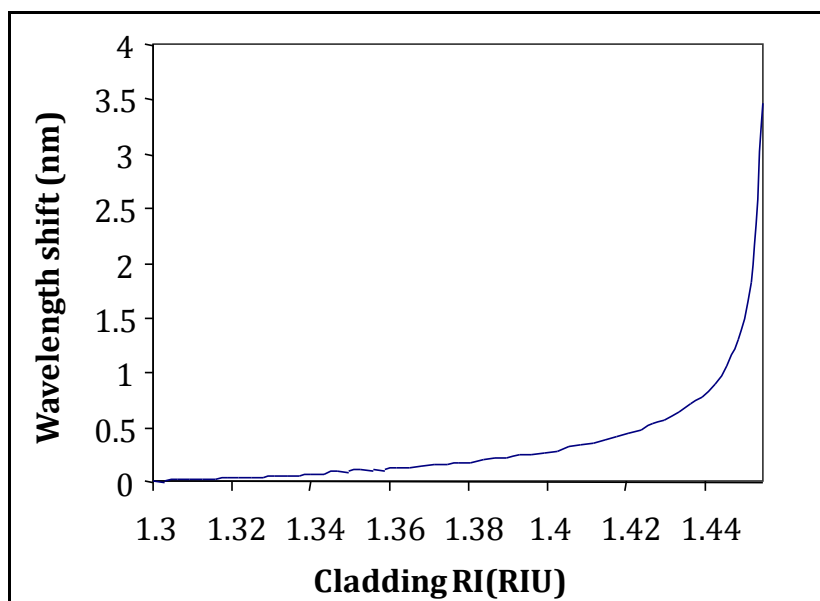


**Figure 4-14** The theoretical representation of shift in Bragg wavelength with outer RI for a standard SMF 28 fibre core (Brodzeli *et al.*, 2009b)

*(b) Experimental analysis*

Reduced cladding FBGs have been successfully demonstrated by using hydrofluoric (HF) acid based etching. The etching of fibre based on HF acid has been reported in (Laine *et al.*, 1999), where a bare fibre was mounted on a translatable stage above a convex meniscus of HF. This method allowed the etching of small lengths of fibre and careful handling is required due to the design of the technique. Another method involved an etching fixture, which was fabricated in two halves out of lexan plastic. An etching well was machined into the lexan to hold the HF and the fibre was mounted onto the fixture and attached at each end by epoxy (Lyons & Lee, 1999). In yet another etching method (Chryssis *et al.*, 2005), the fibre end containing the FBG was submerged into HF and the resulting etched FBG can only be used in reflection. In (Iadicicco *et al.*, 2003), a special packaging was developed in which a PMMA etching tube with two inlet pipes was used as an etching container. Fibre was used with Teflon recoating and fixed at two ends with epoxy.

A fibre can be etched by bending it into the HF acid container but this method will result in sharp unwanted bends, which result in significant loss of power. Also, care should be taken to keep the fibre straight due to the small diameter of the fibre as

the bending of the etched taper can introduce a chirp in the grating structure, due to uneven etching as depicted in Figure 4-15, where excessive tension caused uneven etching of FBG and resulted in chirp in the spectrum. This type of effect is demonstrated by other authors as well where tension was used to fabricate sampled chirped FBGs (Zhao *et al.*, 2004).

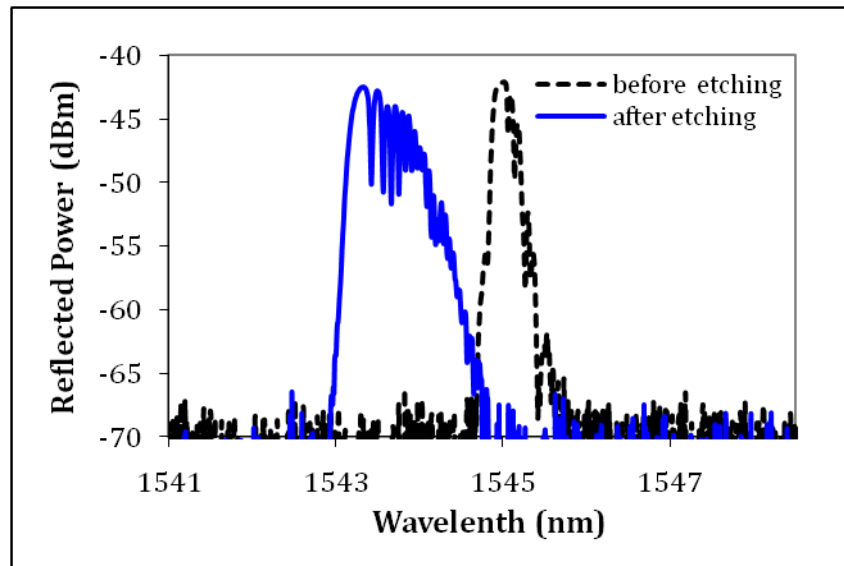


**Figure 4-15** Spectrum of unevenly etched FBG

All of the discussed etching methods are suitable for a very specific application and have specific drawbacks. So a special mount (Figure 4-16) was designed to etch FBGs for this work where the etched FBG can be used in transmission as well as in reflection. Additionally, this mount can etch 6 gratings at one time which is time efficient as HF etching is a time consuming process.

*i. Special etching mount*

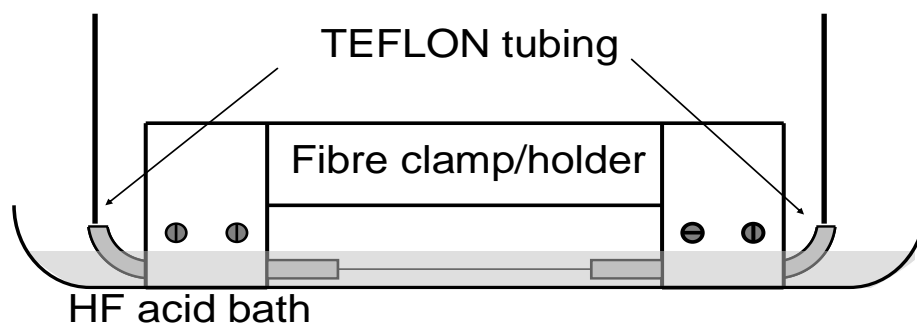


**Figure 4-16** HF acid etching mount

In this mount the fibre clamps were made using Teflon, each clamp holding a single FBG and at least 5 or 6 such clamps can be submerged at same time in the HF bath. A plastic container (non-reactant to HF acid) was used as the HF acid bath. Teflon tubing was used to protect particular sections of the fibre from being etched.

*ii. Fibre preparation for etching*

- FBG was written on the middle section of stripped section of optical fibre using phase-mask writing method;
- suitable Teflon tubing was chosen, which is non reactive to HF;
- a suitable diameter of tubing was used so that it just fit the fibre;
- approximately 3-4 cm long tube was cut and put from the corner of the fibre;
- tubing was used to cover approximately few mm area of stripped section on both sides of the FBG;
- Teflon (DUPONT) spray was used to fill up the any gaps inside the tubing on both tubing ends, to avoid HF acid flow inside the tubing;
- then it was left for 3-4 hours to dry Teflon spray;
- after that, it was mounted on the special mount.

A prepared FBG is depicted in Figure 4-17. Figure 4-18 depicts the set-up used to monitor the etching process. The FBG was connected in reflection through a  $2 \times 2$ , 50% coupler. An erbium broadband source was used to launch light, and an OSA (ANDO, with resolution 0.01 nm) was used to monitor the signal. Real time monitoring was obtained in a computer through GPIB and using LabView.

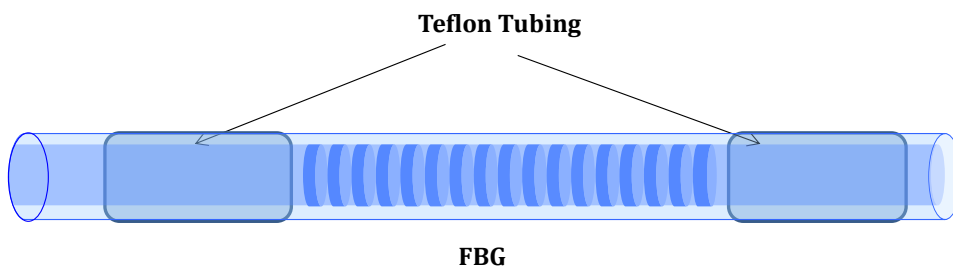


**Figure 4-17** A prepared FBG with Teflon tubing for etching

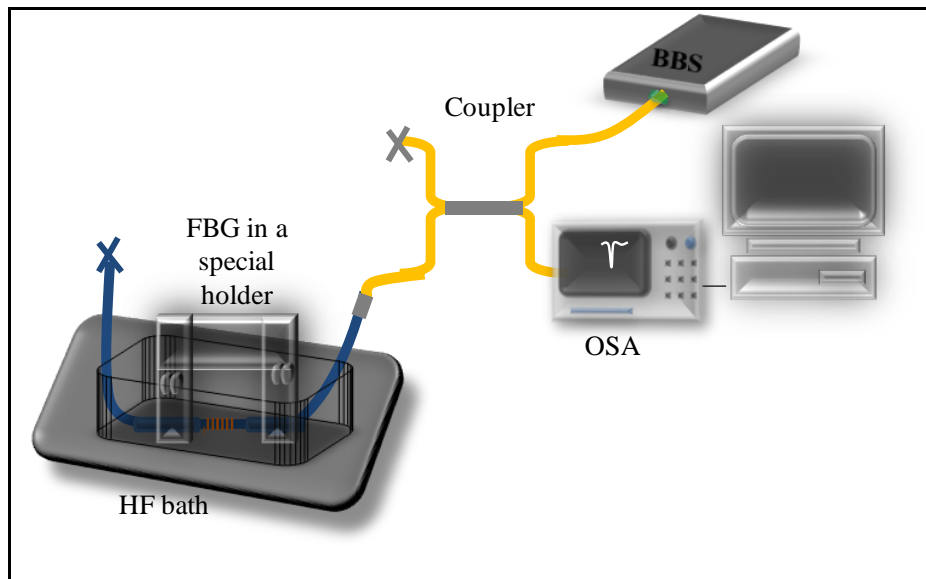


**Figure 4-18** Set-up used for etching of FBG

The shift in the Bragg wavelength was recorded with respect to etching time. Figure 4-19 illustrates the shift of  $\lambda_{\text{Bragg}}$  during the process of etching the cladding off the core of a FBG. The increase of  $\lambda_{\text{Bragg}}$  almost from the start of the process of etching was due to generation of heat caused by chemical reaction of HF with silica glass. After 10 minutes  $\lambda_{\text{Bragg}}$  started to decrease.

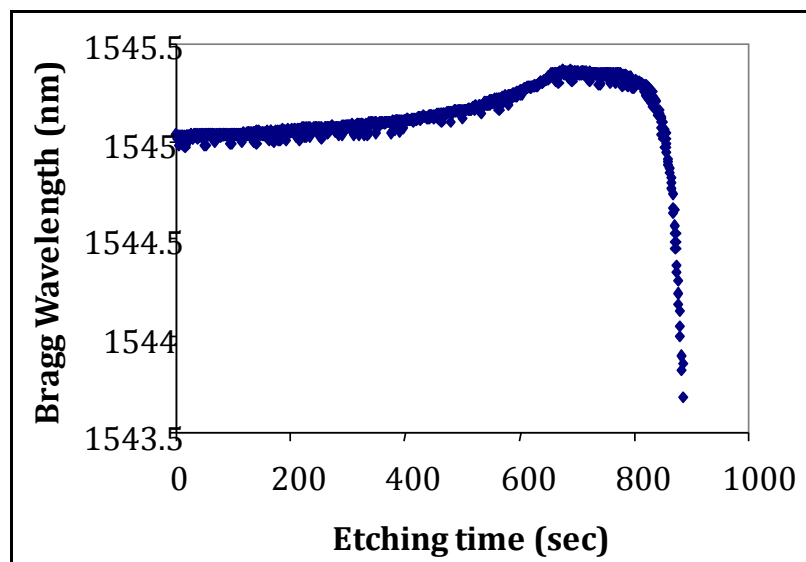


**Figure 4-19** Shift of Bragg wavelength ( $\lambda_{\text{B}}$ ) while etching

A schematic representation of etched FBG is depicted in Figure 4-20, showing that there is no cladding left above the core of the optical fibre.

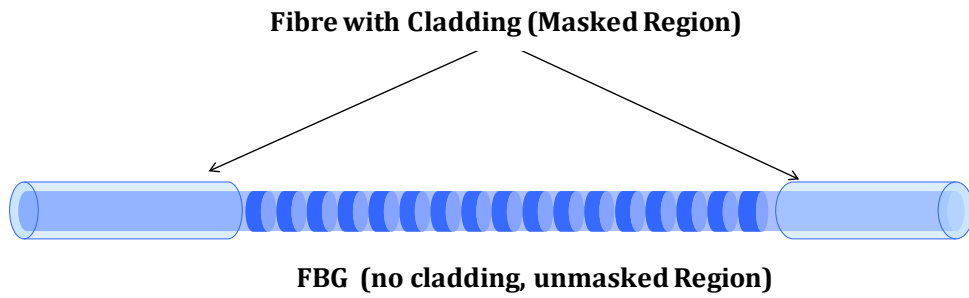


**Figure 4-20** Representation of etched FBG

*iii. Spectral characterization of etched FBGs*

The spectral characterization of thinned FBGs was carried out in reflection using the set-up described in section 3.2.1. Reflection spectra were monitored in air or in water. Several FBGs were etched and characterized in order to optimise the etching time and process.

The process of etching depends highly upon the method used in the etching process. Figure 4-21 depicts the spectrum of the etched FBG when the FBG was etched using Teflon holders but fastened with a tape on both sides. An unwanted chirp in the spectrum was obtained, which can be due to slipping of fibre from the tape resulting in an uneven etching. HF acid also damaged the fibre under the tape.

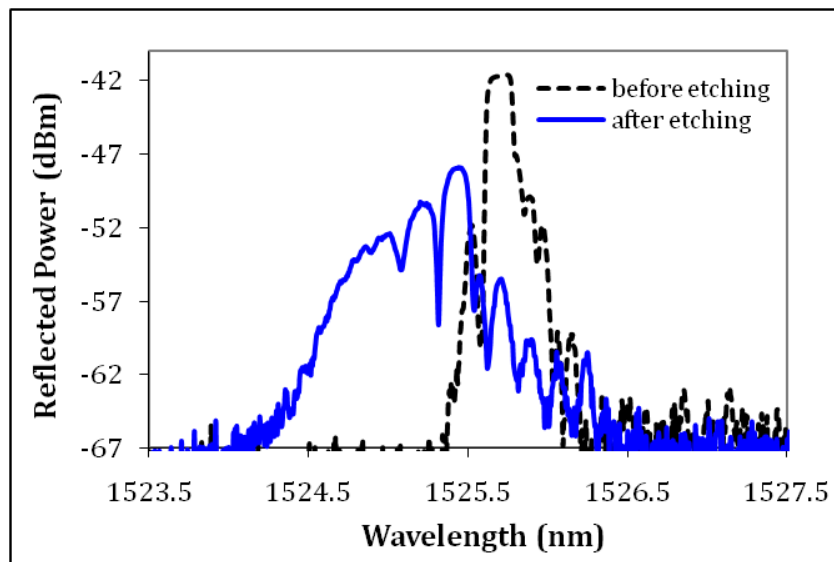


**Figure 4-21** Spectrum of etched FBG, when fixed at the ends on Teflon holder using a sticky tape

Figure 4-22, on the other hand, illustrates the spectrum of a uniformly etched FBG using the special etching mount (Figure 4-16), where the spectral shape before and after etching is the same. A chirped grating was etched to check that the mount was suitable for etching various types and lengths of FBGs. The spectrum of a 40 mm chirped FBG etched using the special etching mount is depicted in Figure 4-23.

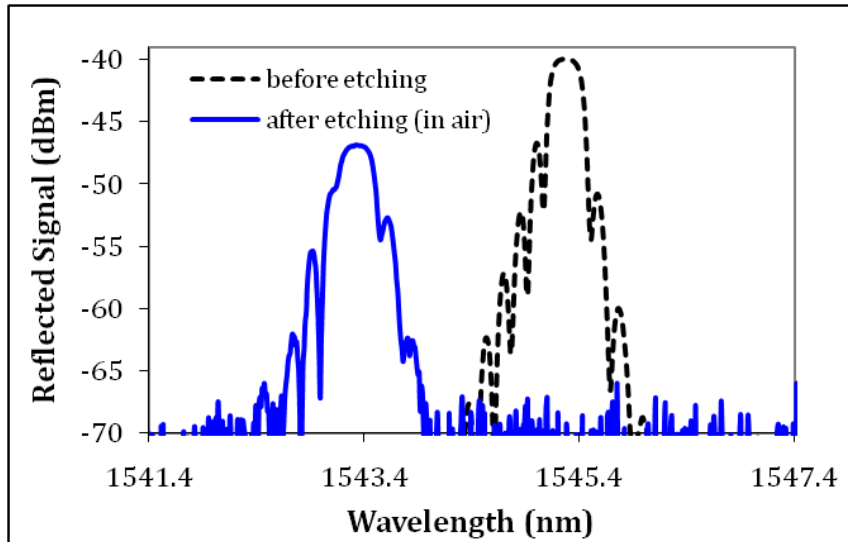


**Figure 4-22** Spectrum of a uniformly etched FBG before and after etching using special etching mount

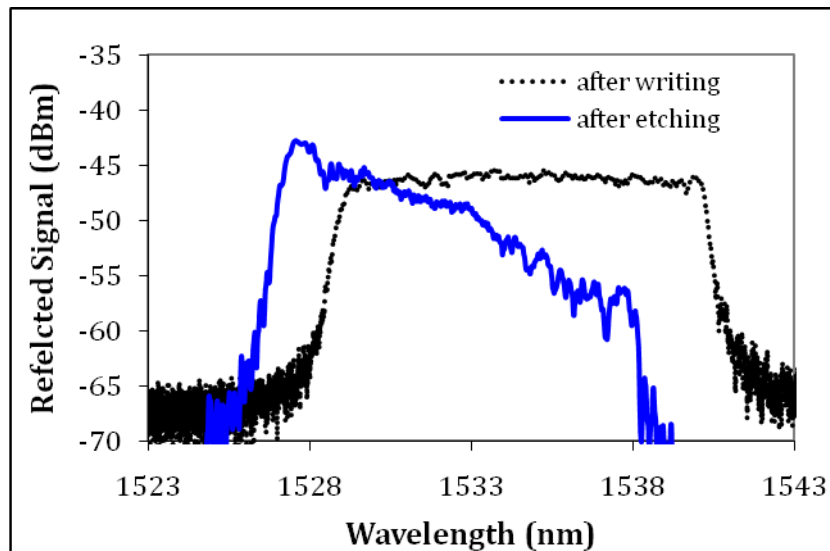


**Figure 4-23** Spectrum of a chirped FBG before and after etching using special etching mount

*iv. Microscopic characterization of etched FBGs*

Figure 4-20 depicts the anticipated results of chemical etching. To evaluate the effectiveness, a microscopic characterization was performed (Section 3.2.2).

Figure 4-24 illustrates the actual DIC images, where (a) depicts fibre with full cladding, and (b) shows the optical fibre core without any cladding around it. Figure 4-24 (c) an unclad fibre with the complex FBG periodic structure is visible (discussed in section 2.2.4.2 (e)); there is no cladding left around the fibre indicating completely etched FBG.

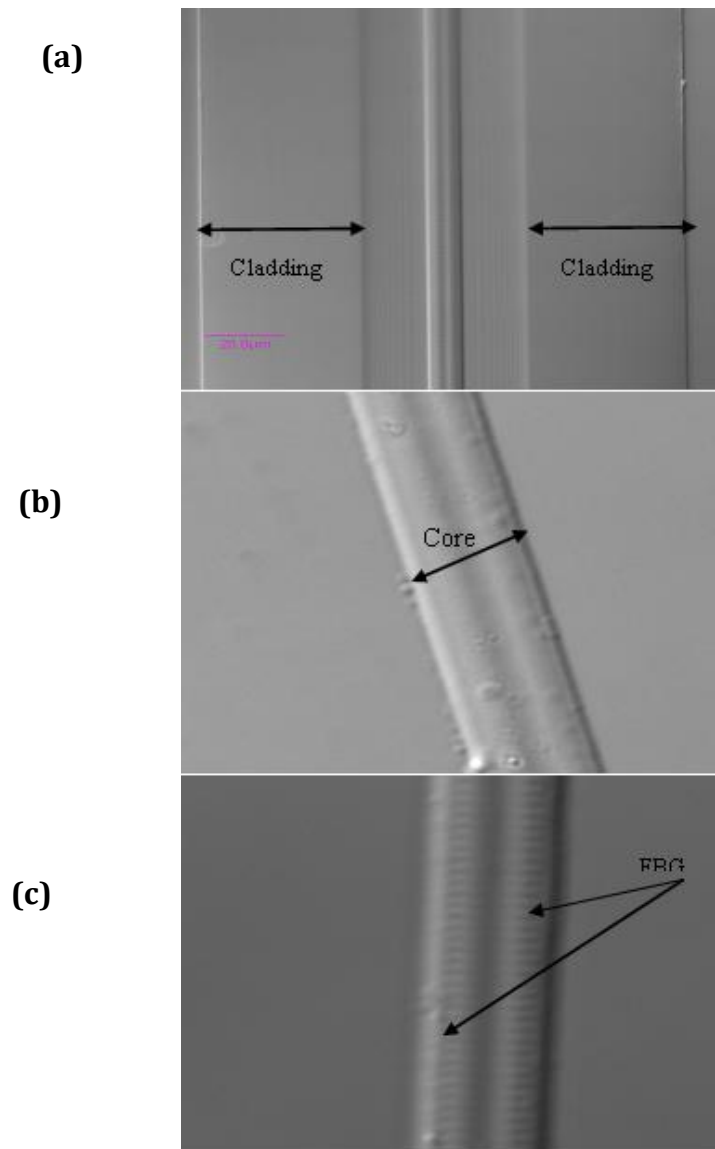


**Figure 4-24** DIC images of (a) un-etched FBG (b) etched fibre without FBG and (c) etched FBG

## 4.5 Applications of Etched FBGs

### 4.5.1 Etched fibre refractometer

The light propagation phenomenon in a reduced cladding fibre was explained using a double cladding fibre with a theoretical model and numerical simulations. If the effective RI of the core and inner cladding is less than the RI of outer medium, a propagation mode will couple with a propagating wave in the outer medium with same propagation constant. In this case the guided mode of the fibre then becomes a leaky wave (Kawakami & Nishida, 1974).

In our experiment we tested this phenomenon in a partially etched fibre (produced as discussed in section 4.4.1.2) present adjacent to the edge of the FBG. This fibre was partially etched along with the FBG. A partially etched fibre has a core and some portion of the original cladding. When the outer RI becomes equal or greater than the core-cladding (portion of cladding left) RI, the guided wave becomes leaky and no reflection will be obtained. As Figure 4-25 illustrates, there was no reflection when the outer RI becomes equal or greater than the core effective RI as expected. This type of etched fibre can be used along with FBGs in switches to swap channels.

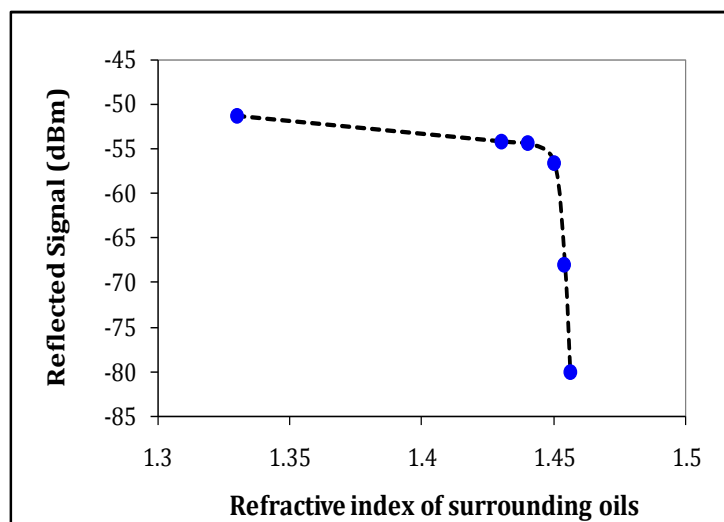


**Figure 4-25** Reflected power intensity of an etched fibre with different surrounding RI

For an etched FBG, where the reflection spectrum of a FBG before etching, after etching and after changing the surrounding RI is illustrated in Figure 4-26. Here

the shift in the FBG Bragg wavelength suggests that the FBG was not fully etched ( $\sim 0.3$  nm shift, refer Figure 4-26), whereas fully etched FBG have shift of  $\sim 2$  nm or more (difference in refractive index of core and air, refer Figure 4-14). An oil (Cargille Series AA) with RI  $1.640 \pm 0.0002$  at  $25^\circ\text{C}$  (with RI sufficiently higher than the RI of the core) was dropped on the edge of the etched FBG, and it is clear from Figure 4-26 that the reflectivity reduced to zero. So in this way, by using an etched fibre and a FBG (can be un-etched), an optical switch is possible for communication applications. Furthermore, an etched optical fibre can be used for intensity-based RI measurements, where the RI of a liquid can be monitored in terms of change of reflectivity of the signal.

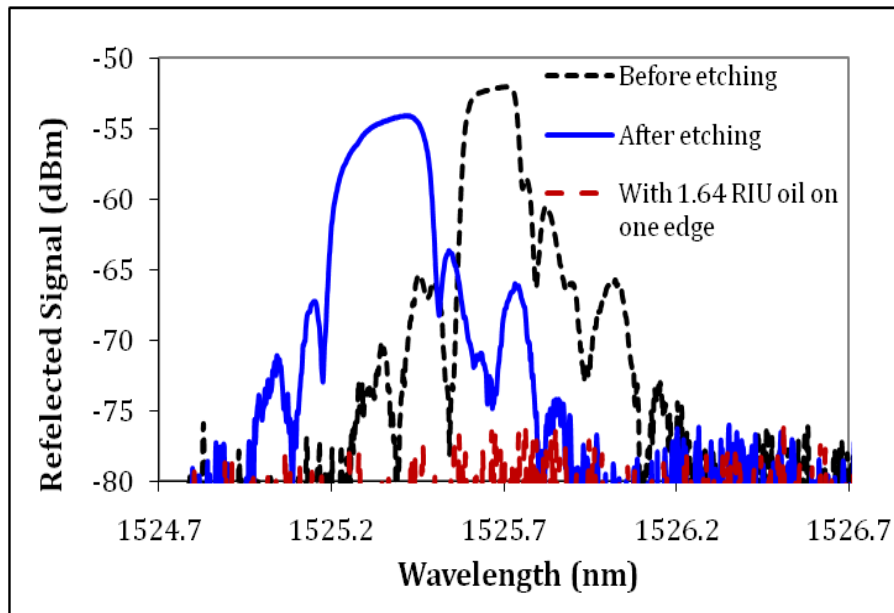


**Figure 4-26** Reflected power of a partially etched FBG with the surrounding RI greater than the core RI

#### 4.5.2 Liquid RI sensor based on etched FBGs

A uniform FBG was fabricated using a using the standard phase-mask writing method as discussed in section 3.1. The FBG region was exposed by etching the cladding of FBGs (refer section 4.4.1.2). The spectrum of a uniform FBG before etching and after full etching of the cladding is depicted in Figure 4-27, where a shift in the Bragg spectrum to lower wavelengths is observed due to the change in the effective RI as given by equation 4-4.

To test the performance of the reduced cladding sensor as a RI sensor, different glycerine compositions were prepared and standard oils (Cargille Series AA) were used. The etched FBG was submerged into the prepared glycerine solution and reflected signal was recorded using an erbium BBS and OSA (resolution 0.01 nm). Before each measurement, the sensor was submerged into isopropyl alcohol to clean any residue left from the previous measurement. The Bragg wavelength was calculated by using FWHM function in OSA and averaged for 10 scans taken for each measurement point.

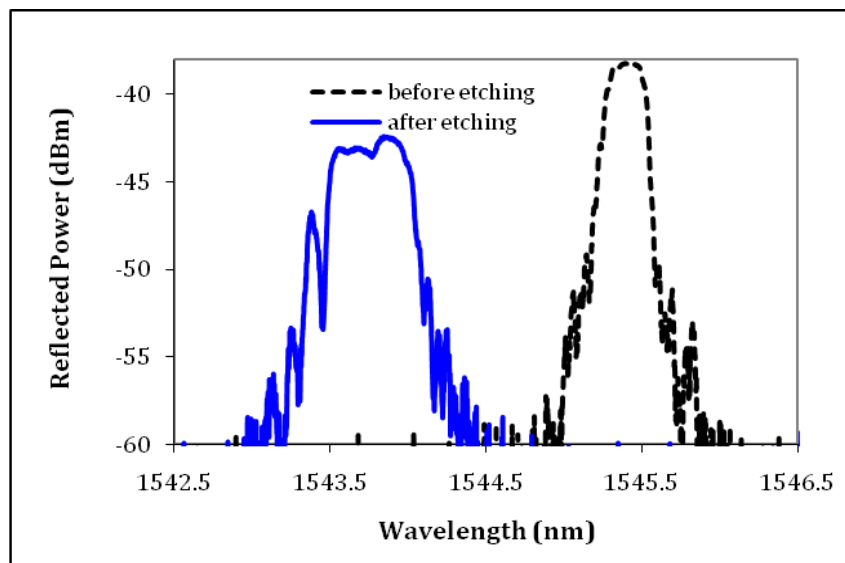


**Figure 4-27** Spectrum of a uniform FBG before and after etching

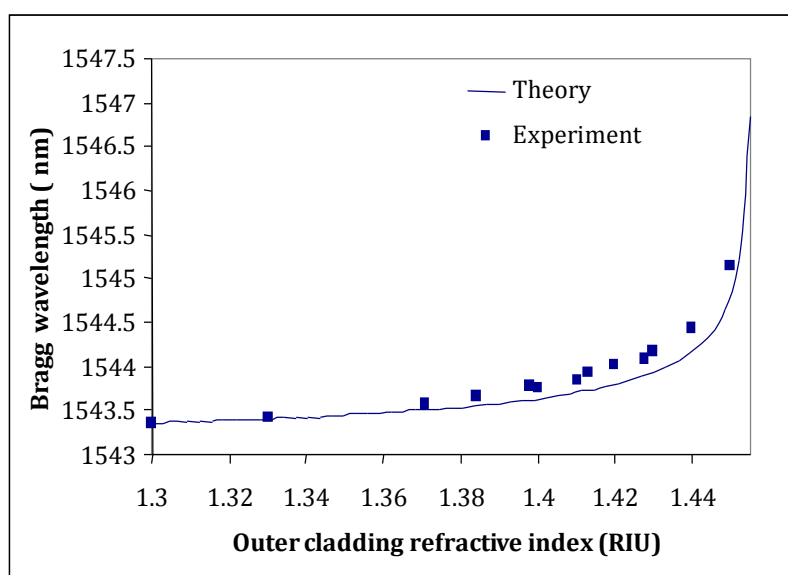


**Figure 4-28** Bragg wavelength shift with respect to RI (Bal *et al.*, 2010e)

Figure 4-28 illustrates the shift in the Bragg wavelength due to glycerine concentration solutions (in water), corresponding to distinct refractive indices. The experimental results are also compared to the theoretical wavelength shift when varying the outer cladding index (Section 4.4.1.2 (a)). The results indicate good correlation between theory and experiment, and agree well with the results presented by other authors (Iadicicco *et al.*, 2004). A small mismatch between these could be due to the difference in core RI; in the theoretical analysis a core RI of  $\sim 1.45$  RIU was used.

The fabricated sensor is of high sensitivity whose response is independent of the power fluctuations of the source. However care was taken to avoid any false results due to bending or straining the etched fibre by taking repeated measurements. In practice a purpose-designed packaging is required to eliminate such effects.

#### 4.5.3 Performance of etched FBGs for longitudinal strain

The axial (or longitudinal) strain response of fibre Bragg gratings arises due to both the physical elongation of the sensor (and corresponding fractional change in grating period), and the change in fibre index due to photo-elastic effects, whereas the thermal response arises due to the inherent thermal expansion of the fibre material and the temperature dependence of the RI (Section 2.2.4.4). The etched FBGs were tested for longitudinal strain and results were compared with un-etched FBG. For this evaluation three FBGs with different cladding diameter were chosen. Table 4-2 shows the FBG characteristics used for this purpose.

FBG1	Un-etched (Full cladding) diameter $\sim 125 \mu\text{m}$
FBG2	Etched for 15 min (a portion of cladding was removed) diameter $\sim 65 \mu\text{m}$
FBG3	Fully etched (no cladding) diameter $\sim 10 \mu\text{m}$

**Table 4-2** Details of FBGs used for longitudinal strain sensing

The set-up used for longitudinal strain is depicted in Figure 4-29 and was the same as that used by other authors (Trpkovski *et al.*, 2005). In this arrangement longitudinal strain was applied with the help of weights attached to the free end of

fibre and the corresponding signal was monitored in reflection. The weight was converted in strain using Hooke's law i.e.  $\epsilon = mg/AE$ , where  $m$  is the applied mass,  $A$  the cross sectional area of the sensing fibre with a value of  $1.23 \times 10^{-8}$  for a fibre with a diameter of  $125 \mu\text{m}$  and  $E$  is the Young's modulus for fused quartz with a value of  $7.31 \times 10^{10} \text{ N/m}^2$  (Wagreich et al., 1996). The same set-up can be used to measure temperature, through use of the tube oven. The response of these FBGs is plotted in Figure 4-30 with respect to applied longitudinal strain.

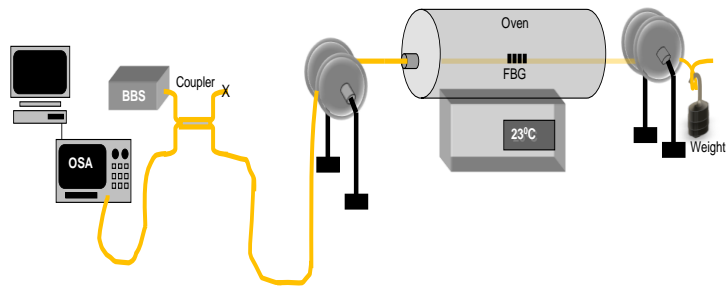


**Figure 4-29** Set-up for longitudinal strain measurement (Trpkovski *et al.*, 2005)

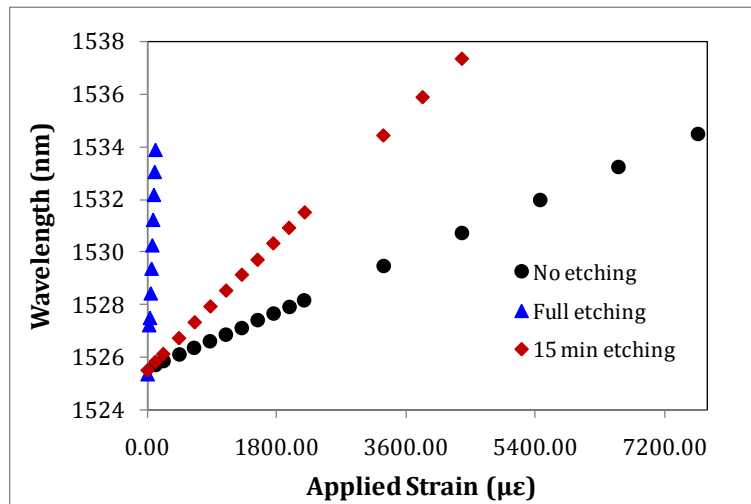


**Figure 4-30** FBGs wavelength shift with applied longitudinal strain

The results indicate that reduced cladding FBGs requires less force (sensitivity  $\sim 0.0027 \text{ nm}/\mu\epsilon$  for 15 min. etched FBG) for tuning as compared to un-etched FBGs (sensitivity  $\sim 0.0012 \text{ nm}/\mu\epsilon$ ). The fully etched FBG requires very small amount of strain to cause corresponding shift (sensitivity  $\sim 0.078 \text{ nm}/\mu\epsilon$ ) in the spectrum. The force required to produce a strain in the fibre is given by Hooke's law where applied stress ( $\sigma$ ) is directly proportional to Young's modulus ( $E$ ) i.e.  $\sigma = E\epsilon$ . So, by

reducing the cross section of the fibre, the Young's modulus is reduced which means a smaller amount of force is required for a given wavelength change in the reduced cladding fibres. Also, for a lower Young's modulus (low cross-section area fibres) a greater longitudinal strain will be produced for a given stress. These results are in good agreement with (Lyons & Lee, 1999), where authors have shown the behaviour of etched FBGs for different applied strains.

#### **4.5.4 Pi-phase FBGs based on wet chemical etching**

Various fabrication methods and applications of pi-phase-shifted FBGs are discussed in section 2.2.4.2 (e). Depending on the application, each fabrication technique can offer certain advantages over the other or certain drawbacks that would prevent the use of the given phase-shifted FBG. For example, phase-shifted FBGs manufactured with the UV post processing method tend to have a slightly unstable profile due to the uneven annealing of the grating as the RI (RI) along the fibre changes in a non-uniform manner. The method involving the use of a phase-shifted phase mask can be quite inflexible since FBGs at different wavelengths require different phase masks, while the method of etching off the middle of the fibre can result to a fibre being very fragile and difficult to handle.

To explore the versatility of the etching method a new and flexible method for manufacturing spectrally stable phase-shifted FBGs was investigated. The application of the non-uniform wet chemical etching fabrication method developed by the authors was used to induce a phase shift in the uniform grating (Brodzeli *et al.*, 2009b). Etching of the cladding of the FBG containing fibre was achieved by submerging it into a 48% aqueous hydrofluoric acid (HF) solution. Fibre was prepared as discussed in section 4.4.1.2.

Different samples were prepared to introduce non-uniform etching. In one sample Teflon spray was employed in order to mask the central part area of the fibre and consequently modify (slow down) the etching rate at that point compared with the unmasked fibre (Figure 4-31(a)). In the second sample a knot was made in the middle section of the FBG with Teflon tape (Figure 4-31(b)). As expected, the modification of the etching rate along the middle of the fibre resulted in the

production of a thicker diameter fibre along that section (Figure 4-31(c)), which introduces a phase-shift in the spectrum of the grating (Figure 4-32).

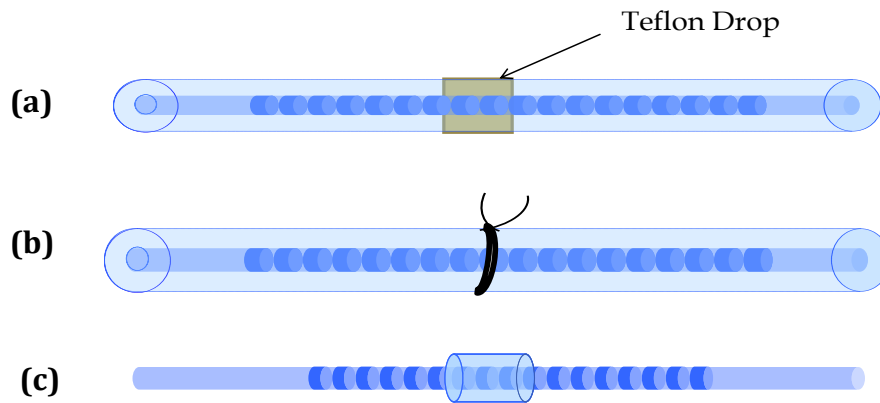


**Figure 4-31** Schematic of FBG (a) with Teflon drop in the middle, (b) Teflon tape knot and (c) an etched phase-shifted FBG

The spectral response of both FBGs samples was monitored in reflection throughout the etching process (set-up in Figure 4-18), and used to control the final diameter of the etched fibre. The FBG with Teflon knot resulted in an unevenly etched micro-structured FBG (Figure 4-33), because the Teflon knot may have resulted in the un-even etching at multiple points due to slipping of the knot during the etching process.

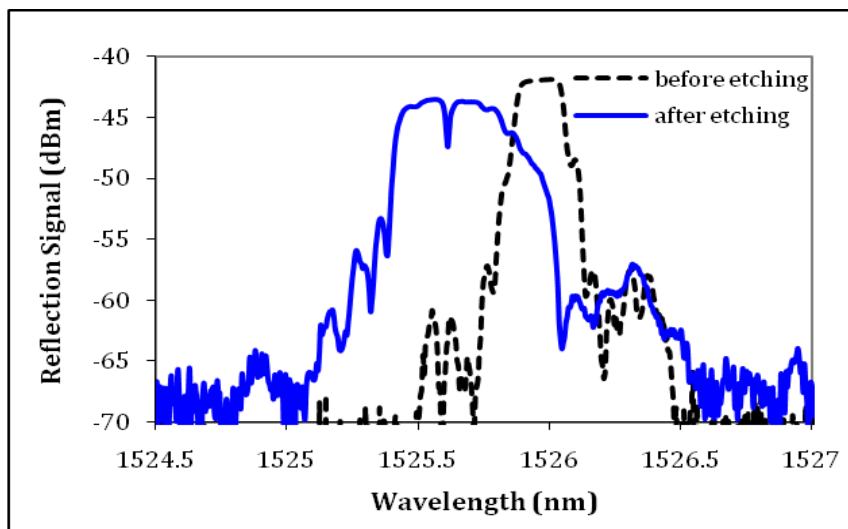


**Figure 4-32** Reflection spectrum of the FBG before (dotted) and after (solid) etching (with Teflon drop)

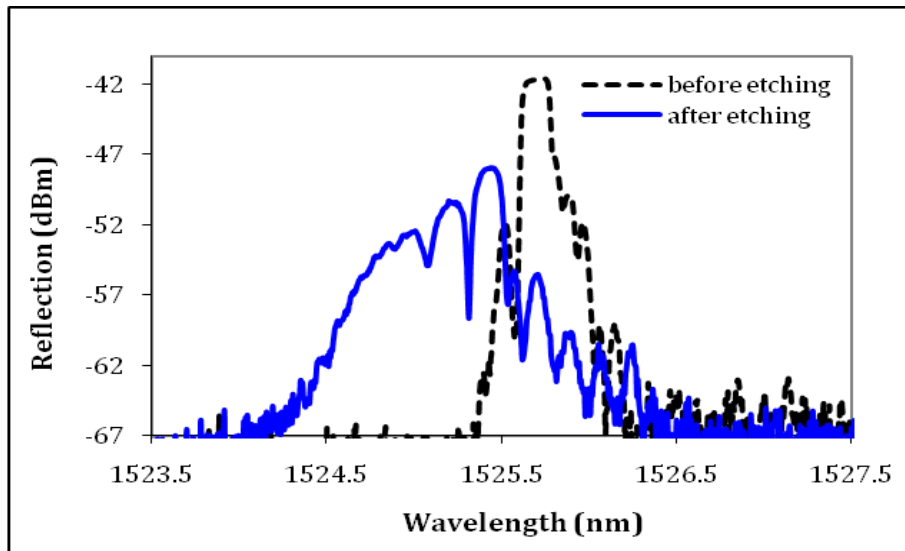


**Figure 4-33** Reflection spectrum of the FBG before (dotted) and after (solid) etching (with Teflon tape knot)

Figure 4-34 (a) & (b) shows the DIC and microscopic images of segments of etched fibre (with Teflon drop) respectively, which shows reduction in cladding and fibre taper at the edges of mask (un-etched region).

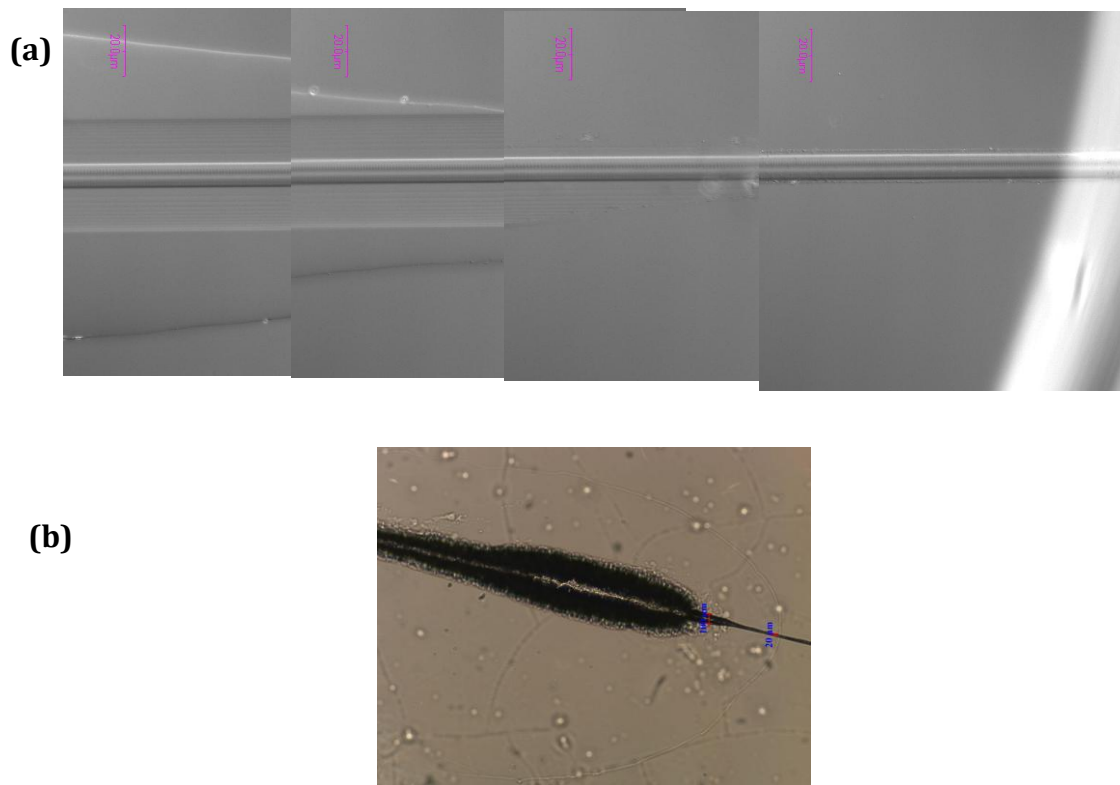


**Figure 4-34 (a)** DIC image of un-evenly etched FBG and **(b)** microscopic image of un-etched fibre region

The effective RI of these phase-shifted FBGs is modified by the cladding etching. The loss in the reflectivity of etched FBGs is due to light coupling loss between etched and un-etched fibre due to different fibre diameters. Full etching of this masked (with Teflon drop) FBG will result in two FBGs: one perturbed pi-phase-shifted FBG that consists of the overall etched and non etched regions of the FBG containing fibre and an unperturbed grating that corresponds to the non-etched portion of the uniform FBG containing fibre (Figure 4-35) (Cusano *et al.*, 2005).

The phase shift in the perturbed grating results due to interference between two etched regions. Figure 4-35 shows the spectrum of a full etched fibre Bragg grating where perturbed grating shows phase shift due to uneven etching whereas unperturbed FBG shows uniform grating due to non-etched middle portion of the grating.

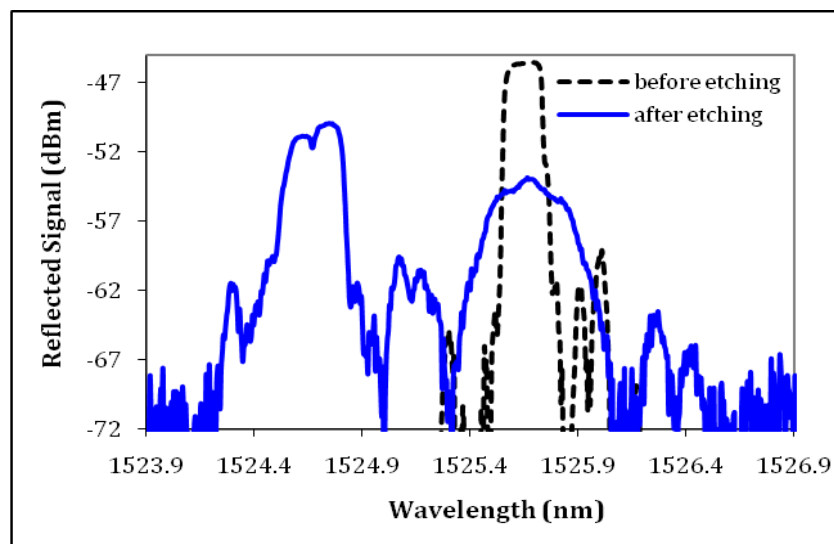


**Figure 4-35** Reflection spectrum of the FBG before (dotted) and after (solid) etching

## 4.6 Conclusions

This chapter describes various RI sensors and their applications. Experimental details and results are provided for a broadband reflector which can measure RI of liquids in terms of intensity of light using the Fresnel equation 2-7. This sensor is demonstrated successfully for measurement of charge of state (SOC) of electrolytic batteries. The estimation of SOC in batteries is very important as it gives user an indication that how long it can be used before recharging. Although different

optical methods are used to estimate it, but all includes either high cost of manufacturing and resources or are complex (discussed in section 4.3.1). In this work a very simple, straightforward and cost effective indicator is demonstrated which provides very reliable results. As most of the fibre optic sensors respond to temperature and there is enough heat generated during operation of batteries so response of sensor can be affected by temperature. In order to compensate variations in response by temperature, a calibration to temperature fluctuations was provided. So this type of sensor can be used as a better alternative to existing SOC of battery indicators. Also, it is quite important to monitor state of charge of several batteries in stock in real time. As batteries consist of electrolyte or gel, while in stock for several months, batteries deplete in charge. A multipoint sensor is proposed for this purpose in which by using FBGs at various wavelengths and optical couplers (or circulators) real time monitoring of SOC of several stock batteries at one time becomes achievable, which is a helpful tool in warehouses to continuously monitor SOC of batteries.

Another application of a multipoint broadband reflector RI sensor was to measure the RI of various liquids at one time. A multiplexing technique of reflective sensor was explored and its use to measure RI of various liquids was studied. The main attractions of this sensor are multiplexing capability, low cost, easy manufacturing process and its simplicity to use and extended lifetime. In this RI sensor the measurements were taken from the cleaved end of the fibre so it is very reliable and, as the FBG part is not used for sensing, it can be used as many times as the only thing required is to cleave the fibre end. The resolution of this sensor is in the range of  $10^{-3}$  RIU which is good enough for several applications. When the RI of fibre becomes equal to liquid under test, it gives no signal. This bifurcation point can be shifted to higher values by using different RI fibre. However, it can easily suffer from fluctuations in the light source which can easily be avoided by calibrating the source and the limitation of intensity of signal due to the configuration of the set-up can be avoided by using a high intensity superluminescent light source (SLD) or by using different configuration where some of the couplers can be replaced by circulators. As it gives reflection for higher

values of refractive indices as well, so this type of configuration can be used to design devices based on liquid crystals (discussed in Chapter 5).

Another RI sensor based on an etched optical fibre is studied. Its prospects for use as a switch in communications networks are also highlighted.

The use of etched FBGs as a highly sensitive RI sensor which was tested to measure different concentrations of glycerine solutions was demonstrated. The etching technique for uniform FBGs was discussed in details and a special mount for uniform etching of FBGs is proposed where 5-6 FBGs can be etched together. It provides resolution of about  $10^{-4}$  RIU. The operation of this sensor is independent of source fluctuation because information is a wavelength modulation. However, as it is a very small diameter fibre, it can easily break and can suffer from micro-bending due to forces in the liquid under test, which could lead to false results. To avoid these deteriorated effects, a special packaging is required (it also requires careful manufacturing process and a special training before handling HF acid). The main precautions which should be considered while dealing with HF are given in Appendix B.

Other applications of etched FBGs such as strain sensing are discussed in detail. A new fabrication method of pi-phase-shifted FBGs is proposed and illustrated.

Different RI sensor applications based on broadband reflector (intensity-based) and etched FBGs (wavelength-modulated) are discussed in details and results of measurements are provided in this chapter. The comparison of RI sensors is presented in the next section, where these sensors are compared in terms of reliability, resolution, and ease of handling.

#### **4.7 Comparison of Intensity-Modulated and Wavelength-Modulated RI Sensor Studied in the Thesis**

Table 4-3 compares the performance of the various RI sensing techniques listed in this chapter with emphasis on major advantages and limitations of each sensor. The performance of a sensor is generally evaluated on the basis of cost of

implementation, life period and accuracy of measurements. The handling, fabrication and implementation were also considered.

Parameters	Intensity-Modulated RI sensor	Wavelength-Modulated RI sensor	Reference
<b>Advantages</b>	<ul style="list-style-type: none"> <li>• Straightforward and simple practical measurement system</li> <li>• Low fabrication cost easy to handle</li> <li>• Long life (sensing head is cleaved fibre end)</li> <li>• Simple and low cost multiplexing capabilities</li> <li>• Requires only intensity spectrum for measurements</li> </ul>	<ul style="list-style-type: none"> <li>• High resolution and sensitivity</li> <li>• Multiplexing capability</li> </ul>	(Bal <i>et al.</i> , 2009a, Krohn, 2000) (Iadicicco <i>et al.</i> , 2004)
<b>Limitations</b>	<ul style="list-style-type: none"> <li>• Comparatively low resolution (However resolution can be improved by using suitable techniques)</li> <li>• Prone to source fluctuations</li> <li>• Possibility of two different RI values giving the same intensity</li> </ul>	<ul style="list-style-type: none"> <li>• High cost</li> <li>• Requires special protective packaging for reduce cladding FBGs</li> <li>• Complex fabrication methods</li> <li>• Comparatively short life as FBG act as a sensing head</li> </ul>	

**Table 4-3** Summary of the performance of the various RI sensing techniques

#### 4.7.1 Comparison of main parameters

Table 4-4 shows a comparison of the performance of the various RI sensing techniques listed in this chapter with emphasis on major advantages and limitations of each sensor. The performance of a sensor is generally evaluated on the basis of cost of implementation, life period and accuracy of measurements. The handling, fabrication and implementation are also considered.

Technique	Resolution (RIU)	Design Complexity	Manufacturability	Cost	Reference
<b>Broadband reflector</b>	$10^{-3}$ - $10^{-5}$	Low	Simple	Low (coupler)	(Bal <i>et al.</i> , 2009a, Zhao <i>et al.</i> , 2009)
<b>Etched fibre</b>	$10^{-5}$	High	Complex	High (etching cost)	(Banerjee <i>et al.</i> , 2007)
<b>Etched FBG</b>	$10^{-4}$ - $10^{-5}$	Very High	Very complex	Very high (FBG+ etching cost)	(Iadicicco <i>et al.</i> , 2004, Liang <i>et al.</i> , 2005)

**Table 4-4** Summary of the performance of the various RI sensing technique

## Chapter 5

### Voltage Sensor: Interfacing Fibre Optic and Liquid Crystal Technology

This chapter outlines a high-voltage sensor for high-voltage transmission lines. This voltage sensor is based on two independently well-established technologies, i.e. fibre optic and liquid crystals (LC) and, a literature review is provided. The use of the broadband reflector (described in section 4.2) for this specific application and the outcomes of this sensor are presented. An electric field amplifying probe (EFAP) to supply sufficient energy to operate high-voltage sensor is proposed and experimentally demonstrated.

#### 5.1 Motivation

Many countries are introducing increasing degrees of competition in their energy markets as part of the process of privatization by the deregulation of the power industry. It is argued that these will translate into substantial economic benefits, which can be redistributed to customers. One of the most important aspects of the power distribution cycle is the ability to measure the quantity and quality of the energy product for each point of power exchange. This makes the development of a low-cost and high-precision voltage measurement technique for high power distribution systems extremely important. Today's current and voltage sensing technology is based on a complicated, large and expensive electrical approach (Sanders *et al.*, 2002). There have been a number of fibre optic current and voltage sensors (Laming & Payne, 1989, Michie *et al.*, 2007, Pacheco *et al.*, 1999, Rahmatian & Jaeger, 1993), but they have resulted in limited commercial success (Sanders *et al.*, 2002) due to complexity and high cost. The emergence of new very high-voltage, i.e. > 800 kV, AC transmission systems and the proliferation of high-voltage DC power transmission systems has placed new demands on voltage measurement systems.

In this work a new approach to this longstanding problem, which would allow direct measurement of up to 800 kV voltage at multiple points along power lines with high precision, is demonstrated.

## **5.2 Introduction to Voltage Sensors**

In transmission lines a distributed voltage sensing device is required which can measure at several points, in order to precisely determine any fluctuations in the power transmission.

### **5.2.1 Background**

Over time there have been different approaches demonstrated for voltage measurements. The optical fibre sensing is an emerging field in the sensor technologies because these have potential advantages over traditional electrical techniques as described previously (Section 1.1). OFSs are immune to electromagnetic interference and thus eliminate the electrical isolation problems between the high-voltage system and the control system. In 1977, Rogers presented a summary of the application of optical methods for measurement of voltage and current in power systems (Rogers, 1977), and, shortly after this, in 1978, optical fibre current sensing was proposed by Smith, using a noise-reduction system in a free-path coupling method (Smith, 1978). Later, in 1979, the detailed extended summary of the optical methods for these measurements was reported by Rogers. These include the magneto-optic effect, the electro-optic effect and the electro-gyration effect. Various detection and noise-reduction techniques were also discussed. A free-path device, which uses a laser beam directed freely towards the transducer, in which signal was also received through a free space coupling. Also an enclosed-path device that utilizes a protected path for light propagation was constructed, which was based on magnetic-optic, electro-optic and electro-gyration effects. The authors successfully demonstrated these devices for simultaneous measurements of electric current and voltage (Rogers, 1979). Later, in 1998, the same author proposed an intrinsic optical fibre current/voltage sensor with sources of noise and noise minimisation procedures where new ideas for vibration immunity were included and experimentally tested (Rogers, 1998).

Optical fibre current sensing has been intensively researched, including sensors based on the Faraday effect in spun highly birefringent optical fibres (Laming & Payne, 1989, Michie *et al.*, 2007), Pockels cells (Rahmatian & Jaeger, 1993), or piezoelectric-modulated FBGs (Pacheco *et al.*, 1999). An optically controlled voltage sensor was demonstrated by Filippov *et al.* based on Pockels effect (Filippov *et al.*, 2000). Another optical approach to high-voltage sensing used glass fibres wound tightly around a piezoelectric quartz cylinder. The stress induced in the fibre through the geometrical changes of the piezo cylinder can then be measured interferometrically (Bohnert *et al.*, 2000a, Bohnert *et al.*, 2005).

### 5.3 Devices based on Interfacing of Liquid Crystals with Optical Fibre

An interest is also growing to use optical fibre with other demanding technologies like liquid crystals and to study some interesting applications. LCs technology for photonic applications is an important topic of research. Liquid crystals (LCs) have electro-optic characteristics and RI compatibility with glass (Table 5-1), allowing the fabrication of devices by combining LCs with optical fibre technology (OFLC). Also LCs allow the dynamic control of their optical properties via applied electric fields, making them very suitable for a wide range of electronic as well as optical applications.

Properties	Optical fibre (light guiding)	Liquid Crystal (optical tuning)
RI (RIU)	1.3-2.4	1.47-2

**Table 5-1** Compatibility of optical fibre and liquid crystal technology for OFLC device

Recent developments in the field of fibre optics (band gap fibre (BGF)) (Pureur *et al.*, 2009), photonic crystal fibres (PCF) (Russell, 2006), electron beam lithography (Tseng *et al.*, 2003) (sub nanometre resolution structures), LCs (new electro optic effect in ferroelectric LCs (Kumar, 2009), new high speed LCs (Chen *et al.*, 2009) and photo alignment of LCs (Chigrinov *et al.*, 2008)) have made it possible to investigate tuneable optical devices. Some possible hybrid devices have been

investigated using Photonic Crystal Fibres (PCFs), an optical fibre which obtains its waveguide properties from an arrangement of very tiny and closely spaced air holes which go through the whole length of fibre (Hu *et al.*, 2009).

Voltage sensing devices based on OFLC technologies have been used for sensing. Wolinski *et al.* proposed photonic crystal fibres filled with LC as a sensing element for electric fields (Wolinski *et al.*, 2007). The authors demonstrated that propagation properties of microstructured fibres filled with nematic liquid crystal (NLC) are strongly influenced by an external electric field. Recently a hybrid voltage sensor based on NLC infiltrated PCFs is proposed, which can sense voltage from 100-850 V (Mathews *et al.*, 2010).

Likewise, Baek *et al.* proposed the usage of liquid crystal cladded fibre Bragg gratings (FBG) (Baek *et al.*, 2006). Indeed, both the reflectivity and Bragg wavelength of such FBGs is influenced by the RI of the liquid crystal cladding. Tabib-Azar *et al.* also reported a simple evanescent field fibre optic electric field sensor constructed by coating an exposed (stripped) fibre core with a polymer-dispersed liquid crystal (Tabib-Azar *et al.*, 2000). Lee *et al.* proposed the usage of liquid crystal core fibres, which is based on the use of hollow core fibre filled with liquid crystal material and with an array of electrodes placed along the fibre. When a voltage is applied, the nematic director aligns along the direction of the applied electric field, which causes modulation of the RI resulting in the appearance of long period gratings (Lee *et al.*, 2002b, Lee *et al.*, 2002a). Similarly, one can substitute the cladding of a conventional long period grating with liquid crystals: when a field is applied, the coupling strength between the core and leaky cladding modes will be affected.

Recent developments in guided optics involve squeezing light out of the bulk and having a large fraction of the optical field outside of the waveguide with low transmission losses. In order to use liquid crystals with optical fibre an extrinsic sensor arrangement shown in Figure 5-1 can be used.

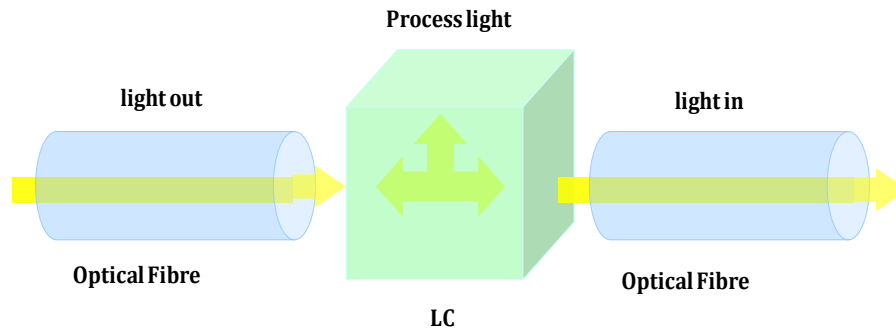


**Figure 5-1** Schematic of a hybrid device based on OFLC

Lastly, in this extrinsic arrangement, liquid crystal can be introduced in a splice by means of ferrules (or Fabry-Perot interferometer) and the power transmission can be monitored as a function of the applied electric field as depicted in Figure 5-1.

Recently different hybrid electromagnetic field photonic sensors were reviewed by Passaro *et al.* In this review intrinsic and extrinsic OFSs for electric and magnetic field measurement were examined. These include the jacketed fibre by magnetostrictive, conductive, electrochromic and polymeric materials and those measuring induced strain by magnetostrictive, electrostrictive and piezoelectric transducers. Extrinsic OFSs exploiting magneto-optic, electro-optic and Joule effects were also discussed (Passaro *et al.*, 2006).

All of the above described (Section 5.2 & 5.3) attempts of development of current and voltage sensors have resulted in limited commercial success (Sanders *et al.*, 2002), due to complexity and thus high cost. Behnert *et al.* proposed a high-voltage sensor based on converse piezoelectric effect of quartz and measured the voltage by a line integration of the electric field. In this scheme the alternating piezoelectric deformations of the crystals were sensed by a common elliptical core dual mode fibre, which is wound onto the circumferential crystal surfaces. The reliability was demonstrated for ac voltages under 520 kV (Bohnert *et al.*, 2000b). It should be noted that at present none of the manufacturers of high-voltage measurement instrumentation offers solutions above 800 kV.

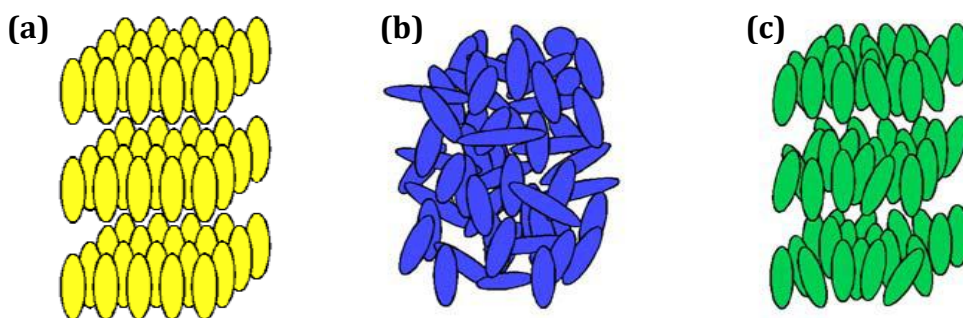
In the following sections a OFLC voltage sensor will be discussed which allows the direct measurement of an electric field up to 800 kV/m at distributed points along

power lines with an precision of 0.1% with measurement distances ranging from 0.02 m up to 200 m, preceded by a brief introduction on LCs.

### 5.3.1 Introduction to liquid crystals

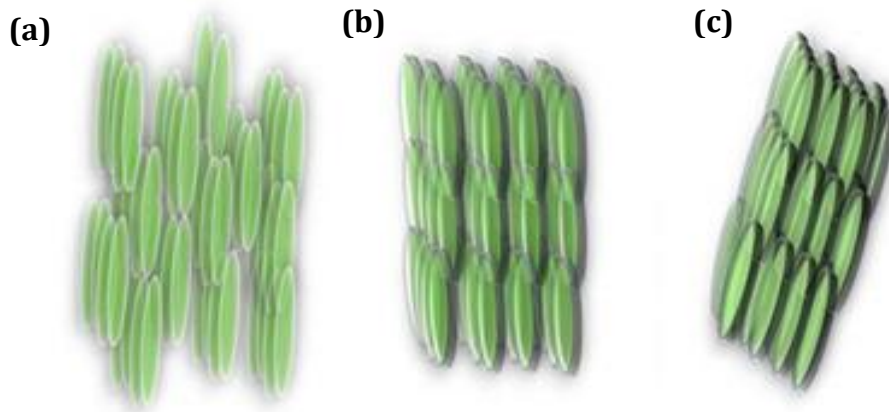
Liquid crystals have a phase in between the liquid and solid phases. So they possess properties of a liquid because they can flow like a liquid as well as properties of a solid because they have an ordered structure. Figure 5-2 (a) depicts a solid where molecules possess orderly arrangement, (b) illustrates a liquid where there is no orderly arrangement and (c) shows an arrangement of molecules in a liquid crystal.

LCs possess different phases depending upon the arrangement of molecules and the dipoles of the molecules help in aligning them along a favoured direction, namely along the director and maintain a highly ordered arrangement.



**Figure 5-2** LC arrangements (a) solid (b) liquid and (c) liquid

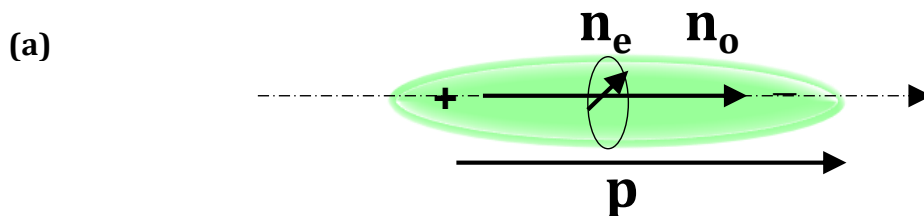
The Nematics have only long-range orientational order and have the director fixed in one direction (Figure 5-3 (a)), while in Smectics (Figure 5-3 (b) & (c)), in addition have long-range positional order in one dimension, resulting in a structure of thin (2-5 nm) layers; several hundred smectic layers thus average up to determine the local optical properties. In Smectic A the molecules orient themselves in layers perpendicular to the director (Figure 5-3 (b)) while in the Smectics C, LCs molecules can orient themselves in layers at an angle other than  $90^\circ$  to the director (Figure 5-3 (c)) (Chandrasekhar, 1992). The well known LC applications in fibre optics include switches, filters, attenuators, equalizers, polarisation controllers and phase emulators (Chigrinov, 2010, Chigrinov, 2007).



**Figure 5-3** Example of orientation of **(a)** Nematic, **(b)** Smectic A and **(c)** Smectic C

### 5.3.1.1 Electro-optical properties of LCs

The characteristic of liquid crystals that allows for most of its applications is that of changing direction of alignment in response to electric fields. When no external electric field is applied, LCs possess ordinary and extraordinary refractive indices as shown in Figure 5-4 (a) and molecules are aligned in a particular direction. A change in the alignment can be achieved by the application of a strong beam of photons or the application of electric fields. The change in alignment can result in a change of polarisation as well as phase shift of any light passing through it. When external electric field is applied the extraordinary component of the director aligns itself in the direction of the applied field, as illustrated in Figure 5-4 (b) and (c). This feature of LCs have been used to make switches and in display applications. The overall change in RI has numerous applications as well.



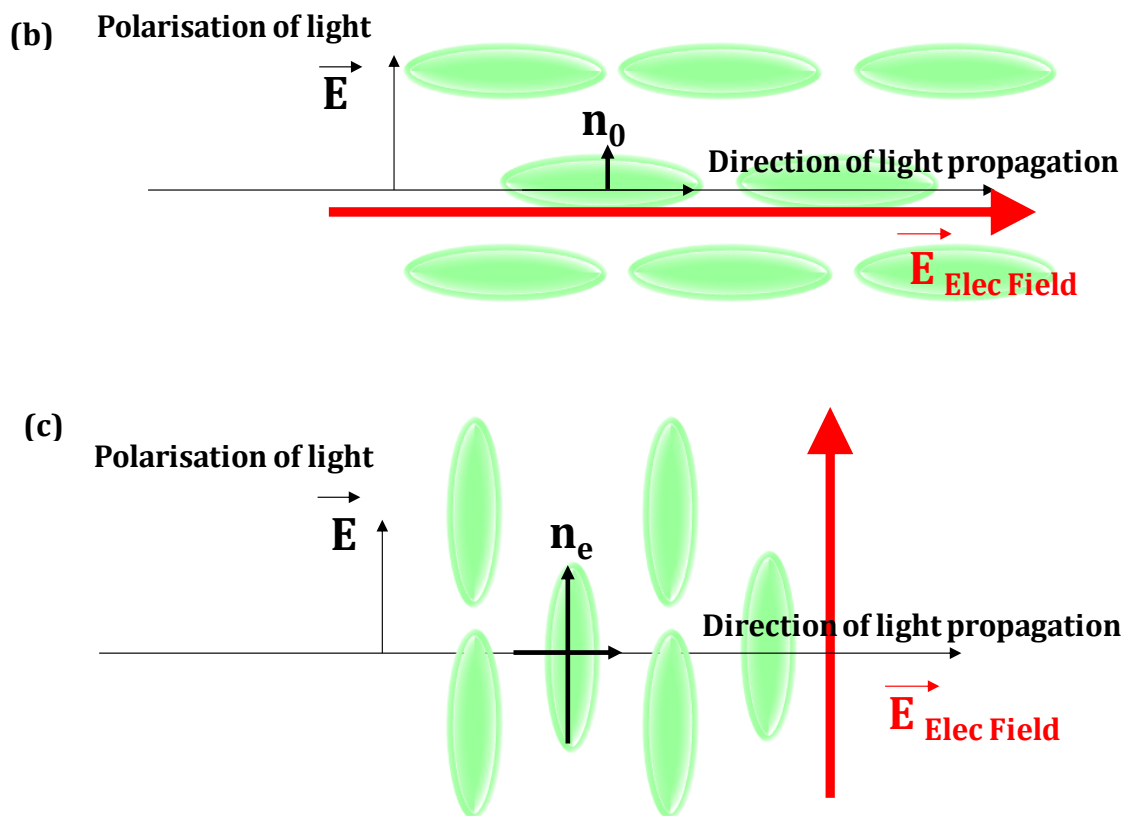


**Figure 5-4** Schematic representing of liquid crystal molecule (a) depicting ordinary and extraordinary refractive indices (b) alignment of molecules when an electric field is applied along direction of propagation of light and (c) alignment of LC molecules when external electric field is applied perpendicular to the direction of propagation of light

Optical properties of liquid crystals are of great interest. They possess birefringence due to orientational ordering of molecules meaning they have different refractive indices along its two directions. Nematic crystals (Figure 5-3 (a)) are the most commonly used liquid phase in liquid crystal displays because they respond to external electric and magnetic fields (Chandrasekhar, 1992). Ferroelectric liquid crystals possess a permanent electric polarisation, and therefore they respond to an electric field without any induction of charge separation. By reversing the direction of an electric field this permanent electric polarisation can be reoriented in two directions. Ferroelectric materials respond very quickly to external electric fields (Collings, 2005, Lagerwall, 2004, Tschierske & Dantlgraber, 2003).

### 5.3.1.2 Alignment of LCs

Initial alignment of LCs is very important because without initial alignment, a drop of liquid crystals appears to have patches where a group of molecules have the same orientation. At the boundary of the crystals where the orientation does not match fault lines appear, breaking up the liquid crystal solution into patches. This is an expected property of nematic liquid crystals whereby the molecules prefer the orientation of the boundary or the surrounding environment. These alignment layers are extensively used to orient the liquid crystal molecule to give a desired optical effect.

There are numerous methods of initial alignment or pre-alignment of nematic liquid crystals. The most common method of pre-aligning liquid crystals has been rubbing of the insulating surface with felt or velvet. Rubbing has various advantages and disadvantages so non-contact alignment method such as use of light or evaporation methods have been use for alignment of liquid crystals. Various other methods used to initially align liquid crystals along the boundary between the liquid crystals and the substrates include surface treatment procedures such as chemical treatment, mechanical abrasion or micro structures. Ion beam, plasma beam, electron irradiation and UV exposure techniques are all practical methods for creating alignment layers. Various methods used to align liquid crystals have been discussed in detail by Martin (Martin, 2008).

To use liquid crystal for switching applications, after initial alignment an external electric field can be used to realign LC molecules, as explained in section 5.6. The application of an electric field affects the alignment of the liquid crystal molecules depending on the field strength as well as proximity to the surface.

## 5.4 Multipoint OFLC Voltage Sensor

As explained earlier the innovative aspect of this sensor lies in novel device designs based on the excellent waveguiding properties of optical fibres, high electro-optic coefficients and sensitivity of liquid crystals together with their proven compatibility (Table 5-1).

### 5.4.1 Principle of operation

The principle of operation of this multipoint RI sensor is similar to that described in section 4.2.1 & 4.2.2. The intensity of reflected light is proportional to the RI of the media from which light reflects, i.e.  $n_2$ .

Equation 2-5 and 2-6 gives the reflectivity for orthogonal polarisations of light perpendicular and parallel to plane of incidence respectively.

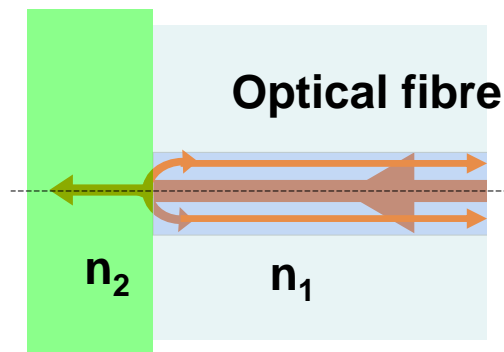


**Figure 5-5** The propagation of light through two transparent materials with different refractive indices when angle of incidence = 0

In case of optical fibre (Figure 5-5) angle of incidence  $\phi$  is 0, so in this case reflectivity is given by equation 2-7. By using equation 2-7, it becomes possible to monitor perturbations of external electric field by surrounding cleaved/polished end of optical fibre with an electro-optic material and measuring intensity of light reflected off the fibre end in similar fashion as depicted in Figure 4-1 (Section 4.2.1).

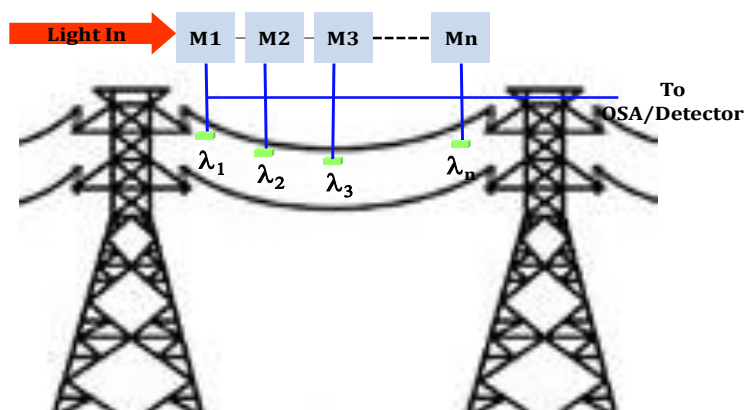


**Figure 5-6** Basic idea of the multipoint sensor

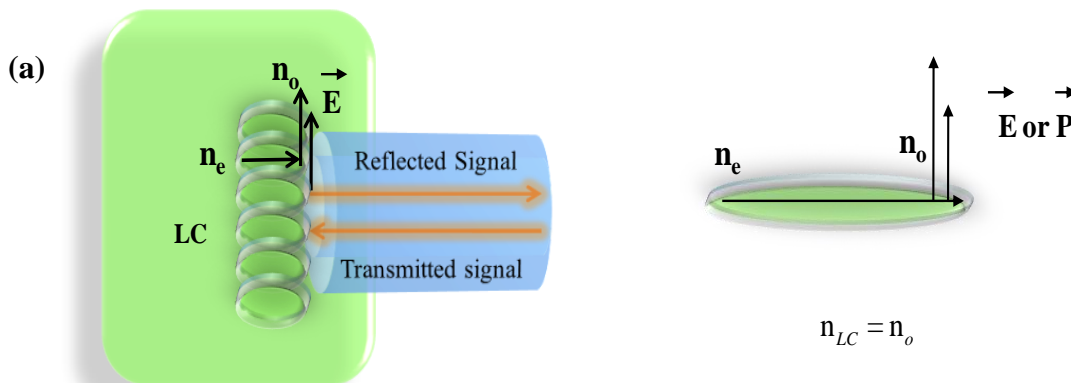
Ability to assign particular wavelength (by using multiplexing capability of FBGs) of light to a certain point where electric field is being measured allows mapping distribution of electric field at various points as given in Figure 5-6, where M1, M2 are different modules as depicted in Figure 4-5.

Light will be reflected from the boundary of the optical fibre and the LC with an intensity that depends upon the difference between the effective RI of the fibre ( $n_F$ ) and that of the LC. The effective RI of LC depends upon the angle between the polarisation direction of light propagating through the fibre and the orientation of the director of the LC molecules at the surface of the fibre end -  $\alpha$  (Figure 5-7 (b)). Figure 5-7 (a) shows the condition when LC molecules are aligned at  $\alpha=0^\circ$ .

$$n_{LC} = n_e n_o / [n_e^2 \sin^2(\alpha) + n_o^2 \cos^2(\alpha)]^{\frac{1}{2}}, \quad 5-1$$

where  $n_o$  is ordinary and  $n_e$  is extraordinary RI of LC. Light reflected off the cleaved end of fibre senses  $n_{LC} = n_o$ , when the electric field between the electrodes is lower than the threshold value and  $n_{LC} \leq n_e$  when it is larger. Substituting  $n_{LC}$  from equation 5-1 into 5-2, it is possible to obtain intensity of light reflected off the cleaved end of the optical fibre while changing RI of LC (Figure 5-8).

$$r_{\perp}^2 = r_{\parallel}^2 = - \left[ \frac{(n_e n_o / [n_e^2 \sin^2(\alpha) + n_o^2 \cos^2(\alpha)]^{\frac{1}{2}}) - n_1}{(n_e n_o / [n_e^2 \sin^2(\alpha) + n_o^2 \cos^2(\alpha)]^{\frac{1}{2}}) + n_1} \right]^2 \quad 5-2$$



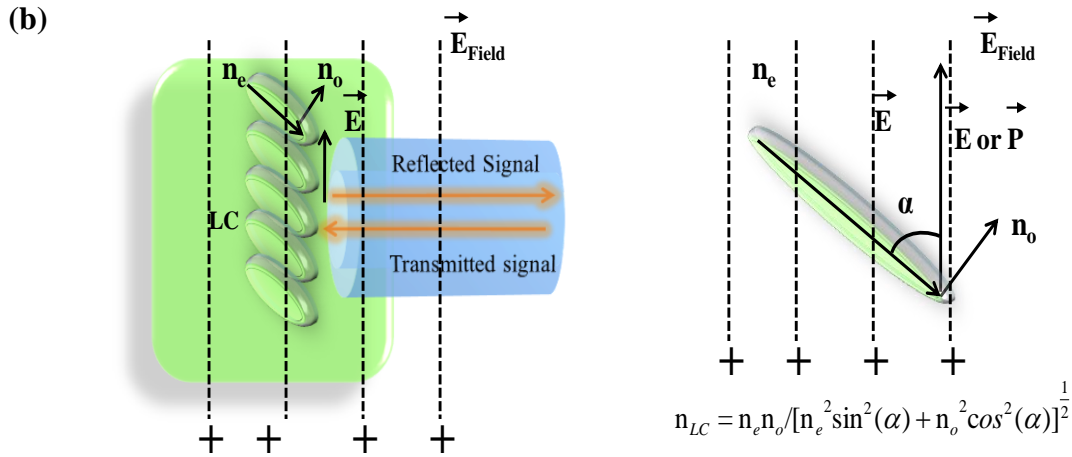


**Figure 5-7** Interaction of light with fibre end and LC **(a)** no external electric field, **(b)** with external electric field

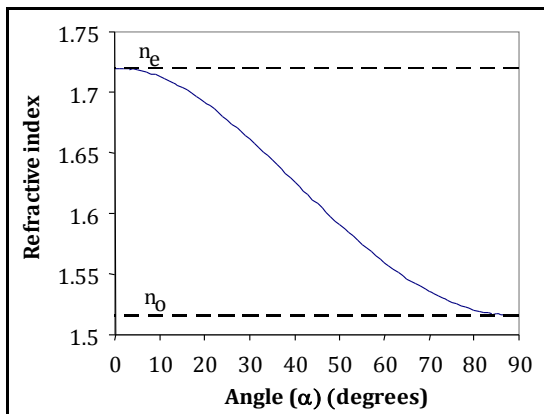


**Figure 5-8** Refractive index vs. angle between the director of the molecule of LC and polarisation of transmitting through LC light (using equation 5-2)

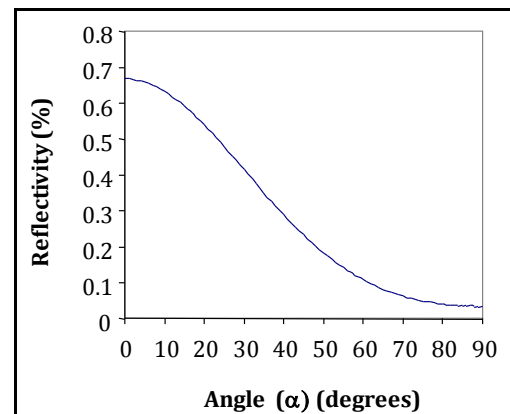


**Figure 5-9** Reflectivity of the cleaved end of fibre emerged into LC vs. angle between the director of the molecule of LC and polarisation of transmitting through optical fibre light

### 5.4.2 Materials and methodologies

Developed multipoint voltage sensor consists of three main parts.

- (a) sensor head containing electro-optic material (LC sensitive to perturbations of the electric field),
- (b) fibre optic circuit multiplexer allowing measurement of electric field at multiple points
- (c) electric field amplifying probe (EFAP) (used to amplify the electric field and to probe it to the LC cell (sensor head)).

(a) Sensor head (SH)

The SH is represented by a cleaved end of a single mode fibre submerged into a LC cell (LCC) (Figure 5-10 (a) & (b)). Any change in the external electric field results in a subsequent change in the LC's RI that can be monitored by the light delivered into the LCC by the optical fibre.

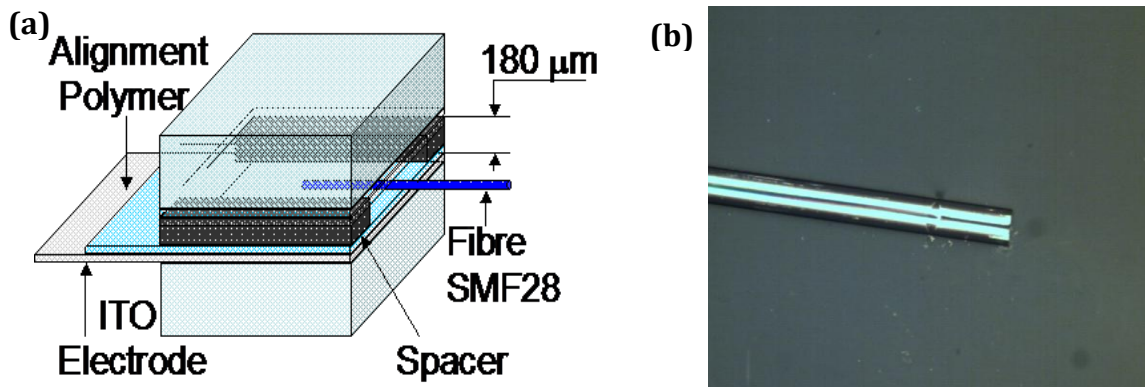


Figure 5-10 (a) Sensor head inside a LCC and (b) Cleaved fibre submerged in LCC

i. Fabrication of liquid crystal cell (LCC)

The LCC was constructed using two glass substrates containing ITO electrodes on the inner surfaces. The thickness of the cell was determined by the thickness of the optical fibre SMF28 ( $\sim 125 \mu\text{m}$ ) and was equal to  $180 \mu\text{m}$ . A polymer film was used as a spacer to form the gap between the substrates of the LCC.

i.i Choice of LC

The gap was filled by LC E7, which is widely used in display applications. The LC E7 (Merck Ltd GB) was used without any further treatments. It exhibits a nematic phase at room temperature. The refractive indices  $n_o$  and  $n_e$  at  $20^\circ \text{C}$  were 1.515 and 1.72 RIU respectively. From the multiplexer characterization (see Figure 4-9 (b)) it was clear that LC with any RI range above or below RI of core of optical fibre can be used for this purpose. And most of the easily available commercial LC possesses RI higher than 1.46 RIU. So any available LC can be used.

i.ii Initial alignment of LC

In this work we achieved the planar alignment of the LC by the standard rubbing method using polymer PIA-3744 (Chisso).

(b) Fibre optic circuit – multiplexer

The module used in this application is, as described in section 4.2.2, capable of measuring voltage at multiple points as illustrated in Figure 5-6. However, only one module was used for the demonstration of LC response with applied voltage.

i. Transmission characterization of LCC

Prior to submerging optical fibre into the LC, the cell was characterized in transmission to determine the minimum voltage required for complete switching. Figure 5-11 shows the bulk optical set-up used to measure the transmittance of the LCC as a function of applied voltage, and the results are given in Figure 5-12. The voltage required for switching of this cell was 50 V.

At this point the cleaved fibre end was introduced in the LCC, where homeotropic orientation of LC molecules on the surface of the cleaved end was achieved by coating it with the VA alignment material JALC 2021.

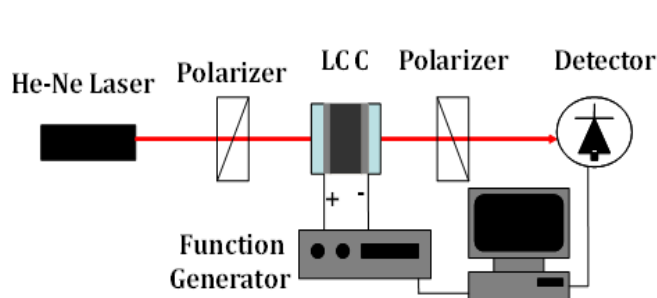


**Figure 5-11** Set-up for characterization of transmittance of LCC

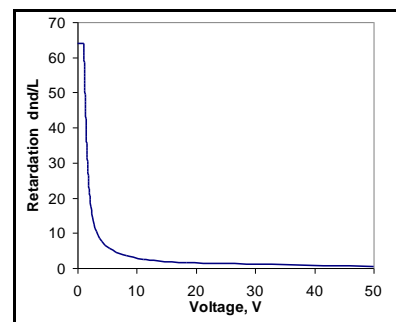


**Figure 5-12** Retardation of 180  $\mu\text{m}$  thick LCC vs. applied voltage (TVC curve)

The sensor was tested by applying a voltage to the LCC containing optical fibre. The voltage required for complete switching was 260 V (Figure 5-13), which is much higher than the 50 V (Figure 5-12) used previously. Experimental data were

compared to the calculated power of reflected signal when changing angle between director and polarisation of light from 0 to 90° using equation 5-2 and using LC - E7 parameters as  $n_e = 1.72$  and  $n_o = 1.515$  (Figure 5-13, Black line).

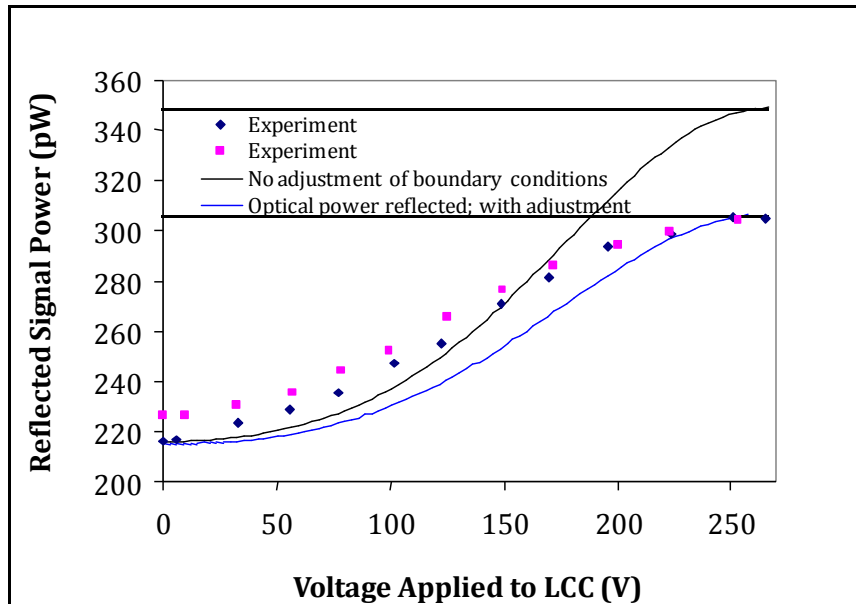


**Figure 5-13** Signal power reflected off FBG vs. external voltage applied to LCC

According to calculation  $p_{power}$  of reflected signal corresponds to 349 pW when complete switching of LCC occurs. In reality reflected signal is equal to 304 pW, which is less than the expected value meaning that RI of LC is less than  $n_e=1.71$  RIU. From theoretical calculations reflected power of 306 pW corresponds to the angle 26° between polarisation of light and director and from Figure 5-8 corresponding RI was 1.67 RIU.

It was not possible to achieve theoretical RI changes of 1.71 RIU with the application of 270 V to the LCC that is due to the presence of anchoring forces, which do not allow molecules close to the surface of the fibre to align along the electric field (Figure 5-14).

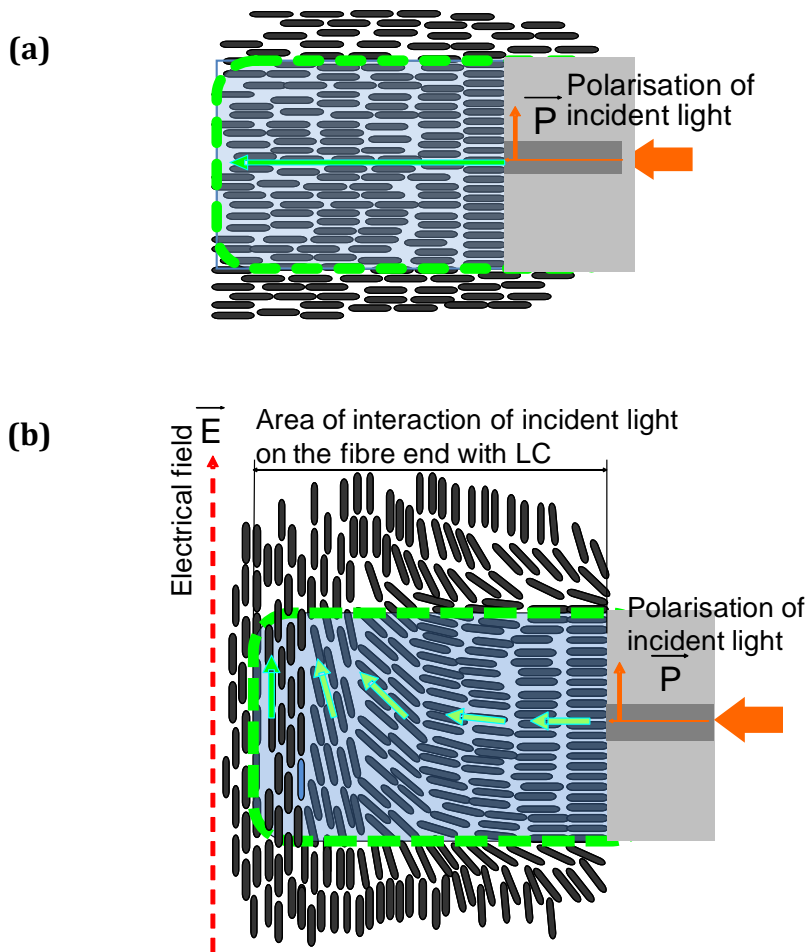


**Figure 5-14** Schematic representation of alignment of LC molecules inside SH around cleaved fibre end; **(a)** no field, **(b)** with electric field

Light, while leaving the fibre at the cleaved end transmits into the evanescent field and interacts with LC. Evanescent field is represented by the square (Dotted line) extended from the fibre end into the LC. When no voltage is applied to the LCC angle between the director of the molecules and polarisation of incident light was equal to  $90^\circ$ . Application of the external electric field reorients molecules in the direction of the field. Due to the anchoring forces the director of the layer of molecules at the surface of the cleaved fibre does not reorient and remains perpendicular to the fibre end. There is some distribution of angle (from  $0^\circ$  to  $90^\circ$ ) between director and polarisation of light in LC present in the space occupied by evanescent field. The average angle is equal to  $26^\circ$ .

During the characterisation of the transmission properties of the cell, saturated switching was achieved by LC in the bulk, while in case of the sensor, light is

delivered into the LCC by the optical fibre and switching is achieved by reorientation of LC molecules at the surface layer next to the cleaved fibre end. The anchoring energy of the molecules closer to the fibre surface is much higher than in the bulk of LC and requires a higher voltage.

There is some mismatch between the two measurements, which is due to the “walk off” of the polarisation of light during the experiment. The LCC is a polarisation sensitive device but the fibre (SMF28) used in the experiments was not polarisation maintaining. The stability of the measurement could be greatly improved by the use of a polarisation maintaining fibre.

*(c) Electric field amplifying probe (EFAP)*

Results indicated that  $\sim 270$  V or more voltage is required to switch  $180 \mu\text{m}$  LCC (Figure 5-13). This voltage will create an electric field  $150 \text{ kV/m}$  inside the LC material. Electric field inside LCC ( $E_{LC}$ ) is lower than the outside when placed into an external electric field ( $E$ ), due to the dielectric nature of the LC (dielectric constant of LC,  $\epsilon = 10$ ) and  $E_{LC} = E_{ext}/\epsilon$ . External electric field under test corresponds to  $100\text{--}400 \text{ kV/m}$ , which translates into  $10\text{--}40 \text{ kV/m}$  inside LCC (Figure 5-15). To increase the voltage applied to LCC (SH) an electric field amplifying probe (EFAP) was constructed using two probes made of conductive material, placed parallel to each other and perpendicular to the direction of external electric field under test (Figure 5-16).

The EFAP used to test LCC consists of two  $25 \times 30 \text{ mm}$  glass substrates coated with ITO electrodes placed parallel to each other at the distance of  $10 \text{ mm}$  in the uniform electric field.

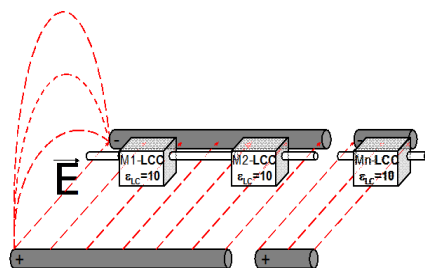


**Figure 5-15** LCC placed inside an electric field

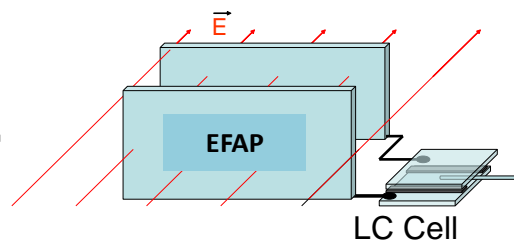


**Figure 5-16** Schematic representation of EFAP connected to LCC (SH)

The LCC similar to one, which will be used in the hybrid voltage sensor but with a smaller gap of 10  $\mu\text{m}$  instead of 180  $\mu\text{m}$ , was constructed. The smaller gap was chosen because it requires lower switching voltages, which can ease the requirements of placing the EFAP into the high external electric fields. The EFAP was placed inside an electric field and the sensor head was connected to the probes of the EFAP as depicted in Figure 5-16.

Prior to connecting to the EFAP the transmittance voltage curve (TVC) was determined by measuring the transmittance of the LCC when varying voltage on the electrodes using the previously described technique (Figure 5-11). It is well known that LC RI change with respect to applied voltage and a point comes when RI changed and molecules tilt in such a way that there will be no reflection or transmission as explained in section 5.4.1. This point is called complete switching of LC. The oscillations in Figure 5-17 shows the response of LC cell to applied voltage means RI of LC changes with applied voltage. It can be seen that at 10 V there are no more oscillations presents (RI changed completely), which indicated that 10 V is required for complete switching of 10  $\mu\text{m}$  LCC (Figure 5-17).

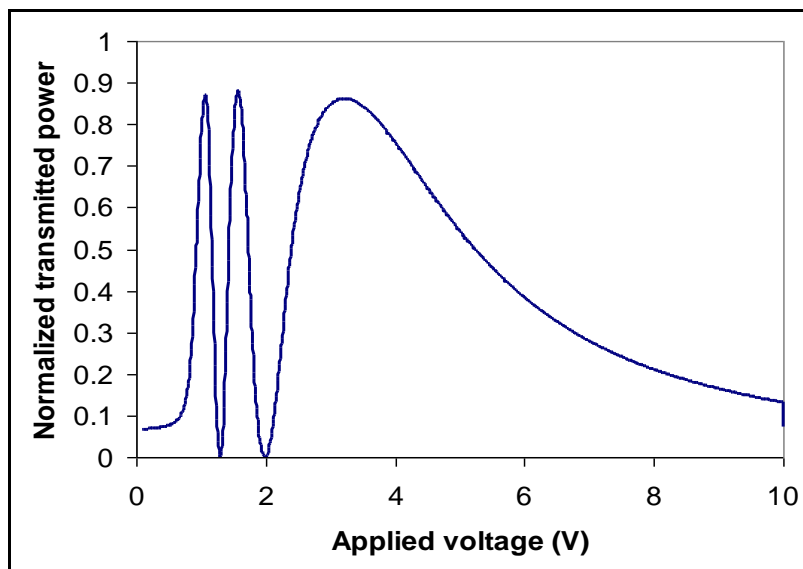


**Figure 5-17** Transmittance of light through the 10  $\mu\text{m}$  gap LCC vs. external voltage

Electrodes of the same cell were connected to the EFAP and TVC was determined by measuring transmittance of the LCC when varying value of electric field surrounding EFAP (Figure 5-18).

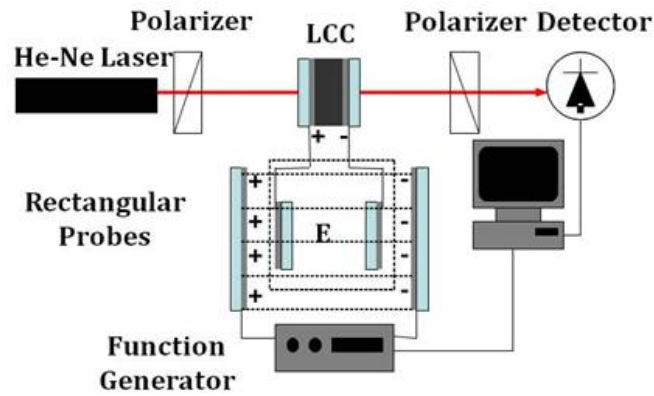


**Figure 5-18** Set-up for demonstrating ability of EFAP to provide enhanced field and switching LCC

An external electric field of 120 kV/m was generating 1.49 V at the output of the EFAP connected to the electrodes of the LCC, which was enough to partially switch it (Figure 5-19). A LCC containing optical fibre requires application of higher voltage, which could be achieved by changing geometrical properties of the EFAP.

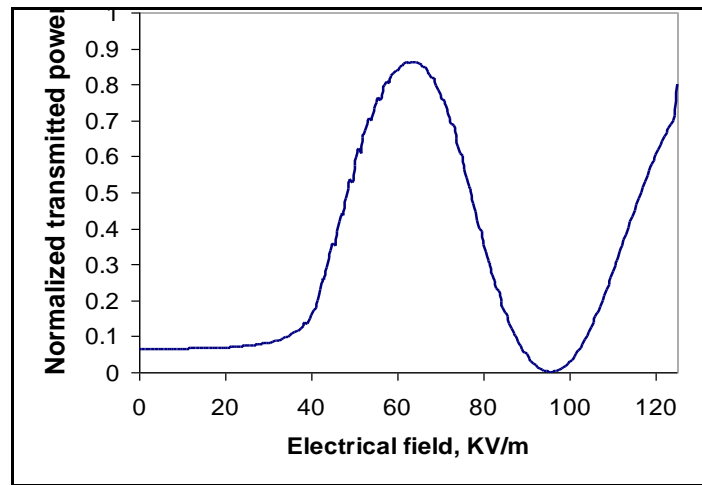


**Figure 5-19** Switching of 10  $\mu\text{m}$  LCC by EFAP placed in an external electric field

### 5.4.3 Characterization of EFAP

Geometrical properties of EFAP were characterized by changing area and distance between the probes of EFAP while measuring output voltage as depicted in Figure 5-20. An external electric field of 2.5 kV/m was created by two aluminium parallel probes of 400  $\times$  400 mm with a separation of 160 mm.

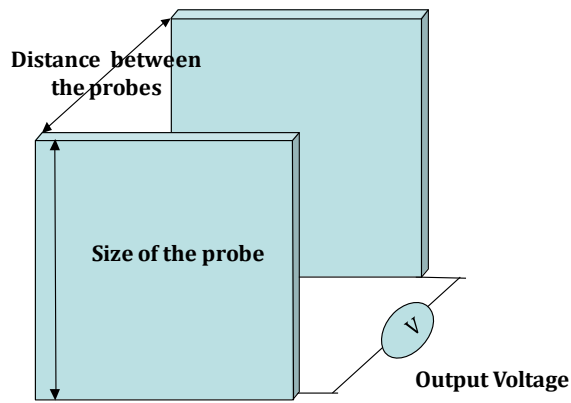


**Figure 5-20** Set-up used to test geometrical properties of EFAP

The size of the probes was much larger than the size of the probes of EFAP (100 × 100 mm, 80 × 80 mm, 60 × 60 mm and 40 × 40 mm). This would guarantee uniformity of external electric field under test related to probes of EFAP. Experimental data of output voltage vs. distance between the probes of EFAP is presented in Figure 5-21.

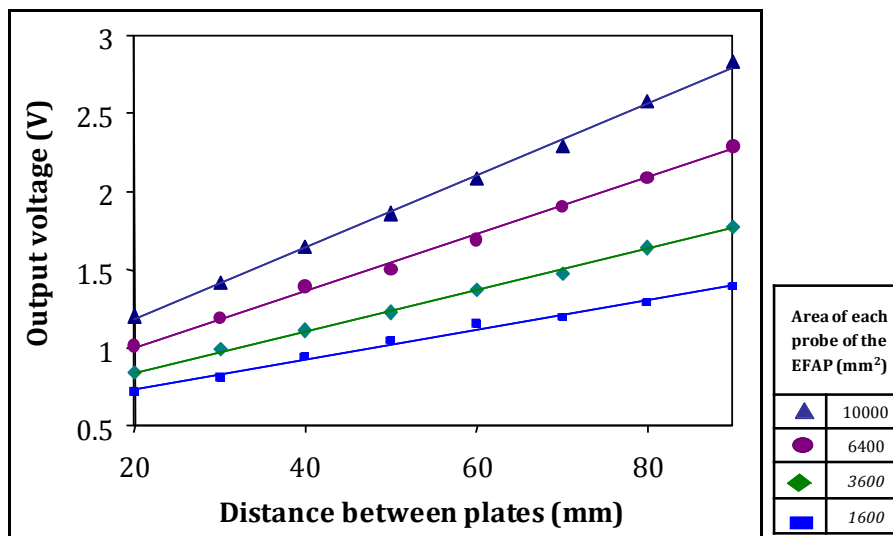


**Figure 5-21** Output voltage vs. distance between the probes of EFAP

More voltage was obtained, when the probes were placed at a larger distance and when the area of the probes was larger. It agrees well with the theory as larger the distance corresponds to larger potential difference between the probes and larger area of the probes corresponds to larger charge accumulated at each probe.

However, it could be noted that voltage obtained is only 2.7 V, when distance between the probes was about 90 mm. It should be  $\sim 225$  V in this case. But this could be explained with the diagram given below (Figure 5-22), where field lines are shown for conductors (in terms of two parallel probes) placed in a uniform electric field.

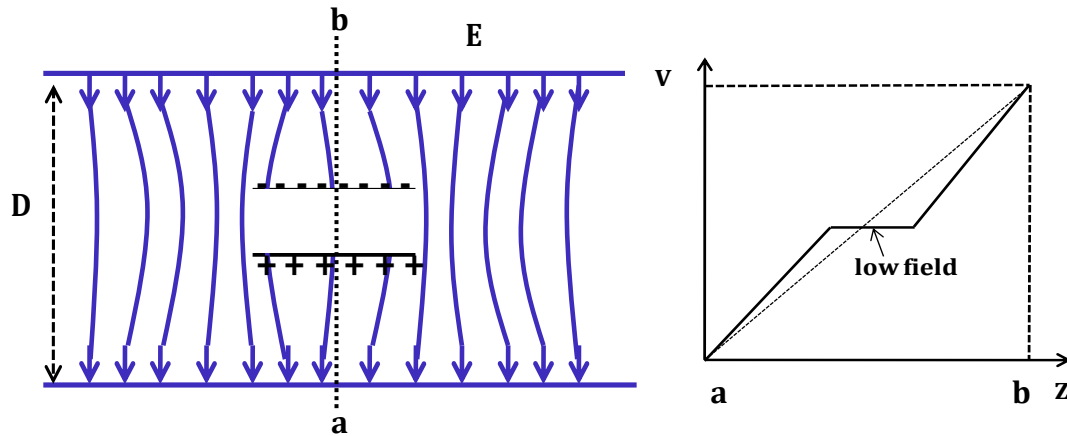


**Figure 5-22** Parallel conducting probes inside uniform electric field (a) inferred field lines (b) electric potential profile along path  $a \rightarrow b$

The field lines at the conductor could be the reason for reduced overall field strength and voltage obtained between these two probes. Although probes inside the electric field formed diminished field, but with suitable parameters of probes sufficiently high electric field can be generated.

Linear fits presented in Table 5-2 allowed predicting value of the output voltage corresponding to a particular surface area of the probe when changing distance between the probes. Constant  $C$  in the linear fits corresponds to the error of the measurement as no voltage could be obtained, when the distance between the probes is equal to 0 mm and should be neglected. Coefficient  $B$  linearly increases with area of the probes (Figure 5-23). Linear fit allows calculating coefficient  $B$  for any area of the probes (Figure 5-24) and predicting performance of the EFAP of any dimensions using equation 5-3 (Figure 5-24).

$$V = (2 \times 10^{-6} z + 0.0072)x, \quad 5-3$$

where  $V$  is output voltage,  $z$  is area of the probe and  $x$  is distance between the probes.

Area of each probe of the EFAP (mm <sup>2</sup> )		Linear fit; y - Output voltage x - Distance between probes y = Bx + C
▲	10000	y = 0.0231x + 0.7208
●	6400	y = 0.0182x + 0.6312
◆	3600	y = 0.0132x + 0.5786
■	1600	y = 0.0095x + 0.5393

Table 5-2

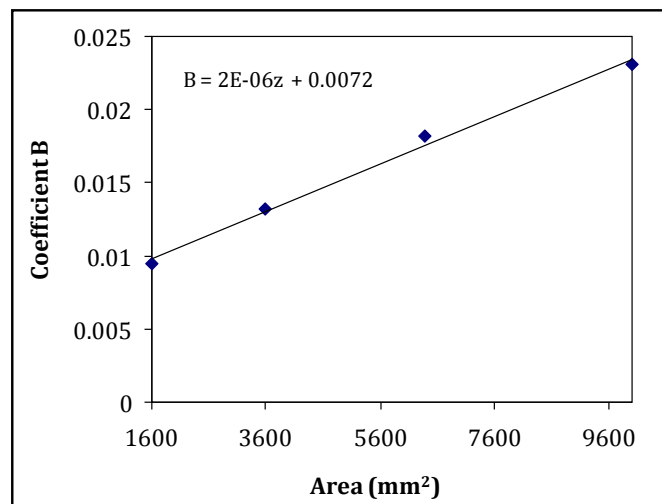


Figure 5-23 Coefficient B vs area of probe of and EFAP

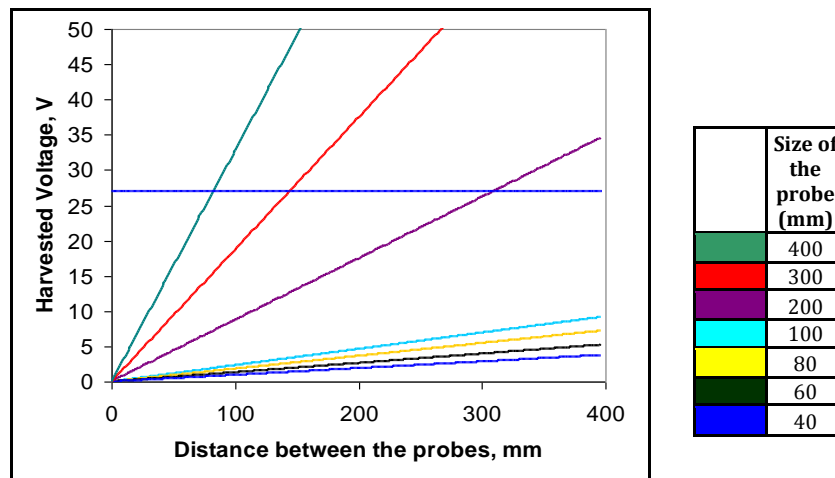


Figure 5-24 Calculated output voltage placed inside uniform electric field of 2.5 kV/m when changing distance between the probes

	Size of the probe (mm)	Distance between the probes (mm)	Output voltage (V)
	400	87	27
	300	147	27
	200	313	27
	100		
	80		
	60		
	40		

**Table 5-3** Calculated output voltage of EFAP for various probe sizes

Calculated output voltage of EFAPs of various sizes placed inside uniform electric field of 2.5 kV/m when changing distance between the probes is presented in Figure 5-24 and Table 5-3. The electric field under actual test will be 10 times larger than the one created in the lab (2.5 kV/m) meaning that use of the EFAP with same parameters described in Table 5-3 would get enough energy to apply 270 V to LCC for complete switching. From Figure 5-24, it is clear that probe sizes below 100 mm are not providing sufficient voltage. So, output voltage is not calculated for these probe sizes in Table 5-3.

## 5.5 Conclusions

This chapter describes a new hybrid high-voltage sensor. The sensor was constructed by combining fibre optics and liquid crystal technologies. In the present study only one module was used to test the performance of the device but multipoint measurements can be achieved easily by using a set-up described in section 4.2.2, Figure 4-5. This voltage sensor allows direct measurement of electric field up to 800 kV/m at distributed points along power lines with an accuracy of 0.1% with measurement distances ranging from 0.02 m up to 200 m (Brodzeli *et al.*, 2009a). The RI of LC is also dependent on temperature. So to avoid change in RI of LC due to temperature in real system proper packaging will be required.

An EFAP was proposed to provide sufficient voltage to switch LCC. This EFAP was experimentally tested and the characterization was acquired in order to estimate the geometrical properties of EFAP. As explained in section 5.5.3 an electric field created in the lab was (2.5 kV/m) that was ~10 times less than the electric field

created in actual situation meaning that use of the EFAP with same parameters described in Table 5-3 would give sufficient voltage (i.e. 270 V) to switch LCC.

## Chapter 6

### Optical Fibre Strain Sensors

**T**his chapter describes several strain sensors based on fibre Bragg gratings. In particular, it details the effect of transverse strain and bending in the alternative type of pi-phase-shifted FBGs (APPhSFBGs). Finally this chapter explores the possibilities of using optical fibre Bragg gratings in pressure sensing in compression garments for biomedical applications. It provides an overview on the use of other types of fibres to enhance the sensitivity of the pressure sensor.

#### 6.1 Optical Fibre Strain Sensor

Conventional metal foil strain gauge sensors are used extensively in many engineering fields in order to measure stress, strain, forces and moments. However, they suffer from signal drift, increased hysteresis, low spatial resolution and they are sensitive to electromagnetic interference. Optical fibre strain sensors offer promising technology for advancing in-situ monitoring, exhibiting advantages as explained in Chapter 2.

The most primitive optical fibre strain sensors were based on intensity variations in a signal transmitted within a multimode optical fibre since the components required for such systems were the only ones available at a reasonable cost. The earliest and simplest strain sensors included intensity-modulated transmission, reflection and micro-bend sensors (Chapter 2). As an optical fibre bends, a portion of the light is lost by means of radiation at the exact point of bending. These losses can be accurately detected by measuring signal attenuation. The sensor effect relies upon correlation between this attenuation and the longitudinal deformation of the optical fibre component.

Technologically simple optical components became available after demonstration of a FBG (band pass filter). FBG can be used to quantify various parameters. The axial (or longitudinal) strain response of fibre Bragg gratings arises due to both the

physical elongation of the sensor (and corresponding fractional change in grating period), and the change in fibre index due to photo-elastic effects (Section 2.2.4.4). The transverse load changes the index of the fibre as well as the polarisation of the axis of the fibre, whereas the thermal response arises due to the inherent thermal expansion of the fibre material and the temperature dependence of the RI.

In this thesis, effects of transverse strain and pressure were studied in detail in different FBG types. The next section will highlight the scope of FBGs as a transverse strain sensor.

## 6.2 Fibre Bragg Grating Transverse Strain Sensor

FBGs are being extensively developed and used as strain sensors. They are able to measure strain locally with high resolution and precision. As the physical size of an optical fibre is extremely small compared with other strain measuring components, it enables fibre to be embedded into structures for determining the strain distribution without influencing the mechanical properties of the host materials. These can provide extremely sensitive strain measurements for various materials and structures. FBGs exhibit sensitivity to transverse strain in addition to longitudinal strain and temperature as discussed in section 2.2.4.4 (c).

When an external force is applied in the transverse direction on a low/non-birefringent single-mode optical fibre, the circular fibre core and surrounding cladding region is deformed and a RI variation is induced which causes birefringence in the fibre (i.e. higher in applied strain axis and lower in those perpendicular direction) (equation 2-20 & 2-21). As the load is increased, however, a broadening of the reflected spectrum is observed and due to induced birefringence the peak finally splits into two. Wagreich *et al.* demonstrated that when a FBG (in standard non-birefringent fibre) is subjected to a static transverse strain along the y-direction, i.e. stress in y-direction and strain in x-direction, where fibre was held in such a way to prevent longitudinal strain ( $\epsilon$ ) via Poisson effect, so the “axial” terms in equation 2-17 had no effect. The separation of the peaks was observed to increase linearly with load. This observation is consistent with equation 2-19; for example if the only strain field present was in the y-

direction and there was only a single Bragg peak initially, then the splitting of the peak is given by equation 2-24 and 2-25 (Wagreich *et al.*, 1996).

Various authors have reported the use of FBGs for transverse strain sensing. A range of effects have been reported for FBGs inscribed in birefringent fibre in which two peaks are present. Through suitable alignment one of the two peaks was observed to split (Abe *et al.*, 2003), whereas in other work the pair of closely spaced Bragg wavelengths separates further when transverse strain is applied (Lawrence *et al.*, 1999). For the later work, the use of two FBGs with different periodicities (in birefringent fibre) produced 4 separate Bragg peaks, enabling the measurement of all three strain directions and temperature, simultaneously. The orientation dependence of APPhSFBGs to applied transverse load is discussed in (Rollinson C. M. *et al.*, 2005).

Table 6-1 summarizes the transverse load effects in different FBG types and its performance at a specific load.

Sensor type, operation and transverse load effect	Performance at a specific load	Reference
Uniform FBGs in standard fibre – the peak split into two polarisation modes.	~ 0.4 nm difference between the peaks for 80 N loading.	(Wagreich <i>et al.</i> , 1996)
Long period gratings – the LP <sub>05</sub> peak splits into two polarisation modes.	~ 20 nm difference between the peaks for 0.04 kg/mm loading.	(Liu <i>et al.</i> , 1999)
Standard pi-phase-shifted gratings – shift of the narrow transmission window (split in two due to “grating birefringence”).	~ 30 pm difference between the peaks for 0.3 N/mm loading.	(LeBlanc <i>et al.</i> , 1999)
Alternative type of pi-phase-shifted FBGs at twice the Bragg wavelength – the two peaks splits with applied transverse load.	Separation of first peak has 0.0039 nm/N. Separation between both peaks increased linearly with applied load	(Bal <i>et al.</i> , 2010b, Bal <i>et al.</i> , 2009c)
Alternative type of pi-phase-shifted FBGs at 2/3 the Bragg wavelength – the two peaks splits with applied transverse load.	Separation between both peaks increased linearly with applied load	(Yam <i>et al.</i> , 2006)
Superstructure gratings – use of the LP <sub>04</sub> peak, which splits into two polarisation modes.	~ 0.4 nm difference between the peaks for 0.3 N/mm loading	(Chi <i>et al.</i> , 2001)

**Table 6-1** Response of various types of FBGs to transverse load

The transverse load sensitivity of fibre Bragg gratings (FBGs) fabricated in a range of commercially available stress and geometrically induced high birefringent (HiBi) fibres have been experimentally investigated by Chehura *et al.* The highest transverse load sensitivity, of  $0.23 \pm 0.02$  nm/ (N/mm), was obtained with FBGs

fabricated in HiBi elliptically clad fibre. Table 6-2 shows fibre type, parameters and transverse load sensitivity for different HiBi fibres.

Fibre Type	Manufacturer/ Cladding diameter ( $\mu\text{m}$ )	Cut-off wavelength (nm)	Nominal Bragg Wavelength (nm)	Measured peak Separation (nm)	Slow axis sensitivity [nm/(N/mm)]	Fast axis sensitivity [nm/(N/mm)]
D - clad	KVH / 125	1320	1556	$0.60 \pm 0.01$	$0.18 \pm 0.02$	$0.12 \pm 0.03$
Elliptical core	KVH / 125	1320	1550	$0.51 \pm 0.01$	$0.12 \pm 0.01$	$0.12 \pm 0.01$
TruePhase	OFS Fitel / 125	1470	1551	$0.56 \pm 0.01$	$0.15 \pm 0.02$	$0.082 \pm 0.009$
Panda	Fujikura / 125	1330	1547	$0.34 \pm 0.01$	$0.14 \pm 0.01$	$0.14 \pm 0.01$
Bow tie	Fibrecore / 125	1275	1549	$0.35 \pm 0.01$	$0.18 \pm 0.02$	$0.098 \pm 0.008$
Elliptical clad	3M / 80	1520	1551	$0.54 \pm 0.01$	$0.23 \pm 0.02$	$0.17 \pm 0.01$

**Table 6-2** Transverse load response for various fibre types (after (Chehura *et al.*, 2004))

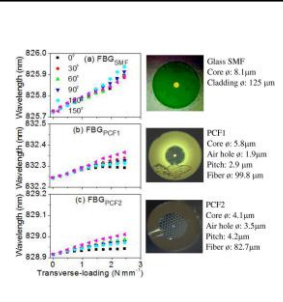
Although chemical composition and core diameter may vary between different types of optical fibres, their cladding diameter is mostly equal to  $(125 \pm 0.5 \mu\text{m})$ . Recently it was experimentally demonstrated by Julich *et al.* that different core diameter and dopant concentration exhibit different transverse strain sensitivity as depicted in Table 6-3.

Fibre Type	Core diameter/ Cladding ( $\mu\text{m}$ )	Dopant concentration (mol % $\text{GeO}_2$ )	Transverse strain sensitivity (nm/N)	Reference
GF1B/ Nufern	9.9 / 125	~5	$45.1 \pm 1.5$	(Julich & Roths, 2010)
PR2008/FBGS Tech.	4.4 / 125	~18	$48.5 \pm 1.0$	(Julich & Roths, 2010)
	9 / 125	-	peak splitting	(Bennett <i>et al.</i> , 2001)
	5 / 125	-	No peak splitting	(Bennett <i>et al.</i> , 2001)

**Table 6-3** Transverse response for various core diameters and dopant concentration

In another approach transverse strain sensitivity of FBGs in micro-structured fibres was investigated by Wang *et al.* by using an active fibre depolarizer. It was demonstrated that transverse strain sensitivity of these FBGs decreases with increasing volume of air holes around fibre core and depends upon the orientation

of fibre. Table 6-4 highlights the transverse strain characteristics of FBGs in microstructured fibres (Wang *et al.*, 2009).

Fibre type		Air filling fractions (%)	FBG length (mm)	Transverse strain sensitivity ( $\text{pm}/\text{N}\cdot\text{mm}^{-1}$ )
Glass SMF	 Glass SMF Core $\phi$ : 8.1 $\mu\text{m}$ Cladding $\phi$ : 125 $\mu\text{m}$	0	5	70
PCF 1	 PCF1 Core $\phi$ : 5.8 $\mu\text{m}$ Air hole $\phi$ : 1.9 $\mu\text{m}$ Pitch: 2.9 $\mu\text{m}$ Fiber $\phi$ : 99.8 $\mu\text{m}$	28	5	30
PCF 2	 PCF2 Core $\phi$ : 4.1 $\mu\text{m}$ Air hole $\phi$ : 3.5 $\mu\text{m}$ Pitch: 4.2 $\mu\text{m}$ Fiber $\phi$ : 82.7 $\mu\text{m}$	52	5	20

**Table 6-4** (after (Wang *et al.*, 2009))

The following section will highlight the transverse strain characteristics of an alternative type of pi-phase-shifted FBGs at twice the Bragg wavelength.

### 6.2.1 Transverse strain measurements at twice the Bragg wavelength

#### (a) Experimental Analysis

The FBG was fabricated in Corning 1060 nm fibre using the phase-mask writing method as explained in section 3.1. Reflection spectra near 1550 nm (twice the Bragg wavelength) were monitored using the set-up discussed in section 3.2.1 (Figure 3-4 (b)).

Figure 3-6 portrays the reflection spectrum at twice the Bragg wavelength, in which the dual peaks (at  $\sim 1552.8$  nm and  $\sim 1553.2$  nm) are due to the existence of a type of pi-phase-shifted grating at twice the Bragg wavelength (Yam *et al.*, 2009a) as discussed in detail in section 2.2.4.2.

The set-up (Figure 6-2) for investigating the response at twice the design Bragg wavelength to transverse strain enabled the transverse strain applied to the grating to be varied by changing the loading of the weights and which prevented longitudinal strains from occurring (Yam *et al.*, 2006). Transverse strain was applied by stressing the fibre between two glass plates as depicted in Figure 6-1. The tested fibre was balanced by an equal diameter support fibre. This configuration enabled the transverse strain applied to the grating to be varied by

changing the loading of the weights. This set-up also known as four-point bending was used to apply uniform transverse load over the FBG (Takahashi *et al.*, 2005). Weights of up to 5.5 kg were applied to the apparatus. Light was launched through the broadband source and a spectrum was measured using the OSA for each weight.

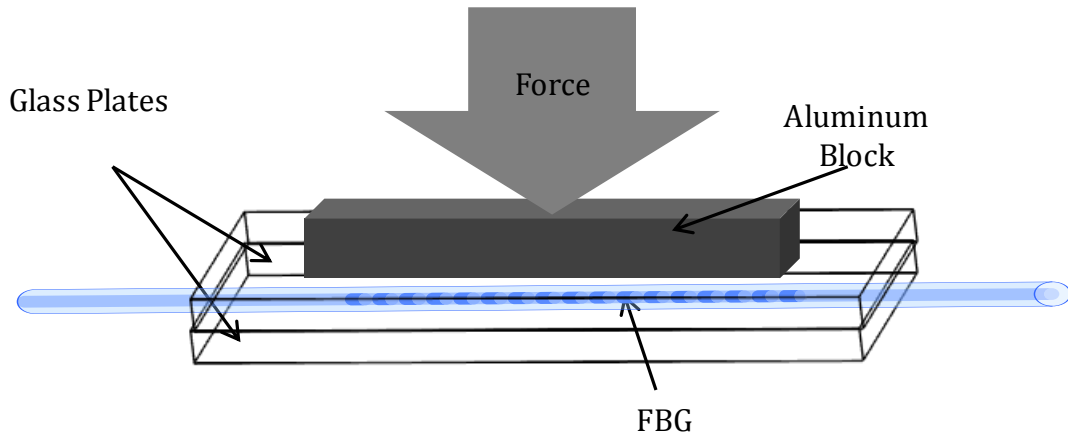


**Figure 6-1** Schematic showing direction of force applied

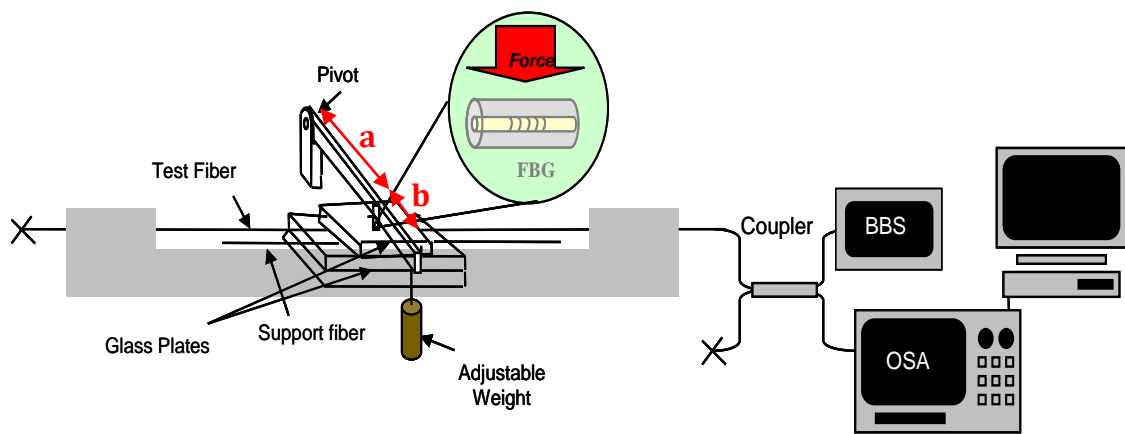
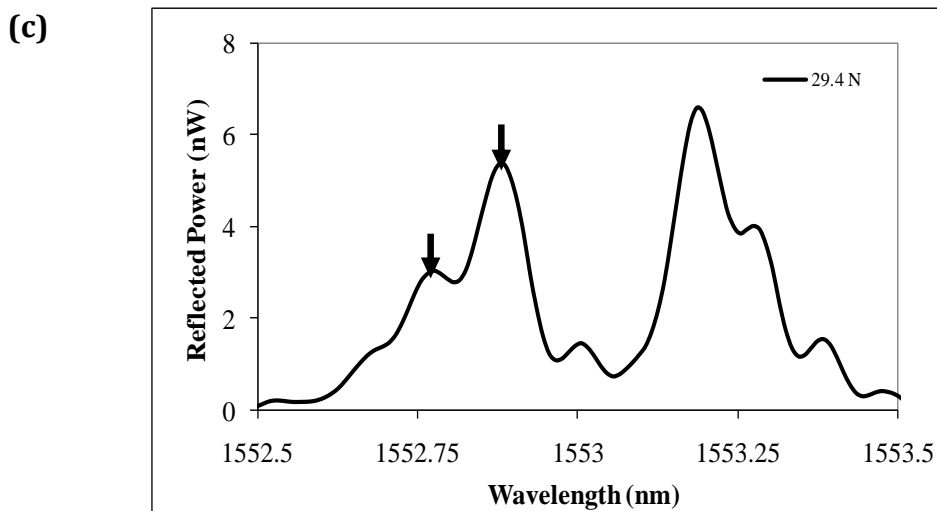
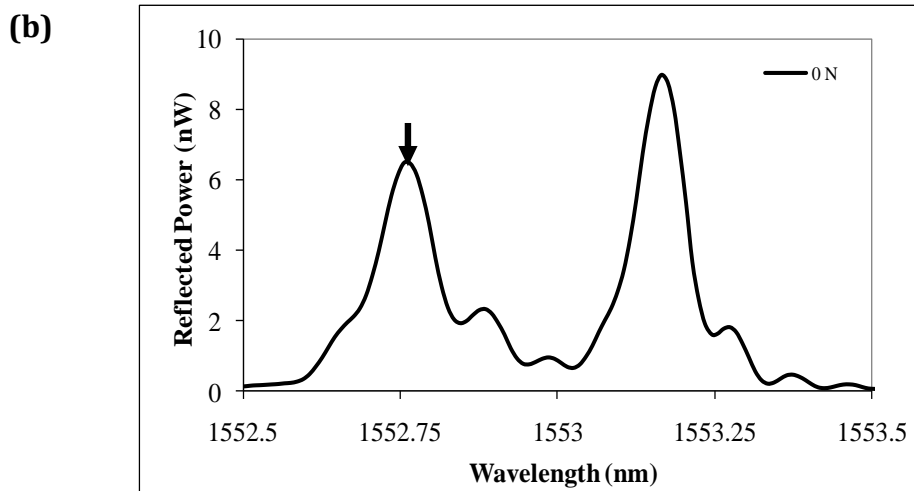
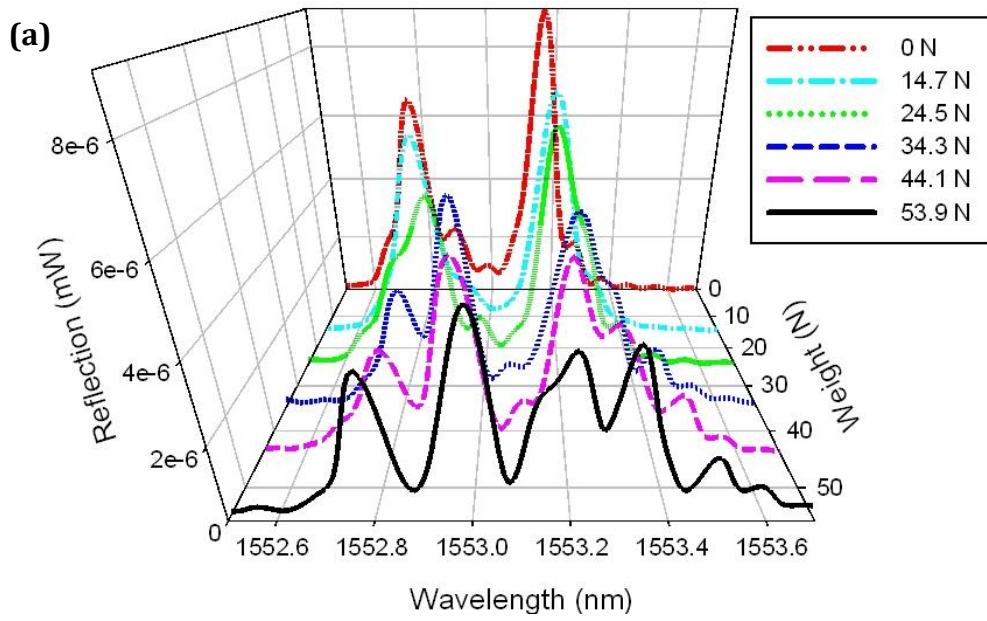


**Figure 6-2** Set-up used for transverse strain measurements

The changes in FBG transmission spectra in response to the applied force on the grating are illustrated in Figure 6-3 (a).



(d)

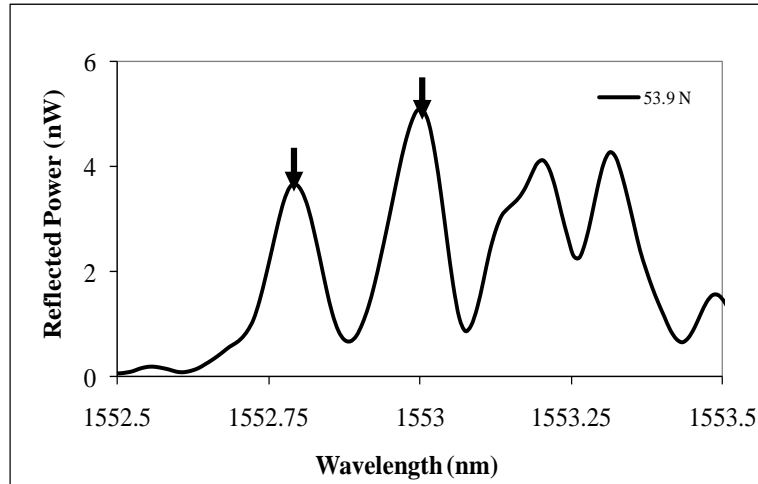


**Figure 6-3** FBG spectra at various applied loads (a) 3D representation and (b), (c), (d) FBG spectra at various applied loads

In Figure 6-3 (b), for which no external transverse strain is applied, two clear peaks are present in the reflection spectrum. There were no significant spectral transformations until force reached 29.43 N. As the applied load increased, the details of the spectrum began to change, including the splitting of the lower wavelength peak as evident in Figure 6-3 (c) and Figure 6-3 (d). It is also evident that the peak at the larger wavelength also splits in a similar fashion. The splitting of the lower wavelength peak (arrows shows peak splitting in first peak) against the applied load is presented in Figure 6-4. The separation of the two dips increased linearly with applied strain and the fitted slope was 3.9 pm/N.

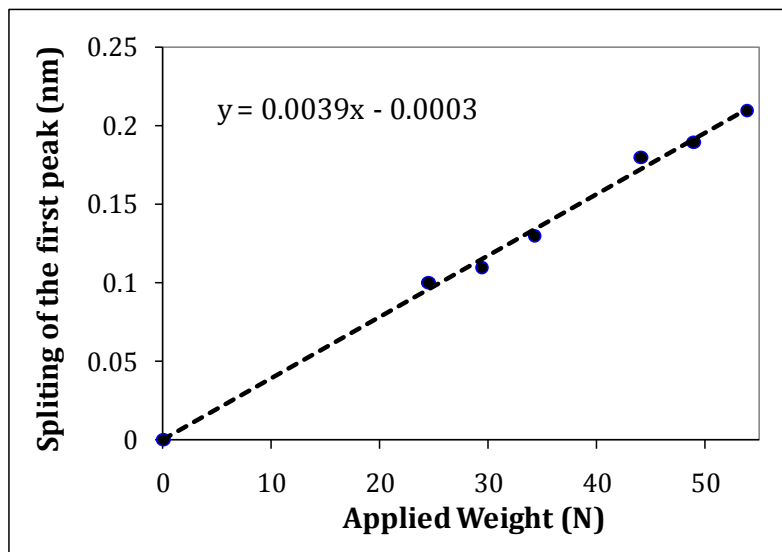


**Figure 6-4** Splitting of the lower wavelength peak vs. applied weight

Under uniform stress the two peak should split uniformly (Wagreich *et al.*, 1996), but in the conduct of 5 similar tests such a uniform split was observed only once, as shown in Figure 6-5. The reason for difference in peak splitting in Figure 6-3 and Figure 6-5 is not very clear, because the splitting of peaks inside uniform pressure chamber (Figure 6-14) was also similar to Figure 6-3. The peak separation of two peaks is given in Figure 6-6.

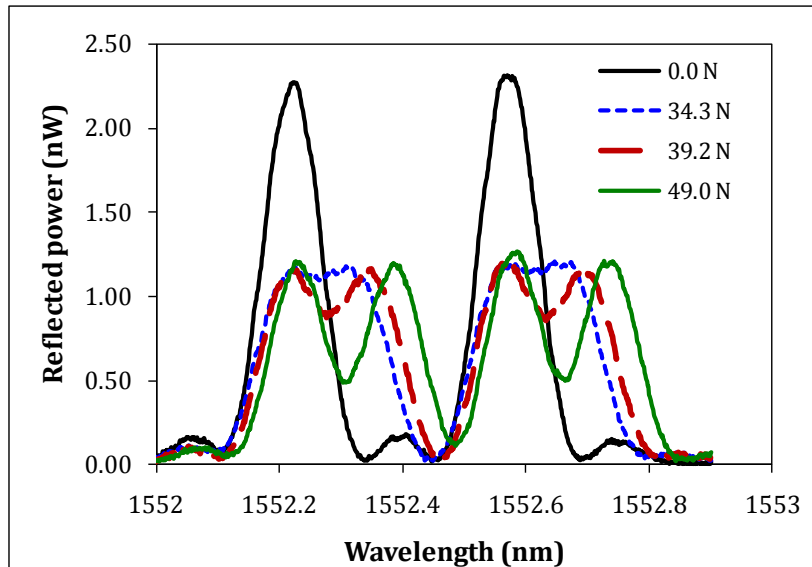


**Figure 6-5** Uniform splitting of two peaks under transverse load

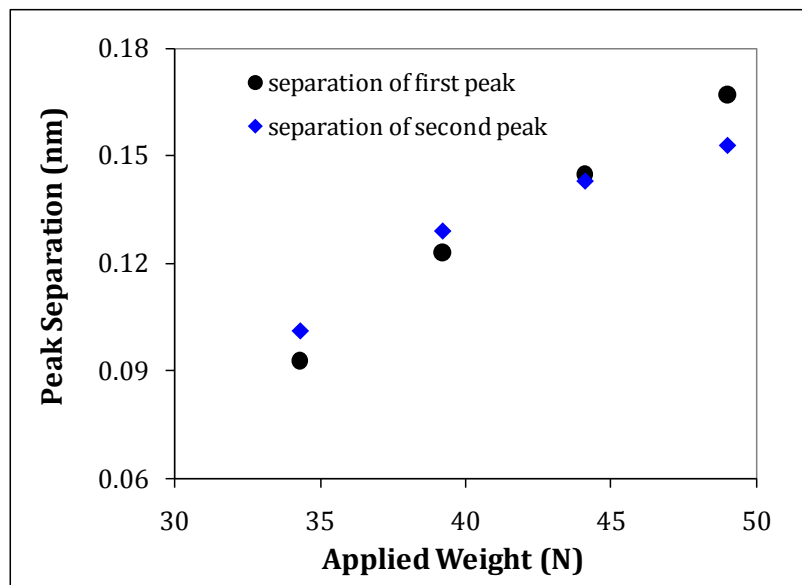


**Figure 6-6** Separation between two peaks with applied load

These double peaks in APPhSFBG also occur at the odd harmonics (such as  $2/3 \lambda_B$ , etc.), and their response to transverse strain was studied at 3<sup>rd</sup> harmonic of a grating periodicity equal to that of the phase mask. For the splitting of the lower wavelength dip in the  $\lambda_{2/3B}$  sensor, the wavelength separation increased linearly with applied load from 0.16 to 0.30 nm. The fitted responsivity was 2.3 pm/N (Yam *et al.*, 2006).

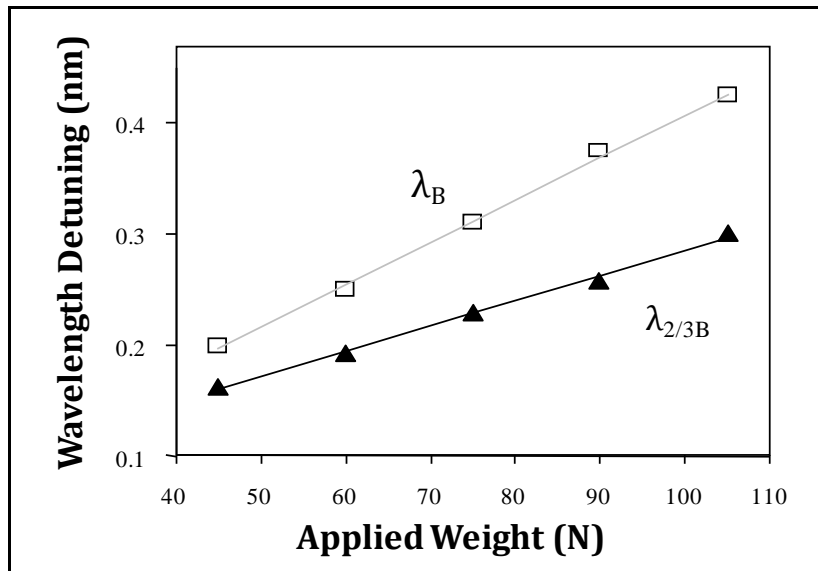


**Figure 6-7** Variation in the dip wavelength against transverse strain at  $\lambda_{2/3B}$  (Yam *et al.*, 2006)

Table 6-5 depicts the response of applied transverse load at different harmonics, where response at twice the Bragg wavelength shows high wavelength splitting per unit applied load. This response was calculated for the weights applied to the end of the lever as shown in Figure 6-2. But the actual load applied to the fibre was different than it, which could be calculated from equation 6-1.

Harmonics	Fibre type	Transverse strain sensitivity (pm/N)	References
$\lambda_B$	SMF-28	$3.8 \pm 0.4$	(Yam <i>et al.</i> , 2006)
$2/3 \lambda_B$	Corning 1060 nm	$2.3 \pm 0.3$	(Yam <i>et al.</i> , 2006)
$2 \lambda_B$	Corning 1060 nm	$3.9 \pm 0.3$	(Bal <i>et al.</i> , 2010b, Bal <i>et al.</i> , 2009c)

**Table 6-5** Transverse strain response at different harmonics of FBG

$$F_f = F_0 + F_G \left( \frac{a+b}{a} \right), \quad 6-1$$

where  $F_f$  is the force applied on the fibre,  $F_G$  is the applied force due to weight and  $a$  &  $b$  are the lengths of the sections of the lever as illustrated in Figure 6-2. The constant  $F_0$  is the load due to weight of lever, plate and hook, which was  $\sim 0.05$  Kg. The transverse line load ( $F_l$ ) (load on the fibre) can be calculated by dividing  $F_f$  by the length of plate = 0.05 m. So,

$$F_l = \frac{F_0}{l} + F_G \left( \frac{a+b}{a} \right) \quad 6-2$$

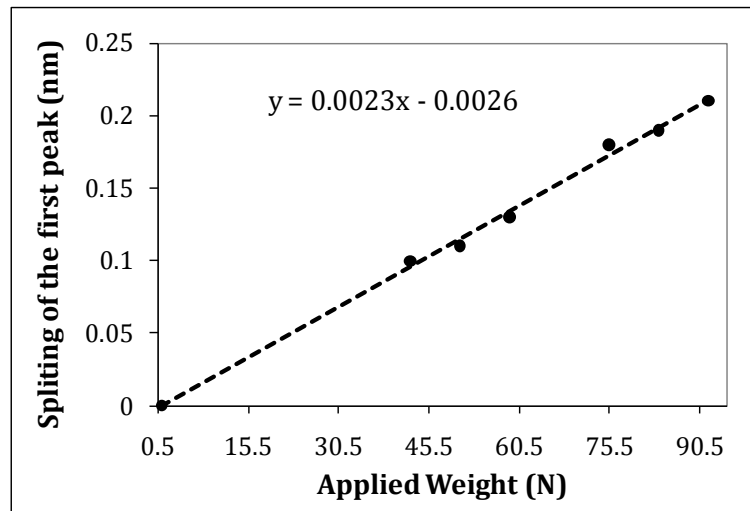


**Figure 6-8** Transverse strain response (Figure 6-4) with respect to actual load on the FBG calculated using equation 6-2

Figure 6-8 shows the splitting of the first peak with respect to applied transverse load on FBG, which was calculated using equation 6-2. This shows sensitivity of  $\sim 0.0023$  nm/N, which is less than the previously reported (Bal *et al.*, 2010b) because the load applied in that case was the weight applied to the fibre end, and was calculated in order to compare the response of this FBG with (Yam *et al.*, 2006) as depicted in Table 6-5 (refer Figure 6-4 & Figure 6-7).

*(b) Theoretical Analysis*

The parameters (Wagreich *et al.*, 1996) given in Table 6-6 were used to calculate the theoretical transverse strain sensitivity. The length of the plate was  $\sim 0.05$  m

and diameter (D) of the fibre was 125  $\mu\text{m}$ . In our case FBG was inscribed in 1060 nm fibre, so  $n_0$  was 1.472 and the Poisson's ratio ( $\alpha$ ) was 0.17.

parameter	$p_{11}$	$p_{12}$	$\xi$	$\nu$	$\alpha$	$n_0$
value	0.113	0.252	$7.0 \times 10^{-6} \text{ }^\circ\text{C}^{-1}$	0.17	$0.5 \times 10^{-6} \text{ }^\circ\text{C}^{-1}$	1.472

**Table 6-6** Properties of optical fibre used for theoretical analysis (Wagreich *et al.*, 1996)

The theoretical value of transverse strain sensitivity was  $\sim 0.0016$  nm/N using equation 2-22 to 2-27 (Julich & Roths, 2010, Wagreich *et al.*, 1996), but the sensitivity obtained in the experiment was  $\sim 0.0023$  nm/N (Figure 6-8) This difference in sensitivity could be due to the variations in precise measurements of the size of the plate or other fibre parameters (h) (equation 2-24 & 2-25). The results obtained were also consistent with the effect reported at 2/3 of the Bragg wavelength, given in Figure 6-7. However, the fitted responsivity, representing the dip wavelength separation per change in applied load, defined as  $\Delta\lambda/\Delta F$ , was different in two cases. However, Julich *et al.* demonstrated the transverse strain sensitivity of  $\sim 48.5 \pm 1$  nm/N for a fibre with 4.4  $\mu\text{m}$  core diameter (Julich & Roths, 2010). The reason for this difference in sensitivity is due to the fact that in our case the sensitivity is calculated as change in wavelength per unit change in force i.e.  $\Delta\lambda/F$ , which is same as (Wagreich *et al.*, 1996), whilst Julich *et al.* calculated the sensitivity as  $\Delta\lambda_{32}(\epsilon)/\lambda_{B,0}$ . By calculating  $\Delta\lambda/F$  for Julich *et al.* parameters, the theoretical sensitivity was  $\sim 0.0072$  nm/N, which however, was higher than in our case due to the difference in Young's modulus and other fibre parameters (Julich & Roths, 2010). The theoretical sensitivity calculated by Wagreich *et al.* was  $0.00289 \pm 0.00012$  nm/N, which is higher than our value due to the use of a different fibre type.

The transverse load sensitivity also depends upon orientation of the fibre (Rollinson C. M. *et al.*, 2005, Wang *et al.*, 2009).

#### 6.2.1.1 Applications of fibre Bragg grating transverse strain sensor

Fibre-Bragg-grating-based transverse strain sensors have been used for various applications and were described in detail by Schulz *et al.* One application is a load cell with embedded distributed transverse strain sensors. This load cell has the capability to measure transverse strains and strain gradients. Another similar application is a “smart” washer which is comprised of embedded distributed transverse strain sensors and is capable of measuring bolt loading, uneven loading, and warn of loosening. These sensors are used in bridges, tunnels and in wells, or are used to detect ice on roadways and thereby warning drivers to avoid a serious accident. FBG based load sensors can be embedded into the roads for traffic monitoring and control (Schulz *et al.*, 1998). Other application areas include smart structures, where FBG based sensors are embedded in the airplane to know the deformations in the structure (Udd *et al.*, 2000).

#### *6.2.1.2 Low cost interrogation technique for simultaneous longitudinal and transverse strain sensor*

OFSs although have many advantages, but they resulted in relatively few real commercial successes due to high manufacturing costs. One of the major costs of the sensors is the interrogation systems. The information about the strain is encoded in the Bragg wavelength and the cost of equipment allowing spectral analysis is fairly high. A low cost interrogation system was demonstrated for measurement of longitudinal and transverse strain simultaneously, where a FBG in a Hi-Bi Bow-Tie fibre was used as a sensor head and two filters with special designed parameters were used for longitudinal and transverse strain (Brodzeli *et al.*, 2008a, Brodzeli *et al.*, 2008b).

The author tested this low cost interrogation system for longitudinal strain measurements. Figure 6-9 depicts the measurement of overall wavelength shift by photo detector w.r.t. applied longitudinal strain using the set up given in low cost equipment (Brodzeli *et al.*, 2008a). Calibration is required to convert the intensity variations to the applied strain values.

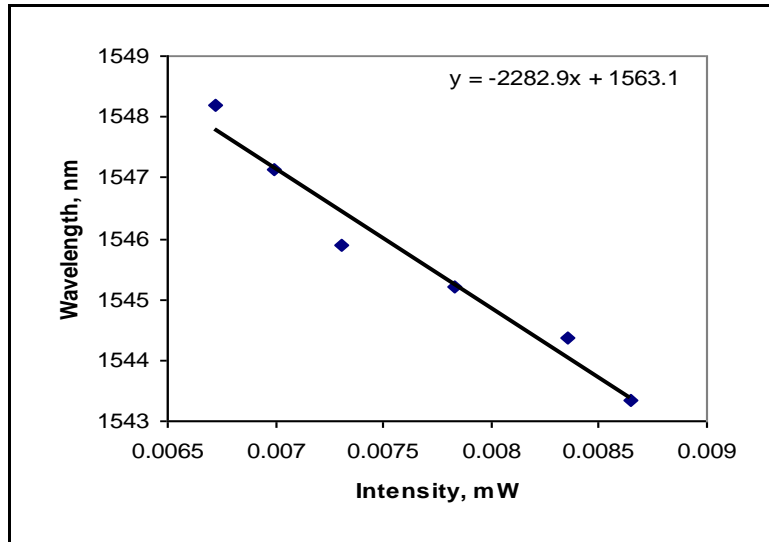


**Figure 6-9** Experimental results of low cost FBG strain interrogation system showing overall wavelength shift on application of longitudinal strain

A comparison of cost of conventional system for interrogation of transverse strain and longitudinal strain is given in Table 6-7, where the discussed method of measurements significantly reduced the cost of the system.

Interrogation Method	Cost
Conventional	OSA+BBS= A\$ 40,000 or more
Proposed method	FBG2+FBG3= A\$10 or 100

**Table 6-7** (after (Brodzeli *et al.*, 2008a))

### 6.2.3 Temperature independent bend measurements at twice the Bragg wavelength

The quantification of bending is very important for the assessment of the deformation of structural materials. Knowledge of deformations provides shape information on flexible structures in aircraft or ships and can verify the material's safety status and improve structural flaws. As a result, a number of bend sensors have been reported in recent times.

Recently, a FBG bend sensor based on tilted FBGs was demonstrated (Liu *et al.*, 2008). Alternatively, a low cost wide tunable FBG filter was proposed based on the

application of bending. FBGs give a red shift or blue shift depending upon the direction of bend. Thus, depending on compression or tension, wavelength tunability can be achieved (Sun *et al.*, 2005). Previously reported bend sensors rely on the demodulation of the reflected wavelength shift, which is sensitive to temperature (Dai *et al.*, 2000). Temperature compensation techniques are therefore necessary that can add to system cost and complexity. Consequently, the requirement for temperature insensitive bend sensors has led to the development of many different approaches employing FBGs (Han *et al.*, 2004, Hao *et al.*, 2006, Guo *et al.*, 2005). Recently in another approach temperature independent bend measurements were achieved using sampled FBGs (Han *et al.*, 2007).

In this work, a bend sensor was developed which gives unique temperature-independent bend measurements based on the application of an alternative pi-phase-shifted FBG (Section 2.2.4.2 (e)) at twice the Bragg wavelength.

In order to investigate the variation of the double peak at twice the Bragg wavelength as a function of applied bend, the fibre containing the FBG was embedded inside a flexible resin where FBG was placed in the middle of the resin. This allowed the resulting flexible slab and thus the embedded FBG to be subjected to a range of possible bending orientations, as shown in Figure 6-10 (a). During this bending FBG reflection spectra were monitored using the  $2 \times 2$  optical coupler, broadband source and OSA set-up, shown in Figure 6-10 (b).

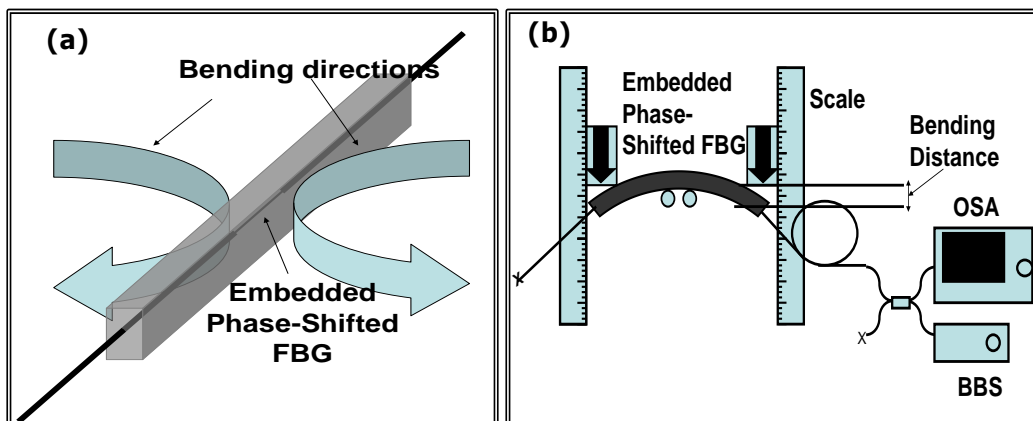


**Figure 6-10** Schematic diagrams, showing (a) bending directions of an embedded FBG, and (b) set-up used for measuring the spectral response of the pi-phase-shifted FBG, when bending in one direction

Changes to the spectrum due to bending are evident in Figure 6-11. Temperature measurements were obtained by placing the FBG into an oven, the temperature of which was varied over a range between room temperature (22 °C) and 110 °C (Figure 4-29). For every 10 °C increase in temperature the corresponding FBG reflection spectrum was recorded using the same experimental set-up shown in Figure 6-10 (b).

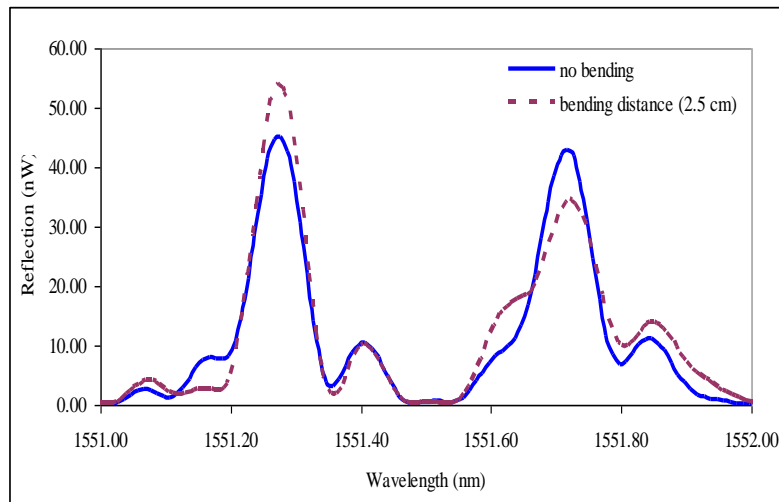


**Figure 6-11** Spectrum of FBG at double the Bragg wavelength without (solid line) and with bending (dotted line)

Bending in one direction (+) caused the double peak to shift towards longer wavelengths (red shift), while a shift to lower wavelengths (blue shift) was observed when bending was in the opposite direction (-). This behaviour is similar to that observed in a uniform FBG. However the relative peak reflectivity of the peaks changed in response to bending. When the fibre was bent in one direction (+), the reflectivity of the first peak (L) increased, while, the reflectivity of the second peak (R) decreased and vice-versa. The normalised peak intensity ratio of two peaks with respect to bending in two directions is depicted in Figure 6-12 (a). It should be noted that the peak separation was constant regardless of the bending direction or the extent of bending (Figure 6-12 (b)). The bending radius R in Figure 6-12 was calculated by using the formula  $D = 2R\sin^2(L/4R)$ , where D is the distance moved and L is the length of the resin.

An increase in temperature caused the two peaks to move simultaneously towards longer wavelengths, as shown in Figure 6-12 (c), while the reflected power

remains unaffected for each peak, as expected. Thus, as is true for all FBGs the temperature can be measured via the wavelength shift. Therefore, it is clear that discrimination between bend and temperature sensitivities may be achieved using the ratio of peak intensities.

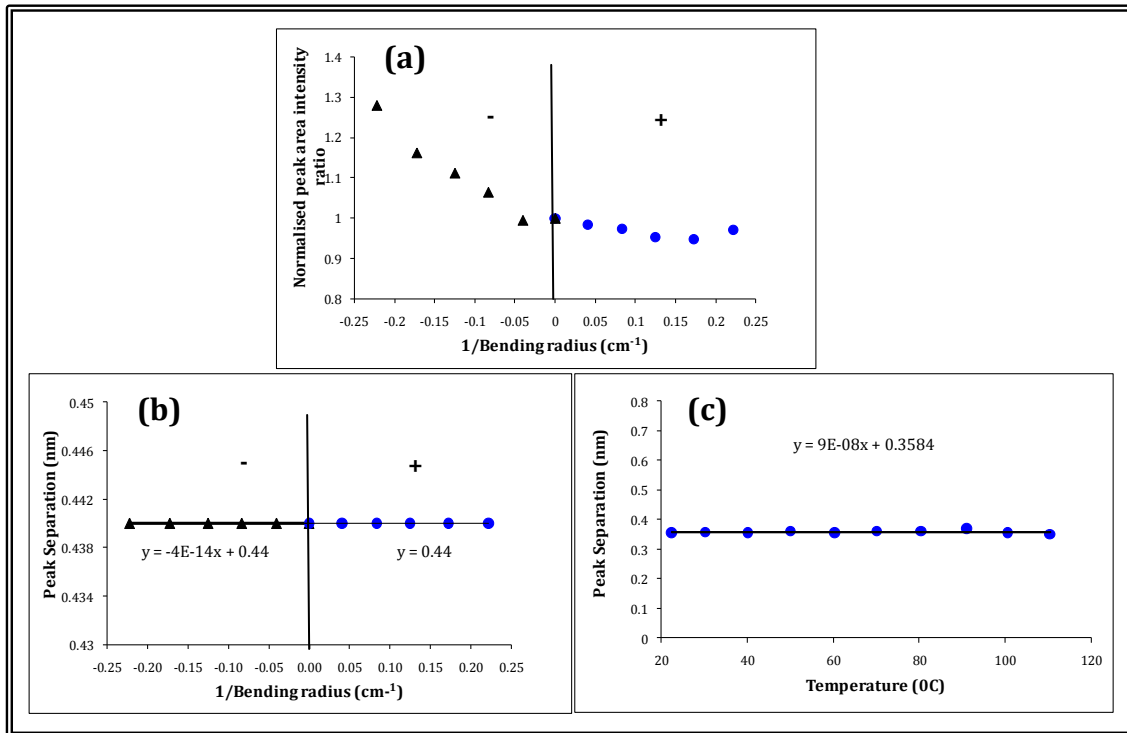


**Figure 6-12** Behaviour of the double peaks (L and R) when subject to bending in two directions (+ and - ), with (a) showing the normalized peak area intensity ratios of two peaks and (b) illustrates the peak separation of wavelength with bending, while (c) depicts the peak separation of wavelength with respect to temperature

As discussed earlier, these pi-phase-shifted FBGs, in which two peaks occur at twice the Bragg wavelength, are due to the formation of a complex RI structure that is a result of the use of a phase mask in fabricating the FBG. The diameter of the fibre used is approximately equal to the Talbot length of the phase mask in use, which means that each of the two grating phases occur only once (Yam *et al.*, 2009a). Thus, when the fibre is bent, the side of the fibre nearest to the centre of curvature experiences compression whilst the far side experiences elongation. The resultant spectral changes therefore must arise from the interference arising from altered Bragg condition from each side of the fibre; there is still a pi relative phase-shift, but the separate Bragg wavelengths have changed. In this case the

wavelength spacing between the two peaks remains the same, but the changes in relative reflected power of the two peaks enable the measurement of bending radius.

### 6.3 Fibre Bragg Grating Pressure Sensor

Most commercial pressure sensors are based on piezoelectric and piezoresistive transducers. Most of the sensors used to measure pressure employ diaphragms or bellows and measure pressure in terms of displacement. These can measure high or low pressure but they suffer from signal drift, increased hysteresis, and low spatial resolution. They all rely on elastic deformation under pressure (Sharifian, 2003). Table 6-8 illustrates the main conventional pressure gauges, their advantages and limitations.

Pressure sensor	Advantages	Disadvantages
Bellows & Bourden tube based	metal used is corrosion resistant & Independent of fatigue, creep or hysteresis	<ul style="list-style-type: none"> <li>slow response</li> <li>used for pressure variations &lt; 1 Hz</li> </ul>
Piezoresistive strain gauge	High sensitivity compared to the conventional metallic strain gauges	<ul style="list-style-type: none"> <li>maximum operating temperature is 120 °C</li> <li>can break if exceed pressure limit</li> <li>not suitable in wet conditions</li> </ul>
Piezoelectric pressure transducer	High sensitivity Good for transient pressure measurements	<ul style="list-style-type: none"> <li>not suitable for static pressure measurements</li> <li>sense acceleration if used for low pressure with strong vibrations</li> <li>high cost (~ A\$1500)</li> </ul>
Pressure sensitive paint (PSP)	Low cost	<ul style="list-style-type: none"> <li>sensitive to temperature</li> <li>trade off between response time and signal to noise ratio (SNR) which limits maximum achievable bandwidth</li> </ul>
Bar gauge	Comparatively fast response	<ul style="list-style-type: none"> <li>large size</li> <li>measured response time ~4 μs</li> </ul>

**Table 6-8** (Sharifian, 2003)

Optical fibre pressure sensors have the potential to measure pressure for various applications. Like other OFSs, these are generally divided into two categories, extrinsic and intrinsic. Intensity-based fibre optic pressure sensors come in various configurations such as transmissive, reflective and microbending, whereas

wavelength-based fibre optic pressure sensors involve FBGs. Another class of pressure sensor, interferometric pressure sensors, typically have high sensitivity, wide bandwidth and accuracy (Krohn, 2000), and can be based on either intrinsic or extrinsic designs.

Recently an optical fibre pressure sensor was reported where an etched single mode fibre was sealed inside a liquid crystal cell and wave-guiding properties of fibre were altered by applying external electric field to LC cell similar to discussed in section 5.5. A pressure sensor with a sensitivity of 0.25 rad/N was demonstrated (Jing *et al.*, 2010).

Wavelength modulated pressure sensors are generally based on FBGs. Pressure measurements using FBGs have been demonstrated by other users. It is reported that a FBG without special coating has very low sensitivity (-0.003 nm/MPa) to pressure (Xu *et al.*, 1993) and the pressure sensitivity can be enhanced by encapsulating the FBG sensor into a silicon casing or polymer coating (Zhang *et al.*, 2001).

Additionally when the fibre is coated with a packaging material, its pressure sensitivity is affected by the elastic properties of this material (Budynas, 1999). The coating material plays a significant role in pressure sensitivity. When, the coating material has a high Young's modulus, the wavelength change per unit load decreases.

In another report a Fabry-Perot type fibre laser sensor for fluid pressure was described, consisting of two identical pieces of Er-doped elliptical-core fibre spliced together with an angle of 90°, interchanging fast and slow polarisation axis. FBGs in circular core and elliptical core (erbium doped) fibres were chosen for measurements where pressure was applied directly on the FBG. It is given that dispersion of the highly birefringent gratings can be used to improve the resolution (Frank *et al.*, 2002).

More recently a hydrostatic pressure sensor was demonstrated which is based on an ultrashort distributed-Bragg-reflector (DBR) fibre laser, where the laser was installed in a high pressure pipe sealed with epoxy glue at one end and connected

to a pressure generator. The laser was pumped by a 980-nm source. The sensor has sensitivity of 418 kHz/MPa with a resolution of 5 kPa. This sensor can measure low pressure with the help of a simple transducer for the laser, where an elastic diaphragm was used to convert the pressure to the lateral force onto the laser. The sensitivity of the sensor was enhanced using transducer and was 69.2 MHz/kPa in a 3 kPa pressure range (Feng *et al.*, 2010).

Interest in using standard pi-phase-shifted FBGs for sensing is that the very narrow spectral feature can be tracked with high precision. Recently a pressure sensor using pi-phase-shifted FBGs was demonstrated by Chehura *et al.* (Chehura *et al.*, 2009).

The next section will highlight the further study on the APPhSFBGs under uniform pressure in order to investigate their behaviour. As it is known that the fibre type can affect the response to certain measurand, APPhSFBGs in two different fibre types were used. A standard pi-phase-shifted FBG was also used for comparison.

### 6.3.1 Response of various pi-phase-shifted FBGs to elevated pressures

A pressure chamber (Figure 6-13) was used for investigating the response of the various FBGs, with the fibre resting on the lower surface. The flatbed pressure chamber had an adjustable control module and applied pressure could range from 0-690 kPa.

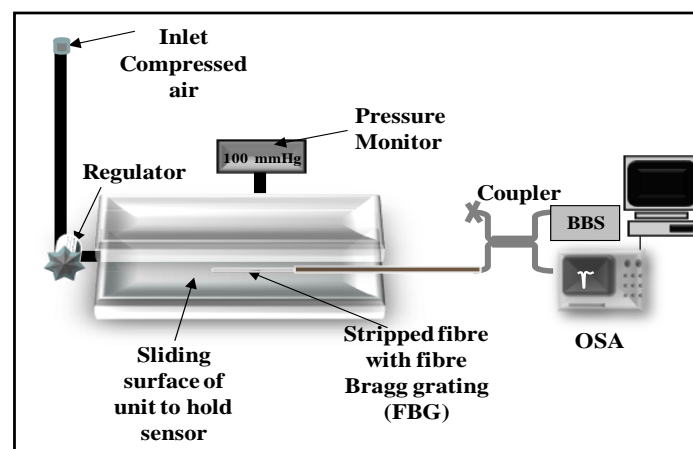


**Figure 6-13** Set-up used for FBG pressure sensor calibration, where BBS - broadband light source, OSA - optical spectrum analyser

This chamber is designed to apply uniform pressure on the sensor. A pressure up to 198 kPa was used for investigating the response of the various FBGs, with the fibre held between two rubber surfaces. APPhSFBGs were fabricated in Corning HI 1060 FLEX and SMF-28 fibre using a 244-nm UV continuous laser source through a phase mask of periodicity 536 nm. The fibre was pre-processed with hydrogen to increase the photosensitivity. Additionally, a standard pi-phase-shifted FBG was fabricated in GF1 fibre using a similar laser source. Reflection spectra were obtained using the set-up shown in Figure 6-13. Table 6-9 shows the parameters of FBGs used for this investigation.

FBG code	Fibre Type	Core diameter ( $\mu\text{m}$ )	FBG Type
FBG1	Hi 1060 Flex	$\sim 3.4$	Alternative type of pi-phase-shifted FBG at $2 \lambda_B$
FBG2	SMF 28	$\sim 8.2$	Alternative type of pi-phase-shifted FBG at $2 \lambda_B$
FBG3	GF1	$\sim 9$	Standard pi-phase-shifted

**Table 6-9** Fibre and FBG types used to measure pressure response

Changes in FBG reflection spectra for the three gratings in response to the applied pressure, for 3 pressures, are shown in Figure 6-14. Each spectrum for atmospheric pressure is different due to the nature of the pi-phase-shifted grating (Yam *et al.*, 2009a) and the fibre type. The standard pi-phase-shifted FBG in GF1 fibre shown in Figure 6-14 (c) exhibits the expected very narrow spectral feature, and whilst the spectrum of the APPhSFBG in HI 1060 FLEX fibre (Figure 6-14 (a)) is similar to those observed previously (Bal *et al.*, 2009c, Bal *et al.*, 2010b, Yam *et al.*, 2006), the two peaks in the SMF-28 fibre (Figure 6-14(b)) are of very different magnitude; it is believed that this is due to the more complex RI structure existing in the larger diameter core of standard telecommunications fibre.

It can be seen from Figure 6-14 that all FBG peaks moved to higher wavelengths as the pressure increased. Since the arrangement involves the application of lateral pressure to the fibre the observed peak changes in the HI 1060 FLEX fibre was more complicated than the expected peak-splitting; the spectral changes resemble the splitting effects observed in the APPhSFBG under transverse loading in the same fibre type (Figure 6-3) (Bal *et al.*, 2010b).

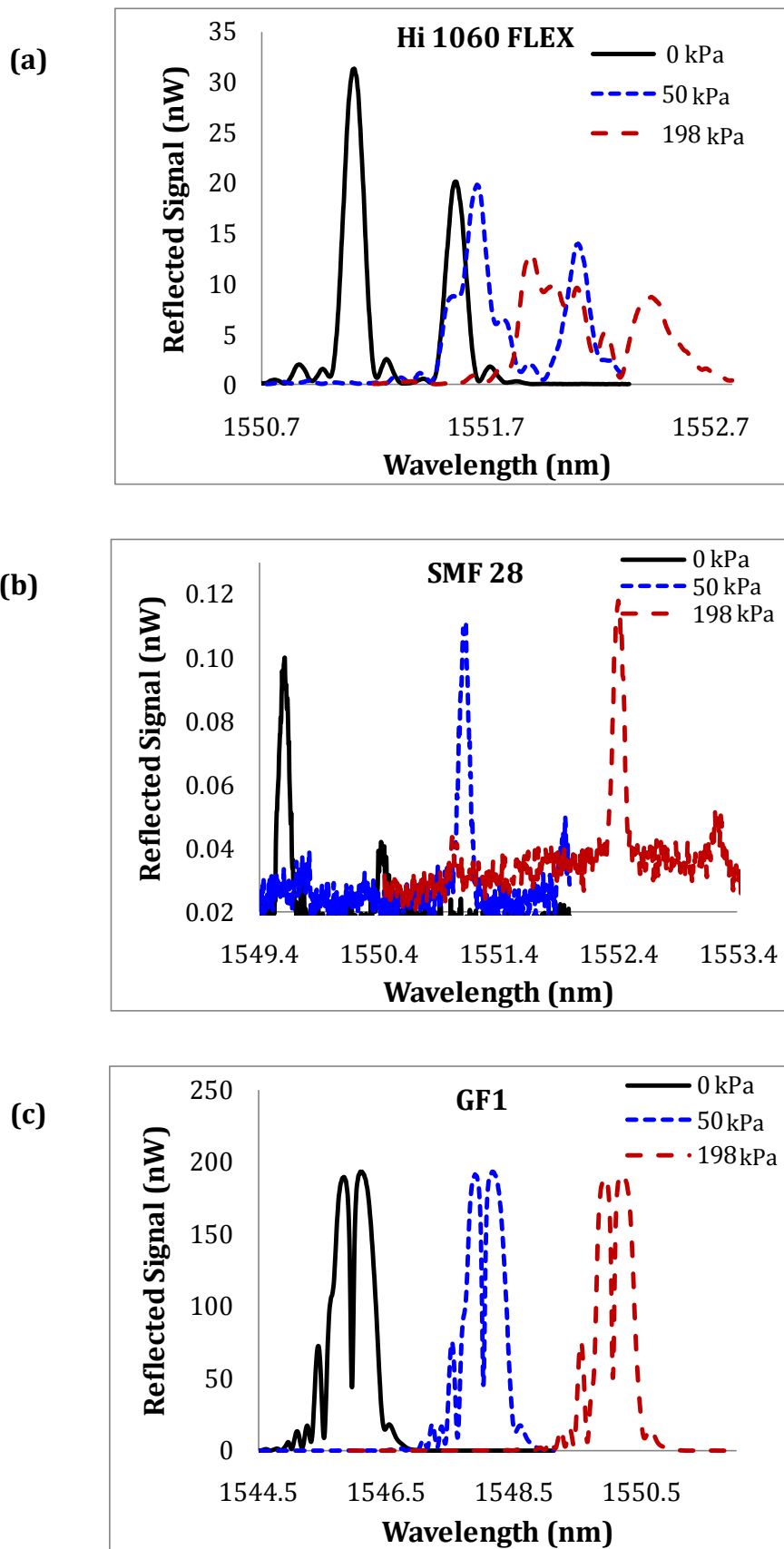


**Figure 6-14** Examples of reflection spectra for 3 different pressures, for the 3 fibre and FBG combinations, where (a) & (b) APPhSFBG and (c) standard pi-phase-shifted FBG

Figure 6-15 illustrates the shifts in the most significant spectral feature for each of the three grating and fibre combinations as a function of the applied pressure. It can be seen that in each case that the wavelength shift per unit pressure change is greater over the first 20 kPa compared with the full pressure range.

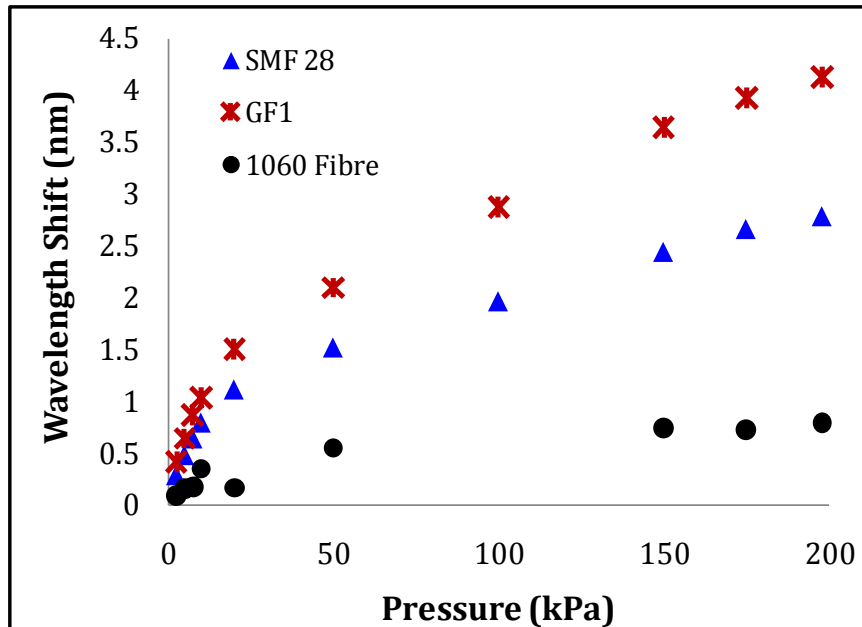


**Figure 6-15** Wavelength shift (first peak) against applied pressure for pi-phase-shifted gratings in the three fibre types

Furthermore, the rate of wavelength shift with pressure was very different for the three fibre types, and the wavelength shift for GF1 fibre at maximum pressure was a factor of about 5 times greater than for the HI 1060 FLEX fibre, indicating the important role of fibre type in determining the pressure sensitivity. Over the linear range (between 20-200 kPa) the sensitivity of the GF1 fibre is approximately 15 nm/MPa.

The response of FBGs to elevated pressure depends upon the manner in which the fibre is suspended within the pressure chamber (Bock, 1990). Thus a freestanding FBG exhibits a slight decrease in Bragg wavelength with applied pressure (Xu *et al.*, 1993) with a linear response of about -0.003 nm/MPa as first reported by Xu *et al.*, whilst a grating which is constrained from undergoing a length change is essentially being subjected to a transverse strain and there is an increase in the Bragg wavelength (Julich & Roths, 2010) due to the strain-optic effect. In one

example of the latter situation, where a FBG in a Hi-Bi fibre was constrained from length change but was under uniform pressure around the core, a linear response of about 0.02 nm/MPa was determined (Chen *et al.*, 2003), which is greater than the magnitude of the response of a freestanding FBG but which is much less than the responses for the three fibres shown in Figure 6-15. Furthermore, these data underscore the advantage of utilizing the effect of transverse strain whilst inhibiting the fibre length change, as this ensures a much greater sensitivity of the Bragg wavelength with increase in pressure. Although the reasons for the non-linear responses in Figure 6-15 are not understood, it is noted that a similar response was observed by Bjerkan *et al.* in a measurement of transverse strain (Bjerkan *et al.*, 1997).

Figure 6-16 illustrates the linear response of various FBGs in different fibres over a pressure range of 0-20 kPa, where fitted slope indicate the sensitivity of the various FBGs.

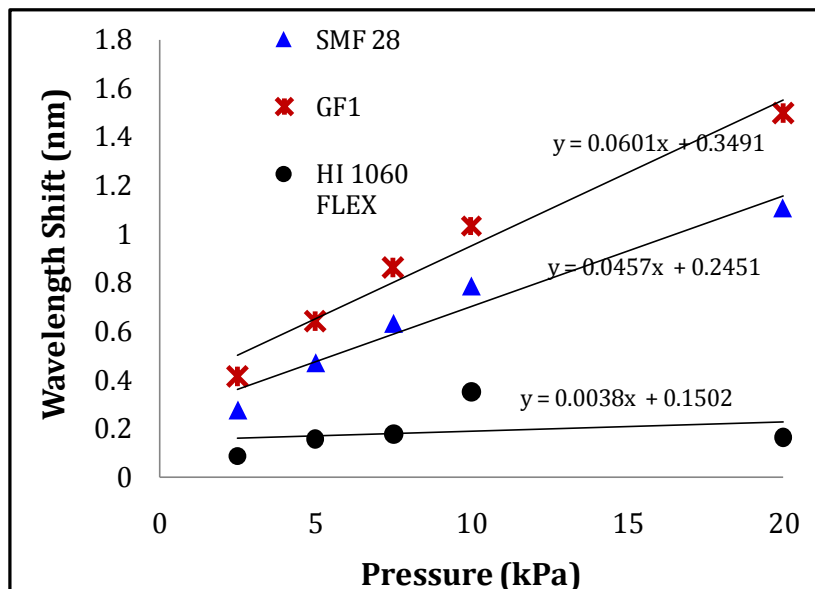


**Figure 6-16** Linear wavelength shift (first peak) against applied pressure (for a range 0-20 kPa) for pi-phase-shifted gratings in the three fibre types

### 6.3.2 Fibre Bragg grating sensors for human skin pressure measurements

Chronic deep venous insufficiency is characterised by a combination of symptoms like varicose veins, lymphoedema, oedema or deep vein thrombosis. The

occurrence rates of these symptoms are very high and graduated compression hosiery has been recognized worldwide as the mainstay of compression therapy in the management and treatment of venous disorders. Graduated compression refers to the application of a varying degree of constant compression to different segments of the leg with pressure being the greatest at the ankle and gradually decreasing proximally, with typical pressures of about 2600 Pa at the ankle then decreasing to approximately 65% at the calf level (Li & Dai, 2006). The compression stockings are designed to apply this graduated compression and are woven in such a way that the compression level lessens towards the top of the hosiery. Graduated compression stockings promote blood flow from superficial veins into deep veins (Herzog, 1993). The improved blood flow and prevention of venous stasis reduce oedema and help compensate for impaired venous return in conditions such as deep vein thrombosis (Byrne, 2001, Byrne, 2002) and venous insufficiency and leg ulcers (Horner *et al.*, 1980, Jonker *et al.*, 2001, Partsch & Partsch, 2008). The medical function of these stockings is to oppose the increased hydrostatic venous pressure, help venous contraction without muscle activity, provide a controlled graduated compression and support the superficial venous system. These stockings are also effective in reducing the occurrence of deep-vein thrombosis (DVT) in travellers (Sigel *et al.*, 1975). These are basically used to

- help control swelling
- assist scar tissue to mature
- protect fragile skin
- promote wound healing.

A compression garment is usually made specifically to suit the person's needs. They can cover any part of the body, encompassing just one limb or the whole body, depending on the person's needs.

*(a) Motivation*

Evaluation of these garments is crucial in order to maintain recommended pressure levels. Portability, as well as real time monitoring of pressure, is also important for some patients. Sensors to monitor such low pressure are based on capacitive sensing (PLIANCE sensor) (Chavan & Wise, 2001) or on traditional

pneumatic sensing (KIKUHIME sensor) (Larsen & Futtrup, 2004, Van *et al.*, 2007). However, they are insufficiently sensitive; suffer from signal drift, increased hysteresis, and low spatial resolution.

As discussed earlier, FBG-based optical sensors have attracted more and more attention in recent years because of their many advantages and potential industrial applications. Although a significant body of research exists in the extensive applications of FBGs in the civil engineering and aerospace industry, limited work has been done in the field of healthcare towards synergizing photonic sensing with biomechanics, orthopaedics or rehabilitation applications. The potential applications of FBGs can revolutionize the health sector. In this work the prospects for FBGs in low pressure sensing in compression stockings is studied. However, as mentioned earlier, recently a distributed Bragg reflector fibre laser based sensor is proposed which is suitable for low pressure measurements (Feng *et al.*, 2010).

The strain dependence of the centre wavelength of the FBG to measure the pressure due to compression garments was evaluated. Various aspects of the optical fibre Bragg gratings in terms of the length and effective RI were considered and the sensor was calibrated under uniform pressure.

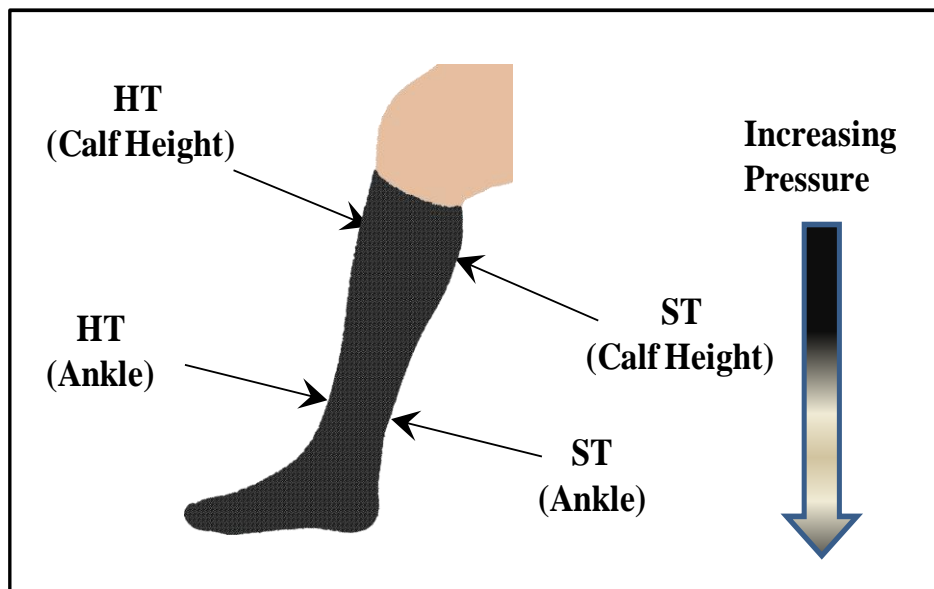


**Figure 6-17** Leg layout showing different positions of measurements, HT- hard tissue & ST-soft tissue

The pressure under the compression stockings was measured using the FBG-based sensor. The positioning of the sensor was chosen to illustrate the graduated compression under the hosiery at the ankle (AK) and calf (CF) respectively, as illustrated in Figure 6-17. The measurement of pressure on a human leg model was made on hard (HT) and soft tissue (ST) to accommodate the non-uniform deformation of the garment relative to these tissues, Figure 6-17.

Three FBGs were fabricated, FBG1, FBG2 and FBG3, in a single mode telecommunication fibre (Nufern, GF1) using a conventional phase-mask writing method (Section 3.1). Two of them had different lengths:  $l_{FBG1} = l_{FBG3} = 10$  mm and  $l_{FBG2} = 40$  mm, and a third (FBG3) had a different RI. Tests were conducted to calibrate all FBG sensors using a flatbed pressure chamber as illustrated in Figure 6-13. Tests were performed using compressed air with pressures ranging from 0 to 10 kPa.

The pressure measurements on the human leg were recorded using the FBG in reflection with a similar set-up to that shown in Figure 6-13 with the stocking rolled over the sensor. The measurements were performed at different positions, illustrated in Figure 6-17, as well as at different postures: sitting, standing and resting with the leg horizontal.

#### *(b) Results and Discussion*

Figure 6-18 depicts the Bragg wavelength shift of FBG1 sensor due to pressure change from 1.9 to 3.0 kPa that are the pressure values in the compression garment at ankle and calf respectively. It illustrates a clear shift of  $\sim 0.004$  nm. As these FBGs were not coated with any specialised coating, we anticipate that polymer coating over the FBG will provide a much clearer shift at such low pressure (Paul *et al.*, 2005). This result validates the use of FBG sensor for low pressure measurement applications.

The uniform pressure calibration curve for all three types of FBG pressure sensors is illustrated in Figure 6-19. Different FBG lengths were chosen to evaluate the effect of length on pressure measurements.

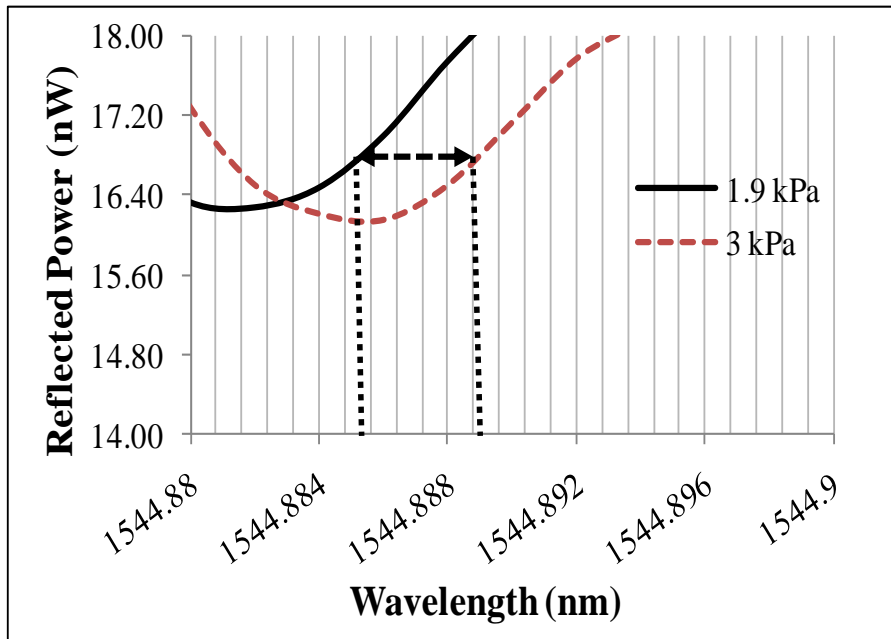


**Figure 6-18** Spectral response of FBG1 sensor for two different loads

As expected, it is clear from Figure 6-19 that the FBG with the shorter length, and with comparatively lower RI change, shows high sensitivity. This result is in good agreement with other work (Mueller, 1938). Accordingly, as illustrated from Figure 6-19, the choice for pressure measurement would be a shorter FBG and RI in the order of  $10^{-4}$ .

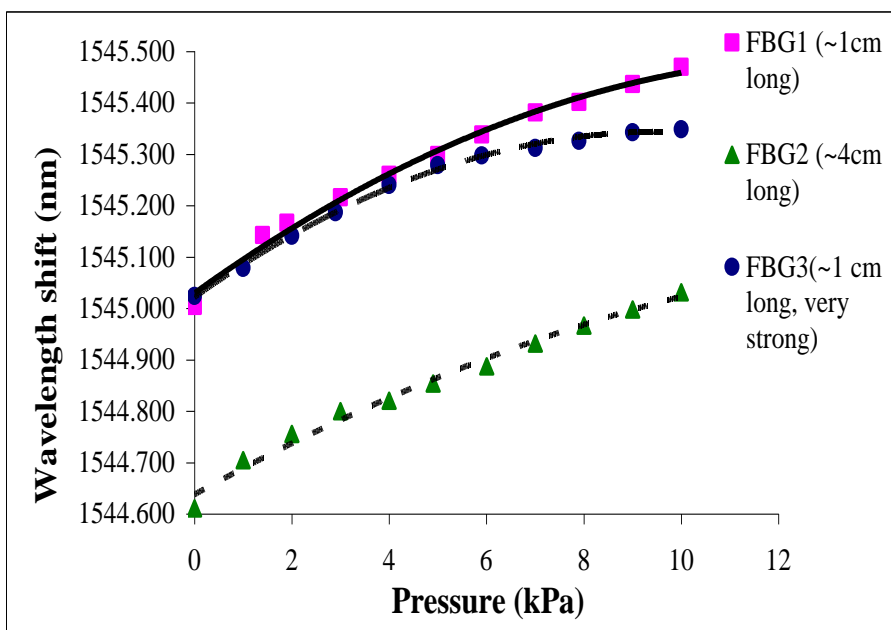


**Figure 6-19** Pressure calibration for different lengths of FBGs

The pressure response due to different body postures and positions on the leg is given in Figure 6-20. Different tissues and muscles in the leg exert different pressure and this pressure is also dependent upon body movements (i.e. at different body positions). As expected, hard tissue (HT) produces different pressures compared to soft tissue (ST) surfaces.

The data from HT surfaces conforms to the expected values of graduated compression stockings – values at the ankle are always higher than values at the calf, irrespective of posture. When assessing the soft tissue data, the ankle values decreases considerably, and the variability in the calf data raises questions about the elasticity of the soft tissue surfaces and the most appropriate measurement site. This issue needs further investigation.

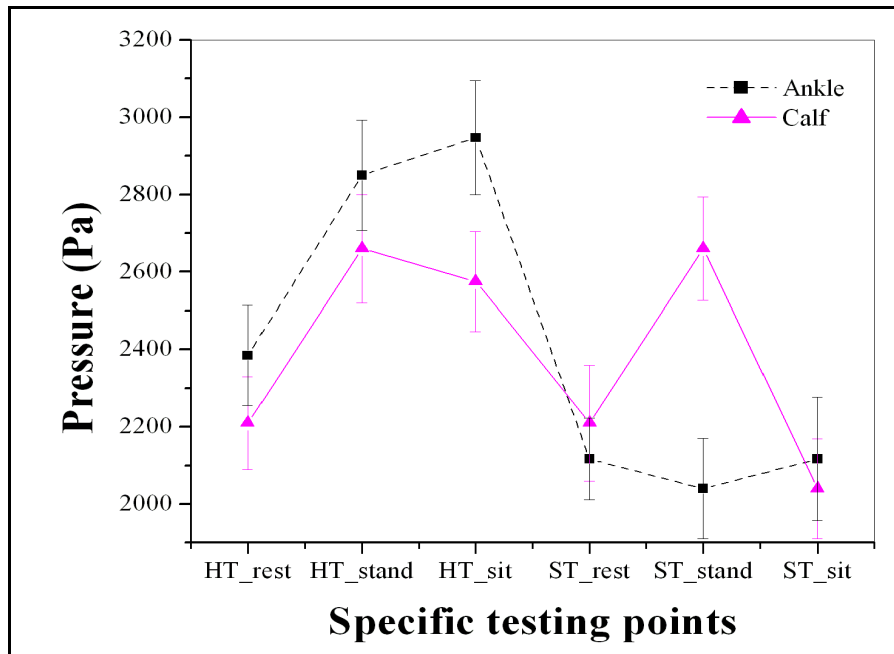


**Figure 6-20** Pressure response demonstrating the effect of changing position and posture

It is well known that FBGs respond to bending and temperature in terms of wavelength shift, and that micro-bending can play a major role in false measurements. Special care was taken to avoid the effect of bending by repeating these measurements, but it can easily be avoided by considering measurements in terms of spectral broadening (spectral width) due to applied pressure. In this way pressure measurements can be distinguished from bending and temperature

changes. Bending can cause spectral broadening as well. So, a special packaging is required in a practical system to avoid it.

It has been observed that an increase in the FBG length did not lead to an increase in the pressure sensitivity. Similarly, the strength of the FBG, i.e. increasing the effective RI did not lead to an increase in the sensitivity of the sensor meaning complex RI structure of FBG plays an important role in these measurements.

## 6.4 Conclusions

This chapter highlights certain strain sensors, mainly transverse strain sensors and pressure sensors. It provides an overview on transverse load effects in different fibre types. It also detailed the response of APPhSFBGs to transverse load and bending, with the aim of understanding these gratings better.

The transverse strain sensitivity for an APPhSFBGs was  $\sim 0.0023$  nm/N, which was less than calculated theoretically using equations 2-22 to 2-27. This difference in sensitivity could be due to the variations in precise measurements of the size of the plate ( $h$ ) or other fibre parameters. A number of experiments were performed with varied results; splitting of the peaks was not very uniform in some of the experiments as can be seen in Figure 6-3, but in an another experiment it was very uniform and given in Figure 6-5. However, the exact cause for non-uniform response is not very clear; it can be due to the way FBG was positioned under test. For example in these experiments APPhSFBGs were fixed at two ends in order to avoid the effect of longitudinal strain. The variation in this position or loosening might have contributed to the above effect. However, when a lateral pressure was applied to these APPhSFBGs using a uniform pressure chamber a non-linear splitting was evident (Figure 6-14 (a)). These effects need to be investigated in future. The response obtained was also consistent with the effect reported at  $2/3$  of the Bragg wavelength, given in Figure 6-7.

Lateral pressure measurements were conducted on pi-phase-shifted FBGs in different fibres. The wavelength shift for GF1 fibre at maximum pressure was a factor of about 5 times greater than for the HI 1060 FLEX fibre. Over the linear

range (between 20-200 kPa) the sensitivity of the GF1 fibre is approximately 15 nm/MPa. Figure 6-16 illustrates the linear response of various FBGs in different fibres over a pressure range of 0-20 kPa. The fitted slope in the linear region shows a very high sensitivity ( $\Delta\lambda/P$ ) for GF1 fibre (0.0601 nm/kPa), whereas APPhSFBG in SMF 28 shows 0.045 nm/kPa. The pressure sensitivity for the small core fibre, i.e. HI 1060 FLEX fibre, was 0.0038 nm/kPa. These results indicate the important role of fibre type in pressure sensitivity.

The suitability of FBG-based pressure sensor in low pressure (1.9 to 3.0 kPa) measurements in compression garments was investigated. A small shift ( $\sim 0.004$  nm) shift in Bragg wavelength was observed in these measurements. This fibre was not coated with any material; however, by suitable coating or using microstructured optical fibre this sensitivity can be enhanced.

## Chapter 7

### Conclusions and Future Work

**T**his chapter concludes this thesis by summarising the results and presenting suggestions on further work based on this research. This research work focused on the study of fibre optic sensors for various applications. The author believes that the results found in this work have made a significant contribution to knowledge in understanding various optical fibre sensors, their fabrication and applications, as described below.

#### 7.1 Summary of the Key Outcomes

The aim of this research work was to develop new OFSs and evaluate them for three major sensing areas, i.e. refractive index, high-voltage for electrical transmission lines and strain. The use of FBGs for multiplexing applications (refractive index sensor and voltage sensor) as well as for sensing (refractive index and strain sensor) was explored. In order to develop these sensors, an outline of the most common types of sensors, i.e. intensity-based and wavelength-based sensors, was provided in Chapter 2.

Chapter 3 provided the details of the fabrication process of various FBGs. Etched FBGs were characterized using a differential interference contrast (DIC) microscope, allowing cross-referencing with their spectral characteristics. This was the first time that etched FBGs had been viewed under a DIC microscope. The extracted 3D images of grating planes were provided, where a dip in the core in GF1 fibre and the grating planes were clearly visible. These images can facilitate the further understanding of the complex structure of FBGs. However, the difficulty of rotating the small diameter fibre needs to be addressed.

A RI sensor based on a well known broadband reflector was discussed and tested experimentally in Chapter 4. In this work, use of an optical coupler (simple approach) for various RI measurements was highlighted. An extension to this broadband reflector for an intensity-based multipoint RI sensor was proposed and

tested for RI measurements of various liquids. This approach is very reliable and straightforward to implement. The resolution of this RI sensor is  $10^{-3}$  RIU, which is suitable for many applications. This type of sensor was shown to be suitable for measuring the state of charge of a battery, in which the concentration of sulphuric acid in water was determined via its RI. Another method used to evaluate external RI behaviour was an etched fibre where RI was measured in terms of reflected power intensity. This is suitable to act as a fibre optic “switch”, i.e. indicate when there is a problem or to add or drop channels. The other method used to measure RI was wavelength dependent and was based on well-known etched FBGs. The core of an optical fibre containing a grating was exposed to a liquid of a certain RI by removing the cladding. Hydrofluoric acid was used for this purpose. The above mentioned methods of determining RI of liquids were compared for their performance, and a comparison table was provided at the end of the chapter. Although there are many etched-FBG-based RI sensors in the literature, the author believes that they are very difficult to fabricate and careful handling is also required as a very thin ( $\sim 6\text{-}8\ \mu\text{m}$ ) FBG portion is used for sensing. Although it gives very high resolution, it can break very easily and is prone to micro-bending. A special packaging is required for these sensors, which adds extra cost to the sensor. So intensity-based sensors (one of the earliest) can serve as a better alternative in many sensing applications. With appropriate techniques these sensors can provide sufficient resolution suitable for many applications.

Chapter 5 summarised a prototype multipoint hybrid voltage sensor designed to measure voltage in power transmission lines that was built by using liquid crystals along with optical fibres. The multipoint fibre optic device, which allows measurement of electric field at multiple points, was similar to that used in chapter 4 for RI measurements. In this case the sensing head was the cleaved end of the fibre embedded inside the liquid crystal cell. Greater spacing between electrodes required more voltage to switch the liquid crystal cell. Fibre embedded inside the cell had  $\sim 180\ \mu\text{m}$  (size of fibre) spacing. However, during the experiments it was noted that a switching cell with such a large gap required a very high voltage. So to provide sufficient voltage to switch LC molecules, an electric field amplifying probe (EFAP) was proposed and characterized. This voltage sensor allows direct

measurement of electric field up to 800 kV/m at distributed points along power lines with a precision of 0.1% for measurement distances ranging from 0.02 m up to 200 m.

Strain sensors based on FBGs were discussed in Chapter 6. APPhSFBGs originated due to the complex refractive index profile within the fibre core, and different measurands were used in order to better understand the behaviour of these APPhSFBGs. There was a clear splitting of both peaks in an APPhSFBG with applied transverse load and the sensitivity was  $\sim 0.0023$  nm/N. The experimental results were compared with the theoretical values. Measurements indicate that these can be used for multiparameter sensing (Collins *et al.*, 2010). The transverse strain sensitivity in FBGs depends on the fibre type (Table 6-2), core diameter (Table 6-3), type of complex microstructure (Table 6-4), concentration of dopants (Table 6-3), fibre orientation and also on the type of FBG (Table 6-1).

The application of bend in one direction reduces the reflectivity of one of the peaks while increases that of other peak and vice-versa. The exact cause of this is required to be further investigated. However, recently DIC images of a FBG in a HI 1060 FLEX fibre (core diameter  $\sim 3.4$   $\mu\text{m}$ ) revealed that the depressed cladding of these fibres is also sensitive to UV irradiation. A highpass filter in the Y direction to original DIC images was used to show the interleaved planes (Figure 7-1).

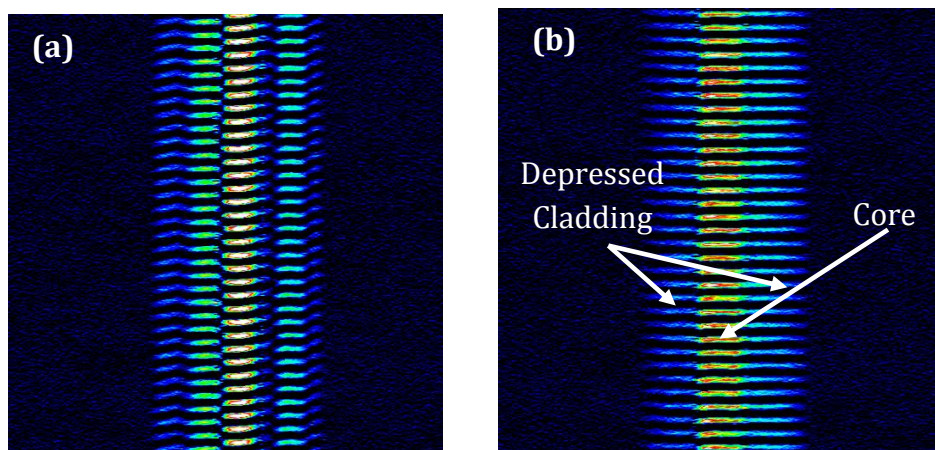


**Figure 7-1** DIC images with highpass filter in Y direction (For display purposes) of the core region of a fibre Bragg grating in small core Hi 1060 FLEX fibre (a) image was taken from a direction orthogonal to that of the writing beam (b) The same fibre Bragg grating, after the fibre has been rotated about its axis by  $\pm 90^\circ$ .

Lateral pressure measurements were carried out with pi-phase-shifted-FBGs (in three different fibres) using a uniform Flatbed pressure chamber. It was observed that GF1 (large core) fibre shows a high sensitivity to lateral pressure. However, splitting of peaks was observed for a FBG in a small core fibre, which is contradictory to the results obtained (Table 6-3) by Bennett *et al.* (Bennett *et al.*, 2001). This variation may be due to different fibre type and dopant concentration and different experimental conditions. It was shown by Julich *et al.* that a fibre having small core with high dopant concentration has a high sensitivity to transverse strain (Julich & Roths, 2010) (Table 6-3).

The application of a FBG pressure sensor to measure pressure in compression garments was demonstrated. These compression garments have graduated pressure increasing upwards and have approximate pressures values at ankle and calf 1.9 to 3.0 kPa respectively. The standard FBG shows very low sensitivity for such a low pressure range. However, these results validate the use of FBG-based sensors for such bio-medical applications.

## **7.2 Directions for Future Work**

### **Chapter 3 Fabrication and characterization of fibre Bragg gratings**

The microscopic characterization of FBGs provided the evidence of a complex grating structure (Rollinson *et al.*, 2005b) with the pattern varying with fibre type and core diameter. This structure may contribute to sensor sensitivity. More research to know the correlation between these structures and sensor sensitivity needs to be investigated in the future. The use of reduced cladding FBGs for evaluation of complex features within a fibre core need to be further studied and compared with unclad fibre.

### **Chapter 4 Refractive index sensor**

The set-up for the multipoint reflective RI sensor could be improved by using circulators, where some of the losses due to couplers could be reduced. By using suitable referencing and a superluminescent diode, the output of the sensor can be improved. There are limited numbers of sensors which can be connected due to

the 3-dB loss at each coupler, but this can be avoided by using a  $1 \times 8$  coupler at the input. To avoid the bifurcation point, the effect of a different fibre RI at the tip of the fibre can be studied in future work.

## **Chapter 5 Hybrid voltage sensor**

The hybrid voltage sensor presented in this research work is a new idea which can be explored further in the future. The sensor presented in this work was a reflective hybrid sensor that could be improved using more sophisticated fibre optic technology as given below.

### *(a) Fabry-Perot interferometer*

A micro-cavity can be obtained using femtosecond laser micromachining (Wei *et al.*, 2008), and the cavity can be filled by a liquid crystal and voltage can be applied using ITO and Nickel electrodes, similar to demonstrated by other authors (Hirabayashi *et al.*, 1993, Bao *et al.*, 1996).

### *(b) Corrugated Fibre Bragg gratings*

The design of corrugated or surface relief FBGs allows light to escape the waveguide and then be recaptured. The gaps of a corrugated grating filled with LC would allow interaction of the propagating light with an electro-optic material, as the light in the guided mode is not confined entirely inside the core. However, the manufacturing process of these corrugated FBGs is not a simple process and requires great engineering expertise. Recently, these FBGs have been successfully fabricated and demonstrated for different sensing applications (Alemohammad *et al.*, 2008, Smith *et al.*, 2006), and this might be a better way to realise a voltage sensor.

### *(c) Fibre Taper*

Another way to access the evanescent field is using a fibre taper. It can be manufactured using a heat flame or using wet chemical etching. Recently a pressure sensor was demonstrated, where an etched fibre was embedded inside a liquid crystal cell and pressure was applied over it (Feng *et al.*, 2010).

*(d) Etched fibre Bragg gratings*

The reduced cladding FBGs can also be used as a high-voltage sensor. The real challenge is to find a suitable liquid crystal with compatible RI. However, a tuned electric field sensor was demonstrated using FBG filled with LCs (Baek *et al.*, 2006), but the liquid crystal would have been especially designed for this purpose.

*(e) Long period gratings*

The other choice is to use long period gratings, which can be used in higher order leaky modes and possess high sensitivity.

Furthermore, fibre used inside the LC cell can be embedded in a different manner to reduce the cell gap. The next step is the implementation of this sensor in real time in power transmission lines.

## **Chapter 6 Strain sensor**

*Pi-phase-shifted FBGs*

As suggested by Yam *et al.* (Yam, 2010) a full model of gratings similar to those investigated by (Tomljenovic-Hanic & Love, 2005), having the interleaving pi-phase-shifted gratings in parallel, would be extremely useful for the understanding of characteristics of their higher-order diffraction wavelengths. Effects of different writing conditions and phase mask alignment on peaks of APPhSFBGs at twice the Bragg wavelength and at other harmonics are currently under investigation.

*Transverse strain measurements*

The splitting of APPhSFBGs peaks was not always uniform under transverse strain. The exact cause for this response needs to be investigated in future. A number of experiments can be performed to understand it. The effect of transverse strain on a FBG when it is not fixed at two ends (Transverse +longitudinal strain) and when it is fixed at two ends (Transverse strain) can be compared. This response is also different if a uniform pressure is applied on a freestanding FBG (as observed by Xu *et al.*, 1993).

As APPhSFBGs are a special class of pi-phase-shifted FBGs and these are highly responsive to transverse strain, the transverse strain effect on these pi-phase-shifted FBGs at different FBG positions could be investigated. By applying pressure at one half of the FBG, the response could be helpful to understand more about these FBGs.

Furthermore, how transverse strain in FBGs fabricated in different fibres depends upon complex RI structure may be investigated using DIC microscope.

#### *Bend measurements*

The results of a bend measurement on an APPhSFBG at twice the Bragg wavelength embedded inside silicon resin gives a change in peak reflected power of both peaks, where the intensity of the first peak increases while for other peak it decreases and vice versa for bending in the other direction. The exact cause of this behaviour is still unclear. Few more experiments can be performed in order to determine the exact cause.

- (a) Comparing the bend measurements and DIC images for two different grating conditions. One is slightly slanted and the other should be a normal FBG. For the slightly tilted FBG, bending would cause more leakage of light than the normal. The above mentioned change in intensities could be due to a slight tilt in the FBG during writing.
- (b) The effect of different diameter and uniform flexible embedding materials could be investigated. The embedding material exerts compression on FBG, which could be changed by changing the diameter of the outer layer. Modelling can help to understand this effect.
- (c) This effect could be investigated in different fibre types to see the effect of extended FBG patterns in a depressed cladding region.

#### *Lateral Pressure measurements*

The response of lateral pressure on pi-phase shifted FBGs in different fibre types is different and non-linear. The exact cause of difference in response in various fibre types and non-linear behaviour needs to be investigated in the future. The use of

uniform FBGs for low pressure measurements was presented. However, as expected the results indicate that uniform FBGs are not sufficiently sensitive for such measurements. In future work FBGs in other types of fibre, for example, bow-tie fibre or micro-structured fibres would be considered. Long period gratings could also be considered for such applications. The best choice would be the use of a plastic optical fibre.

## References

- Abe I., Kalinowski H. J., Nogueira R., Pinto J. L. & Frazao O., 2003, Production and characterisation of Bragg gratings written in high-birefringence fibre optics, *Proc. IEEE Circuits, Devices and Systems*, 150, 495-500.
- Accetta J. S., 2008, Fiber sensing to measure battery state of charge, *Sensors article*, URL:<http://www.sensormag.com/sensors/electric-magnetic/fiber-sensing-measure-battery-state-charge-1484>.
- Acevedo J. M., Paz A., Fernandez-Gomez S. & Soria M. L., 2008, Life testing of plastic optical fibers for lead-acid battery fast charge equipment, *IEEE Reliability and Maintainability Symposium (RAMS 2008)*, Annual, 126-31.
- Aglzim E. H., Rouane A. & El-Moznine R., 2007, An electronic measurement instrumentation of the impedance of a loaded fuel cell or battery, *Sensors*, 7, 2363-77.
- Albert J., Hill K. O., Johnson D. C., Bilodeau F. & Rooks M. J., 1996, Moire phase masks for automatic pure apodisation of fibre Bragg gratings, *Electronics Letters*, 32, 2260-1.
- Albert J., Hill K. O., Malo B., Theriault S., Bilodeau F., Johnson D. C. & Erickson L. E., 1995, Apodisation of the spectral response of fibre Bragg gratings using a phase mask with variable diffraction efficiency, *Electronics Letters*, 31, 222-3.
- Alemohammad H., Toyserkani E. & Pinkerton A. J., 2008, Femtosecond laser micromachining of fibre Bragg gratings for simultaneous measurement of temperature and concentration of liquids, *Journal of Physics D: Applied Physics*, 41, 185101.
- Arregui F. J., Matias I. R., Cooper K. L. & Claus R. O., 2002, Simultaneous measurement of humidity and temperature by combining a reflective intensity-based optical fiber sensor and a fiber Bragg grating, *IEEE Sensors Journal*, 2, 482-7.
- Atkins R. M., Lemaire P. J., Erdogan T. & Mizrahi V., 1993, Mechanisms of enhanced UV photosensitivity via hydrogen loading in germanosilicate glasses, *Electronics Letters*, 29, 1234-5.
- Baek S., Roh O., Na J. H., Jeong Y., Jeong C., Lee S. D. & Lee B., 2006, Liquid-crystal-cladding fiber Bragg gratings with electrically controllable polarization-dependent characteristics, *Japanese Journal of Applied Physics Part 1- Regular Papers Brief Communications & Review Papers*, 45, 4044-50.

- Bakalidis G. N., Glavas E., Voglis N. G. & Tsalides P., 1996, A low-cost fiber optic force sensor, *IEEE Transactions on Instrumentation and Measurement*, 45, 328-31.
- Bal H. K. & Brodzeli Z., 2010a, Fibre optic reflective sensor to measure state of charge of battery, Proc. 4<sup>th</sup> European Workshop on Optical Fibre Sensors (EWOFS 2010), Porto, Portugal, Proc. SPIE, (Post deadline poster).
- Bal H. K., Sidiroglou F., Brodzeli Z., Wade S. A., Baxter G. W. & Collins S. F., 2010b, Fibre Bragg grating transverse strain sensing using reflections at twice the Bragg wavelength, *Measurement Science and Technology*, 21, 094004.
- Bal H. K., Sidiroglou F., Brodzeli Z., Wade S. A., Baxter G. W., & Collins S. F., 2010c, Temperature independent bend measurement using a pi-phase shifted FBG at twice the Bragg wavelength, Proc. 4<sup>th</sup> European Workshop on Optical Fibre Sensors (EWOFS 2010), Porto, Portugal, Proc. SPIE, 7653, 76530H.
- Bal H. K., Sidiroglou F., Collins S. F. & Brodzeli Z., 2010d, Multiplexing of fibre optic reflective sensors using Bragg gratings, *Measurement Science and Technology*, 21, 094011.
- Bal H. K., Sidiroglou F., Collins S. F. & Brodzeli Z., 2009a, Multipoint optic refractive index sensor for liquids, Proc. IEEE 14<sup>th</sup> OptoElectronics and Communications Conference (OECC 2009), Hong Kong, 5222773.
- Bal H. K., Sidiroglou F., Ladouceur F., Dragomir N. M., Collins S. F. & Brodzeli Z., 2010e, Fabrication of a fibre Bragg grating liquid composition sensor based on wet etching technique, Proc. 35<sup>th</sup> Australian Conference on Optical Fibre Technology (CD-ROM: 19<sup>th</sup> Australian Institute of Physics Congress, Australian Institute of Physics, Australian Optical Society & Engineers Australia, ISBN 978-0-9775657-6-4), Melbourne, Australia, paper no. 663.
- Bal H. K., Sidiroglou F., Yam S. P., Brodzeli Z., Wade S. A., Baxter G. W. & Collins S. F., 2009b, Response of fiber Bragg grating transmission dips at twice the Bragg wavelength to transverse strain, Proc. Australasian Conference on Optics, Lasers and Spectroscopy and 34<sup>th</sup> Australian Conference on Optical Fibre Technology 2009 (CD-ROM: ACOFT ACOLS 09, Australian Optical Society & Engineers Australia, ISBN 1 876346 61 2), Adelaide, Australia, ACOFT paper 26, pp. 487–488.
- Bal H. K., Sidiroglou F., Yam S. P., Brodzeli Z., Wade S. A., Baxter G. W. & Collins S. F., 2009c, Response of fiber Bragg grating transmission dips at twice the Bragg wavelength to transverse strain, Proc. 20<sup>th</sup> International Conference on Optical Fibre Sensors (OFS 2009), Edinburgh, UK, Proc. SPIE, 7503, 750337.
- Bal H. K., Soin K., Mclaughlin P., Collins S. F. & Dragomir N. M., 2010f, Fibre Bragg grating sensors for human skin pressure measurements, Proc. 35<sup>th</sup>

Australian Conference on Optical Fibre Technology (CD-ROM: 19th Australian Institute of Physics Congress, Australian Institute of Physics, Australian Optical Society & Engineers Australia, ISBN 978-0-9775657-6-4), Melbourne, Australia, paper no. 607.

Bali L. M., Shukla R. K., Srivastava P., Srivastava A., Srivastava A. & Kulshreshtha A., 2005, New approach to the measurement of refractive index, *Optical Engineering*, 44, 058002.

Banerjee A., Mukherjee S., Verma R. K., Jana B., Khan T. K., Chakroborty M., Das R., Biswas S., Saxena A., Singh V., Hallen R. M., Rajput R. S., Tewari P., Kumar S., Saxena V., Ghosh A. K., John J. & Gupta-Bhaya P., 2007, Fiber optic sensing of liquid refractive index, *Sensors and Actuators B-Chemical*, 123, 594-605.

Bao Y., Sneh A., Hsu K., Johnson K. M., Liu J. Yu, Miller C. M., Monta Y. & McClain M. B., 1996, High-speed liquid crystal fiber Fabry-Perot tunable filter, *IEEE Photonics Technology Letters*, 8, 1190-2.

Baptista J. M., Abad S., Rego G., Ferreira L. A., Araujo F. M., Santos J. L. & Lage A. S., 2002, Multiplexing of self-referenced fibre optic intensity sensors using fibre Bragg gratings and wavelength division couplers, Proc. 15<sup>th</sup> International Conference on Optical Fiber Sensors Conference Technical Digest (OFS 2002), Portland, USA, Proc. IEEE (IEEE Catalog No. 02EX533, ISBN: 0 7803 7289 1), 1, 243-6.

Baptista J. M., Santos J. L. & Lage A. S., 2001, Measurement of refractive index in oils using a self-referenced fiber optic intensity sensor, The 14<sup>th</sup> Annual Meeting of the IEEE Lasers and Electro-Optics Society (LEOS 2001), 2, 875-6.

Barbu M., Jovanovich K., Trahan R. & Chirlian P., 2002, The use of tapered fibers in an intensity based single mode temperature sensor, 2<sup>nd</sup> ISA/IEEE Sensors for Industry Conference, 47-50.

Basell M. C. & Hawkins J. M., 1998, *Method and apparatus for determining the charge condition of an electrochemical cell*, United States Patent 5717336

Bennett J., El-Sherif M. & Froggatt M., 2001, Transverse loading effects on embedded Bragg fiber system, Proc. Fiber Optic Sensor Technology II, Boston, MA, Proc. SPIE, 4204, 50-60.

Bernardin J. P. & Lawandy N. M., 1990, Dynamics of the formation of Bragg gratings in germanosilicate optical fibres, *Optics Communications*, 79, 194-9.

Bhatia V. & Vengsarkar A. M., 1996, Optical fiber long-period grating sensors, *Optics Letters*, 21, 692-4.

- Bjerkan L., Johannessen K. & Guo X., 1997, Measurements of Bragg grating birefringence due to transverse compressive forces, Proc. 12<sup>th</sup> International Conference on Optical Fiber Sensors (OFS, OSA Technical Digest Series), Optical Society of America, OTuC7.
- Blanke H., Bohlen O., Buller S., De Doncker R. W., Fricke B., Harnmouche A., Linzen D., Thele M. & Sauer D. U., 2005, Impedance measurements on lead-acid batteries for state-of-charge, state-of-health and cranking capability prognosis in electric and hybrid electric vehicles, *Journal of Power Sources*, 144, 418-25.
- Bock W. J., 1990, High-pressure polarimetric sensor using birefringent optical fibers, *IEEE Transactions on Instrumentation and Measurement*, 39, 233-7.
- Bohnert K., Brandle H., Gabus P., Kostovic J. & Talir J., 2000a, *Fiber-optic voltage sensor for outdoor high-voltage installations*, United States patent application 6140810.
- Bohnert K., Gabus P., Kostovic J. & Brandle H., 2005, Optical fiber sensors for the electric power industry, *Optics and Lasers in Engineering*, 43, 511-26.
- Bohnert K., Kostovic J. & Pequignot P., 2000b, Fiber optic voltage sensor for 420 kV electric power systems, *Optical Engineering*, 39, 3060-7.
- Brennan J. F., Sloan D. A., Fahey M. T. & Novack J. C., 2001, *Accelerated method for increasing the photosensitivity of a glassy material*, United States patent application 6311524.
- Brodzeli Z., Bal H. K., Sidiroglou F., Collins S. F., Chigrinov V., Murauski A. & Fan F., 2009a, Multipoint fibre optic voltage sensor, Proc. Australasian Conference on Optics, Lasers and Spectroscopy and 34<sup>th</sup> Australian Conference on Optical Fibre Technology 2009 (CD-ROM: ACOFT ACOLS 09, Australian Optical Society & Engineers Australia, ISBN 1 876346 61 2), Adelaide, Australia, ACOLS paper 235, 185–186.
- Brodzeli Z., Bal H. K., Sidiroglou F., Collins S. F., Chigrinov V., Murauski A. & Fan F., 2010, Fibre optic/liquid crystal multipoint voltage sensor, Asia-Pacific Optical Sensors (APOS) Conference 2010, Guangzhou, China.
- Brodzeli Z., Bal H. K., Sidiroglou F., Dragomir N. M. & Ladouceur F., 2009b, Fabrication of phase-shifted fibre Bragg gratings with non-uniform etching, Proc. Australasian Conference on Optics, Lasers and Spectroscopy and 34<sup>th</sup> Australian Conference on Optical Fibre Technology 2009 (CD-ROM: ACOFT ACOLS 09, Australian Optical Society & Engineers Australia, ISBN 1 876346 61 2), Adelaide, Australia, ACOFT paper 46, 525–526.

- Brodzeli Z., Baxter G. W., Collins S. F., Bal H. K., Canning J., Michael S., Buryak A. & Vasiliev M., 2008a, Implementation of a low cost interrogation technique for an optical fibre Bragg grating sensor for simultaneous transverse and longitudinal strain measurement, *18<sup>th</sup> National Congress of Australian Institute of Physics (AIP 2008)*, The University of Adelaide, South Australia.
- Brodzeli Z., Baxter G. W., Collins S. F., Canning J., Stevenson M. & Buryak A., 2008b, Low cost interrogation technique for a FBG sensor for combined transverse and longitudinal strain measurement, Proc. 19<sup>th</sup> International Conference on Optical Fibre Sensors (OFS), Perth, WA, Australia, Proc. SPIE, 7004, 700466.
- Brodzeli Z. M. & Stepanov D. Y., 1999, Direct observation of optical fibre densification under UV irradiation, Proc. 24<sup>th</sup> Australian Conference on Optical Fibre Technology (ACOFT 1999), IREE, N.S.W, Australia.
- Buck J. A., 2004, *Fundamentals of optical fibers*, John Wiley & Sons Inc., New Jersey, USA.
- Budynas R. G., 1999, *Advanced strength and applied stress analysis*, WCB/McGraw-Hill.
- Byrne B., 2001, Deep vein thrombosis prophylaxis: The effectiveness and implications of using below-knee or thigh-length graduated compression stockings, *Heart Lung*, 30, 4, 277-84.
- Byrne B., 2002, Deep vein thrombosis prophylaxis: The effectiveness and implications of using below-knee or thigh-length graduated compression stockings, *Journal of vascular nursing: official publication of the Society for Peripheral Vascular Nursing*, 20, 53-9.
- Canning J. & Sceats M. G., 1994, Pi-phase-shifted periodic distributed structures in optical fibres by UV post-processing, *Electronics Letters*, 30, 1344-5.
- Canning J., 2008, Progress in photosensitivity for writing Bragg gratings, Proc. 19<sup>th</sup> International Conference on Optical Fibre Sensors (OFS 2008), Perth, WA, Australia, Proc. SPIE, 7004, 700409.
- Castrejon-Pita J. R., Morales A. & Castrejon-Garcia R., 2006, Critical angle laser refractometer, *Review of Scientific Instruments*, 77, 035101-4.
- Caucheteur C., Wuilpart M., Chen C., Megret P. & Albert J., 2009, Multi-point in-line refractometry using tilted fiber Bragg gratings, IEEE/LEOS Winter Topicals Meeting Series, 2009, 75-6.
- Chandrasekhar S., 1992, *Liquid crystals*, Cambridge University Press, UK.

- Chavan A. V. & Wise K. D., 2001, Batch-processed vacuum-sealed capacitive pressure sensors, *Journal of Microelectromechanical Systems*, 10, 580-8.
- Chehura E., Ye C. C., Staines S. E., James S. W. & Tatam R. P. 2004, Characterization of the response of fibre Bragg gratings fabricated in stress and geometrically induced high birefringence fibres to temperature and transverse load, *Smart Materials and Structures*, 13, 888.
- Chehura E., James S. W., Lawson N., Garry K. P. & Tatam R. P., 2009, Pressure measurements on aircraft wing using phase-shifted fibre Bragg grating sensors, Proc. 20<sup>th</sup> International Conference on Optical Fibre Sensors (OFS 2009,), Edinburgh, United Kingdom, Proc. SPIE, 7503, 750334.
- Chen C. H., Tang J. L. & Wu W. T. 2010, Fabrication of the novel multi-D-shape fiber sensor by femtosecond laser machining with the diffractive optical element, Symposium on Design Test Integration and Packaging of MEMS/MOEMS (DTIP), Seville, 382-6.
- Chen G., Liu L., Jia H., Yu J., Xu L. & Wang W., 2003, Simultaneous pressure and temperature measurement using Hi-Bi fiber Bragg gratings, *Optics Communications*, 228, 99-105.
- Chen H. W., Tien C. L., Liu W. F. & Lin S.-W., 2007, The measurement of liquid refractive index by D-shaped fiber Bragg grating, IEEE International Conference on Optical MEMS and Nanophotonics, 2007 (IEEE/LEOS), Hualien 119-20.
- Chen J., Morris S. M., Wilkinson T. D., Freeman J. P. & Coles H. J., 2009, High speed liquid crystal over silicon display based on the flexoelectro-optic effect, *Optics Express*, 17, 7130-7.
- Chi H., Tao X. M., Yang D. X. & Chen K. S., 2001, Simultaneous measurement of axial strain, temperature, and transverse load by a superstructure fiber grating, *Optics Letters*, 26, 1949-51.
- Chiang K. S. & Liu Q., 2006, Long-period grating devices for application in optical communication, 5<sup>th</sup> International Conference on Optical Communications and Networks (ICOON), Chengdu, China, 128-33.
- Chigrinov V., 2010, Liquid crystal applications in photonics, *Frontiers of Optoelectronics in China*, 3, 103-7.
- Chigrinov V. G., 2007, Liquid crystal devices for photonics applications, Proc. Passive components and fiber-based devices IV, Wuhan, China, Proc. SPIE, 6781, 67811M.

- Chigrinov V. G., Kozenkov V. M. & Kwok H. S., 2008, *Photoalignment of LCs*, John Wiley & Sons, Ltd.
- Chiu M. H. & Wang S. F., 2004, New-type fiber optical liquid refractometer, *Novel Optical Systems Design and Optimization VII*, Proc. SPIE, 5524, 169.
- Chryssis A. N., Lee S. M., Lee S. B., Saini S. S. & Dagenais M., 2005, High sensitivity evanescent field fiber Bragg grating sensor, *IEEE Photonics Technology Letters*, 17, 1253-5.
- Cole M. J., Loh W. H., Laming R. I., Zervas M. N. & Barcelos S., 1995, Moving fibre/phase mask-scanning beam technique for enhanced flexibility in producing fibre gratings with uniform phase mask, *Electronics Letters*, 31, 1488-90.
- Collings P. J., 2005, Ferroelectric liquid crystals: The 2004 Benjamin Franklin medal in physics presented to Robert B. Meyer of Brandeis University, *Journal of the Franklin Institute-Engineering and Applied Mathematics*, 342, 599-608.
- Collins S. F., Yam S. P., Bal H. K., Kouskousis B. P., Rollinson C. M., Sidiroglou F., Brodzeli Z., Wade S. A. & Baxter G. W., 2010, Fiber Bragg gratings at twice the Bragg wavelength: Properties and sensor applications, 2<sup>nd</sup> Asia-Pacific Optical Sensors Conference (APOS 2010) Guangzhou, China, (Invited Paper).
- Cordaro M. H., Rode D. L., Barry T. S. & Krchnavek R. R., 1994, Precision fabrication of D-shaped single-mode optical fibers by in situ monitoring, *Journal of Lightwave Technology*, 12, 1524-31.
- Cortazar O. D. & Feliu V., 2006, A simple and robust fiber optics system for measuring the lead-acid battery state-of-charge, *Journal of Power Sources*, 159, 728-33.
- Cortes P. Y., Ouellette F. & Larochelle S., 1998, Intrinsic apodisation of Bragg gratings written using UV-pulse interferometry, *Electronics Letters*, 34, 396-7.
- Cusano A., Iadicicco A., Campopiano S., Giordano M. & Cutolo A., 2005, Thinned and micro-structured fibre Bragg gratings: Towards new all-fibre high-sensitivity chemical sensors, *Journal of Optics A-Pure and Applied Optics*, 7, 734-41.
- Dai C., Yang D., Tao X. & Tam H. Y., 2000, Effects of pure bending on the sensing characteristics of fiber Bragg gratings, Proc. International Conference on Sensors and Control Techniques (ICSC 2000), Wuhan, China, Proc. SPIE, 4077, 92-6.

- Dakin J. & Brown R.G.W., 2006, *Handbook of optoelectronics*, CRC Press (Taylor & Francis group), Florida.
- Dowgiallo E. J. Jr., 1976, *Method for determining battery state of charge by measuring A.C. Electrical phase angle change*, United States Patent 3984762.
- Dragomir N. M., Rollinson C., Wade S. A., Stevenson A. J., Collins S. F., Baxter G. W., Farrell P. M. & Roberts A., 2003, Nondestructive imaging of a type I optical fiber Bragg grating, *Optics Letters*, 28, 789-91.
- Dutta S., Basak S., Kumar R. & Samanta P. K., 2010, Fabrication of intensity based fiber optic pH sensor, 3<sup>rd</sup> International Nanoelectronics Conference (INEC 2010), 370-1.
- Dyer P. E., Farley R. J. & Giedl R., 1995, Analysis of grating formation with excimer laser irradiated phase masks, *Optics Communications*, 115, 327-34.
- El-Sherif M., Bansal L. & Yuan J. M., 2007, Fiber optic sensors for detection of toxic and biological threats, *Sensors*, 7, 3100-18.
- Fang J. X., Taylor H. F. & Choi H. S., 1998, Fiber-optic Fabry-Perot flow sensor, *Microwave and Optical Technology Letters*, 18, 209-11.
- Fang X., Liao C. R. & Wang D. N., 2010, Femtosecond laser fabricated fiber Bragg grating in microfiber for refractive index sensing, *Optics Letters*, 35, 1007-9.
- Feng Z., Zhang Y., Tan Y. N. & Wu C., 2010, Hydrostatic pressure sensors based on ultrashort distributed-Bragg-reflector fiber lasers, *Optical Engineering*, 49, 100502-3.
- Filippov V. N., Starodumov A. N., Minkovich V. P. & Barmenkov Y. O., 2000, Optically controlled fiber voltage sensor, *IEEE Photonics Technology Letters*, 12, 870-2.
- Frank A., Haroud K., Rochat E., Bohnert K. & Brandle H., 2002, High resolution fiber laser sensor for hydrostatic pressure, Proc. IEEE 15<sup>th</sup> Optical Fiber Sensors Conference Technical Digest (OFS 2002), Portland, USA, Proc. IEEE (IEEE Catalog No. 02EX533, ISBN: 0 7803 7289 1), 359-62
- Gafsi R. & El-Sherif M. A., 2000, Analysis of induced-birefringence effects on fiber Bragg gratings, *Optical Fiber Technology*, 6, 3, 299-323.
- Gordon J. D., 2007, *Using an optical D-fiber as a chemical sensor*, Bachelor of Science, Brigham Young University, URL: <http://www.physics.byu.edu/faculty/rees/416/Samples/John%20Gordon/thesis/Template.pdf>.

- Govindan G., Gokul R. S. & Sastikumar D., 2009, Measurement of refractive index of liquids using fiber optic displacement sensors, *Journal of American Science*, 5, 13-7.
- Grattan K. T. V. & Meggitt B. T., 1994, *Optical fibre sensor technology*, Chapman & Hall London & Kluwer Academic, Dordrecht, Netherlands.
- Guo T., Zhao Q., Dou Q., Zhang H., Xue L., Huang G. & Dong X., 2005, Temperature-insensitive fiber Bragg grating liquid-level sensor based on bending cantilever beam, *IEEE Photonics Technology Letters*, 17, 2400-2.
- Han Y. G., Lee J. & Lee S., 2004, Discrimination of bending and temperature sensitivities with phase-shifted long-period fiber gratings depending on initial coupling strength, *Optics Express*, 12, 3204-8.
- Han Y. G., Dong X., Lee J. H. & Lee S. B., 2007, Temperature insensitive bending sensor based on a sampled fiber Bragg grating, Conference on Optical Fiber Communication and the National Fiber Optic Engineers Conference, 2007 (OFC/NFOEC 2007), 1-3.
- Hancke G. P., 1990, A fibre-optic density sensor for monitoring the state-of-charge of a lead-acid battery, *IEEE Transactions on Instruments and Measurements* 39, 1, 247-250.
- Hao J., Cai Z., Ng J. H., Gong Y. & Varghese P., 2006, Simultaneous temperature and lateral force measurement using simple arc-shaped FBG sensor module, *Electronics Letters*, 42, 1446-7.
- Hecht J., 2004, *City of light: The story of fiber optics*, Oxford University Press, New York.
- Herzog J. A., 1993, Deep vein thrombosis in the rehabilitation client: Diagnostic tools, prevention, and treatment modalities, *Rehabilitation Nursing*, 18, 8-11.
- Hill K. O., 2000, Photosensitivity in optical fiber waveguides: From discovery to commercialization, *IEEE Journal of Selected Topics in Quantum Electronics* 6, 1186-9.
- Hill K. O., Fujii Y., Johnson D. C. & Kawasaki B. S., 1978, Photosensitivity in optical fiber waveguides: Application to reflection filter fabrication, *Applied Physics Letters*, 32, 647-9.
- Hill K. O. & Meltz G., 1997, Fiber Bragg grating technology fundamentals and overview, *Journal of Lightwave Technology*, 15, 1263-76.

- Hirabayashi K., Tsuda H. & Kurokawa T., 1993, Tunable liquid-crystal Fabry-Perot interferometer filter for wavelength-division multiplexing communication systems, *Journal of Lightwave Technology*, 11, 2033-43.
- Horner J., Fernandes J., Fernandes E. & Nicolaides A. N., 1980, Value of graduated compression stockings in deep venous insufficiency, *British Medical Journal*, 280, 820-1.
- Hu D. J. J., Shum P., Lu C., Sun X., Ren G., Yu X. & Wang G., 2009, Design and analysis of thermally tunable liquid crystal filled hybrid photonic crystal fiber coupler, *Optics Communications*, 282, 2343-7.
- Huang D. W., Liu W. F., Wu C. W. & Yang C. C., 2000, Reflectivity-tunable fiber Bragg grating reflectors, *IEEE Photonics Technology Letters*, 12, 176-8.
- Huang X. F., Chen Z. M., Shao L. Y., Cen K. F., Sheng D. R., Chen J. & Zhou H., 2008, Design and characteristics of refractive index sensor based on thinned and microstructure fiber Bragg grating, *Applied Optics*, 47, 504-11.
- Iadicicco A., Campopiano S., Cutolo A., Giordano M. & Cusano A., 2005a, Nonuniform thinned fiber Bragg gratings for simultaneous refractive index and temperature measurements, *IEEE Photonics Technology Letters*, 17, 1495-7.
- Iadicicco A., Campopiano S., Cutolo A., Giordano M. & Cusano A., 2005b, Refractive index sensor based on microstructured fiber Bragg grating, *IEEE Photonics Technology Letters*, 17, 1250-2.
- Iadicicco A., Cusano A., Cutolo A., Bernini R. & Giordano M., 2004, Thinned fiber Bragg gratings as high sensitivity refractive index sensor, *IEEE Photonics Technology Letters*, 16, 1149-51.
- Iadicicco A., Campopiano S., Paladino D., Cutolo A. & Cusano A., 2007, Microstructured fiber Bragg gratings: Optimization of the fabrication process, *Optics Express*, 15, 15011-21.
- Iadicicco A., Cusano A., Persiano G. V., Cutolo A., Bernini R. & Giordano M., 2003, Refractive index measurements by fiber Bragg grating sensor, Proc. IEEE Sensors Conference 2003, 1, 101-5.
- Ibsen M., Eggleton B. J., Sceats M. G. & Ouellette F., 1995, Broadly tunable DBR fibre laser using sampled fibre Bragg gratings, *Electronics Letters*, 31, 37-8.
- Ibsen M., Fu A., Geiger H. & Laming R. I., 1999, All-fibre 4 x 10Gbit/s WDM link with DFB fibre laser transmitters and single sine-sampled fibre grating dispersion compensator, *Electronics Letters*, 35, 982-3.

- Ignacio R. M., Francisco J. A. & Richard O. C., 2007, *Novel fiber optic sensing architectures based on sensitive nanofilms* [Online], Available: [http://www.iaria.org/conferences2007/filesSENSORCOMM07/Matias\\_SensorComm07.pdf](http://www.iaria.org/conferences2007/filesSENSORCOMM07/Matias_SensorComm07.pdf) [Accessed 2011].
- Jackson D. A. & Jones J. D. C., 1986, Extrinsic fibre-optic sensors for remote measurement: Part one, *Optics & Laser Technology*, 18, 243-52.
- Jarzynski J., 1984, Frequency response of a single-mode optical fiber phase modulator utilizing a piezoelectric plastic jacket, *Journal of Applied Physics*, 55, 3243-50.
- Jing F., Yun Z., Su-Shan L., Xiao-Wen L., Fei X. & Yan-Qing L., 2010, Fiber-optic pressure sensor based on tunable liquid crystal technology, *IEEE Photonics Journal* 2, 292-8.
- Jonker M. J., De Boer E. M., Ader H. J. & Bezemer P. D., 2001, *The oedema-protective effect of lycra support stockings*, *Dermatology*, 203, 4, 294-8.
- Jorgenson R. C. & Yee S. S., 1993, A fiber-optic chemical sensor based on surface plasmon resonance, *Sensors and Actuators B: Chemical*, 12, 213-20.
- Julich F. & Roths J., 2010, Comparison of transverse load sensitivities of fibre Bragg gratings in different types of optical fibres, Proc. Optical Sensing and Detection, Brussels, Belgium, Proc. SPIE, 7726, 77261N-9.
- Kaddu S. C., Booth D. J., Garchev D. D. & Collins S. F., 1997, Intrinsic fibre Fabry-Perot sensors based on co-located Bragg gratings, *Optics Communications*, 142, 189-92.
- Kalvoda L., Aubrecht J., Klepacek R. & Lukasova P., 2010, Sensing applications of U-optrodes, Proc. 4<sup>th</sup> European Workshop on Optical Fibre Sensors (EWOFS 2010.), Proc. SPIE, 7653, 765329.
- Kao K. C. & Hockham G. A., 1966, Dielectric-fibre surface waveguides for optical frequencies, *Proceedings of the Institution of Electrical Engineers*, 113, 1151-8.
- Kashyap R., 1999, *Fiber Bragg gratings*, Academic Press, London, UK.
- Kashyap R., Mckee P. F. & Armes D., 1994, UV written reflection grating structures in photosensitive optical fibres using phase-shifted phase masks, *Electronics Letters*, 30, 1977-8.
- Kawakami S. & Nishida S., 1974, Characteristics of a doubly clad optical fiber with a low-index inner cladding, *IEEE Journal of Quantum Electronics*, 10, 879-87.

- Keck D. B., 1981, *Fundamentals of Optical Fiber Communications*, Academic Press, New York.
- Kejalakshmy N. & Srinivasan K., 2001, Simple method of Brewster-angle measurement for the determination of refractive indices in transparent biaxial crystal, *Optical Engineering*, 40, 2594-7.
- Kersey A. D., Davis M. A., Patrick H. J., LeBlanc M., Koo K. P., Askins C. G., Putnam M. A. & Friebele E. J., 1997, Fiber grating sensors, *Journal of Lightwave Technology*, 15, 1442-63.
- Kim C. B. & Su C. B., 2004, Measurement of the refractive index of liquids at 1.3 and 1.5 micron using a fibre optic Fresnel ratio meter, *Measurement Science & Technology*, 15, 1683-6.
- Kouskousis B. P., 2009, *Microscopic characterisation of fibre Bragg gratings*, PhD Thesis, Victoria University, Australia.
- Kouskousis B. P., Rollinson C. M., Kitcher D. J., Collins S. F., Baxter G. W., Wade S. A., Dragomir N. M. & Roberts A., 2006, Quantitative investigation of the refractive-index modulation within the core of a fiber Bragg grating, *Optics Express*, 14, 10332-8.
- Krohn D. A., 2000, *Fibre optic sensors: fundamentals and applications*, ISA, USA.
- Kumar S., 2009, *Biaxial liquid crystal electro-optic devices*, United States patent application 7604850.
- Lagerwall S. T., 2004, Ferroelectric and antiferroelectric liquid crystals, *Ferroelectrics*, 301, 15-45.
- Laine J. P., Little B. E. & Haus H. A., 1999, Etch-eroded fiber coupler for whispering-gallery-mode excitation in high-Q silica microspheres, *IEEE Photonics Technology Letters*, 11, 1429-30.
- Laming R. I. & Payne D. N., 1989, Electric current sensors employing spun highly birefringent optical fibers, *Journal of Lightwave Technology*, 7, 2084-94.
- Larsen A. M. & Futtrup I., 2004, Watch the pressure - it drops, *European Wound Management Association Journal*, 4, 1-12.
- Lawrence C., Nelson D., Udd E. & Bennett T., 1999, A fiber optic sensor for transverse strain measurement, *Experimental Mechanics*, 39, 202-9.

- Le Goullon D. & Goswami K., 1990, *Fiber optic refractive index sensor using a metal clad*, United States patent application 4929049.
- LeBlanc M., Vohra S. T., Tsai T. E. & Friebele E. J., 1999, Transverse load sensing by use of pi-phase-shifted fiber Bragg gratings, *Optics Letters*, 24, 1091-3.
- Lee B., Jeong Y., Baek S., Kim H. R., Kim Y., Lee Y. W. A. & Lee S. D., 2002a, Electromagnetic field sensing using liquid crystal optical fibers, Proc. 15<sup>th</sup> Optical Fiber Sensors Conference Technical Digest (OFS 2002), Portland, USA, Proc. IEEE (IEEE Catalog No. 02EX533, ISBN: 0 7803 7289 1), 403-6.
- Lemaire P. J., Atkins R. M., Mizrahi V. & Reed W. A., 1993, High pressure h<sub>2</sub> loading as a technique for achieving ultrahigh UV photosensitivity and thermal sensitivity in GeO<sub>2</sub> doped optical fibres, *Electronics Letters*, 29, 1191-3.
- Li H. & Xie S., 1996, Measurement method of the refractive index of biotissue by total internal reflection, *Applied Optics*, 35, 1793-5.
- Li Y. & Dai X. Q. D., 2006, Clothing comfort and compression therapy, *Biomechanical engineering of textiles and clothing*, Woodhead Publishing Limited, Cambridge, UK.
- Liang W., Huang Y. Y., Xu Y., Lee R. K. & Yariv A., 2005, Highly sensitive fiber Bragg grating refractive index sensors, *Applied Physics Letters*, 86, 151122-3.
- Liang X. J., Liu A. Q., Lim C. S., Ayi T. C. & Yap P. H., 2007, Determining refractive index of single living cell using an integrated microchip, *Sensors and Actuators A: Physical*, 133, 349-54.
- Liao C. R., Wang Ying, Wang D. N. & Yang Minwei, 2010, Multi-parameter sensor using fiber in-line MZ interferometer embedded in fiber Bragg grating, Proc. 4<sup>th</sup> European Workshop on Optical Fibre Sensors (EWOFS 2010), Proc. SPIE, 7653, 765310.
- Liu B., Miao Y. P., Zhou H. B. & Zhao Q. D., 2008, Pure bending characteristic of tilted fiber Bragg grating, *Journal of Electronic Science and Technology of China*, 6, 470-3
- Liu Y., Zhang L. & Bennion I., 1999, Fibre optic load sensors with high transverse strain sensitivity based on long-period gratings in B/Ge co-doped fibre, *Electronics Letters*, 35, 661-3.
- Lyons E. R. & Lee H. P., 1999, Demonstration of an etched cladding fiber Bragg grating filter with reduced tuning force requirement, *IEEE Photonics Technology Letters*, 11, 1626-8.

- Martelli C., Canning J., Kristensen M. & Groothoff N., 2007, Refractive index measurement within a photonic crystal fibre based on short wavelength diffraction, *Sensors*, 7, 2492-8.
- Martin P. J., 2008, Recent patents on liquid crystal alignment, *Recent Patents on Materials Science*, 1, 21-8.
- Masuda S. & Iwama T., 1982, Single-mode fiber-optic directional coupler, *Applied Optics*, 21, 3484-8.
- Mathews S., Farrell G. & Semenova Y., 2010, Liquid crystal filled photonic crystal fibers for voltage sensing applications, Proc. Optical Sensing and Detection Conference, Brussels, Belgium, Proc. SPIE, 7726, 77260R.
- Matsuhara M. & Hill K. O., 1974, Optical-waveguide band-rejection filters - design, *Applied Optics*, 13, 2886-8.
- Matsui T., 1987, Portable type optical hydrometer for lead-acid batteries, *Prog. Batteries Solar Cells*, 6, 130-2.
- Mears R. J., Reekie L., Jauncey I. M. & Payne D. N., 1987, Low-noise erbium-doped fibre amplifier operating at 1.54  $\mu\text{m}$ , *Electronics Letters*, 23, 1026-8.
- Meltz G., Morey W. W. & Glenn W. H., 1989, Formation of Bragg gratings in optical fibers by a transverse holographic method, *Optics Letters*, 14, 823-5.
- Menadier C., Kissenger C. & Adkins H., 1967, The photonic sensor, *Instrumentation & Control Systems*, 40, 114.
- Michie A., Canning J., Bassett I., Haywood J., Digweed K., Ashton B., Stevenson M., Digweed J., Lau A. & Scandurra D., 2007, Spun elliptically birefringent photonic crystal fibre for current sensing, *Measurement Science and Technology*, 18, 3070.
- Mueller H., 1938, The theory of photoelasticity, *Journal of the American Ceramic Society*, 21, 27-33.
- Nagai Y., Tomokuni Y., Matsui T., 1987, Optical-type hydrometer for lead-acid batteries and its applications, Proceedings of the INTELEC, International Telecommunications Energy Conference, 640-7.
- Nand A., 2007, *Intragrating sensing using chirped optical fibre Bragg gratings*, PhD Thesis, Victoria University, Australia.

- Ohsawa N., Tsurumi T, Maeda T, 2001, *Battery voltage measuring device*, US Patent 6255826.
- Othonos A. & Kalli K., 1999, *Fiber Bragg gratings: fundamentals and applications in telecommunication and sensing*, Boston, USA, Artech House.
- Pacheco M., Santoyo F. M., Méndez A. & Zenteno L. A., 1999, Piezoelectric-modulated optical fibre Bragg grating high-voltage sensor, *Measurement Science and Technology*, 10, 777.
- Partsch B. & Partsch H., 2008, Compression stockings for treating venous leg ulcers: Measurement of interface pressure under a new ulcer kit, *Phlebology*, 23, 1, 40-6.
- Passaro V. M. N., Dell'olio F. & De Leonardis F., 2006, Electromagnetic field photonic sensors, *Progress in Quantum Electronics*, 30, 45-73.
- Paul J., Zhao L. & Ngoi B. K. A., 2005, Fiber-optic sensor for handgrip-strength monitoring: Conception and design, *Applied Optics*, 44, 3696-704.
- Paz A. M. C. Y., Acevedo J. M., Vazquez A. D R., Penalver C. M., Ferreiro A. L., Melendez A. A. N. & Gandoy J. D., 2010, A multi-point sensor based on optical fiber for the measurement of electrolyte density in lead-acid batteries, *Sensors*, 10, 2587-608.
- Paz A. M., Cao Y. & Acevedo J. M., 2006, Fibre optic sensor for multipoint measurement in lead acid batteries, Proc. 18<sup>th</sup> International Conference on Optical Fiber Sensors (OFS 2006), Cancún, Mexico, Optical Society of America, TuE56.
- Phan H. M. C., Laffont G., Dewynter V., Ferdinand P., Roy P., Auguste J. L., Pagnoux D., Blanc W. & Dussardier B., 2007, Three-hole microstructured optical fiber for efficient fiber Bragg grating refractometer, *Optics Letters*, 32, 2390-2.
- Photon Design, *What is fimmwave?* [Online], Available: <http://www.photond.com/products/fimmwave.htm> [Accessed 2009].
- Pluta M., 1994, Nomarski's DIC microscopy: A review, Proc. Phase Contrast and Differential Interference Contrast Imaging Techniques and Applications, Warsaw, Poland, Proc. SPIE, 1846, 10.
- Pureur V., Bouwmans G., Delplace K., Quiquempois Y. & Douay M., 2009, Birefringent solid-core photonic bandgap fibers assisted by interstitial air holes, *Applied Physics Letters*, 94, 131102-3.

- Rahmatian F. & Jaeger N. A. F., 1993, An integrated optics sensor for high-voltage measurement applications, Proc. IEEE Canadian Conference on Electrical and Computer Engineering, 2, 672-5.
- Rao Y. J., 1999, Recent progress in applications of in-fibre Bragg grating sensors, *Optics and Lasers in Engineering*, 31, 297-324.
- Rao Y. J., Wang W., Zhu T. & Duan D., 2009, In-line fiber-optic Fabry-Perot ultrasound sensor formed by hollow-core photonic-crystal fiber, IEEE Sensors Conference 2009, 858-60.
- Rao Y. J., Webb D. J., Jackson D. A., Zhang L. & Bennion I., 1996, High-resolution, wavelength-division-multiplexed in-fibre Bragg grating sensor system, *Electronics Letters*, 32, 924-6.
- Renner R., Kehrli M., Lüthy W. & Weber H. P., 2003, Manufacturing of a D-shaped fiber, *Laser Physics*, 13, 232-3.
- Ribeiro A. B. L. & Jackson D. A., 1993, Low coherence fiber optic system for remote sensors illuminated by a 1.3  $\mu\text{m}$  multimode laser diode, *Review of Scientific Instruments*, 64, 2974-7.
- Rogers A. J., 1977, Optical methods for measurement of voltage and current on power systems, *Optics & Laser Technology*, 9, 273-83.
- Rogers A. J., 1979, Optical measurement of current and voltage on power systems, *IEEE Journal on Electric Power Applications* 2, 120-4.
- Rogers A. J., 1998, Intrinsic optical fibre current sensors, *Sensor Review*, 18, 17-22.
- Rollinson C. M., Wade S. A., Dragomir N. M., Roberts A., Baxter G. W. & Collins S. F., 2005, Three parameter sensing with a single Bragg grating in non-birefringent fiber, Proc. Bragg Gratings Poling & Photosensitivity/Australian Conference on Optical Fibre Technology 2005 (Proc. BGPP/ACOFT 2005) (CD-ROM, ISBN 1877040339), 92-4.
- Rollinson C. M., Wade S. A., Dragomir N. M., Baxter G. W. & Collins S. F., 2005a, Strain and temperature response of transmission dips at 2/3 of the Bragg wavelength in type I and IIA fiber Bragg gratings, Proc. 17<sup>th</sup> International Conference on Optical Fibre Sensors (OFS 2005), Proc. SPIE, 5855, 310-3.
- Rollinson C. M., Wade S. A., Dragomir N. M., Baxter G. W., Collins S. F. & Roberts A., 2005b, Reflections near 1030 nm from 1540 nm fibre Bragg gratings: Evidence of a complex refractive index structure, *Optics Communications*, 256, 310-8.

- Rui S., Xianfeng C., Kaiming Z., Lin Z. & Bennion I., 2008, 800 nm WDM interrogation system for strain, temperature, and refractive index sensing based on tilted fiber Bragg grating, *IEEE Sensors Journal*, 8, 1273-9.
- Russell P. St J., 2006, Photonic-crystal fibers, *Journal of Lightwave Technology*, 24, 4729-49.
- Sandbank C. P., 1977, Fibre Optic Communication Systems, IEEE 7<sup>th</sup> European Microwave Conference, 3-12.
- Sanders G. A., Blake J. N., Rose A. H., Rahmatian F. & Herdman C., 2002, Commercialization of fiber-optic current and voltage sensors at NxtPhase, Proc. 15<sup>th</sup> International Conference on Optical Fiber Sensors, Conference Technical Digest, 2002 (OFS 2002), Portland, USA, Proc. IEEE (IEEE Catalog No. 02EX533, ISBN: 0 7803 7289 1), 1, 31-4.
- Sang X., Yu C., Mayteevarunyoo T., Wang K., Zhang Q. & Chu P. L., 2007, Temperature-insensitive chemical sensor based on a fiber Bragg grating, *Sensors and Actuators B-Chemical*, 120, 754-7.
- Sang X. Z., Yu C. X., Yan B. B., Ma J. X., Meng Z. F., Mayteevarunyoo T. & Lu N. G., 2006, Temperature-insensitive chemical sensor with twin Bragg gratings in an optical fibre, *Chinese Physics Letters*, 23, 3202-4.
- Sastikumar D., Gobi G. & Renganathan B., 2008, Fiber optic sensor for determination of thickness of transparent plates, Proc. SPIE, 19<sup>th</sup> International Conference on Optical Fibre Sensors (OFS 2008), 7004, 2, 70044Q.1-4.
- Schawlow A. L., Townes C. H., 1960, *Masers and maser communications system*, United States patent application 2929922.
- Schulz W. L., Udd E., Seim J. M. & McGill G. E., 1998, Advanced fiber-grating strain sensor systems for bridges, structures, and highways, Proc. Smart Structures and Materials 1998: Smart Systems for Bridges, Structures, and Highways, San Diego, CA, USA, Proc. SPIE, 3325, 212-21.
- Sean J. H. & Tomasz A. L., 2006, Refractive index determination of biological particles, Report no. NRL/MR/6110-06-8967, Naval Research Lab Washington DC.
- Shampo M. A., Kyle R. A. & Steensma D. P., 2011, Charles K. Kao—Father of Fiber Optics, *Mayo Clinic Proceedings*, 86, e45.

- Sharifian S. A., 2003, *Fibre optic pressure transducers for disturbance measurements in transient aerodynamic research facilities*, PhD Thesis, University of Southern Queensland, Australia.
- Shi J., Chen Z. Y., Shen Y. Q. & Guo Q., 2007, Solution-concentration sensor using a fused fiber-optic coupler, *ICEMI 2007: Proceedings of 2007 8th International Conference on Electronic Measurement & Instruments, Vol. IV*, 178-81.
- Shugar G. J., Ballinger J. T. & Dawkins L. M., 1996, *Chemical technicians' ready reference handbook*, McGraw-Hill Professional, New York.
- Sigel B., Edelstein A. L., Savitch L., Hasty J. H. & Felix W. R., 1975, Type of compression for reducing venous stasis: A study of lower extremities during inactive recumbency, *Arch Surg*, 110, 171-5.
- Singh S., 2002, Refractive index measurement and its applications, *Physica Scripta*, 65, 167-180.
- Sirkis J., Berkoff T. A., Jones R. T., Singh H., Kersey A. D., Friebele E. J. & Putnam M. A., 1995, In-line fiber etalon (ILFE) fiber-optic strain sensors, *Journal of Lightwave Technology*, 13, 1256-63.
- Sirkis J. S., 1993, Unified approach to phase-strain-temperature models for smart structure interferometric optical fiber sensors: Part 1, applications, *Optical Engineering*, 32, 752-61.
- Smietana M., Korwin-Pawlowski M. L., Bock W. J., Pickrell G. R. & Szmids J., 2008, Refractive index sensing of fiber optic long-period grating structures coated with a plasma deposited diamond-like carbon thin film, *Measurement Science and Technology*, 19, 085301.
- Smith A. M., 1978, Polarization and magneto-optic properties of single-mode optical fiber, *Applied Optics*, 17, 52-6.
- Smith K. H., Ipson B. L., Lowder T. L., Hawkins A. R., Selfridge R. H. & Schultz S. M., 2006, Surface-relief fiber Bragg gratings for sensing applications, *Applied Optics*, 45, 1669-75.
- Snyder A. W. & Love J. D., 1983, *Optical waveguide theory*, Chapman and Hall.
- Stepanov D. Y., Canning J. & Brodzeli Z., 1998, Real-time characterisation of fibre grating Fabry-Perots and phase-shifted gratings with 100 kHz resolution, *Symposium on Optical Fibre Measurements, Boulder, Colorado*, ISBN 0 7881 8374 5, 149-152.

- Stephens T., Krug P. A., Brodzeli Z., Dhosi G., Ouellette F. & Poladian L., 1996, 257 km transmission at 10 Gbit/s in non-dispersion-shifted fibre using an unchirped fibre Bragg grating dispersion compensator, *Electronics Letters*, 32, 1599-601.
- Stewart G., Johnstone W. & Culshaw B., 1989, *Metal clad fibre optic polarizer*, UK patent application 8722338.
- Storoy H., Engan H. E., Sahlgren B. & Stubbe R., 1997, Position weighting of fiber Bragg gratings for bandpass filtering, *Optics Letters*, 22, 784-6.
- Su H. & Huang X. G., 2007, Fresnel-reflection-based fiber sensor for on-line measurement of solute concentration in solutions, *Sensors and Actuators B: Chemical*, 126, 579-82.
- Suhadolnik A., 2007, An optical fibre interferometric refractometer, *Measurement Science and Technology*, 18, 1205.
- Sun J., Chan C. C. & Dong X. Y., 2005, A wide tunable range fiber Bragg grating filter, Lasers and Electro-Optics (CLEO/Pacific Rim 2005), Baltimore, MD, 1080-1.
- Tabib-Azar M., Sutapun B., Srihirin T., Lando J. & Adamovsky G., 2000, Fiber optic electric field sensors using polymer-dispersed liquid crystal coatings and evanescent field interactions, *Sensors and Actuators A-Physical*, 84, 134-9.
- Takahashi S., Hao J. Z., Lee Y. W. A., Cai Z., Do T. T. & Ng B. Y. R., 2005, Effect of bending methods on FBG lateral force sensor, *Electronics Letters*, 41, 1270-1.
- Taylor H. F., 2002, Fiber optic sensors based upon the Fabry-Perot interferometer, *Fiber optic sensors*, Marcel Dekker Inc., New York.
- Tomljenovic-Hanic S. & Love J. D., 2005, Symmetry-selective reflection gratings, *Journal of Optical Society of America A*, 22, 1615-9.
- Trpkovski S., Wade S. A., Collins S. F. & Baxter G. W., 2005, Er<sup>3+</sup>:Yb<sup>3+</sup> doped fibre with embedded FBG for simultaneous measurement of temperature and longitudinal strain, *Measurement Science and Technology*, 16, 488-96.
- Tschierske C. & Dantlgraber G., 2003, From antiferroelectricity to ferroelectricity in smectic mesophases formed by bent-core molecules, *Pramana*, 61, 455-81.
- Tseng A. A., Kuan Chen, Chen C. D. & Ma K. J., 2003, Electron beam lithography in nanoscale fabrication: Recent development, *IEEE Transactions on Electronics Packaging Manufacturing*, 26, 141-9.

- Tsubota M., 1985, Sensor for specific gravity of lead-acid battery electrolyte, *New Material New Processes*, 3, 248-52.
- Turan J., Carome E. F. & Ovsenik L., 2001, Fiber optic refractometer for liquid index of refraction measurements, 5<sup>th</sup> International Conference on Telecommunications in Modern Satellite, Cable and Broadcasting Service, 2001 (TELSIKS 2001), Nis, Yugoslavia, 2, 489-92.
- Udd E., Schulz W. L., Seim J. M., Trego A., Hauge E. D. & Johnson P. E., 2000, Transversely loaded fiber optic grating strain sensors for aerospace applications, Proc. Nondestructive evaluation of aging aircraft, airports, and aerospace hardware IV, Newport Beach, CA, USA, Proc. SPIE, 3994,96-104.
- Ullrich M., Folge H. W., Schmitz C., 2004, *Method for determining the state of charge of rechargeable batteries by integration of the amounts of current flowing during charging and discharging*, United States Patent 6777914.
- Van D. K. E., Fieuws S., Massage P., Hierner R., Boeckx W., Deleuze J. P., Laperre J. & Anthonissen M., 2007, *Reproducibility of repeated measurements with the Kikuhime pressure sensor under pressure garments in burn scar treatment*, Burns, 33, 5, 572-578.
- Vengsarkar A. M., Lemaire P. J., Judkins J. B., Bhatia V., Erdogan T. & Sipe J. E., 1996, Long-period fiber gratings as band-rejection filters, *Journal of Lightwave Technology*, 14, 58-65.
- Wagreich R. B., Atia W. A., Singh H. & Sirkis J. S., 1996, Effects of diametric load on fibre Bragg gratings fabricated in low birefringent fibre, *Electronics Letters*, 32, 1223-4.
- Wang Y., Bartelt H., Ecke W., Schroeder K., Willsch R., Kobelke J., Rothhardt M., Latka -I. & Brueckner S., 2009, Investigating transverse loading characteristics of microstructured fiber Bragg gratings with an active fiber depolarizer, *IEEE Photonics Technology Letters*, 21, 1450-2.
- Wei T., Han Y. K., Tsai H. L. & Xiao H., 2008, Miniaturized fiber inline Fabry-Perot interferometer fabricated with a femtosecond laser, *Optics Letters*, 33, 536-8.
- Weisenbach L., 2008, Fiber optic sensors, [Available online], URL: <http://www.opticalfibersensors.org/news/been/155/detail/item/1500/>
- Weiss J. D., 2002, *Fiber optic refractive index monitor*, United States patent application 6356675.

- Wolinski T. R., Ertman S., Czapla A., Domanski A. W., Wojcik J., Dabrowski R. & Nowinowski-Kruszelnicki E., 2007, Photonic liquid crystal fiber as a sensing element for electric field measurement, Proc. Instrumentation and Measurement Technology Conference (IMTC 2007, IEEE), 1-4.
- Wong D., Poole S. B. & Sceats M. G., 1992, Stress-birefringence reduction in elliptic-core fibres under ultraviolet-irradiation, *Optics Letters*, 17, 1773-5.
- Xu M. G., Reekie L., Chow Y. T. & Dakin J. P., 1993, Optical in-fibre grating high pressure sensor, *Electronics Letters*, 29, 398-9.
- Yam S. P., 2010, *Higher order diffraction wavelengths of fibre Bragg gratings and applications*, PhD Thesis, Victoria University, Australia.
- Yam S. P., Brodzeli Z., Kouskousis B. P., Rollinson C. M., Wade S. A., Baxter G. W. & Collins S. F., 2009a, Fabrication of a pi-phase-shifted fiber Bragg grating at twice the Bragg wavelength with the standard phase mask technique, *Optics Letters*, 34, 2021-3.
- Yam S. P., Brodzeli Z., Wade S. A., Rollinson C. M., Baxter G. & Collins S. F., 2009b, Use of first-order diffraction wavelengths corresponding to dual-grating periodicities in a single fibre Bragg grating for simultaneous temperature and strain measurement, *Measurement Science & Technology*, 20, 034008.
- Yam S. P., Kitcher D. J., Baxter G. W. & Collins S. F., 2007, Comparison of FBG wavelengths, in the regions of 2/3 of the Bragg wavelength and the Bragg wavelength, by piecewise irradiation of a chirped phase mask, Proc. 3<sup>rd</sup> European Workshop on Optical Fibre Sensors (EWOFS 2007), Napoli, Italy, Proc. SPIE, 6619, 61910-1.
- Yam S. P., Rollinson C. M., Kitcher D., Baxter G. W. & Collins S. F., 2006, Transverse strain response of transmission dips at 2/3 of the Bragg wavelength in a fiber Bragg grating, Proc. 18<sup>th</sup> International Conference on Optical Fiber Sensors (OFS 2006), Cancun, Mexico, Optical Society of America, TuE47.
- Zaatar Y., Zaouk D., Bechara J., Khoury A., Llinaress C. & Charles J. P., 2000, Fabrication and characterization of an evanescent wave fiber optic sensor for air pollution control, *Materials Science and Engineering B-Solid State Materials for Advanced Technology*, 74, 296-8.
- Zhang Y. , Feng D. , Liu Z. , Guo Z., Dong X., Chiang K. S. & Chu B. C. B., 2001, High-sensitivity pressure sensor using a shielded polymer-coated fiber Bragg grating, *IEEE Photonics Technology Letters*, 13, 618-9.

- Zhang Z.W., Wu Z. F. & Wen T. D., 2007, A simple model for measuring refractive index of a liquid based upon Fresnel equations, *Chinese Physics Letters*, 24, 3133.
- Zhao J. R., Huang X. G. & Chen J. H., 2009, A Fresnel-reflection-based fiber sensor for simultaneous measurement of liquid concentration and temperature, *Journal of Applied Physics*, 106, 083103-5.
- Zhao Z. Y., Zhang S. A., Yu Y. S., Zhuo Z. C., Zhang J., Zheng W. & Zhang Y. S., 2004, Fabrication of tunable sampled nonlinearly chirped fiber Bragg gratings with a simple method, *Optical and Quantum Electronics*, 36, 499-506.
- Zyskind J. L., Sulhoff J. W., Sun Y., Stone J., Stulz L. W., Harvey G. T., Digiovanni D. J., Presby H. M., Piccirilli A., Koren U. & Jopson R. M., 1991, Singlemode diode-pumped tunable erbium-doped fibre laser with linewidth less than 5.5 kHz, *Electronics Letters*, 27, 2148-9.

## List of Publications

### Journal Publications

Bal H. K., Sidiroglou F., Collins S. F., & Brodzeli Z., 2010, Multiplexing of fibre optic reflective sensors using Bragg gratings, *Measurement Science and Technology*, 21(9), 094011.

Bal H. K., Sidiroglou F., Brodzeli Z., Wade S. A., Baxter G. W., & Collins S. F., 2010, Fibre Bragg grating transverse strain sensing using reflections at twice the Bragg wavelength, *Measurement Science and Technology*, 21(9), 094004.

### International Conference Publications

Bal H. K., & Brodzeli Z., 2010, Fibre optic reflective sensor to measure state of charge of battery, *Proc. SPIE 4<sup>th</sup> European Workshop on Optical Fibre Sensors (EWOFS 2010)*, Porto, Portugal (Post deadline Poster Session).

Bal H. K., Brodzeli Z., Sidiroglou F., & Collins S. F., 2010, Transverse strain sensor based on etched phase-shifted fiber Bragg gratings, *Proc. 4<sup>th</sup> European Workshop on Optical Fibre Sensors (EWOFS 2010)*, Porto, Portugal, *Proc. SPIE*, 76530, 76530P.

Bal H. K., Sidiroglou F., Brodzeli Z., Wade S. A., Baxter G. W., & Collins S. F., 2010, Temperature independent bend measurement using a pi-phase shifted FBG at twice the Bragg wavelength, *Proc. 4<sup>th</sup> European Workshop on Optical Fibre Sensors (EWOFS 2010)*, Porto, Portugal, *Proc. SPIE*, 7653, 76530H.

Collins S. F., Yam S. P., Bal H. K., Kouskousis B. P., Rollinson C. M., Sidiroglou F., Brodzeli Z., Wade S. A. & Baxter G. W., 2010, Fiber Bragg gratings at twice the Bragg wavelength: Properties and sensor applications, *Asia-Pacific Optical Sensors (APOS 2010)*, Guangzhou, China, (Invited Paper).

Bal H. K., Sidiroglou F., Collins S. F., & Brodzeli Z., 2009, Multipoint refractive index sensor for liquids based on optical fiber Bragg-gratings, *Proc. 20<sup>th</sup> International Conference on Optical Fibre Sensors (OFS 2009)*, Edinburgh, UK, *Proc. SPIE*, 7503, 75031U.

Bal H. K., Sidiroglou F., Yam S. P., Brodzeli Z., Wade S. A., Baxter G. W. & Collins S. F., 2009, Response of fiber Bragg grating transmission dips at twice the Bragg wavelength to transverse strain, *Proc. 20<sup>th</sup> International Conference on Optical Fibre Sensors (OFS 2009)*, Edinburgh, UK, *Proc. SPIE*, 7503, 750337.

Bal H. K., Sidiroglou F., Collins S. F., & Brodzeli Z., 2009, Multipoint optic refractive index sensor for liquids, Proc. 14<sup>th</sup> OptoElectronics and Communications Conference (OECC 2009), Hong Kong, Proc. IEEE, 5222773.

## **National Conference Publications**

Bal H. K., Ladouceur F. & Brodzeli Z., 2010, State of charge of battery indicator based on fibre optic probe, Proc. 35<sup>th</sup> Australian Conference on Optical Fibre Technology (CD-ROM: 19th Australian Institute of Physics Congress, Australian Institute of Physics, Australian Optical Society & Engineers Australia, ISBN 978-0-9775657-6-4), Melbourne, Australia, paper no. 463.

Bal H. K., Sidiroglou F., Ladouceur F., Dragomir N. M., Collins S. F. & Brodzeli Z., 2010, Fabrication of a fibre Bragg grating liquid composition sensor based on wet etching technique, Proc. 35<sup>th</sup> Australian Conference on Optical Fibre Technology (CD-ROM: 19th Australian Institute of Physics Congress, Australian Institute of Physics, Australian Optical Society & Engineers Australia, ISBN 978-0-9775657-6-4)(Proc. ACOFT 2010), Melbourne, Australia, paper no. 663.

Bal H. K., Soin K., Mclaughlin P., Collins S. F. & Dragomir N. M., 2010, Fibre Bragg grating sensors for human skin pressure measurements, Proc. 35<sup>th</sup> Australian Conference on Optical Fibre Technology (CD-ROM: 19th Australian Institute of Physics Congress, Australian Institute of Physics, Australian Optical Society & Engineers Australia, ISBN 978-0-9775657-6-4), Melbourne, Australia, paper no. 607.

Brodzeli Z., Bal H. K. , Chigrinov V., Murauski A. & Ladouceur F., 2010, Electrical energy harvesting device for current/voltage fibre-based sensors, Proc. 35<sup>th</sup> Australian Conference on Optical Fibre Technology (CD-ROM: 19th Australian Institute of Physics Congress, Australian Institute of Physics, Australian Optical Society & Engineers Australia, ISBN 978-0-9775657-6-4), Melbourne, Australia, paper no. 300.

Bal H. K., Sidiroglou F., Yam S. P., Brodzeli Z., Wade S. A., Baxter G. W. & Collins S. F., 2009, Response of fiber Bragg grating transmission dips at twice the Bragg wavelength to transverse strain, Proc. Australasian Conference on Optics, Lasers and Spectroscopy and 34th Australian Conference on Optical Fibre Technology 2009 (CD-ROM: ACOFT ACOLS 09, Australian Optical Society & Engineers Australia, ISBN 1 876346 61 2), Adelaide, Australia, ACOFT paper 26, pp. 487–488.

Brodzeli Z., Bal H. K., Sidiroglou F., Dragomir N. M. & Ladouceur F., 2009b, Fabrication of phase-shifted fibre Bragg gratings with non-uniform etching, Proc. Australasian Conference on Optics, Lasers and Spectroscopy and 34th Australian Conference on Optical Fibre Technology 2009 (CD-ROM: ACOFT ACOLS 09, Australian Optical Society & Engineers Australia, ISBN 1 876346 61 2), Adelaide, Australia, ACOFT paper 46, 525–526.

- Brodzeli Z., Bal H. K., Sidiroglou F., Collins S. F., Chigrinov V., Murauski A. & Fan F., 2009a, Multipoint fibre optic voltage sensor, Proc. Australasian Conference on Optics, Lasers and Spectroscopy and 34th Australian Conference on Optical Fibre Technology 2009 (CD-ROM: ACOFT ACOLS 09, Australian Optical Society & Engineers Australia, ISBN 1 876346 61 2), Adelaide, Australia, ACOLS paper 235, 185–186.
- Bal H. K., Sidiroglou F., Collins S. F., & Brodzeli Z., 2009, Multipoint refractive index sensor based on optical fibre Bragg gratings, Proceedings of the Australasian Conference on Optics, Lasers and Spectroscopy and 34th Australian Conference on Optical Fibre Technology 2009 (CD-ROM: ACOFT ACOLS 09, Australian Optical Society & Engineers Australia, ISBN 1 876346 61 2), Adelaide, Australia, ACOLS paper 428, 428–429.
- Brodzeli Z., Baxter G. W., Collins S. F., Bal H. K., Canning J., Michael S., 2008, Implementation of a low cost interrogation technique for an optical fibre Bragg grating sensor for simultaneous transverse and longitudinal strain measurement, 18<sup>th</sup> National Congress of Australian Institute of Physics (AIP), Proc. AIP, ISBN 1 876346 57 4.

## Appendix B

### Precautions while dealing with HF acid

- Special chemical handling training is required before handling HF
- An assistance of trained lab attendant is required to suitably store HF acid.
- Wear suitable HF resistance clothes all over the body, cover your head.
- Use transparent plastic helmet to cover your face and goggles for eyes.
- Always use double gloves (nylon and rubber gloves).
- Keep first aid tube and tablets near to access.
- Use well ventilated fume hood.